APPLICATION OF POINT-PROCESS SYSTEM IDENTIFICATION TECHNIQUES TO COMPLEX PHYSIOLOGICAL SYSTEMS.

A Thesis

submitted to the Faculty of Engineering

of the University of Glasgow

for the degree of

Doctor of Philosophy

by

David M. Halliday

October 1986

This Thesis is dedicated to

my family.

ACKNOWLEDGMENTS

I am indebted to my supervisor Professor D.J. Murray-Smith for his help and many useful suggestions throughout this project. I would also like to express my thanks to Dr. J. Rosenberg of the Department of Physiology for his advice and assistance with the physiological background and also for many useful discussions in the course of this project.

I am grateful to Professor J. Lamb for the provision of research and computing facilities for the duration of this research, and I would also like to acknowledge the financial support of the Science and Engineering Research Council.

Thanks are also due to the many people who provided neurophysiological data used in this research. These include G. P. Moore from the Department of Biomedical Engineering, University of Southern California (this work was supported in part by UPHS grants NS11298 and GM23732), Professor I. Boyd, Dr. M. Gladden and S. Thompson from the Department of Physiology. I would also like to thank Dr. P. Ellaway, Dr. N. Davey, and Professor J. Stephens from U.C.L., London, for providing data.

Thanks are also due to the Medical Illustrations Unit of the Physiology Department for the preparation of the illustrations in chapter one and other non-graphical illustrations. The figures in chapter one and figure 4.5.5a appear courtesy of Professor I. Boyd.

Finally, I would like to express my appreciation to all my friends and fellow research students for making my stay here so enjoyable. In particular Messrs K.Y. Lee, V.M. Airaksinen, L.D. Bradley and J.P.F. Duffy deserve a special mention. The many useful discussions which were had over a quiet drink with W.J. Adamson and J.S. Denheen are also gratefully acknowledged.

SUMMARY

This thesis is concerned with the application of system identification techniques to the analysis of complex physiological systems. The techniques are applied to neuronal spike-train data obtained from elements of the neuromuscular system.

A brief description of the neuromuscular system is given in chapter 1, along with a more detailed discussion of the muscle spindle, which is the component of the neuromuscular system which this study deals with. In addition, some possibilities for system identification studies of the muscle spindle are discussed.

The identification procedure is based on statistical methods for the treatment of point-process data. The point-process representation of a spike-train is introduced in chapter 2 with definitions of time and frequency domain point-process parameters. Estimates for these parameters are given, along with expressions for their asymptotic distributions. The linear point-process system identification model is introduced and estimates are described for the model parameters in terms of the previously defined point-process parameters. These point-process and linear parameter estimates are applied to muscle spindle spike-train data. In the analysis of a single spike-train certain important features only show up in the frequency domain, and for input and output spike-trains a linear transfer function type description is constructed in the frequency domain. The mathematical model of this transfer function is used as the basis for an analogue computer simulation of a subsystem of the muscle spindle. This consists of a linear first order filter followed by an encoder which generates output spikes. Data logged from the simulation is processed in the same manner as experimental data, and the effect

of varying the simulation parameters on the linear model estimates is looked at. It is shown that in general the linear model description reflects the properties of the linear filter in the simulation, and varying the simulation parameters can be used to accurately match results from simulated data with those obtained from real data.

Chapter 3 compares the point-process approach with a more conventional filtering and sampled data approach to estimate power spectra. The filtering of spike-trains with broad band spectra is investigated, and this shows up a pitfall in the choice of filter cut-off frequency. It is concluded that the point-process approach is preferable due to shorter computational times, and the well documented statistical properties of the point-process estimates.

The application of the point-process techniques described in chapter 2 to the analysis of more general spike-train data is considered in chapter 4. Three techniques for measuring the degree of coupling between two spike-trains are compared, and the point-process frequency domain measure is found to be the most sensitive. This measure is also applied to a data set containing a strong single periodicity, and the ability to detect coupling at a single harmonic is demonstrated. The analysis of coupling between spike-trains in the frequency domain is extended to deal with multiple spike-trains, and the ability to distinguish genuine coupling from the effect of a common input is shown to be a powerful tool which can be used to investigate communications pathways in neural systems. Finally, one special feature of the muscle spindle response to a spike-train input is analysed using the simulation. It is demonstrated that the point-process

approach can produce results about a particular phenomenon from a single experiment much more rapidly than using a repetitive trial and error approach.

Chapter 5 considers the extension of the linear point-process identification model introduced in chapter 2. Higher order time and frequency domain point-process parameters are defined and estimates given. In the time domain, a new technique for rapidly generating higher order time domain parameters is developed. The quadratic point-process model is introduced and solutions for its parameters given. These estimates are applied to muscle spindle data and more complex models are looked at. The two input linear model shows how one input tends to dominate the output when both inputs are applied simultaneously. The single input quadratic model is investigated in the time and frequency domain, providing two different representations of how non-linear interactions can affect the output. The two input quadratic model parameter estimates agree with the findings of the two input linear model, with one input making a larger contribution than the other input to non-linear interactive effects upon the output.

Finally chapter 6 summarises the main findings of the thesis, and makes some suggestions for further research.

CONTENTS

CHAPTER ONE

1.1 INTRODUCTION

Under normal operating conditions many biological systems can be acted upon by several simultaneous inputs. These inputs may in turn give rise to several outputs, and these signals are often of different types. The field of neurophysiology provides many examples of such systems where continuous signals (such as muscle length) can interact with neuronal signals to produce other neuronal signals. These neuronal signals consist of a series of spikes, or spike-train, and can be represented as a series of isolated events by considering the spike-train as a point-process. Any element of the neuromuscular system which is acted upon or generates spike-trains can then be considered as a point-process system. One example of such a system is the muscle spindle. The muscle spindle is thought to play an important role in the control of movement and the maintenance of posture. Several independent point-process inputs and a length input interact within the spindle to produce point-process output signals. This chapter will present a simplified account of the organisation of part of the neuromuscular system and then consider the structure and operation of the spindle in more detail. The response of the spindle to a combination of different inputs will be mentioned and finally some of the possibilities for system identification studies based on muscle spindle data will be discussed.

1.2 THE PERIPHERAL NEUROMUSCULAR SYSTEM

The neuromuscular system in mammals consists of all parts of the nervous and muscle systems which maintain posture, and initiate and control movement. This system has been divided, on

anatomical and functional grounds, into central and peripheral parts. At the level of the spinal cord, the peripheral nervous system is arranged in a sequence of identically organised repeating segmental layers. Figure 1.2.1 outlines one of these levels along with the other components which form the peripheral neuromuscular system at this level.

The main load-bearing muscle consists of muscle fibres lying in parallel. These extrafusal fibres are attached to bone by tendons and generate forces and change length in response to signals sent from the spinal cord, and in response to any applied external forces. These signals are nerve impulses of approximately 100mv. in amplitude and 1msec. in duration which originate from large groups of cell bodies located in the spinal cord. These groups of cells, called alpha-motoneurones, may contain as many as 2000 cells and have long processes called axons which leave the spinal cord and innervate the extrafusal fibres. Nerve impulses propagate down the cell axons as localised voltage changes between the membrane surrounding the cell body and the axon, with conduction velocities in the range 50-120m/sec.. These nerve impulses are also called action potentials or, because they have a short duration, spikes. Nerve cells can generate these action potentials repetitively to produce spike-trains which may vary in frequency from one spike every few seconds up to several hundred spikes per second. It is the arrival of a spike at the junction of the axon and extrafusal fibre which causes muscle contraction. The force of the contraction can be increased over the whole muscle by either increasing the number of alpha-motoneurones or increasing the frequency of the nerve impulses reaching the muscle via the alpha-motoneurones. A single alpha-motoneurone may innervate

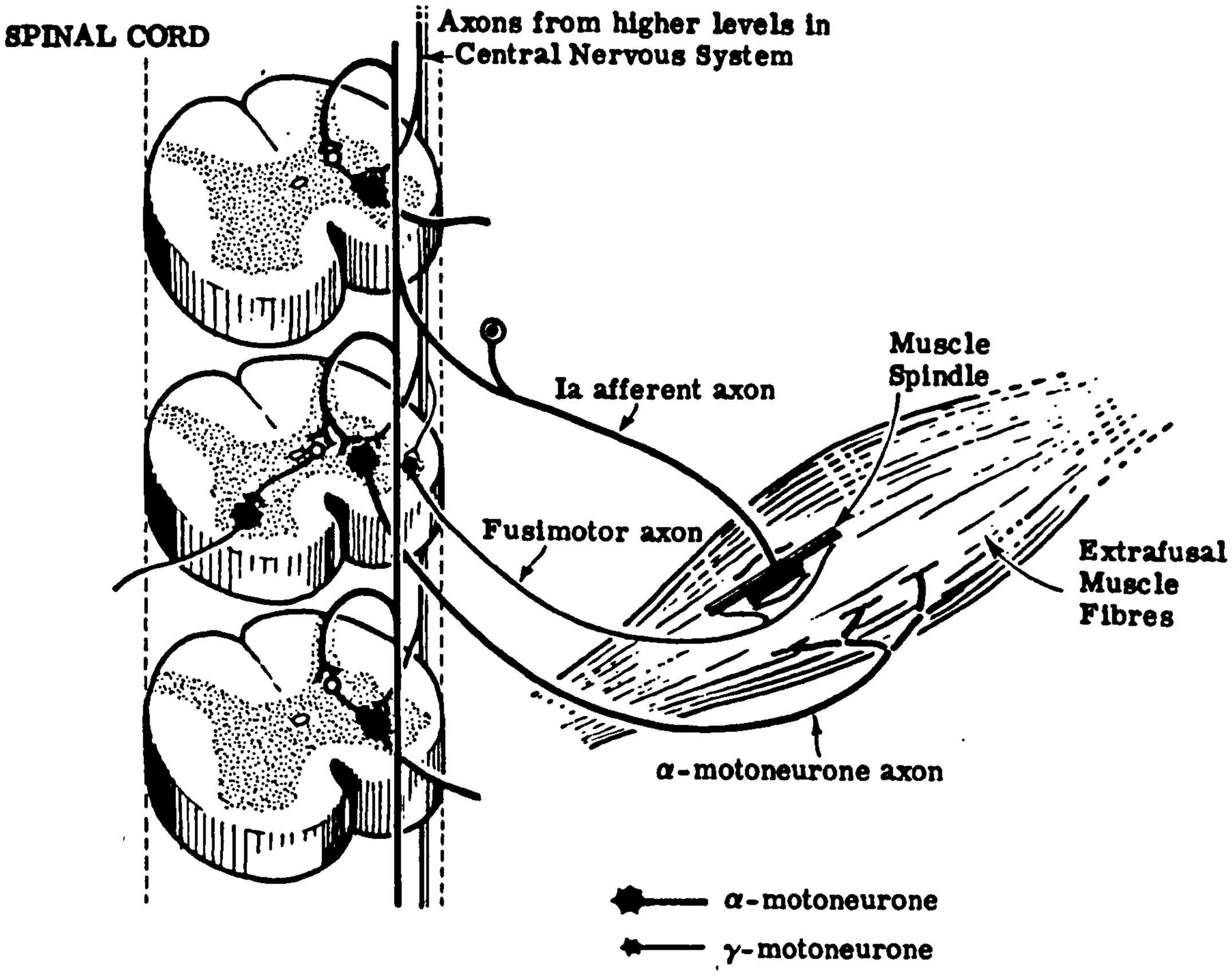

Fig. 1.2.1 Diagram of peripheral neuromuscular system showing pathways between the spinal cord, a muscle spindle and its parent muscle.

several extrafusal fibres, all of which lie within the same muscle, and an alpha-motoneurone together with all the muscle fibres that it innervates is called a motor-unit. The number of muscle fibres in a motor-unit and the number of motor-units within a muscle depend on the function of that muscle. Muscles concerned with the control of delicate movement have small motor-units capable of generating small incremental units of force, whereas large scale muscles which simply maintain posture have large motor-units.

Buried within the main muscle are receptors which are sensitive to changes of length or forces acting on the parent muscle. These receptors send information to the spinal cord, via sensory axons, in response to disturbances in the parent muscle. This information is again in the form of nerve impulses and these nerve impulses, once they reach the spinal cord, modify the activity in the alpha-motoneurone cell bodies. Each sensory axon may make contact with a large number of nerve cells over several segmental layers in the spinal cord, and each nerve cell in the spinal cord may receive information from a large number of sensory axons in the same muscle. In addition nerve cells within the same segmental layer may interact with each other and interactions between different segmental layers may also occur. It is possible for a single alpha-motoneurone to be affected by up to 10000 different inputs. An introduction to the organisation of the spinal cord can be found in Sheperd (1974), and a detailed review of this along with the properties of the spinal cord and its interconnections is given in Burke and Rudomin (1977).

1.3 THE MUSCLE SPINDLE

One class of muscle receptors which are thought to have an important role in controlling movement and maintaining posture are the muscle spindles. Spindles respond mainly to length changes in the parent muscle, and consist of a number of specialised fibres which lie parallel to the extrafusal fibres. These spindle or intrafusal fibres are much shorter than the extrafusal fibres and are partially surrounded by a fluid filled capsule. Three different types of intrafusal fibres are found in spindles, these are the dynamic-bag fibres (Db_1), static-bag fibres (Sb_1) and the chain fibres (C). These fibres all have different mechanical properties and respond differently to length changes (Bessou and Pages, 1975; Boyd et al, 1977). A spindle will typically have one of each bag fibre and up to six chain fibres. There are two types of sensory axon which transmit the information about length change to the spinal cord. These are the primary or group Ia and the secondary or group II axons, each spindle having one primary and several secondary axons associated with it. The primary ending has branches which form spirals around the central regions of the intrafusal fibres, the secondary endings lie to either side of this and are associated with the chain and static-bag fibres. Conduction velocities of the action-potentials to the spinal cord range from 72-120m/sec. for the primary and 24-72m/sec. for the secondary.

If the parent muscle is held at a fixed length, the spindle will generate action-potentials at a constant rate, dependent upon the muscle length (Matthews and Stein, 1969). This is termed the spontaneous discharge. Increasing the muscle length increases the rate of discharge in both primary and secondary axons by a

process not fully understood, but believed to be due to the distortion of the fine terminals of the axons where they are in contact with intrafusal fibres.

As well as sending pulse coded information to the spinal cord, muscle spindles also receive pulse coded information from the spinal cord. This information originates from groups of cells within the spinal cord which lie close to the alpha-motoneurone cells. The axons of these cells, called gamma-motoneurones, have conduction velocities of 10-50m/sec. and innervate only intrafusal muscle fibres. These neurones are also called fusimotor neurones and each one may innervate different spindle fibres within the same parent muscle. Fusimotor axons have been divided into two categories, gamma dynamic and gamma static axons (Matthews, 1962; Emonet-Denand et al, 1977). Gamma dynamic axons innervate only dynamic bag fibres whereas gamma static axons innervate static bag or chain fibres, or both (Boyd, 1980; Matthews, 1981). A single spindle may have as many as six fusimotor inputs. Activity in the fusimotor axons alters the primary and secondary axon responses to any length changes in the parent muscle. The main features of the muscle spindle are illustrated in figure 1.3.1a showing a photograph of a single isolated spindle in which the spirals of the primary ending can be seen wrapped around all the intrafusal fibres. The spirals of the secondary ending are restricted mainly to chain fibres. Figure 1.3.1b is a simplified block diagram of the innervation of a spindle incorporating the features mentioned.

Muscle spindles are very sensitive to length disturbances in the parent muscle. A sinusoidal length variation of 0.1mm will produce an appreciable modulation of the spontaneous discharge from the primary sensory ending. Primary and secondary endings

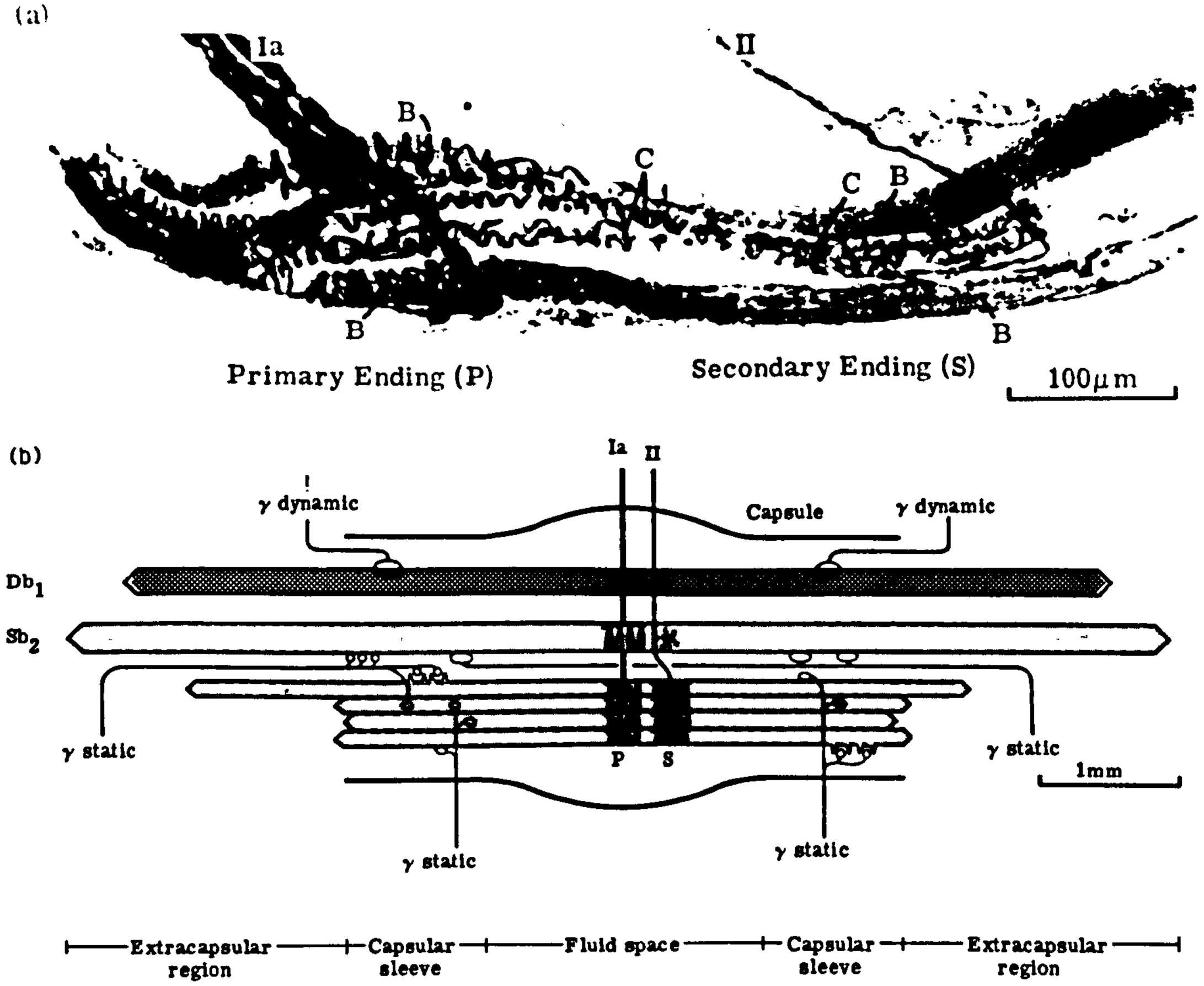

Fig. 1.3.1 (a) Photograph of isolated muscle spindle showing primary and secondary endings.

(b) Diagram of the innervation of the muscle spindle.

respond differently to a ramp stretch and hold applied to the parent muscle. Figure 1.3.2a shows a typical primary response, while figure 1.3.2b shows a typical secondary response to this input. The upper trace shows the sensory axon response in each case, the middle trace shows the instantaneous frequency of the discharges. This is calculated by taking the reciprocal of the time between one spike and the previous spike in the discharge. The lower trace in each figure illustrates the applied stretch and hold input.

The primary ending discharge increases rapidly during the applied stretch, and then settles at a new higher constant value due to the increased muscle length, disappearing almost completely during the relaxation stage and returning again to a constant rate representing the resting length. The instantaneous frequency of the secondary ending follows the general shape of the length input, suggesting that the secondary is more sensitive to muscle length and the primary is more sensitive to change in muscle length, or muscle velocity. These different responses also suggest different electro-mechanical properties of the intrafusal fibres associated with each sensory ending.

The effect of fusimotor inputs on the ramp response of the primary ending is illustrated in figure 1.3.3 showing the effect of individually stimulating a fusimotor input associated with the three different types of intrafusal fibre at a constant rate. In each case the upper trace shows the instantaneous frequency of the Ia response in the presence, the lower trace in the absence, of the fusimotor input. Figure 1.3.3a shows that innervating a dynamic bag fibre at a constant 75 pulses/sec. increases both the rate of discharge during the dynamic phase and the overshoot following the end of the ramp. Stimulation of a gamma axon

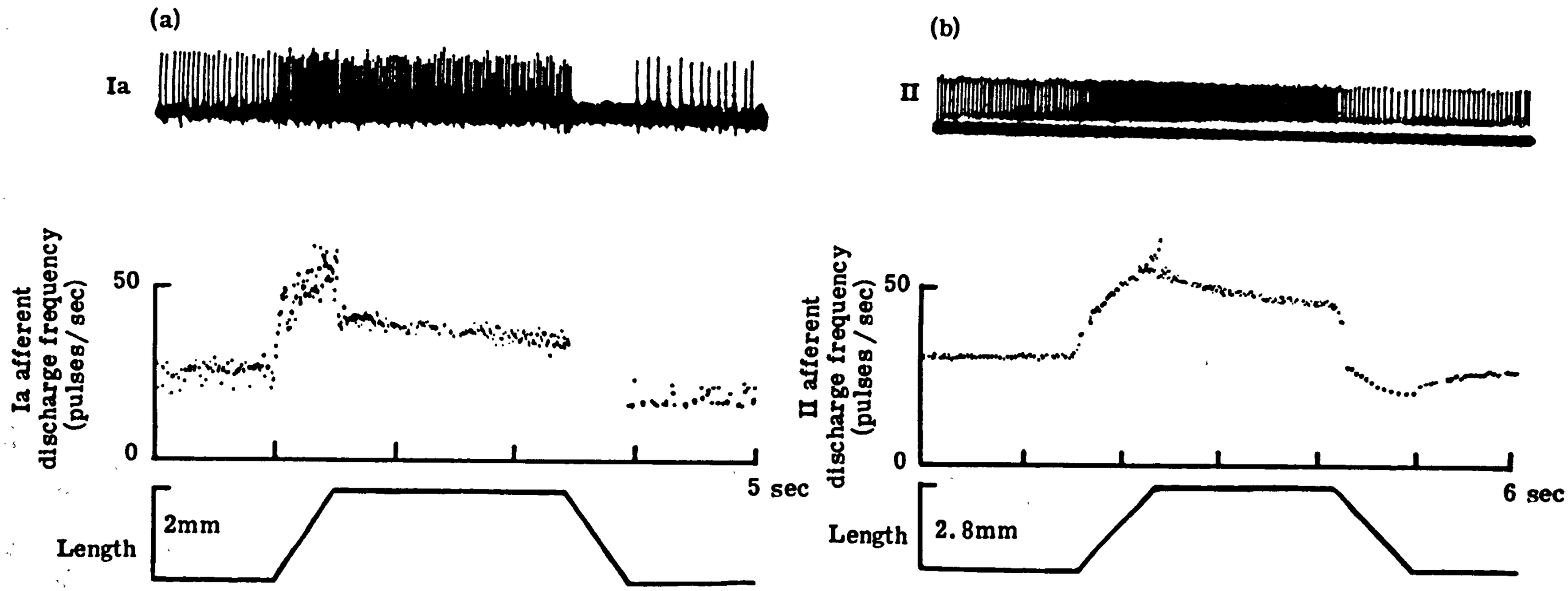

Fig. 1.3.2 (a) Primary response to ramp stretch and hold.

(b) Secondary repsonse to ramp stretch and hold.

Upper trace shows record of spikes, middle trace shows instantaneous frequency, and lower trace shows length stimulus.

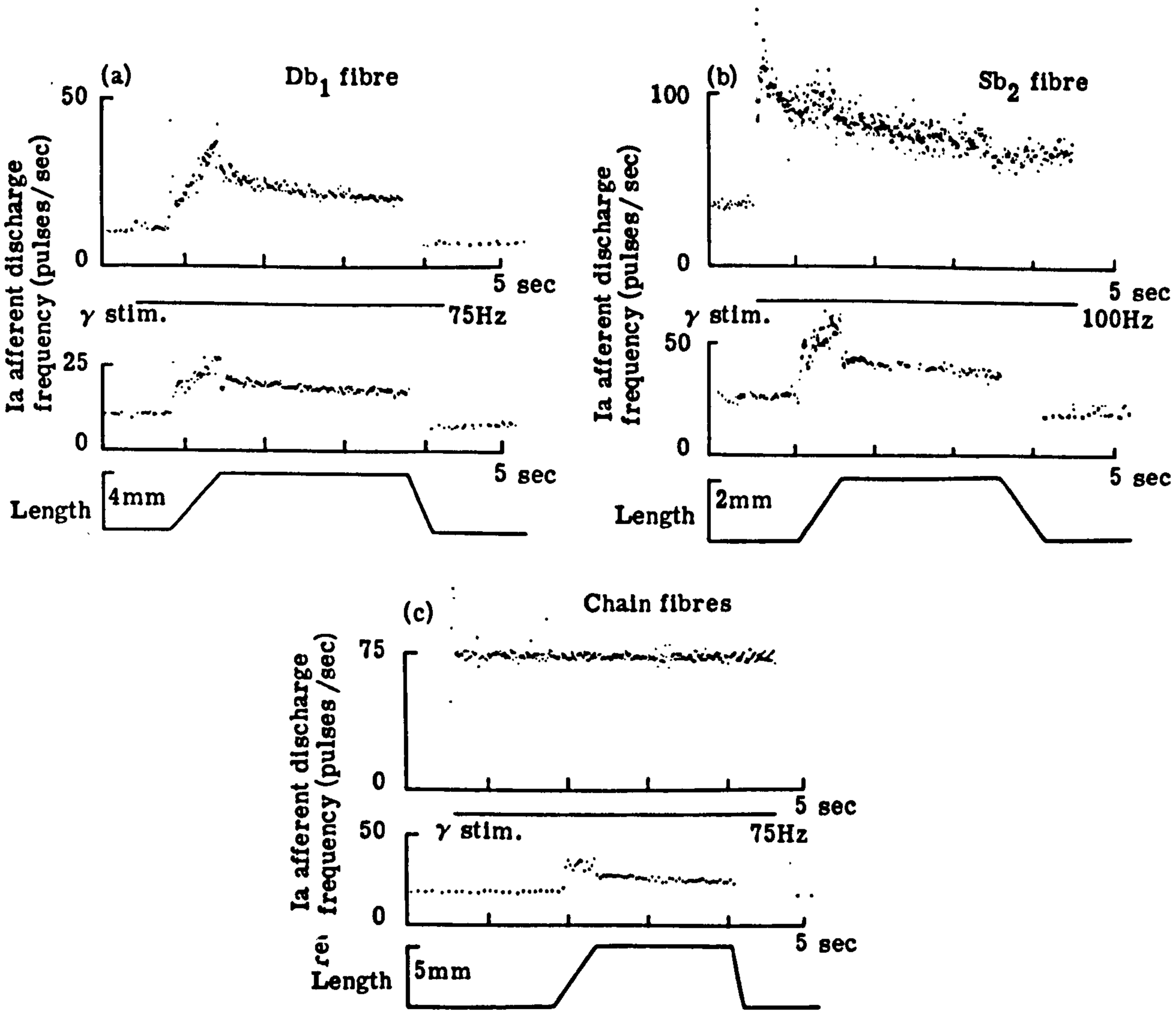

Fig. 1.3.3 Primary response to ramp stretch and hold stimulus with constant rate of fusimotor stimulation applied to :

(a) dynamic bag (Db_1) intrafusal fibre,

(b) static bag (Sb_2) intrafusal fibre and

(c) chain (C) fibre.

Upper trace is instantaneous frequency of primary discharge in presence of stimulation, middle trace in absence of fusimotor stimulation and lower trace shows length stimulus. Straight line between upper and middle trace indicates duration of fusimotor stimulation.

associated with either static bag or chain fibres appears to override the Ia ramp and hold response. Figure 1.3.3b shows that static bag fusimotor innervation on its own produces a strong dynamic response in the primary ending which almost obscures the length response. The constant rate of innervation of the axon leading to the chain fibres, 75 pulses/sec. is imposed on the primary discharge, and changes in length no longer modulate the primary discharge. These three responses suggest that fusimotor innervation may modify the mechanical properties of the intrafusal fibres or influence the conversion of strain in the fibres to action potentials in the sensory axons.

The types of signal associated with the muscle spindle are illustrated in figure 1.3.4. This figure shows a section of the primary discharge resulting from stimulation using a random fusimotor input and a random length signal, which are also shown. The isolated spikes in the primary and fusimotor spike-trains can clearly be seen in the upper two traces.

The muscle spindle data used in this study was obtained from the tenuissimus muscle in the rear limb of anaesthetized cats. This involved isolating a muscle spindle within the parent muscle and cutting the fusimotor nerves from the spinal cord and the primary and secondary axons to the spinal cord, while leaving the spindle and its blood supply intact. The parent muscle was clamped in a muscle puller which allowed it to be held at constant length, or stretched randomly. Electrodes were attached to the cut nerve endings and the fusimotor ending stimulated with voltage pulses. This sequence of pulses was recorded along with the resulting primary response to form the data sets.

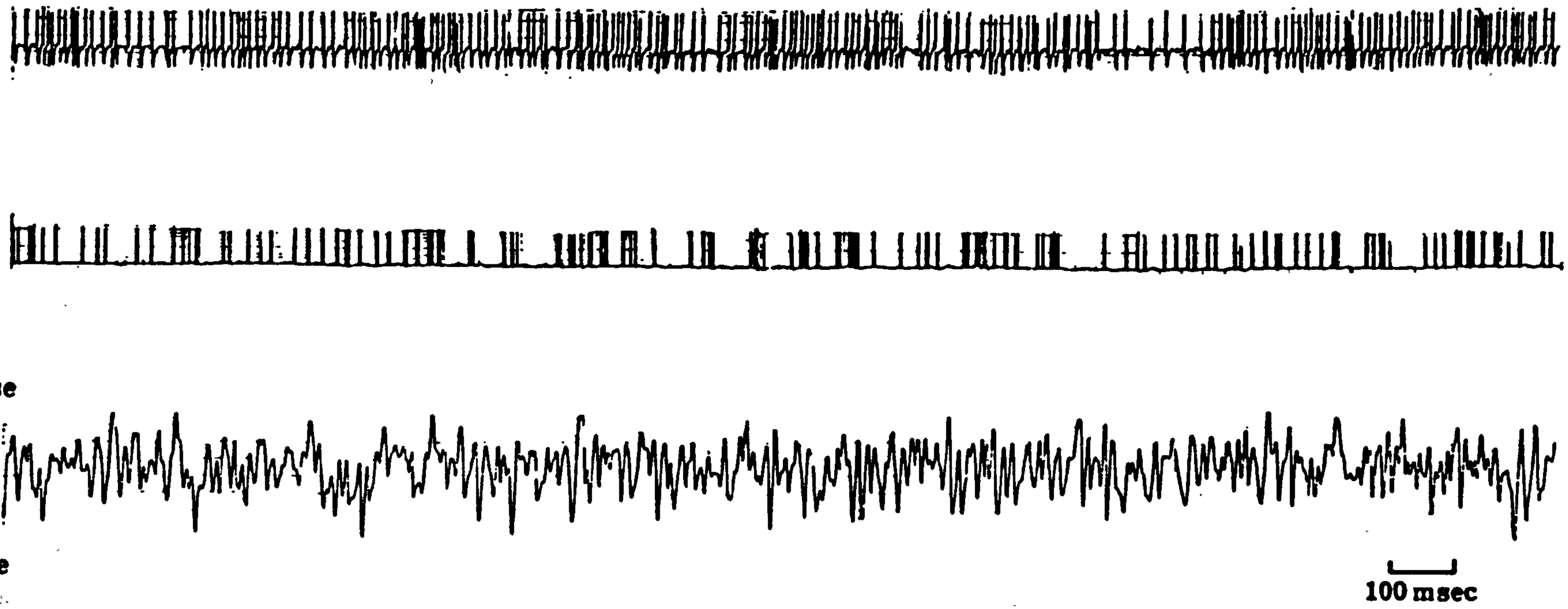

Fig. 1.3.4 Section of primary discharge recorded during an experiment which results from random fusimotor stimulation and a random length change.

1.4 IDENTIFICATION OF SPINDLE SYSTEMS

This brief outline of the peripheral neuromuscular system shows that the muscle spindle is a very complex structure, which forms only one component of the neuromuscular system. Considering the possibilities of the interactions that must exist within each level and between levels illustrates the size of the problem encountered when investigating the control function of the whole neuromuscular system. However, application of engineering techniques to individual elements of the neuromuscular system, will allow models of the component elements to be built up. Interactions within these component elements can then be looked at and more accurate and complex models of these elements constructed if results are related to physiologically meaningful effects.

In the case of the muscle spindle investigation of the mechanism by which fusimotor activity modifies sensory axon response at fixed muscle length will aid in determining the role of the spindle in the maintenance of posture. A useful starting point is to look at the relationship between a single fusimotor input and the primary axon response to this input at fixed length. Interactive effects can be studied by looking at the combined effects of two fusimotor inputs on the primary discharge, or the effects of a single fusimotor input on the primary and secondary discharges simultaneously. The characterisation and study of these interactive effects will allow a more complex model of the spindle to be constructed as each new interactive term is studied. Repeating these studies using a length input will add another interactive term to the model and allow the investigation of the spindle role in the control of movement.

In a physiological context overall aims include the characterisation of the properties of the intrafusal fibres and the characterisation of the process which converts the strain in these fibres into action potentials in the primary and secondary sensory axons. In particular studies of the spindle at fixed length can be used to investigate the mechanism by which fusimotor activity can modify the mechanical properties of the intrafusal fibres. Altering the muscle length is attempting to characterize how mechanical deformation of the intrafusal fibres alters the rate of discharge of action potentials in the sensory neurones.

In an engineering context overall aims include the determination of the information content of the primary discharge for various inputs, and the characterisation of the spindle using the input and output signals recorded experimentally. In the simplest case involving one fusimotor input and the resultant primary response, the identification process is that of a system which has a single spike-train input and output, with a spontaneous discharge due to the fixed muscle length. This process can be extended to the identification of systems with two spike-train inputs representing two fusimotor inputs and one output representing the primary discharge. Considering both the primary and secondary discharges means the identification process is that of a system with two spike-train outputs.

Treating the spike-train signals of the fusimotor inputs and the primary and secondary discharges as realisations of point-processes allows point-process system identification techniques to be applied to the analysis of the muscle spindle.

CHAPTER TWO

2.1 INTRODUCTION

Previous identification studies of the muscle spindle have tended to concentrate on single-input single-output models, particularly upon experiments using length inputs and the resulting primary discharge pattern. These types of model produce a linearised description about a particular operating point and are of limited value since they do not attempt to characterize any non-linearities present, and cannot be readily extended to consider more than one input variable. A review of these and other single input/output studies, containing references, as well as an introduction to identification methods based upon point-process parameters can be found in Rosenberg et al (1982).

Point-process identification techniques can be applied to muscle spindle data if the neuronal spike-trains are treated as point-process data. The short duration of the action potentials, compared with the time interval between successive pulses provides the basis for considering the spike-trains in the neuromuscular system as realisations of stochastic point-processes. The analysis of point-process data uses statistical methods which can be related to conventional time-series analysis. These techniques are both particular cases of a general class of processes called stochastic processes which deal with the theory of random functions (Doob, 1953; Bartlett, 1955). The theory and applications of time-series can be found in monographs by Jenkins and Watts (1968), Brillinger (1975a) and Bloomfield (1976). Reviews of different stochastic models applicable to neuronal data can be found in Fienberg (1974), Holden (1976) and Sampath and Srinivassan (1977).

The problem of characterising point-processes was considered by Bhabha and Ramakrishnan (1950) for the distribution of

particles over a continuous infinity of energy states. Only probability densities can be attached to a particular energy state, and not non-zero probabilities. Integration of the probability density function will only give the first-order expectation of the numbers of particles in a prescribed energy range. To study fluctuations in the distribution of the particles Bhabha and Ramakrishnan introduced higher-order density functions. These functions were later called product-densities (Bahbha,1950; Ramakrishnan, 1950, 1953) and are analogous to moment functions used to characterize other stochastic processes. Cox (1955) defined a class of random point-processes and Bartlett (1963) considered the spectral analysis of these processes to detect clustering in traffic data derived from the timing of vehicles passing a fixed point. Bartlett's approach was developed and given a firmer mathematical basis by Lewis (1970), Daley (1971) and Brillinger (1972). Monographs were published by Cox and Lewis (1966) and Lewis (1972), the latter containing papers covering the development, theory and applications of statistical analysis of point-processes. This provided the basis for the system identification technique studied here which was introduced by Brillinger (1974a, 1975b, 1975c) and is similar to the method proposed by Wiener (1958) for the identification of polynomial systems using Gaussian noise. The advantage of this approach is that it can be readily extended to include non-linearities as well as multi-input, multi-output descriptions. The proposed model parameters can be expressed in terms of stochastic point-process parameters. More extensive bibliographies concerning the historical development, and applications of point-process theory can be found in the references mentioned above.

This chapter will introduce the general theory of stochastic point-processes along with Brillinger's model for the identification of point-process systems. Estimates will be given for the relevant parameters and these will be applied to the analysis of muscle spindle data. Based on the model parameter estimates, a computer simulation of a spindle subsystem will be constructed and results from this will be compared with experimental results.

2.2 STOCHASTIC POINT-PROCESS PARAMETERS

A stochastic point-process M is defined as a random non-negative integer valued measure. In practice this will give the times of occurrence of the M events in terms of an integer number of some sampling period. The parameters will be defined on the assumption that the point-processes are stationary (with respect to time) and orderly (Brillinger, 1975b). An orderly process is one with isolated events, this is achieved in the present study by digitising the spike-trains with a sampling interval of 1msec. and storing the times of the events as an integer number of milliseconds. This also avoids any aliasing of frequencies, since a sampling period of T_s = 1msec. in conventional time-series analysis gives a Nyquist frequency of $1/2T_s$ = 500Hz., which is outside the range of frequencies of interest.

2.2a Time Domain Parameters

For two point-processes M and N satisfying the above assumptions, M(t) and N(t) represent the number of events that have occurred in the interval (0,t] in the processes M and N respectively. Differential increments at time t are given by :

$$\{dM(t)\} = \{M(t,t+dt]\}$$

$$\{dN(t)\} = \{N(t,t+dt]\}, \qquad (2.2.1)$$

these count the number of events occurring in the interval dt. In practice, since we are dealing with isolated events, then the differential increments will have the value 1 if an event occurs in the interval dt, 0 otherwise. The first order intensity function of events of type M, P_m, is defined as :

$$E\{dM(t)\} = P_m dt, \qquad (2.2.2)$$

where E is the expectance operator. This may be interpreted as :

$$\text{Prob}\{\text{ M point in } (t,t+dt] \}, \qquad (2.2.3)$$

giving a measure of the mean rate of the process M. P_n is defined in a similar manner (Brillinger, 1975b). The second order product density at lag u, of the process M, $P_{mm}(u)$, is defined as :

$$E\{dM(t+u)dM(t)\} = P_{mm}(u)\ dudt. \qquad (2.2.4)$$

This may be interpreted as :

$$\text{Prob}\{\text{M point in } (t+u,t+u+du] \ \&\ \text{M point in } (t,t+dt]\}, \qquad (2.2.5)$$

and gives a probabalistic measure of the occurrence of an M event u time units after a previous M event (Brillinger, 1976a).

Extending this approach to the bivariate case allows the second order cross product density $P_{nm}(u)$ to be defined as :

$$E\{dN(t+u)dM(t)\} = P_{nm}(u)\ dudt, \qquad (2.2.6)$$

giving a measure of the relative number of occurrences of an N event u time units after an M event. A similar interpretation

applies as for the univariate case and is given in (2.2.7).

Prob{N point in (t+u,t+u+du] & M point in (t,t+dt]}. (2.2.7)

The conditional mean intensity of the process M, $m_{mm}(u)$, is defined by :

$$E\{dM(t+u) \mid M(t)=1\} = m_{mm}(u)\ du. \qquad (2.2.8)$$

Using the rules of conditional probability this can be written as :

$$m_{mm}(u) = P_{mm}(u)/P_m, \qquad (2.2.9)$$

and interpreted as :

Prob{M point in (t+u,t+u+du] | M event at t}. (2.2.10)

This provides a measure of the probability of occurrence of an M event given that another M event occurs u time units previously. The corresponding equations for the conditional mean intensity in the bivariate case are given below.

$$E\{dN(t+u) \mid M(t)=1\} = m_{nm}(u)\ du. \qquad (2.2.11)$$

$$m_{nm}(u) = P_{nm}(u)/P_m. \qquad (2.2.12)$$

Prob{N point in (t+u,t+u+du] | M event at t}. (2.2.13)

In the univariate case the conditional mean intensity is called the auto-intensity function, and in the bivariate case it is known as the cross-intensity function (Cox and Lewis, 1972). The cross-intensity function gives the short term intensity of the N process u time units after an M event. If M and N are the input and output of a point-process system respectively, then the cross-intensity function is useful in predicting whether an

output event will occur u time units after an input event. If the processes are independent then process M will have no effect on process N and $m_{nm}(u) = P_n$ for all u. A dependence of N upon M will result in $m_{nm}(u) < P_n$ if the process N slows down, and an acceleration of process N after an M event will give $m_{nm}(u) > P_n$. In practice all correlating influences have a finite time of dependence. This phenomenon is known formally as a mixing condition (Rosenblatt, 1956), and results from the fact that as u increases the differential increments dN(t+u) and dM(t) tend to become independent. Using this the asymptotic distribution of the cross-intensity function can be defined as :

$$\lim_{u\to\infty} m_{nm}(u) = P_n. \qquad (2.2.14)$$

Similar arguments can be applied to the auto-intensity function giving :

$$\lim_{u\to\infty} m_{mm}(u) = P_m. \qquad (2.2.15)$$

Product densities are considered in Cox and Lewis (1972) and Brillinger (1975b, c)

Cumulant density functions can now be defined using the above parameters and equations (2.2.16) and (2.2.17) do so for the univariate and bivariate cases respectively.

$$q_{mm}(u) = P_{mm}(u) - P_m^2 \qquad (2.2.16)$$

$$q_{nm}(u) = P_{nm}(u) - P_n P_m \qquad (2.2.17)$$

Cumulant density functions are also known as the auto-covariance density in the univariate case and as the cross-covariance density when considering the bivariate case. For completeness equation (2.2.16) needs to be extended to allow for the singularity at zero lag (Bartlett, 1963). This is achieved by

adding $P_m\delta(u)$ and $P_n\delta(u)$ to the auto-covariance densities of the processes M and N respectively. The mixing condition again allows the asymptotic distribution for the cumulant densities to be defined as :

$$\lim_{u\to\infty} q_{mm}(u) = 0 \qquad (2.2.18)$$

$$\lim_{u\to\infty} q_{nm}(u) = 0. \qquad (2.2.19)$$

For a Poisson point-process the increments dM(t+u) and dM(t) will be independent for all u, thus $q_{mm}(u)=0$ for a Poisson point-process.

2.2b Frequency Domain Parameters

Two methods can be used to calculate frequency domain point-process parameters. They can be defined indirectly by taking the Fourier transform of the cumulant density functions (Bartlett, 1963; Brillinger, 1974a, b, 1975d), or directly by taking the finite Fourier transform of the differential increments of a segment of the process (Brillinger, 1972, 1974a, b). Both methods give equivalent results.

Considering the indirect method first, the auto spectrum of the process M, $f_{mm}(\lambda)$ at frequency λ, is defined as the Fourier transform of the complete auto-covariance density :

$$f_{mm}(\lambda) = 1/2\pi \int_{-\infty}^{\infty} (q_{mm}(u)+\delta(u)P_m)\ e^{-i\lambda u}\, du, \qquad (2.2.20)$$

and similarily for the cross-spectrum between processes N and M at frequency λ :

$$f_{nm}(\lambda) = 1/2\pi \int_{-\infty}^{\infty} q_{nm}(u)\ e^{-i\lambda u}\, du. \qquad (2.2.21)$$

Due to the symmetrical nature of the auto-covariance function $f_{mm}(\lambda)$ is a real quantity, however since the cross-covariance density is not symmetrical about u=0 then the cross-spectrum is a complex quantity and has gain and phase components associated with it.

If the process M is Poisson then (2.2.20) simplifies to :

$$f_{mm}(\lambda) = P_m/2\pi, \qquad (2.2.22)$$

since $q_{mm}(u)$ is zero. The spectrum of a Poisson process is thus a constant value (Lewis, 1970). This illustrates the equivalence of Poisson noise in point-process system identification to Gaussian white noise in continuous systems identification. For processes which are non-Poisson in nature any dependence of dM(t+u) upon dM(t) as shown by the auto spectrum will cover a finite range of frequencies (Brillinger et al, 1976). This gives an asymptotic distribution for $f_{mm}(\lambda)$ of :

$$\lim_{\lambda \to \infty} f_{mm}(\lambda) = P_m/2\pi. \qquad (2.2.23)$$

Any deviation from this level will indicate a non-Poisson process.

The second method for calculating point-process spectra involves taking the finite Fourier transform of the differential increments of the process. For a section of length T of the process M this is defined as :

$$d_M^{(T)}(\lambda) = \int_0^T e^{-i\lambda t}\, dM(t), \qquad (2.2.24)$$

with a similar definition for $d_N^{(T)}(\lambda)$. The periodogram of the process M is defined as :

$$I_{MM}^{(T)}(\lambda) = 1/2\pi T \; d_M^{(T)}(\lambda) \; \overline{d_M^{(T)}(\lambda)}, \qquad (2.2.25)$$

where the bar indicates a complex conjugate quantity. The cross-periodogram between processes N and M is defined as :

$$I_{NM}^{(T)}(\lambda) = 1/2\pi T \; d_N^{(T)}(\lambda) \; \overline{d_M^{(T)}(\lambda)}. \qquad (2.2.26)$$

The periodogram itself is not a consistent estimate of the spectrum and requires further smoothing to provide consistent spectral estimates (Brillinger 1972, 1975a).

2.3 ESTIMATES OF POINT-PROCESS PARAMETERS

This section will consider estimates of the parameters defined in section 2.2. Where appropriate expressions for the asymptotic distributions and the variance of the estimates will be given.

2.3a Estimates of Time Domain Parameters

Estimates of product densities are discussed in Griffith and Horn (1963), Cox (1965), Cox and Lewis (1972), and Brillinger (1975b, d). Brillinger (1976b), and Brillinger et al (1976) also discuss estimates of product densities and give expressions for the variance of the estimates which they use to construct confidence intervals for the estimates. A detailed discussion of univariate and bivariate point-process parameter estimates, along with expressions for variances and asymptotic distributions is contained in Rigas (1983, ch's 3 and 4).

The mean intensity, P_m, of the process M can be estimated as :

$$\hat{P}_m = M(R)/R, \qquad (2.3.1)$$

where R is the period of observation of the spike-train. The hat symbol above P_m is used to indicate an estimate. All the first

order intensity functions are equivalent as shown by (2.3.2).

$$q_m = m_m = P_m \qquad (2.3.2)$$

Estimates of the second order intensity and density functions of the process M are based upon the counting variate defined in (2.3.3).

$$J_{MM}^{T}(u) = \#^{(1)}\{\ (k,l)\ :\ u-h/2 < t_k - t_l < u+h/2\ \}, \qquad (2.3.3)$$

where t_k and t_l denote the times of the M spikes (k,l=1,2,...) and h is the bin width used in the estimate.

In discrete form this variate can be written as $J_{MM}^{T}(u_j)$, where $u_j=jh$ and (j=...,-2,-1,0,1,2,...). This variate counts the number of M events falling inside a bin of width h whose midpoint is u time units along from another M event. The expected value of this histogram type estimate can be shown to be (Cox and Lewis, 1972):

$$E\{J_{MM}^{T}(u)\} = h\ T\ P_{mm}(u). \qquad (2.3.4)$$

From this estimates for the second order intensity and density functions for the univariate process M can be derived :

$$\hat{P}_{mm}(u_j) = J_{MM}^{T}(u_j)/h\ T, \qquad (2.3.5)$$

$$\hat{m}_{mm}(u_j) = J_{MM}^{T}(u_j)/h\ M(T), \qquad (2.3.6)$$

$$\hat{q}_{mm}(u_j) = \hat{P}_{mm}(u_j)-\hat{P}_m^{\,2} = (\hat{m}_{mm}(u_j)-\hat{P}_m)\hat{P}_m, \qquad (2.3.7)$$

where h is the bin width, and T is the record length used in the estimate. For the bivariate case the counting variate becomes $J_{NM}^{T}(u)$ and is defined as :

$$J_{NM}^{T}(u) = \#\{\ (k,l)\ :\ u-h/2 < s_k - t_l < u+h/2\ \}, \qquad (2.3.8)$$

(1) here #{A} denotes the number of elements in set A.

where s_k denote the times of the N events and t_l the M events (k,l=1,2,...). This variate counts the number of N events falling in a bin of width h whose midpoint is u time units along from an M event. The expected value of this variate is given in (2.3.9).

$$E\{J_{NM}^{T}(u)\} = h\ T\ P_{nm}(u), \tag{2.3.9}$$

giving the following estimates for the second order bivariate intensity and density functions :

$$\hat{P}_{nm}(u_j) = J_{NM}^{T}(u_j)/h\ T, \tag{2.3.10}$$

$$\hat{m}_{nm}(u_j) = J_{NM}^{T}(u_j)/h\ M(T), \tag{2.3.11}$$

$$\hat{q}_{nm}(u_j) = \hat{P}_{nm}(u_j)-\hat{P}_n\hat{P}_m = (\hat{m}_{nm}(u_j)-\hat{P}_n)\hat{P}_m. \tag{2.3.12}$$

The asymptotic distributions for these estimates are given by :

$$\lim_{u\to\infty} \hat{P}_{nm}(u) = \hat{P}_m^{\,2}, \tag{2.3.13}$$

$$\lim_{u\to\infty} \hat{P}_{nm}(u) = \hat{P}_n\hat{P}_m, \tag{2.3.14}$$

$$\lim_{u\to\infty} \hat{m}_{nm}(u) = \hat{m}_m, \tag{2.3.15}$$

$$\lim_{u\to\infty} \hat{m}_{nm}(u) = \hat{m}_n, \tag{2.3.16}$$

$$\lim_{u\to\infty} \hat{q}_{nm}(u) = 0, \tag{2.3.17}$$

$$\lim_{u\to\infty} \hat{q}_{nm}(u) = 0. \tag{2.3.18}$$

Considering the estimate of the cross-intensity function in more detail, $\hat{m}_{nm}(u)$ has an approximately Poisson distribution with mean $m_{nm}(u)$ and variance given by :

$$\mathrm{Var}\{\ \hat{m}_{nm}(u)\ \} = (h\ M(T))^{-1}\ m_{nm}(u). \tag{2.3.19}$$

Confidence limits can easily be constructed for an estimate if

the variance is constant. However from (2.3.19) the variance of the estimate (2.3.11) is proportional to the quantity being estimated. This can be overcome by applying a variance stabilizing transform to (2.3.11) (Jenkins and Watts, 1968, pp75-77). The appropriate transform here is a square root transformation (Brillinger, 1976b), giving the following two results :

$$\lim_{u\to\infty} (\hat{m}_{nm}(u))^{1/2} = (\hat{P}_n)^{1/2}, \qquad (2.3.20)$$

$$\mathrm{Var}\{ (\hat{m}_{nm}(u))^{1/2} \} = (4\ h\ M(T))^{-1}. \qquad (2.3.21)$$

Approximate 95% confidence limits can be constructed by adding plus and minus 1.96 standard deviations to the estimate of the asymptotic distribution. Therefore when considering the cross-intensity function, the estimate $(\hat{m}_{nm}(u))^{1/2}$ should be plotted along with the values $(\hat{P}_n)^{1/2} \pm (h\ M(T))^{-1/2}$ representing the asymptotic distribution and the approximate 95% upper and lower confidence limits. This asymptotic distribution and confidence band is based upon the assumption of independence, and the upper and lower confidence intervals give the range of expected values of $(\hat{m}_{nm}(u))^{1/2}$ if the two processes N and M are independent. Dependence of one process upon another will lead to a deviation of the estimate outside these intervals, as discussed in the previous section.

For the univariate process M confidence limits can be constructed in a similar manner, by taking the square root of the estimate (2.3.6) of the auto-intensity function. Expression (2.3.20) then becomes :

$$\lim_{u\to\infty} (\hat{m}_{mm}(u))^{1/2} = (\hat{P}_m)^{1/2}, \qquad (2.3.22)$$

while the variance will be given approximately by $(4\ h\ M(T))^{-1}$,

giving an asymptotic distribution and 95% confidence limits of $(P_m)^{1/2} \pm (h\ M(T))^{-1/2}$.

2.3b Estimates of Frequency Domain Parameters

In the frequency domain the spectra can be estimated indirectly by taking the Fourier transform of the cumulant density functions (Bartlett, 1963; Brillinger, 1974a, b, 1975b, c, Brillinger et al, 1976; Rigas, 1983 ch's 3 and 4). For the univariate process M the autospectrum can be estimated by :

$$\hat{f}_{mm}(\lambda) = \hat{P}_m/2\pi + h/2\pi \sum_j \hat{q}_{mm}(u_j)\ K_T(u_j)\ e^{-i\lambda u}\ , \qquad (2.3.23)$$

where $u_j=hj$ $(j=\ldots,-2,-1,0,1,2,\ldots)$. $K_T(u_j)$ is a convergence factor or data window which improves the convergence properties of the Fourier transform (Brillinger, 1975a; Harris, 1978). Since $q_{mm}(-u) = q_{mm}(u)$ expression (2.3.23) can be re-written as :

$$\hat{f}_{mm}(\lambda) = 1/2\pi\ (\hat{P}_m + 2h \sum_{j=1}^{m} \hat{q}_{mm}(u_j)\ K_T(u_j)\ e^{-i\lambda u}\ ). \qquad (2.3.24)$$

For the bivariate case the cross-spectrum between processes N and M can be estimated as :

$$\hat{f}_{nm}(\lambda) = h/2\pi \sum_j \hat{q}_{nm}(u_j)\ K_T(u_j)\ e^{-i\lambda u}\ , \qquad (2.3.25)$$

where $u_j=hj$ $(j=\ldots,-2,-1,0,1,2,\ldots)$ and $K_T(u_j)$ is again a convergence factor.

Estimating the frequency domain parameters directly from the original data uses the periodogram of a point-process (Brillinger, 1972, 1974a, b; Rigas, 1983 ch's 3 and 4). The periodogram is based on the finite Fourier transform of the counting process, and for the process M can be estimated as :

$$d_M^{(T)}(\lambda) = \int_0^T e^{-i\lambda t}\, dM(t) = \sum_{t=0}^{T-1} e^{-i\lambda t}\, \{M(t+1)-M(t)\}, \qquad (2.3.26)$$

where the difference {M(t+1)-M(t)} has the value 1 if an event occurs in the interval (t,t+1], 0 otherwise, (t=0,...,T-1). In discrete form this is expressed as $d_M^{(T)}(\lambda_j)$, where $\lambda_j = 2\pi j/T$ (j=0,...,T/2). The frequency of the j^{th} ordinate in cycles per second will be $j/T\ T_s$, where T_s is the sampling interval used to convert the spike-train to a point-process, and T is the number of samples in the discrete Fourier transform. The periodogram is then given by :

$$I_{MM}^{(T)}(\lambda_j) = 1/2\pi T\ \ d_M^{(T)}(\lambda_j)\ \ \overline{d_M^{(T)}(\lambda_j)}. \qquad (2.3.27)$$

The periodogram requires further smoothing to obtain a more consistent estimate of the power spectrum. One effective method of smoothing the periodogram is to divide the whole record R into a number of disjoint sections each of length T (Bartlett, 1948) so that :

$$R = KT. \qquad (2.3.28)$$

The periodogram for each section can then be calculated, and an estimate of the autospectrum of the process M constructed as in (2.3.29).

$$\hat{f}_{mm}(\lambda_j) = 1/K \sum_{i=1}^{K} I_{MM}^{(Ti)}(\lambda_j), \qquad (2.3.29)$$

where $I_{MM}^{(Ti)}(\lambda_j)$ is the periodogram of the i^{th} disjoint section.

An estimate for the cross-spectrum between processes N and M can be constructed in a similar manner giving :

$$I_{NM}^{(T)}(\lambda_j) = 1/2\pi T\ \ d_N^{(T)}(\lambda_j)\ \ \overline{d_M^{(T)}(\lambda_j)}, \qquad (2.3.30)$$

and

$$\hat{f}_{nm}(\lambda_j) = 1/K \sum_{i=1}^{K} I_{NM}^{(Ti)}(\lambda_j), \qquad (2.3.31)$$

where $d_N^{(T)}(\lambda_j)$ is defined for the process N in a similar manner to (2.3.26).

From (2.2.23) the asymptotic distribution of the autospectrum is $P_m/2\pi$, and this can be estimated as $\hat{P}_m/2\pi$. The variance of the estimate (2.3.30) can be shown to be (Brillinger et al, 1976):

$$\text{Var}\{\ \hat{f}_{mm}(\lambda)\ \} = 1/K\ (f_{mm}(\lambda))^2. \qquad (2.3.32)$$

When dealing with conventional time-series it is usual to plot the logarithmic form of the spectral estimates. This also has the effect of simplifying expression (2.3.32) to give (Bloomfield, 1976, pp189-197):

$$\text{Var}\{\ \text{Ln}(\hat{f}_{mm}(\lambda))\ \} = 1/K. \qquad (2.3.33)$$

This allows 95% confidence intervals to be constructed by adding $\pm 1.96(K)^{-1/2}$ to the asymptotic distribution. Plots of $\text{Log}_{10}(\hat{f}_{mm}(\lambda))$ should therefore contain the the values : $\text{Log}_{10}(\hat{P}_m/2\pi) \pm 1.96(K)^{-1/2}\text{Log}_{10}(e)$. These limits will give the range of expected values of $\text{Log}_{10}(\hat{f}_{mm}(\lambda))$ if M is a Poisson process. Any deviation outside these limits at a particular frequency will indicate that the process is not Poisson at this frequency.

Unless stated otherwise, all spectral estimates will be calculated by the direct method based upon the estimates (2.3.29) and (2.3.31).

2.4 SYSTEM IDENTIFICATION: THE LINEAR POINT-PROCESS MODEL

For a time invariant system with input process M and output process N the essential feature of the identification procedure

is the conditional probability of the occurrence of an N spike in the interval dt given the times of occurrence of the input events (Brillinger, 1974a, 1975b). This can be expressed as :

$$\text{Prob}\{\ N \text{ point in } (t,t+dt] \mid M\ \} = E\{\ dN(t) \mid M\ \}, \qquad (2.4.1)$$

and the proposed model is given by :

$$\lim_{h\to 0} \text{Prob}\{\ N \text{ point in } (t,t+dt] \mid M\ \}/h = x_M(t). \qquad (2.4.2)$$

A series of models for $x_M(t)$ can then be constructed as follows (Brillinger, 1975b). If there is no input to the system then it is assumed that $x_M(t)$ is equal to a constant :

$$x_M(t) = s_o. \qquad (2.4.3)$$

The system is then said to be emitting points at a constant rate s_o. If the input M now consists of a single event at time t_1 then (2.4.3) can be written as :

$$x_M(t) = s_o + s_1(t-t_1), \qquad (2.4.4)$$

where the function $s_1(t)$ represents the effect on the output process N of a single M event at time t=0. Extending this to 2 input events at times t_1 and t_2 and neglecting any interactive effects (2.4.3) becomes :

$$x_M(t) = s_o + s_1(t-t_1) + s_1(t-t_2). \qquad (2.4.5)$$

Equation (2.4.5) can be written in a more general form to include all the events in the process M as :

$$x_M(t) = s_o + \int s_1(t-u)\ dM(u), \qquad (2.4.6)$$

where dM(u) are the differential increments of the process M

having the value 1 if an event occurs in the interval du, or 0 otherwise.

If the interactive effects between two input events are considered equation (2.4.3) is modified to :

$$x_M(t) = s_o + s_1(t-t_1) + s_1(t-t_2) + s_2(t-t_1,t-t_2), \quad (2.4.7)$$

where the function $s_2(u,v)$ gives the effect on the output process of the interaction between two separate events at times t=u and t=v. Generalising (2.4.7) to include all M events gives :

$$x_M(t) = s_o + \int s_1(t-u)\ dM(u) + \iint_{u\neq v} s_2(t-u,t-v)\ dM(u)\ dM(v). \quad (2.4.8)$$

This model may be expanded in a recursive manner to build up a functional series which includes interactive effects of several input spikes on the output point-process. The model has the form :

$$x_M(t) = s_o + \sum_{k=1}^{K} \int\cdots\int s_k(t-u_1,\ldots,t-u_k)\ dM(u_1)\ldots dM(u_k), \quad (2.4.9)$$

where $u_1,\ldots,u_k$ are all distinct. The function $s_k(t-u_1,\ldots,t-u_k)$ gives the interactive effects of k input events at times $u_1,\ldots,u_k$ on the output point-process. These functions are also referred to as kernels, the function s_k being the kernel of order k. This functional series can be considered as the point-process analogue of the Volterra expansion for Gaussian processes. When K=1 in (2.4.9) the model is given by equation (2.4.6), and this is known as the linear point-process model involving only the kernels of order zero and one. By analogy with ordinary time series $s_1(u)$ may be called the average impulse response of the system. In the point-process case it is defined as the best linear predictor of the average rate of change of the

instantaneous frequency of the output process at time u, given that an input event occurs at time t=0.

The significance of the contribution of each term in the summation to the model (2.4.9) can be determined by the use of coherence functions. Coherence functions are defined in the frequency domain and have a value which lies between 0 and 1, with zero occurring in the case of independence. For the linear model the linear coherence function is known as the coherence (Brillinger, 1975b; Brillinger et al, 1976) and is defined as :

$$\lim_{T\to\infty} \left| \mathrm{Corr}\{ d_N^{(T)}(\lambda), d_M^{(T)}(\lambda) \} \right|^2 = \left| R_{nm}(\lambda) \right|^2, \quad (2.4.10)$$

where $\left|R_{nm}(\lambda)\right|^2$ is the coherence and $d_N^{(T)}(\lambda)$ and $d_M^{(T)}(\lambda)$ are as defined in (2.2.24). Equation (2.4.10) can be re-written as :

$$\left| R_{nm}(\lambda) \right|^2 = \lim_{T\to\infty} \frac{\mathrm{Cov}\{ d_N^{(T)}(\lambda), d_M^{(T)}(\lambda) \}^2}{\mathrm{Var}\{ d_N^{(T)}(\lambda) \}\mathrm{Var}\{ d_M^{(T)}(\lambda) \}}$$

which gives :

$$\left|R_{nm}(\lambda)\right|^2 = \left|f_{nm}(\lambda)\right|^2 / f_{nn}(\lambda)\, f_{mm}(\lambda) \quad , \quad (2.4.11)$$

where $f_{nm}(\lambda)$ is the cross-spectrum, and $f_{nn}(\lambda)$ and $f_{mm}(\lambda)$ are the component autospectra for the processes N and M. The coherence will give a measure of the usefuleness of the linear model (2.4.6) by showing the strength of dependence of the output process N upon the input process M at a frequency λ. If the coherence is zero then the two processes are not linearly dependent and the linear model is not valid.

2.5 ESTIMATES OF THE LINEAR POINT-PROCESS MODEL PARAMETERS

Identification of a linear point process system requires the solution of the linear model (2.4.6) in terms of the previously

defined point-process parameters. The following four identities can all be derived (Brillinger, 1975b) from the relationship (2.4.6) :

$$P_n = s_o + \int s_1(u)\ du, \qquad (2.5.1)$$

$$P_{nm}(t) = s_o\ P_m + s_1(t)\ P_m + \int s_1(t-u)\ P_{mm}(u)\ du, \qquad (2.5.2)$$

$$q_{nm}(t) = s_1(t)\ P_m + \int s_1(t-u)\ q_{mm}(u)\ du, \qquad (2.5.3)$$

$$f_{nm}(\lambda) = S_1(\lambda)\ f_{mm}(\lambda). \qquad (2.5.4)$$

Equations (2.5.1), (2.5.2) and (2.5.3) are derived in Brillinger (1975b) and Rigas (1983, App.III). Equation (2.5.4) follows directly from equation (2.5.3) and the definition of $f_{nm}(\lambda)$ in (2.2.21). The two quantities $s_1(t)$ and $S_1(\lambda)$ form a Fourier transform pair and by analogy with ordinary time series $S_1(\lambda)$ may be thought of as the transfer function of a linear point-process system, and will have gain and phase components associated with it.

Relation (2.5.4) suggests the estimate :

$$\hat{S}_1(\lambda) = \hat{f}_{nm}(\lambda)/\hat{f}_{mm}(\lambda), \qquad (2.5.5)$$

where $\hat{f}_{nm}(\lambda)$ and $\hat{f}_{mm}(\lambda)$ are estimates of the cross-spectrum and auto spectrum given in section 2.3. An estimate of s_o can be constructed from (2.5.1) giving :

$$\hat{s}_o = \hat{P}_n - \hat{P}_m\ \hat{S}_1(0). \qquad (2.5.6)$$

In practice a zero-mean sequence is used in the F.F.T. to calculate the periodogram, this improves convergence properties and reduces leakage, therefore :

$$\hat{s}_o = \hat{P}_n. \qquad (2.5.7)$$

In the time domain the first kernel can be estimated as :

$$\hat{s}_1(t) = \int_{-\infty}^{\infty} \hat{s}_1(\lambda)\ e^{\ i\lambda t}\ dt, \qquad (2.5.8)$$

or by noting that if the input is a Poisson process with independent increments then $q_{mm}(u)$ equates to zero and equation (2.5.3) gives :

$$\hat{s}_1(t) = \hat{q}_{nm}(t)/\hat{P}_m. \qquad (2.5.9)$$

However this is only valid if the system is probed with a Poisson point-process.

The coherence can be estimated by :

$$\left|R_{nm}(\lambda)\right|^2 = \left|\hat{f}_{nm}(\lambda)\right|^2 / \hat{f}_{nn}(\lambda)\ \hat{f}_{mm}(\lambda) \quad . \qquad (2.5.10)$$

This follows directly from (2.4.11) and will indicate the range of frequencies over which the estimates for the linear model parameters are valid. A confidence interval can be constructed for this estimate, and is based upon the null hypothesis that the coherence is zero if the two processes are not linearly dependent. This requires the computation of the 100α per cent point of $\left|R_{nm}(\lambda)\right|^2$ (Brillinger et al, 1976; Rigas, 1983, pp195-197). This is given by :

$$1-(1-\alpha)^{1/(z-1)}, \qquad (2.5.11)$$

where z is determined by :

$$z = R/\int K_T(u)^2\ du, \qquad (2.5.12)$$

R is the total record length and $K_T(u)$ is the convergence factor used to smooth the spectral estimates (see section 2.3). If the

cross-spectral and autospectral estimates are formed by averaging the periodograms of disjoint sections, then (2.5.12) simplifies to :

$$z = R/T = 1/K, \tag{2.5.13}$$

according to (2.3.28). To estimate the 95% point of the distribution α=0.95 and (2.5.11) becomes :

$$1-(0.05)^{1/(z-1)}. \tag{2.5.14}$$

This level will show the 95% confidence limit assuming the two processes M and N are not linearly dependent. Coherence values less than this level will indicate the non-validity of the linear model (2.4.6) for these two point-processes.

2.6 EXAMPLES OF ESTIMATES OF UNIVARIATE POINT-PROCESS PARAMETERS

If a situation arises where access to both input and output processes is not available, then system identification using bivariate point-process parameters is not possible. However, if the output process is accessible then univariate point-process parameters can be used to characterize changes in this process which may result from the application of any inputs to the system. Analysing typical primary discharge patterns for a number of different input conditions can be used to provide a quantitative description of the information content of the primary discharge.

In the case of the muscle spindle the primary discharge is relatively constant under conditions of fixed length with no fusimotor activity. Any imposed length change or the initiation of fusimotor activity, or a combination of both, alters the nature of this discharge in a characteristic way. Using time and

frequency domain univariate point-process parameters to characterize this change will allow a comparison of these two approaches to be made. In particular estimates of the auto-intensity function and auto spectrum will be used here to try and describe the variety of discharge patterns that occur in the primary sensory axon.

The primary discharge that occurs at fixed length with no fusimotor activity is termed the spontaneous discharge. Figure 2.6.1 shows estimates of the square root of the auto-intensity and the logarithmic transform of the auto spectrum of a typical spontaneous Ia discharge. The auto-intensity uses the estimate given in (2.3.6), with a record length of 15872. The auto spectrum uses the estimate (2.3.29), with T=256. For this data set M(R)=416, R=15872 and $\hat{P}_m$=0.0262, giving a mean interspike interval of 38.2 msec., with a fundamental frequency of 26.2 cycles/sec.. The equi-spaced peaks in the estimate $(\hat{m}_{mm}(u))^{1/2}$ indicate the regularity of the discharge with the spacing between the peaks in figure 2.6.1a being equal to the mean interspike interval. The amplitude of these peaks decrease at higher values of lag indicating the ephemeral nature of the correlating influences as defined by the mixing condition, and at higher lag values the estimate tends towards the asymptotic distribution of $(\hat{P}_m)^{1/2}$, (=0.16). The logarithm of the auto spectrum in figure 2.6.1b also illustrates the regularity of the discharge and has peaks which occur at multiples of the fundamental frequency of the mean rate of the discharge. These peaks also decrease in magnitude and tend to the asymptotic distribution of $Log_{10}(\hat{P}_m/2\Lambda)$, (=-2.38dB), this again is due to the mixing condition. The time and frequency domain descriptions provide essentially similar information about the regularity of the

discharge, as shown by the equispaced peaks in the two estimates. The range of lag values or frequency values over which these peaks extend give an indication of the exactness of the periodicity. An exact periodicity will be correlated to the same degree over all the increments of the process and will result in equispaced peaks of equal magnitude in both auto-intensity and auto spectral estimates.

If this analysis is extended to typical Ia discharge patterns for a number of different input conditions, the frequency domain approach would appear to yield more information about the effects of these inputs on the primary response. Three input conditions are considered here, a random gamma-static input with fixed muscle length, a random length applied to the parent muscle in the absence of any fusimotor activity and both length and fusimotor stimulation applied simultaneously. Figure 2.6.2 illustrates the estimates of $(m_{mm}(u))^{1/2}$ for these three conditions, while fiqure 2.6.3 shows the corresponding estimates of the logarithm of the autospectrum. A static fusimotor input appears to override the regularity of the discharge observed at fixed length , this is indicated by the loss in regularity of the auto-intensitv estimate. Apart from this loss in regularity the three auto-intensity estimates only change slightly with changes to the imposed inputs on the spindle and do not provide any further insight into the nature of the changes in the primary response to these inputs.

Examination of the auto spectral estimates reveals significant differences in the nature of the primary response resulting from these input conditions. The loss of regularity due to the fusimotor input is also shown by the autospectrum estimate

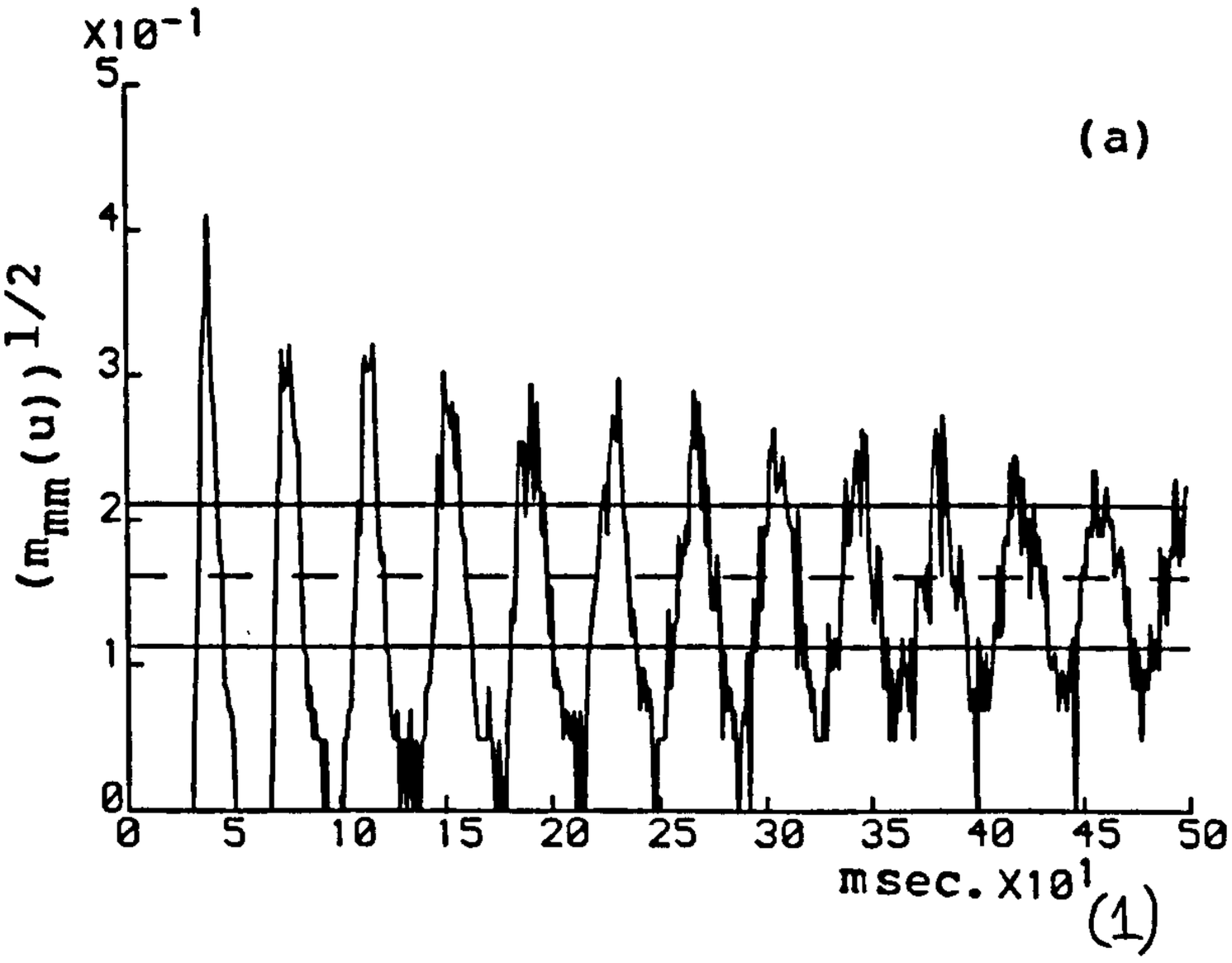

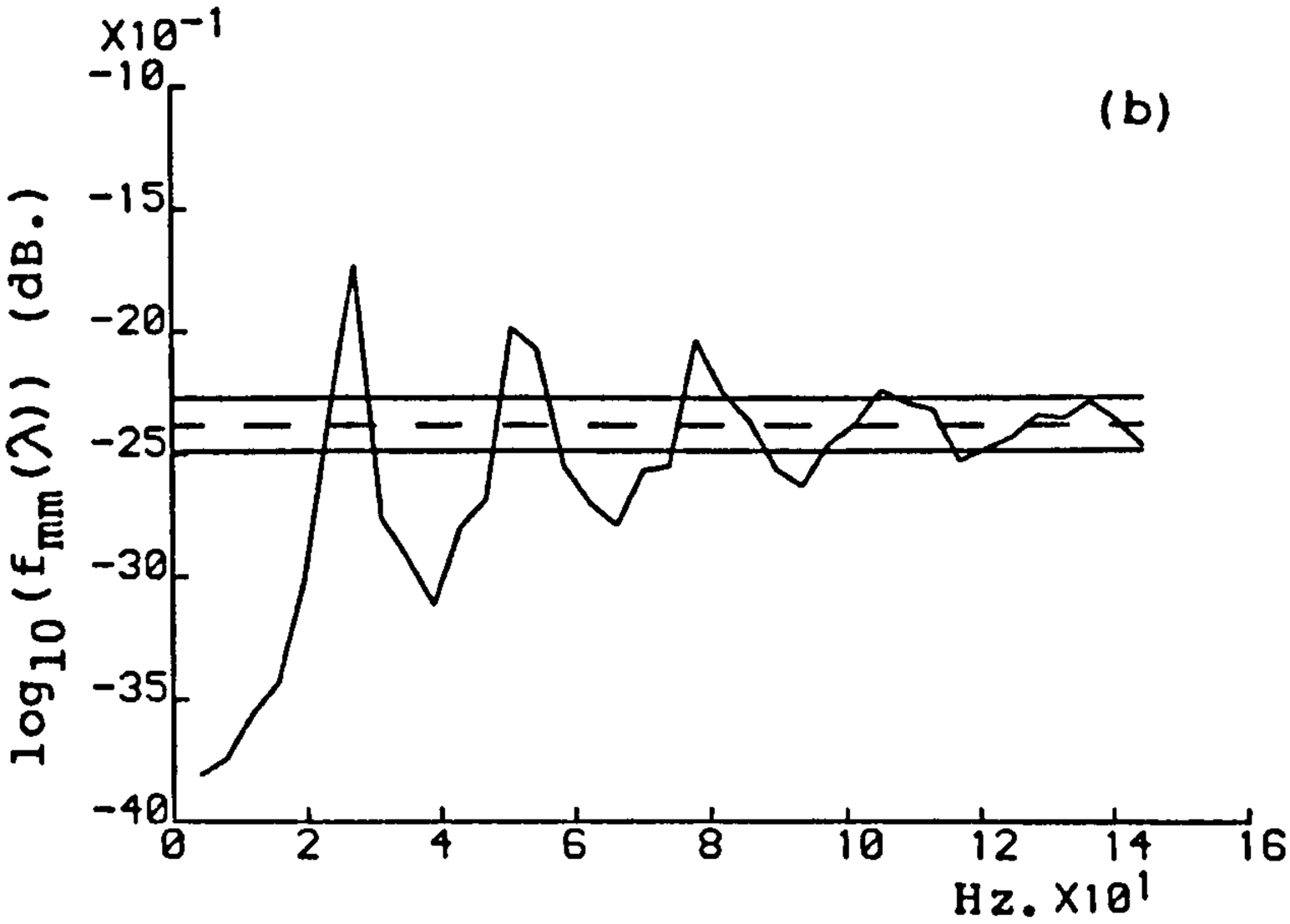

Fig. 2.6.1 (a) Square root of estimate of auto-intensity function (2.3.6) for a spontaneous primary discharge.

(b) Log_{10} of estimate of auto spectrum (2.3.29) of spontaneous discharge. R=15872, T=256 and M(R)=416.

Dashed lines represent estimates of asymptotic distributions, and solid lines indicate the approximate 95% confidence limits.

(1) To obtain correct scaling on Horizontal scale of this and all subsequent graphs labelled x10¹, all values should be multiplied by 10.

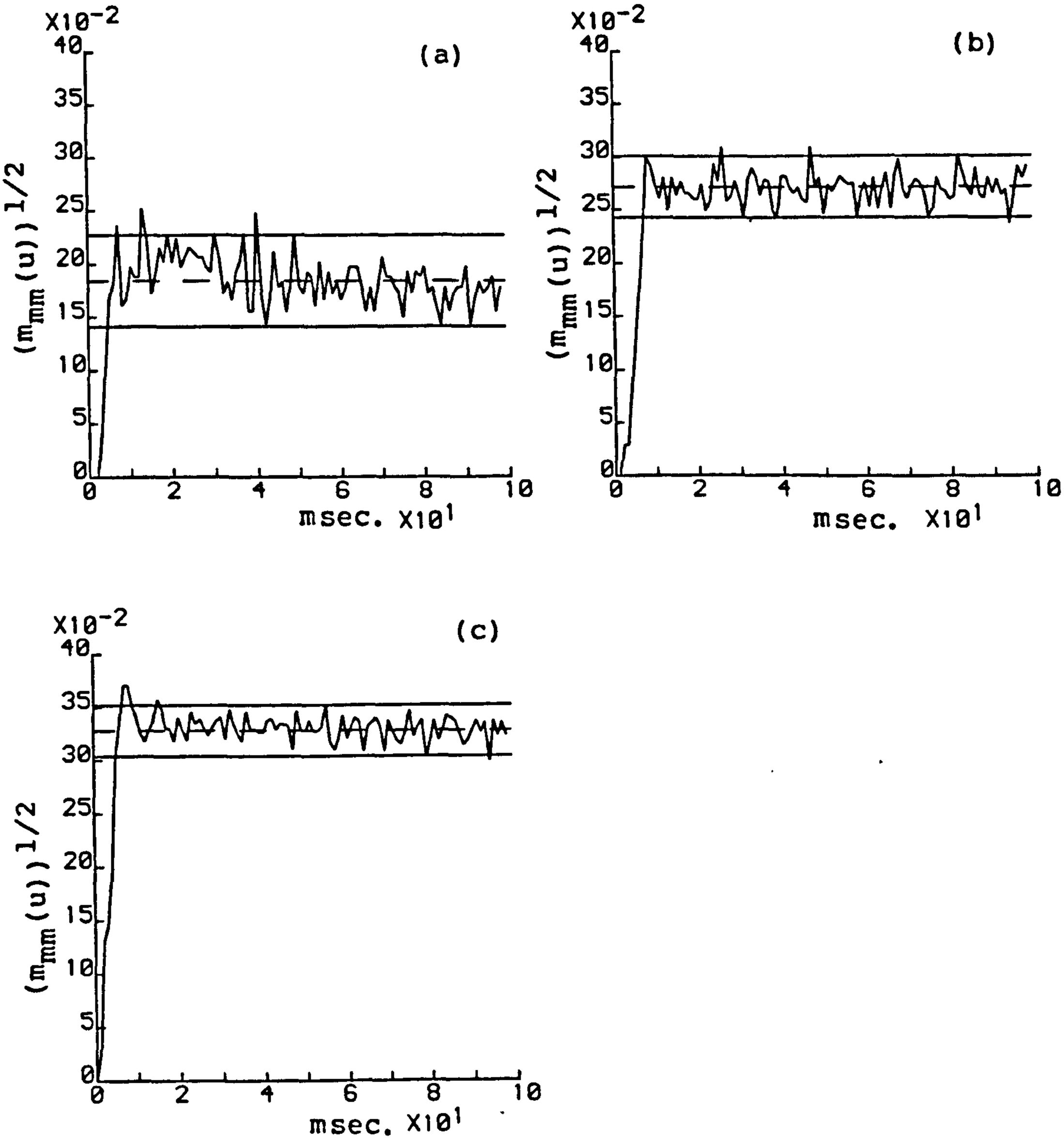

Fig. 2.6.2 Square root of estimate of auto-intensity function (2.3.6) for :

(a) Random static fusimotor input,

(b) Random length change and

(c) Combination of both inputs.

Dashed lines represent estimates of asymptotic distributions, and solid lines indicate approximate 95% confidence limits.

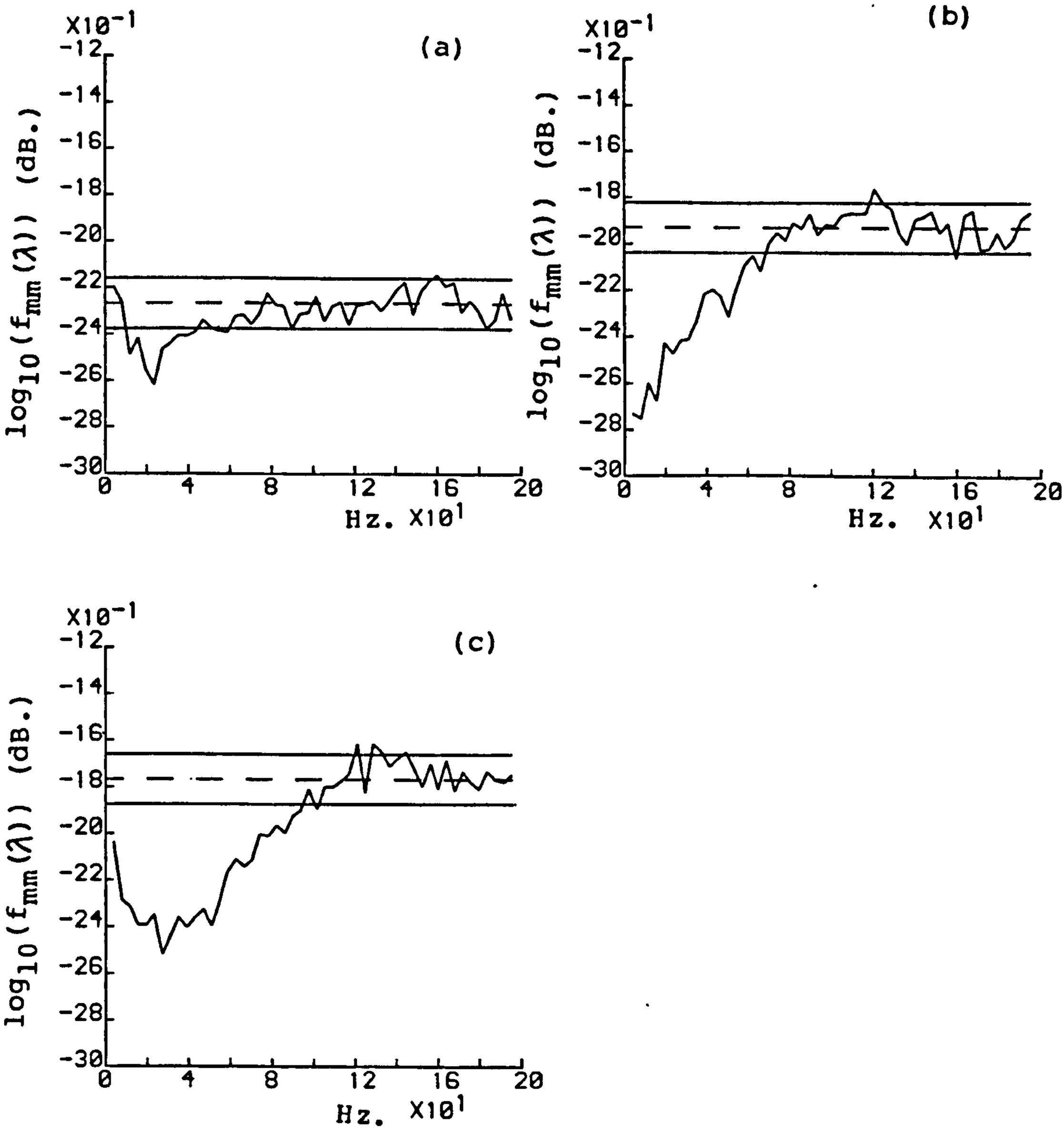

Fig. 2.6.3 Log_{10} of estimate of auto spectrum (2.3.29) with T=256 for :

(a) Random static fusimotor input,

(b) Random length change and

(c) Combination of both inputs.

Dashed lines represent estimates of asymptotic distributions, and solid lines indicate approximate 95% confidence limits

in figure 2.6.3a losing its periodic appearance. Also evident from figures 2.6.3a and 2.6.3b is that a length input on its own reduces the spectral power of the primary signal over a much wider range of frequencies than a static fusimotor input on its own. The effects of the fusimotor input are concentrated in a band from 5 to 50 Hz., whereas the length input can modify the frequency content of the Ia signal up to about 70 Hz..

The interaction between the two inputs affects the Ia discharge over the widest range of frequencies and has a region concentrated between 5 and 50 Hz. where a maximal reduction in frequency content of the Ia occurs, with an overall reduction in spectral power occurring up to about 100 Hz.. The differences in the nature of the signal reaching the central nervous system through the primarv sensory neurone indicate that the spindle transmits different information to the spinal cord in response to the different input conditions imposed on it.

These differences can only be extracted from the estimates of the auto spectrum for the various input conditions, the auto-intensity function does not seem to provide as much useful information about these data sets. This would seem to recommend the use of the auto spectrum for the analysis of physiological problems involving univariate point-process data.

2.7 EXAMPLES OF BIVARIATE AND LINEAR-MODEL PARAMETERS

Treating a muscle spindle subsystem consisting of a single fusimotor input and the primary output, at fixed muscle length, as a realisation of a point-process system, allows the estimates of the bivariate point-process parameters defined in section 2.3 to be constructed. Using these the parameters of the linear

point-process model can be estimated and used to try and characterize the system. As in the univariate case both time and frequency domain parameters will be estimated, and a comparison of the two approaches made.

Figure 2.7.1a shows an estimate of $(m_{nm}(u))^{1/2}$ for a typical bivariate process, constructed using the estimate (2.3.11). To obtain the data set a Possion spike-train was applied to a fusimotor input and the primary discharge recorded. A Geiger counter and weak radioactive source was used to provide the stimulus spike-train, which ensured a Poisson distribution of intervals. Considering the cross-intensity estimate in terms of the probabilistic interpretation given in (2.2.13) shows that after each input event there is a delay of approximately 13 msec. after which there is a rapid rise in the probability of occurrence of an output spike. This increased probability tails off and merges in with the asymptotic distribution. The deviation of this estimate outside the confidence band indicates a dependence of the primarv response upon the fusimotor input. The delay is due to the conduction delay that the impulses require to propagate down the axons plus an additional delay for the effects of the fusimotor impulses to propagate through the spindle.

Estimates of the gain and phase of the cross-spectrum are shown in figure's 2.7.1b and 2.7.1c. The phase is plotted in unrestrained form (Chatfield, 1980, p181), to show the delay between the two processes. The cross-spectrum gives a measure of the dependence of the output process N upon the input process M at a frequency λ. The magnitude plot shows that this dependence is at a maximum at low frequencies and decreases as λ increases. This is consistent with the characteristics of a low pass filter.

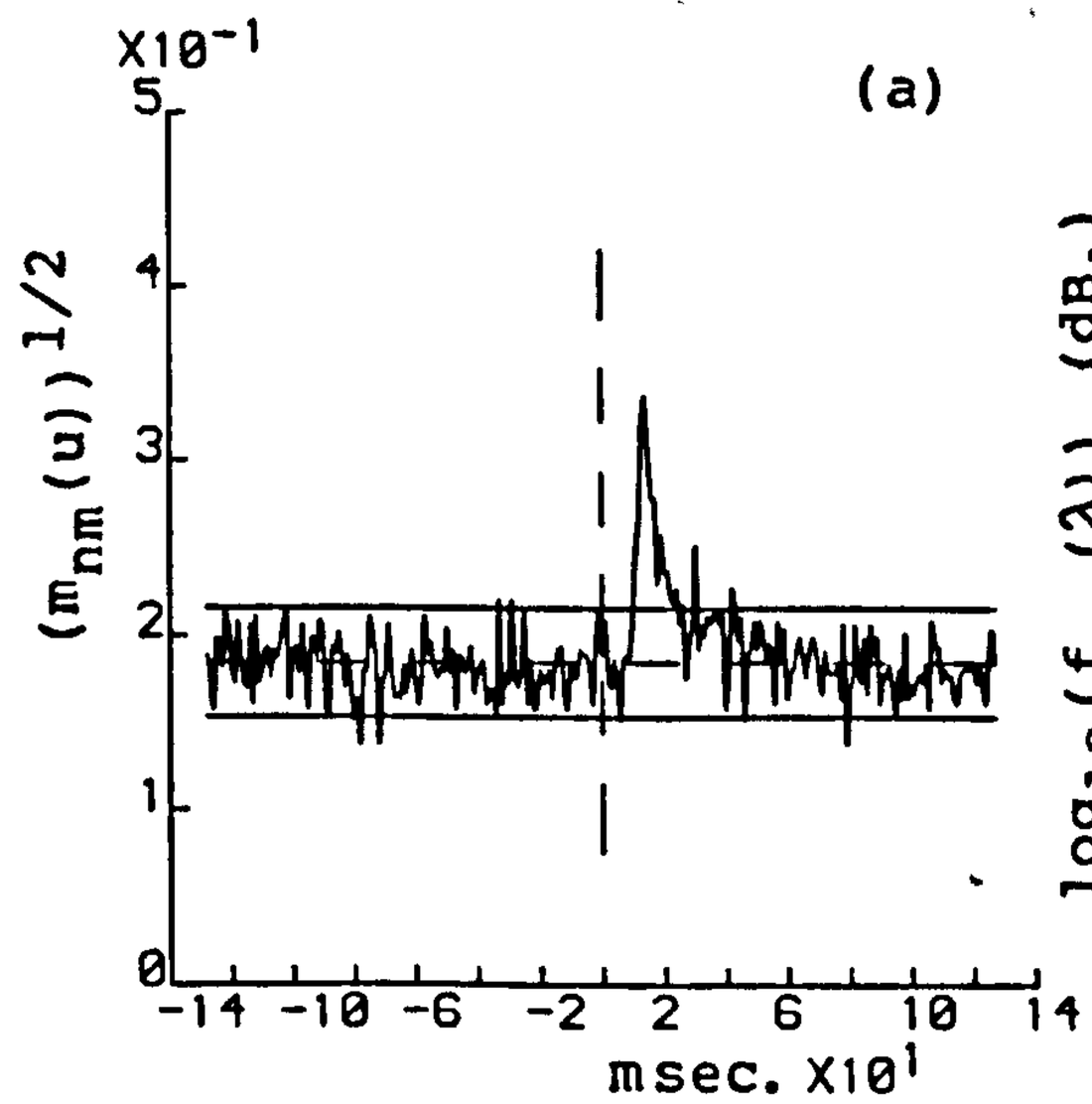

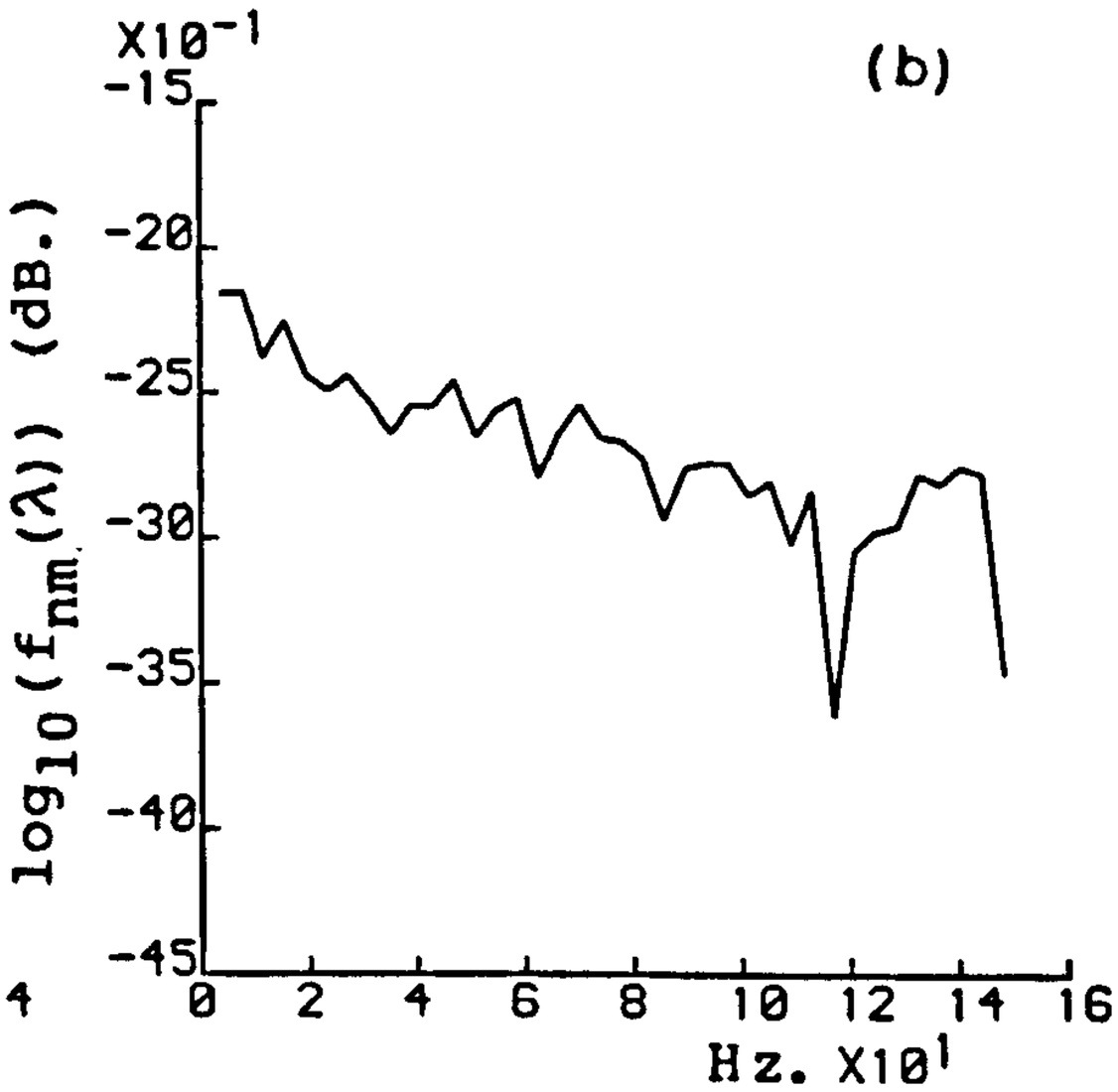

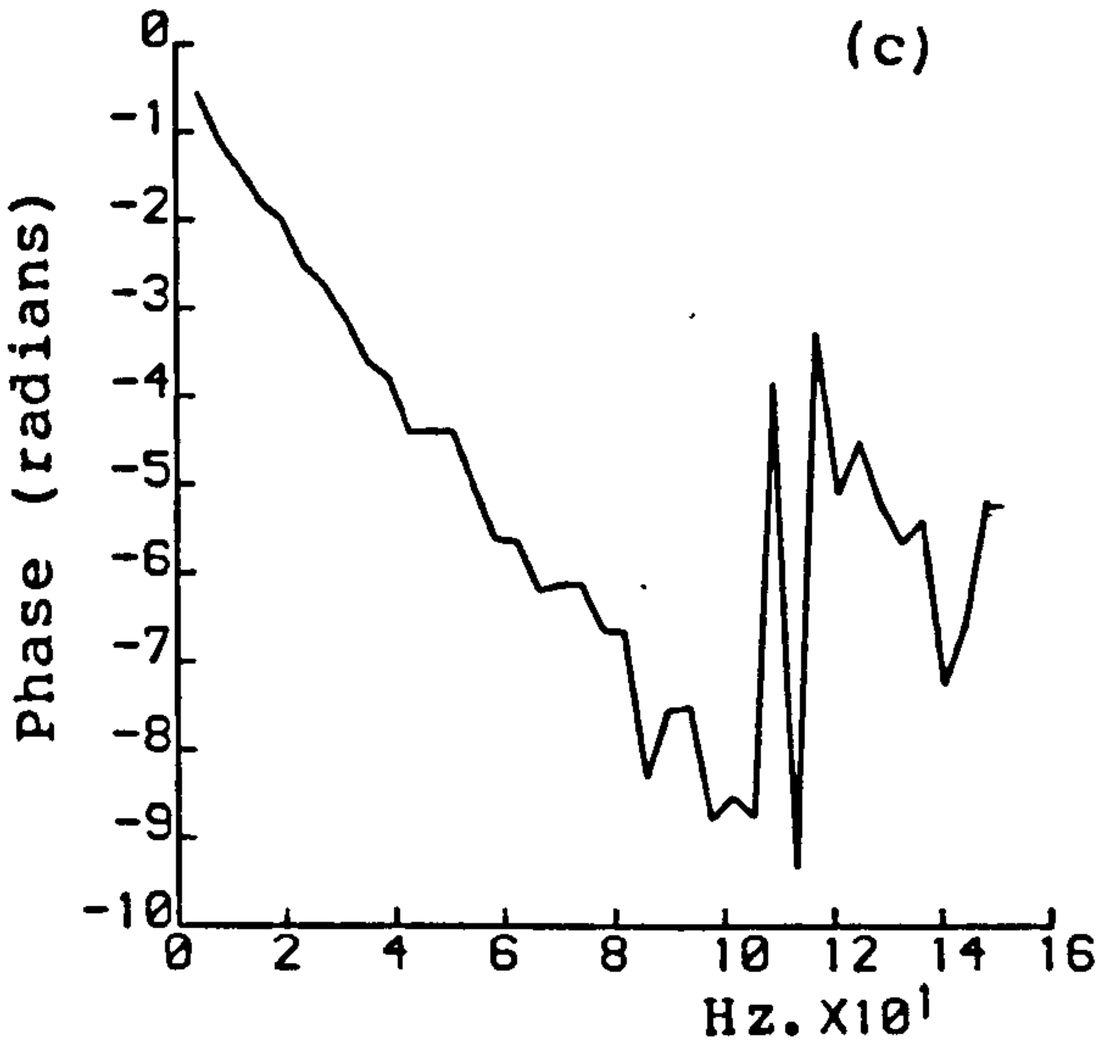

Fig. 2.7.1 (a) Square root of estimate of cross-intensity function (2.3.11),

(b) Magnitude of $\log_{10}$ of estimate of cross-spectrum (2.3.31), with T=256 and

(c) Phase of estimate of cross-spectrum for static fusimotor input and primary discharge at fixed muscle length.

R=15872, M(R)=1010 and N(R)=538.

The phase can be considered as a straight line with a constant slope. This indicates a delay between the harmonics of the two processes M and N, this delay being equal to the slope of the line. The delay at each frequency can be estimated by the expression $\phi(\lambda)/\lambda$, giving an estimate of 11 msec.. This is in agreement with the value obtained from the cross-intensity function.

Estimates of the linear model parameters can now be constructed. In the frequency domain $S_1(\lambda)$ can be estimated according to equation (2.5.5). This will have gain and phase components and since $f_{mm}(\lambda)$ is a real quantity the phase of $S_1(\lambda)$ will be the same as of $\hat{f}_{nm}(\lambda)$ as shown in figure 2.7.1c. Figure 2.7.2a shows an estimate of $20\text{Log}_{10}\left|(S_1(\lambda))\right|$ and figure 2.7.2c shows an estimate of the coherence for this data set calculated from equation (2.5.10). Since the estimation of $S_1(\lambda)$ is concerned with system parameter estimation and not the detection of single frequencies, further smoothing was done in the frequency domain using Hanning (Harris, 1978). This was found to facilitate the fitting of theoretical curves to the estimate $\hat{S}_1(\lambda)$. The form of the coherence suggests that the magnitude and phase of $S_1(\lambda)$ are significant up to about 60 cycles/second. This indicates that the primary discharge is linearly dependent upon the fusimotor input up to moderately high frequencies. This broad range of dependence also illustrates the validity of the linear point-process model for this spindle system. Within this frequency range the gain of the transfer function estimate is consistent with the frequency response of a first order lag with a time constant of 9.5 msec.. The dashed line in figure 2.7.2a shows the theoretical gain curve for such a transfer function. The delay estimated from the cross-intensity and phase can also

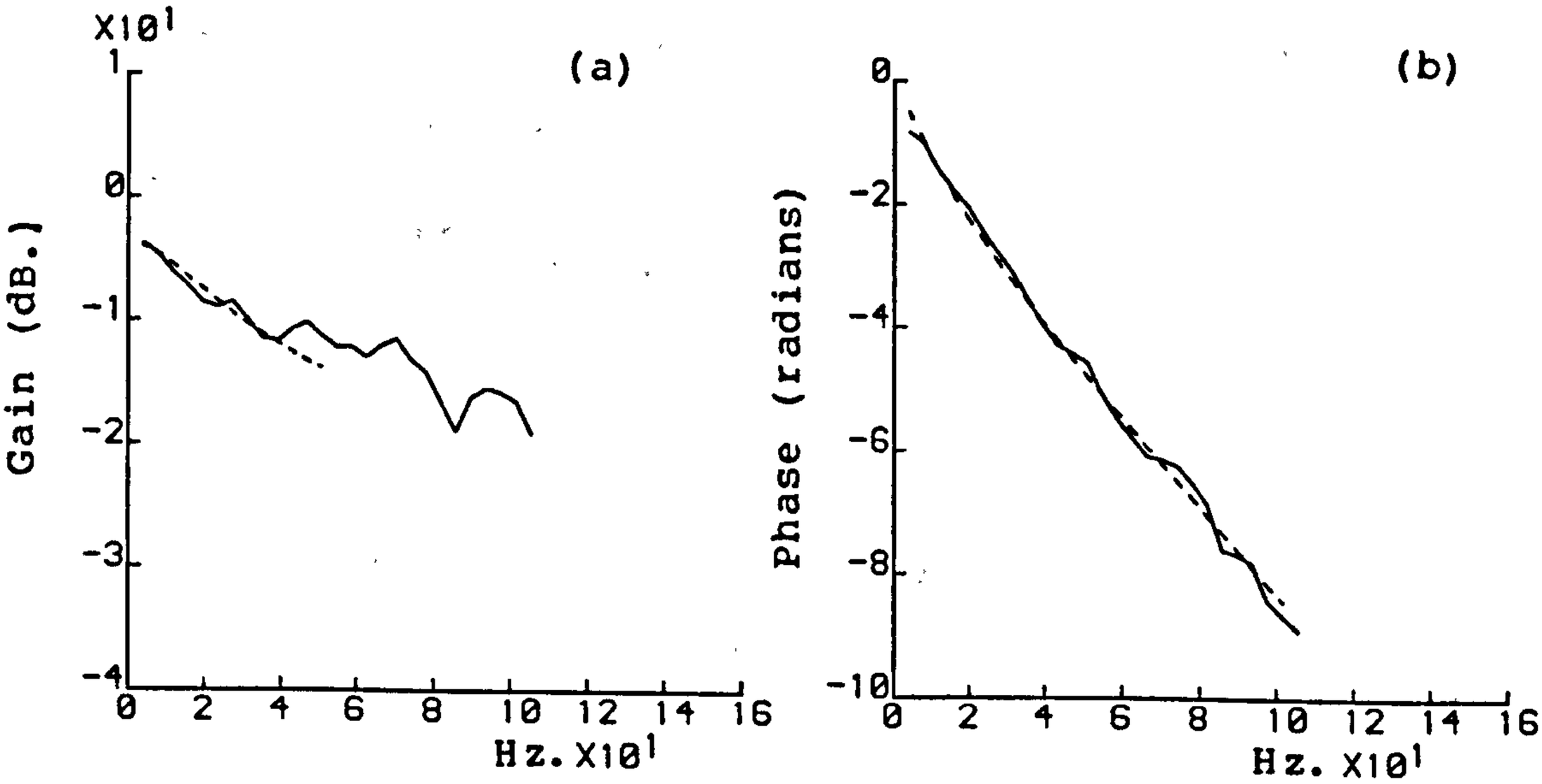

Fig. 2.7.2 (a) Gain and

(b) Phase of estimate of $S_1(\lambda)$ (2.5.5), dashed lines show theoretical response (2.7.1) for K=0.65, τ =9.5msec. and a delay of llmsec., and

(c) Coherence estimate, dashed line shows approximate 95% confidence limit.

be incorporated into this transfer function resulting in an expression of the form :

$$S_1(\lambda) = K\, e^{-\lambda\sigma} / (1+\lambda\tau), \qquad (2.7.1)$$

with K=0.65, τ =9.5msec., and a delay of σ=11msec., providing one possible solution which fits (2.7.1) to the estimate of $S_1(\lambda)$. Since the break point is not clearly visible, and the phase estimate is dominated by the delay, then an exact estimation of the time constant is not possible. However it can be deduced that a time constant of the order of 10 msec. in (2.7.1) can accurately model the estimate of the transfer function $S_1(\lambda)$ for this data set. This agrees with the findings of the previous studies of Rosenberg et al (1982) using this method, and Andersson et al (1968). The approach used by Andersson et al involved sinusoidal modulation of a fusimotor input for each frequency required in the transfer function. This new approach is much less time consuming and results can be obtained from a single experiment.

In the time domain s_o can be obtained from equation (2.5.7), giving $\hat{s}_o$=0.034, which equates to the mean rate of the output process N. The impulse response can be estimated by taking the inverse Fourier transform of the transfer function $S_1(\lambda)$. Since the fusimotor input is Poisson then equation (2.5.9) can be used to estimate $s_1(t)$ directly. This assumption can be justified by examining the estimate of the auto spectrum of the input shown in figure 2.7.3a. At no point does the estimate deviate outside the confidence band indicating no dependence of one differential increment upon another i.e. a Poisson point-process. If the input process is not Poisson then $s_1(t)$ must be estimated via the

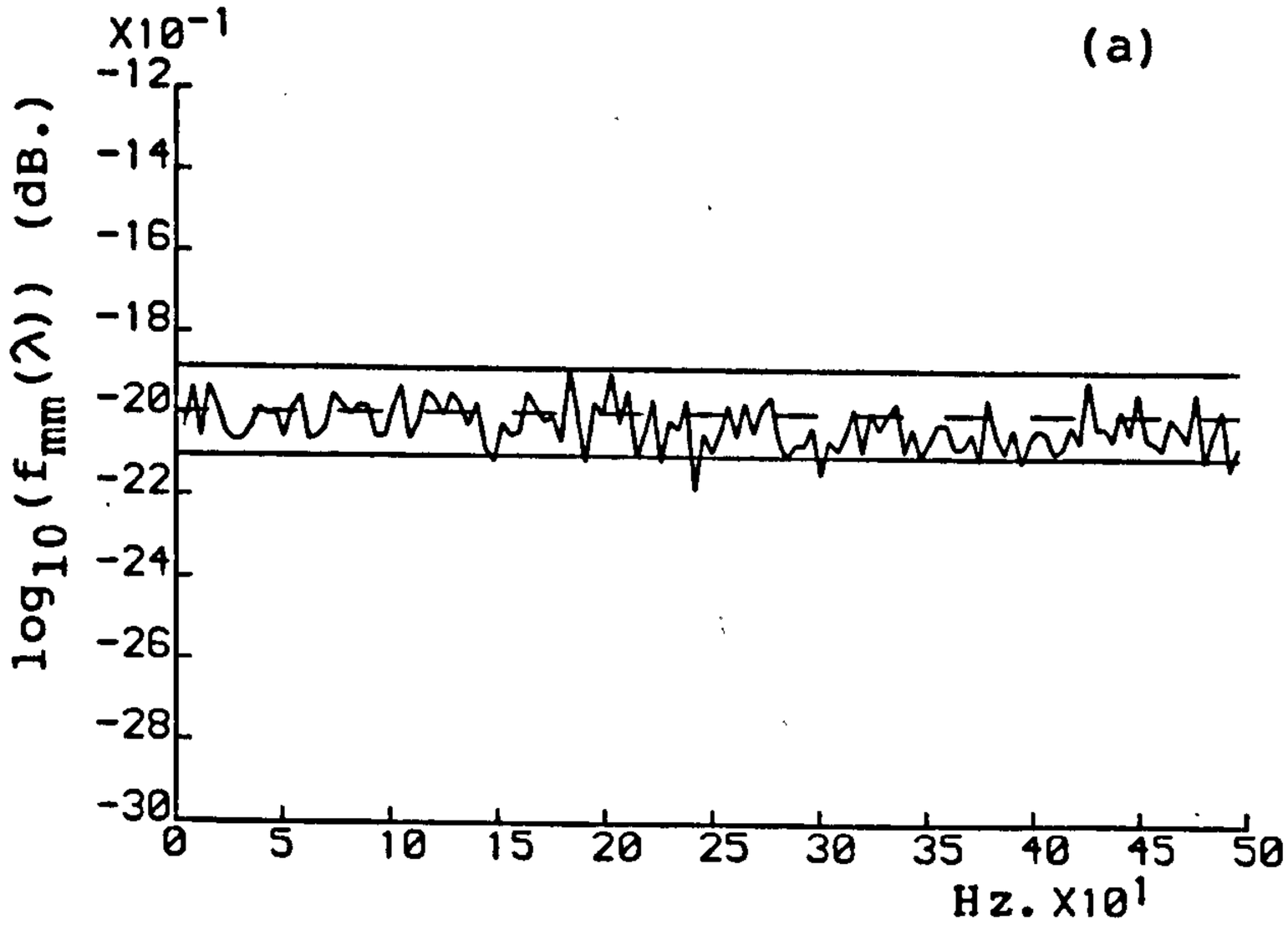

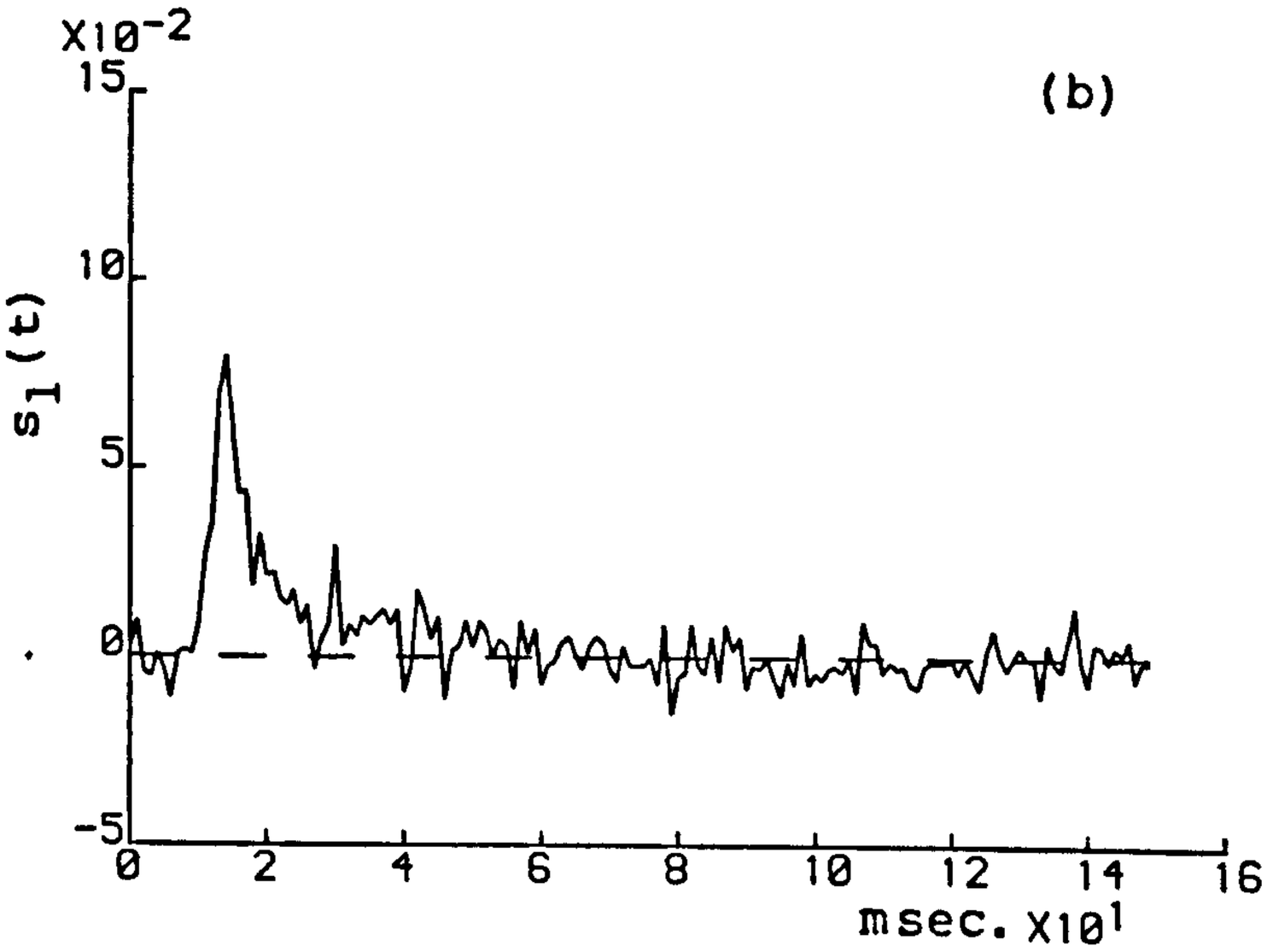

Fig. 2.7.3 (a) Log_{10} of estimate of auto spectrum (2.3.29) with asymptotic distribution and 95% confidence limits, and (b) Estimate of first kernel, $s_1(t)$, (2.5.9) for static fusimotor input and primary discharge at fixed muscle length.

frequency domain using (2.5.8), since an estimate of the cross-covariance density will contain a term which convolves the impulse response with the input auto-covariance density. Figure 2.7.3b shows the estimate of the impulse response for this data set. This impulse response also reflects the exponential form expected of a first order lag.

The results in figures 2.7.2 and 2.7.3 indicate a similarity between the Fourier transform pair formed by $S_1(\lambda)$ and $s_1(t)$ of the linear point-process model and the transfer function and average impulse response of a conventional time-series. The relations between ordinary time-series and point-processes have been discussed in detail by Brillinger (1974b, 1978). Also apparent from figures 2.7.1a and 2.7.3b is the similarity between the cross-intensity function and the function $s_1(t)$. For this example the cross-intensity function consists of the sum of the two kernels in the linear model (2.4.6). This can be proved using equations (2.3.12), (2.5.7) and (2.5.9). This only applies for a Poisson input process as explained above.

Although the probabilistic interpretation which can be applied to the cross-intensity function is a useful aid in the interpretation of this estimate, it does not give an exact indication of the strength of any dependence. The coherence, however, provides an absolute measure of the degree of linear dependence on a scale from 0 to 1. The cross-intensitv function gives an indication of the average delay between input and output events, whereas the phase can estimate the delay at each frequency. As in the univariate case the frequency domain approach appears more useful in the identification of the linear bivariate point-process system.

2.8 SIMULATION OF A FUSIMOTOR SUBSYSTEM

Based on the solution of the linear model in equation (2.7.1), an analogue computer simulation of a single fusimotor subsytem was developed. A first order lag without the time delay, similar to that qiven in (2.7.1), is used to simulate the mechanical properties of the intrafusal fibres. Since the time delay in (2.7.1) is likely to be dominated by the conduction delays of the fusimotor and Ia pulses, it may be disregarded when considerinq the mechanical properties of the intrafusal fibres. The output of this section of the simulation represents the strain at the receptor nerve endinqs. An encoder then converts this continuous signal into a spike-train representing the primary disharge. In the simulation the spikes are represented by rectangular pulses lmsec. wide. A simplified block diagram of the simulation is shown in figure 2.8.1. A constant bias is added at the input to the encoder to simulate the effect of fixed muscle lenqth. The effect of changing muscle length can be simulated by altering this bias.

The type of encoder used is of the sigma pulse-frequency modulator type first suqqested by Meyer (1961) and Pavlidis and Jury (1965). Pulse frequency modulators must observe the input signal for a finite time before a pulse can be emitted. Integral pulse frequency modulation is the simplest method of doing this, and integrates the input signal, emitting a pulse when this integral exceeds a fixed threshold level. The output of the integrator is then reset to its resting value and the process repeated. The more general case of sigma pulse frequency modulation involves feeding the input to the encoder through a low-pass filter and deciding on the emission of a pulse when the output of this filter reaches the threshold level. The filter

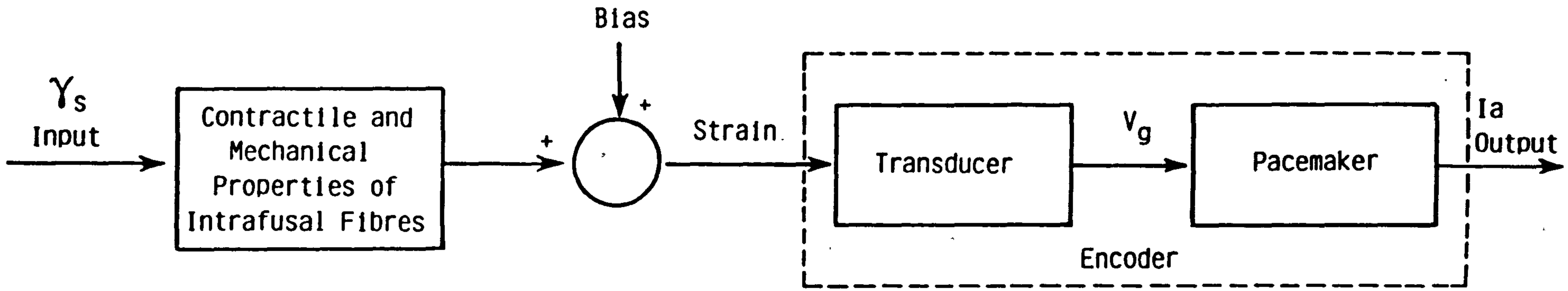

Fig. 2.8.1 Block diagram of simulation of a fusimotor subsystem.

output is similarily reset to its resting value as in integral pulse frequency modulation.

Integral pulse frequency modulation can be described by the two equations :

$$dp/dt = x - r.\delta(|p|-r), \qquad (2.8.1)$$

and

$$y = \delta(|p|-r), \qquad (2.8.2)$$

where x is the input to the modulator, y is the output, r is the threshold value and p is the instantaneous value of the integral. The delta function $\delta(|p|-r)=1$ if $|p| = r$, 0 otherwise. This term represents the resetting of the integrator in (2.8.1), and the generation of an output spike in (2.8.2). Equation (2.8.1) can be extended for the more general case of sigma pulse frequency modulation to give :

$$dp/dt + g(p) = x - r\,\delta(|p|-r), \qquad (2.8.3)$$

where g(p) gives the function of the integrator output which is fed back to the input. In this simulation a linear first order filter is used, this has been found to give better agreement between simulated and physiological results in previous simulation studies (Angers and Delilse, 1971; Downie and Murray-Smith, 1981). For a linear first order filter then g(p)=cp, with $c \propto 1/t_m$, where t_m is the time constant in the filter, and (2.8.3) can be written as :

$$dp/dt = (G/t_m)x - r\,\delta(|p|-r) - (1/t_m)p, \qquad (2.8.4)$$

where G is the gain in the filter. In this encoder a time constant of 50msec. was chosen as being representitive of a

primary encoder (Angers and Delilse, 1971; Kroin, 1974).

2.9 SIMULATION RESULTS AND COMPARISON WITH EXPERIMENTAL RESULTS

Values of time constant ranging from 5 to 50 msec. were tried in the linear sub-system, with the gain in this sub-system set equal to 1. The gain in the encoder was adjusted to give a ratio of input to output spikes roughly equal to 1, this being similar to the ratio obtained in spindle experiments using the same random fusimotor stimulation. The simulation was run in real time and the input and output spike-trains recorded on an F.M. recorder and digitised in the same manner as experimental data. Fifteen second runs were generated to allow a comparison with experimental results to be made.

Figure 2.9.1 shows estimates of the magnitude of $\hat{S}_1(\lambda)$ for three values of time constant, 5, 10, and 20 msec., in the linear subsystem, while figure 2.9.2 shows the corresponding phase estimates. The dashed line in each of the gain and phase plots shows the theoretical response for the transfer function (2.7.1), without the delay, with γ set equal to 5, 10 and 20 msec. in agreement with the simulation, and values of K of 0.90, 0.92, and 0.93 respectively. These theoretical responses are graphed over the range of frequencies for which the linear model is valid, as given by the coherence estimate for each example, these are shown in figure 2.9.3.

The results in figures 2.9.1 and 2.9.2 illustrate that, even although the output of the linear sub-system undergoes an inherently non-linear operation to generate the output spike-train, the estimate of $S_1(\lambda)$ still reflects accurately the properties of this linear sub-system. The coherence estimates in

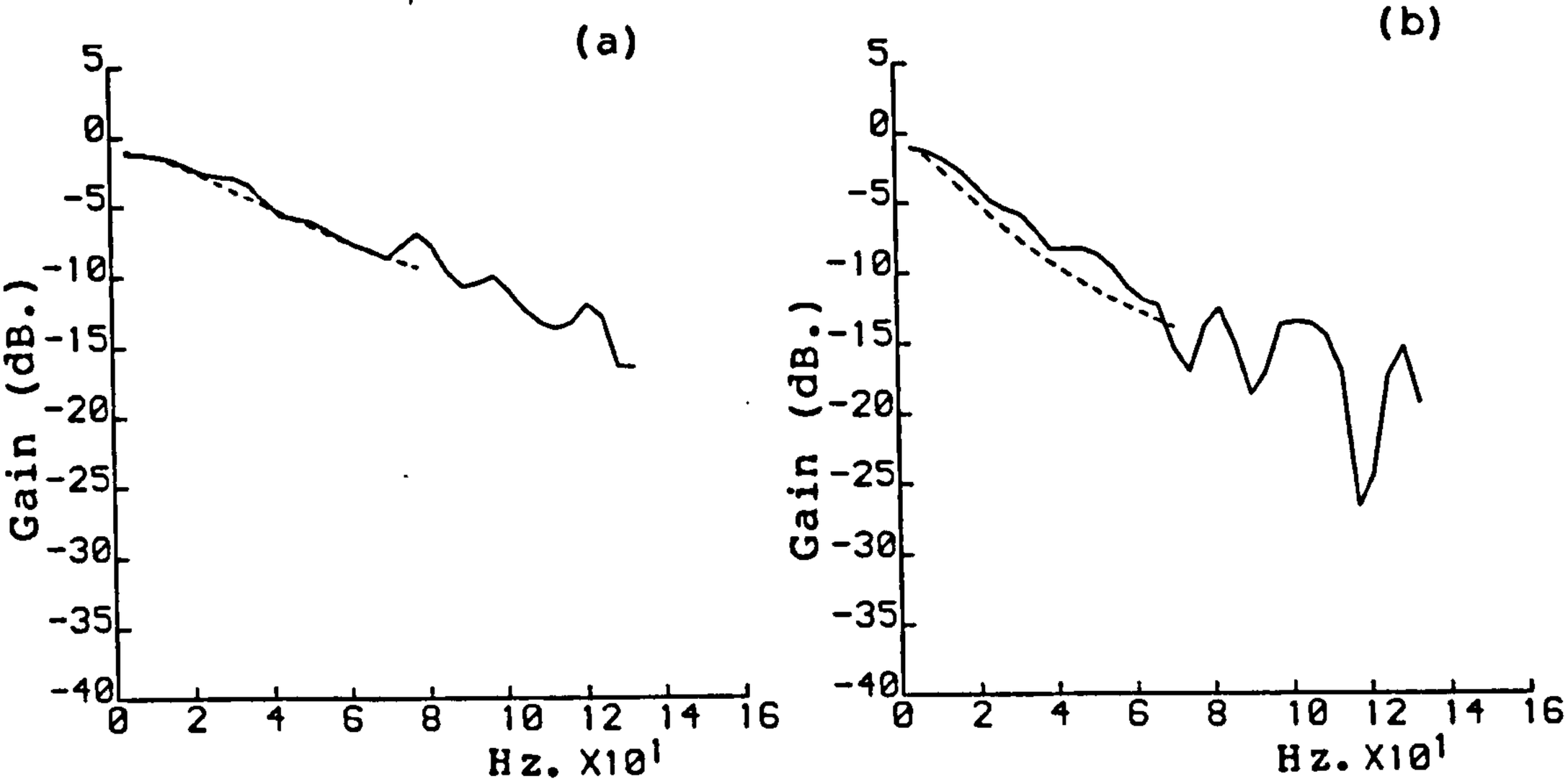

Fig. 2.9.1 Gain for estimates of $S_1(\lambda)$ for simulated data, G_m=30 and t_m=50msec., for :

(a) t_d=5msec.,

(b) t_d=10msec. and

(c) t_d=20msec..

Theoretical responses (2.7.1) are shown by dashed lines.

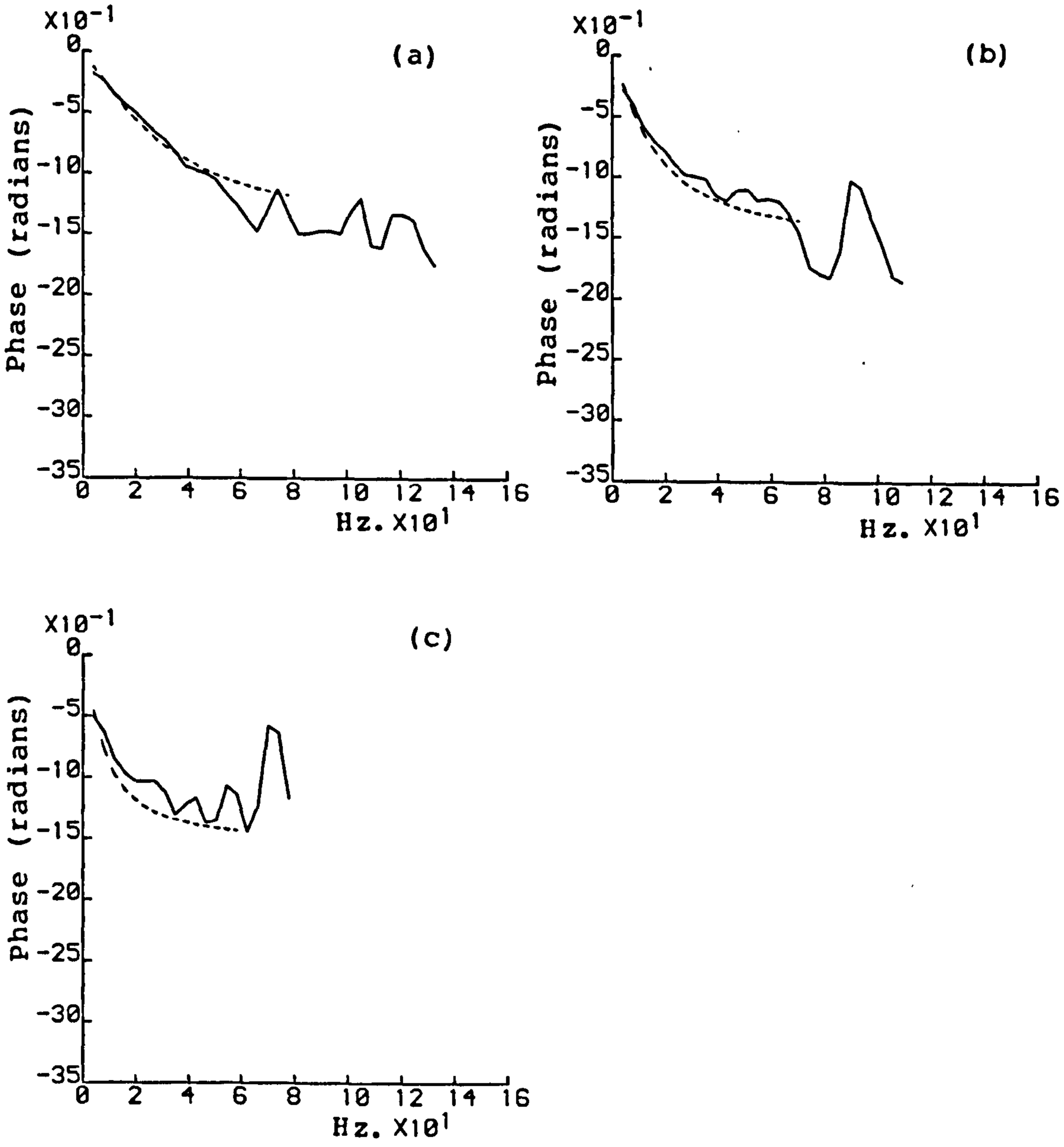

Fig. 2.9.2 Phase for estimates of $S_1(\lambda)$ for simulated data, G_m=30 and t_m=50msec., for :

(a) t_d=5msec.,

(b) t_d=10msec. and

(c) t_d=20msec..

Theoretical responses (2.7.1) are shown by dashed lines.

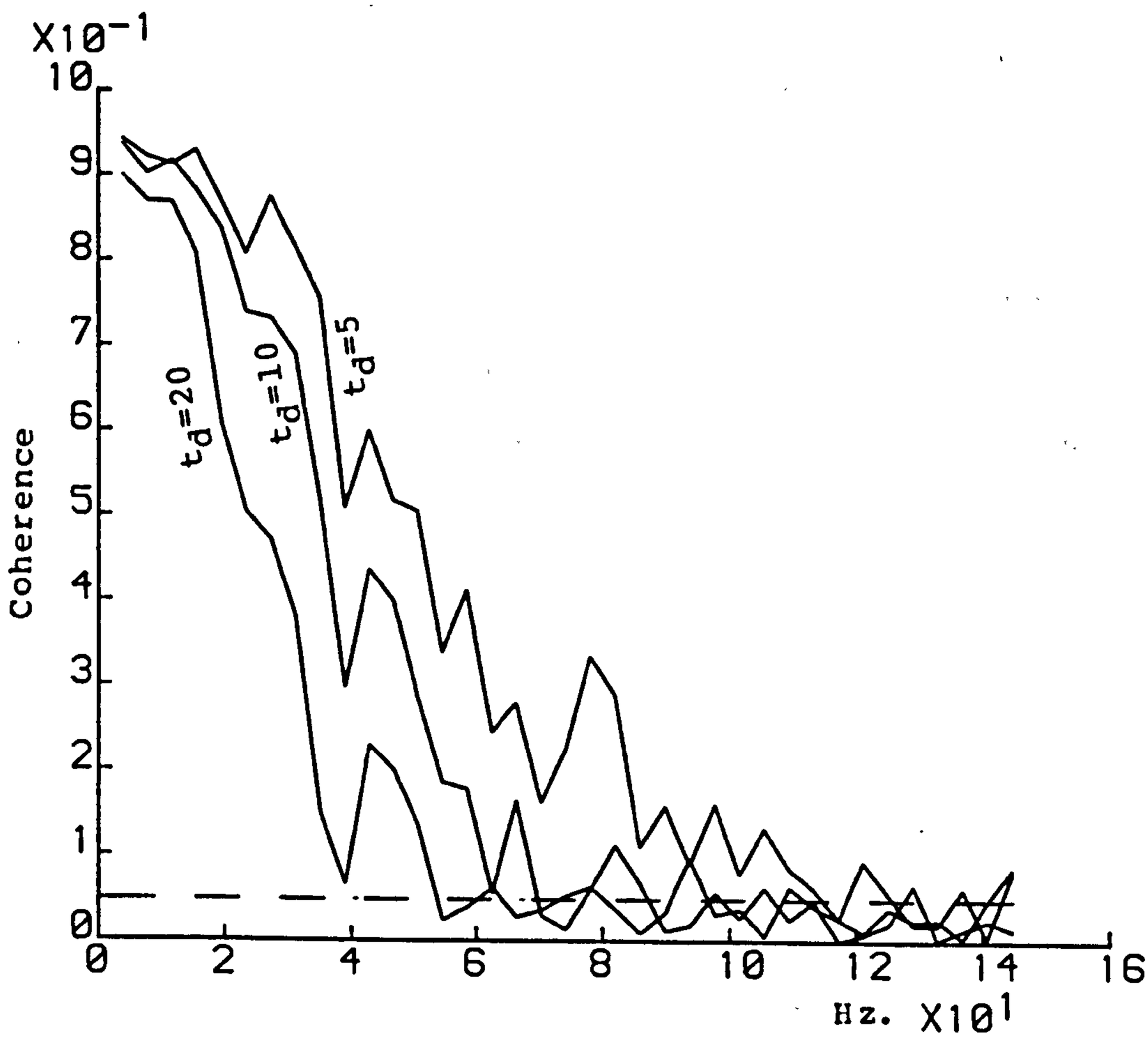

Fig. 2.9.3 Coherence estimates for simulated data, G_m=30 and t_m=50msec. with t_d varied (t_d=5, 10 and 20msec.)
Dashed line represents approximate 95% confidence limit.

figure 2.9.3 are significantly high over a wide range of frequencies, and the range of frequencies over which the linear model is valid decreases as the time constant in the linear sub-section of the simulation increases. This may be related to the greater filtering effect a longer time constant would have on the input spike-train. From the results in figures 2.9.1 and 2.9.2 it would appear that the modulator in the simulation does not make any contribution to the linear model (2.4.6), however it has been found that altering the modulator parameters in the simulation results in changes occurring in the estimates $\hat{s}_o$ and $\hat{S}_1(\lambda)$.

The gain value used in the modulator in the simulations above was 30. This was found to give a ratio of output to input spikes of approximately 1. The effect of varying the modulator gain from 20 to 50, with the time constant in the modulator fixed at 50msec., can be seen in figure 2.9.4. A fixed value of 10msec. was used for the time constant in the linear section. Figure 2.9.4a shows the estimates of the magnitude of $\hat{S}_1(\lambda)$ for gain values of 20, 30 and 50 in the modulator, the corresponding coherence estimates are shown in figure 2.9.4b. The numbers of output spikes for these gain values were 582, 925, and 1582 respectively giving estimates for s_o of 0.037, 0.058, 0.100. The number of input spikes was the same for each data set, M(R)=1008, with R=15872. The three gain estimates in figure 2.9.4a are very similar apart from having different D.C. gain values. In terms of the transfer function (2.7.1), values of K of 0.66, 0.92 and 1.51 result in the close agreement of the theoretical response for this transfer function with the magnitude of $\hat{S}_1(\lambda)$ over the relevant range of frequencies. This range of frequencies increases as the gain increases, as shown by the coherence estimates in figure 2.9.4b.

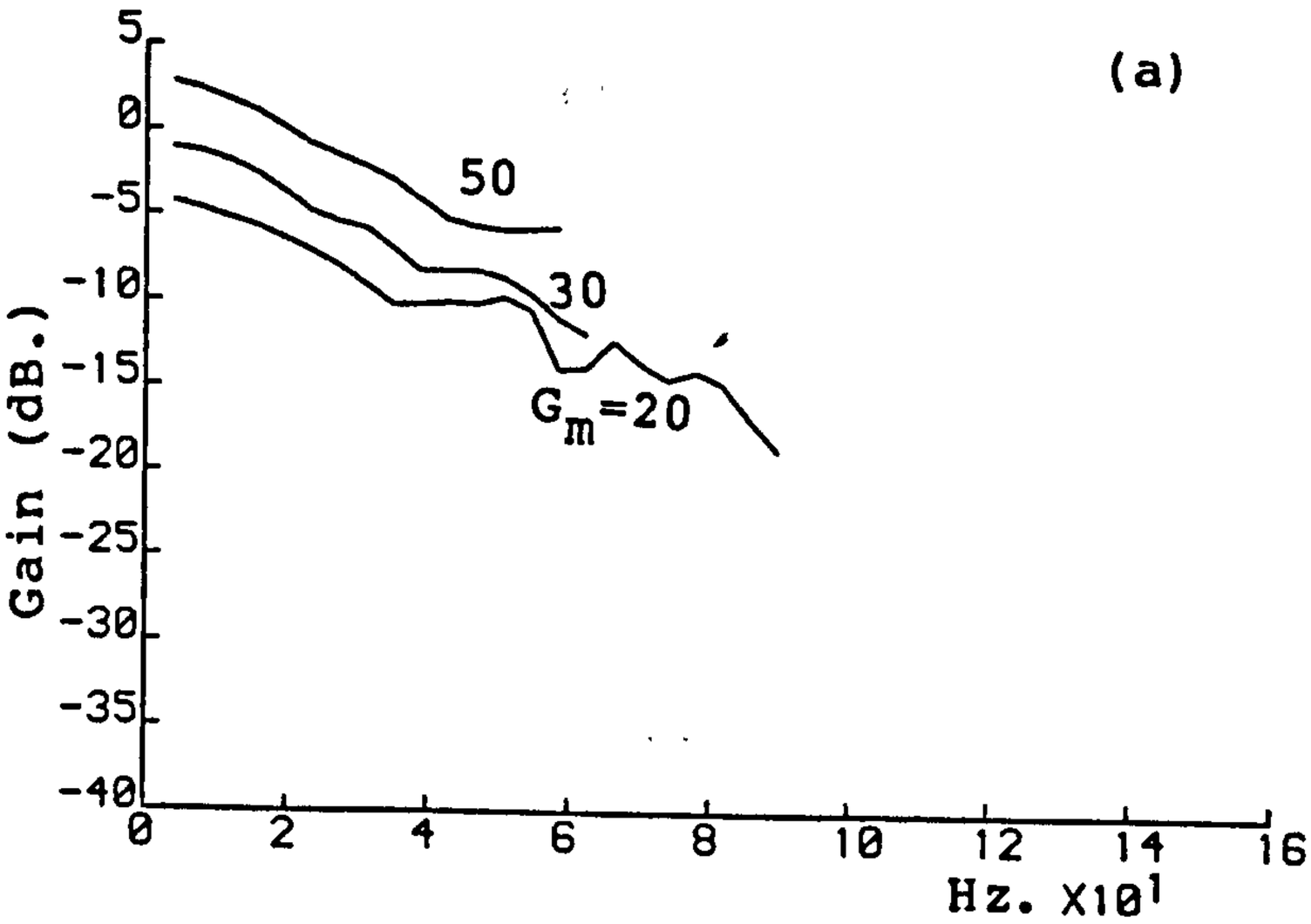

Fig. 2.9.4 (a) Gain of estimates of $S_1(\lambda)$ and (b) Coherence estimates for simulated data with t_d=10msec., t_m=50msec. and varying modulator gain (G_m=20, 30 and 50).

A higher gain in the encoder will allow the filter section of the modulator to rise more rapidly for a fixed input level. This will result in the filter output reaching the threshold level in a shorter time interval, and accounts for the larger number of output spikes and the increased frequency response of the simulation with higher gain values in the modulator. The phase estimates for modulator gains of 20 and 50 being very similar to the estimate in figure 2.9.2b for a modulator gain of 30.

Altering the gain in the modulator changes the gain value K required to match the transfer function (2.7.1.) response with that of the simulation, however the phase estimate and the general shape of the magnitude of $\hat{S}_1(\lambda)$ still accurately reflect the properties of the linear sub-section of the simulation. It is interesting to note that for the two higher gain values, 30 and 50, the value of K calculated for the solution of (2.7.1) is the same as the ratio of output to input spikes for these simulations. This was not found to be the general case with other simulation studies.

Altering the time constant in the modulator also has an effect on estimates of the linear model parameters. Only short time constants in the linear sub-section of the simulation produced different results with diferent modulator time constants. These studies use time constants ranging from 5 to 50 msec. in the linear sub-section, and only simulations using a time constant of 5msec. in the linear sub-section were found to be affected by altering the time constant in the modulator. The range of time constants tried in the modulator ranged from 5 to 50 msec. The gain in the modulator was also varied, this was

required to maintain the ratio of output to input spikes around unity. Although the main object was to study the effect of varying only the modulator time constant it was decided that more physiologically meaningful results would be obtained if modulator gain/time constant (G_m/t_m) pairs were used, since keeping the gain fixed and altering the time constant led to a very large variation in the ratio of output to input spikes.

Figure 2.9.5 shows the gain, phase and coherence estimates for G_m/t_m pairs 7/5, 19/25, and 30/50msec.. The dashed line in the gain and phase plots is the theoretical response of the transfer function (2.7.1) with K=1 and a time constant of 5msec.. This solution is only a good approximation to $\hat{S}_1(\lambda)$ for the longer modulator time constant, and as G_m and t_m are decreased then $\hat{S}_1(\lambda)$ deviates further from this solution.

The effect appears to give a broader frequency response and introduce extra phase lag into the estimate $S_1(\lambda)$. This may be due to some interactive effect between the time constants in the linear section and the modulator, or it may be a phenomenon caused by this type of pulse frequency modulator. The coherence estimates in figure 2.9.5c show that decreasing G_m/t_m increases the range of frequencies covered by the linear model, however unlike the above example the ratio of output to input spikes remains fairly constant in this example, with values of 1.06, 1.01 and 0.86 for the three G_m/t_m pairs 7/5, 19/25 and 30/50 respectively.

When the time constant in the linear dynamics (t_d) was increased to values of 10msec. and higher, this effect was not present and the gain and phase estimates agreed closely with the transfer function (2.7.1) using the value of t_d for τ and

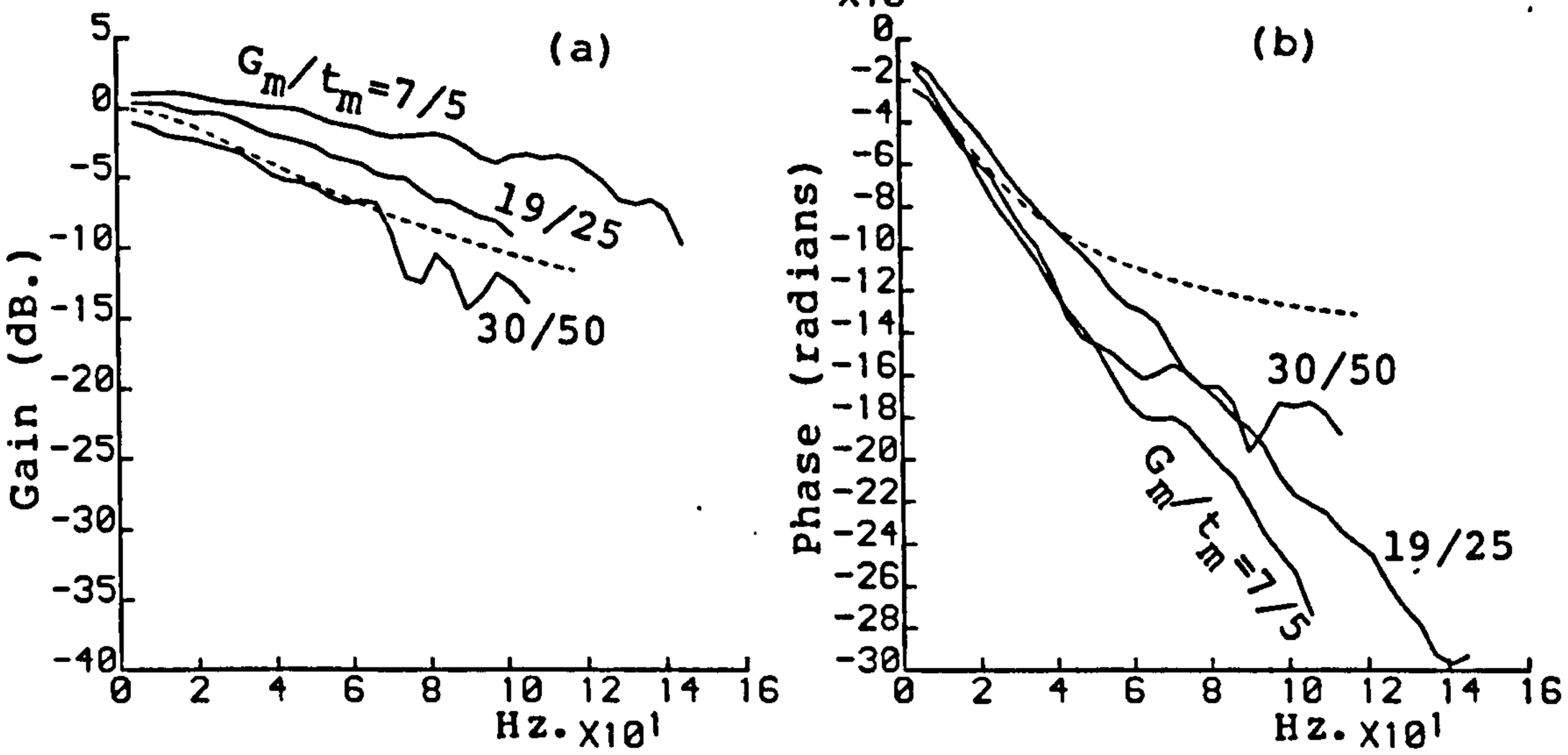

Fig. 2.9.5 (a) Estimates for gain and

(b) Phase of $S_1(\lambda)$, and

(c) Coherence estimates for simulated data with t_d=5msec., and varying modulator gain and time constant (G_m/t_m=7/5, 19/25 and 30/50).

Theoretical responses are shown as dashed lines in (a) and (b). Dashed line in (c) indicates the approximate 95% confidence limit.

choosing an appropriate value for K. All these simulation studies had an output to input spike ratio around unity and it was found that in general as G_m/t_m values increased then the value of K required to fit the theoretical gain curve to the estimate $\hat{S}_1(\lambda)$ decreased. More specifically for t_d=15msec. the value of K required fell from K=1.8 for G_m/t_m=7/5 to K=1.0 for G_m/t_m=30/50. For each value of t_d the phase estimates from $\hat{S}_1(\lambda)$ were very similar for all G_m/t_m pairs tried, and the range of frequencies over which the coherence estimate was significant increased as G_m/t_m values decreased, in a manner similar to that shown in figure 2.9.5c. Figure 2.9.6 illustrates these points showing the gain, phase and coherence plots for t_d=25msec. and the two G_m/t_m pairs 9/5 and 30/50. The similarity between the gain and phase estimates is apparent for these two G_m/t_m pairs representing the smallest and largest values tried.

The above simulation studies show that in general the estimate $S_1(\lambda)$ reflects the properties of the linear sub-section of the simulation in agreement with the transfer function (2.7.1.). Also apparent is the similarity between the results from the simulation and results from muscle spindle fusimotor experiments.

Figure 2.9.7 compares the autospectral estimates, (2.3.29), of a typical fusimotor experiment with a simulated data set using the same random input. For this particular simulation the value of t_d was 50msec.. The similarity between the two estimates indicates how accurately the simulation can model the behaviour of a muscle spindle fusimotor sub-system. Altering t_d in the simulation also has a clear and consistent effect on autospectral estimates. Increasing t_d tends to increase the magnitude and decrease the width of the characteristic dip present in the

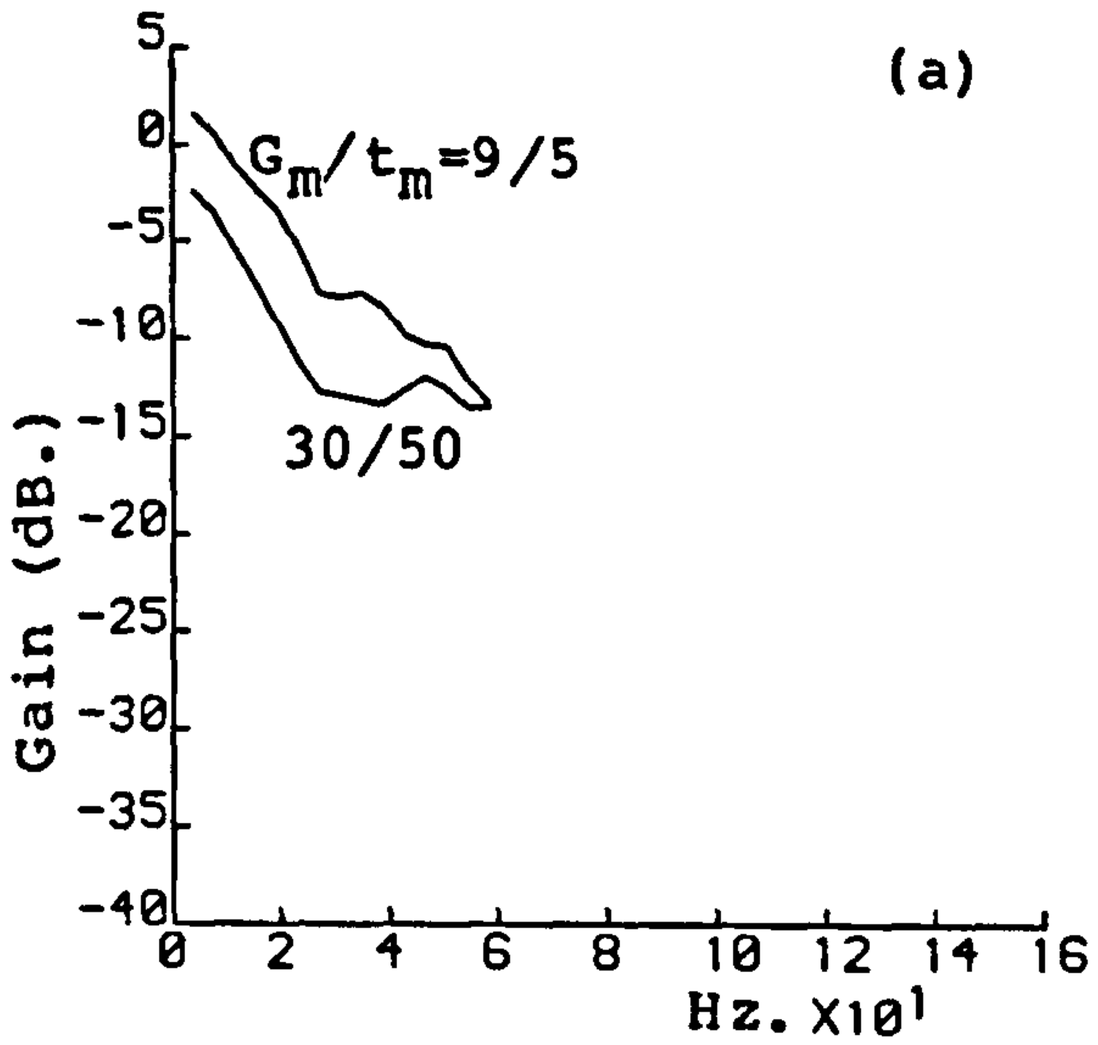

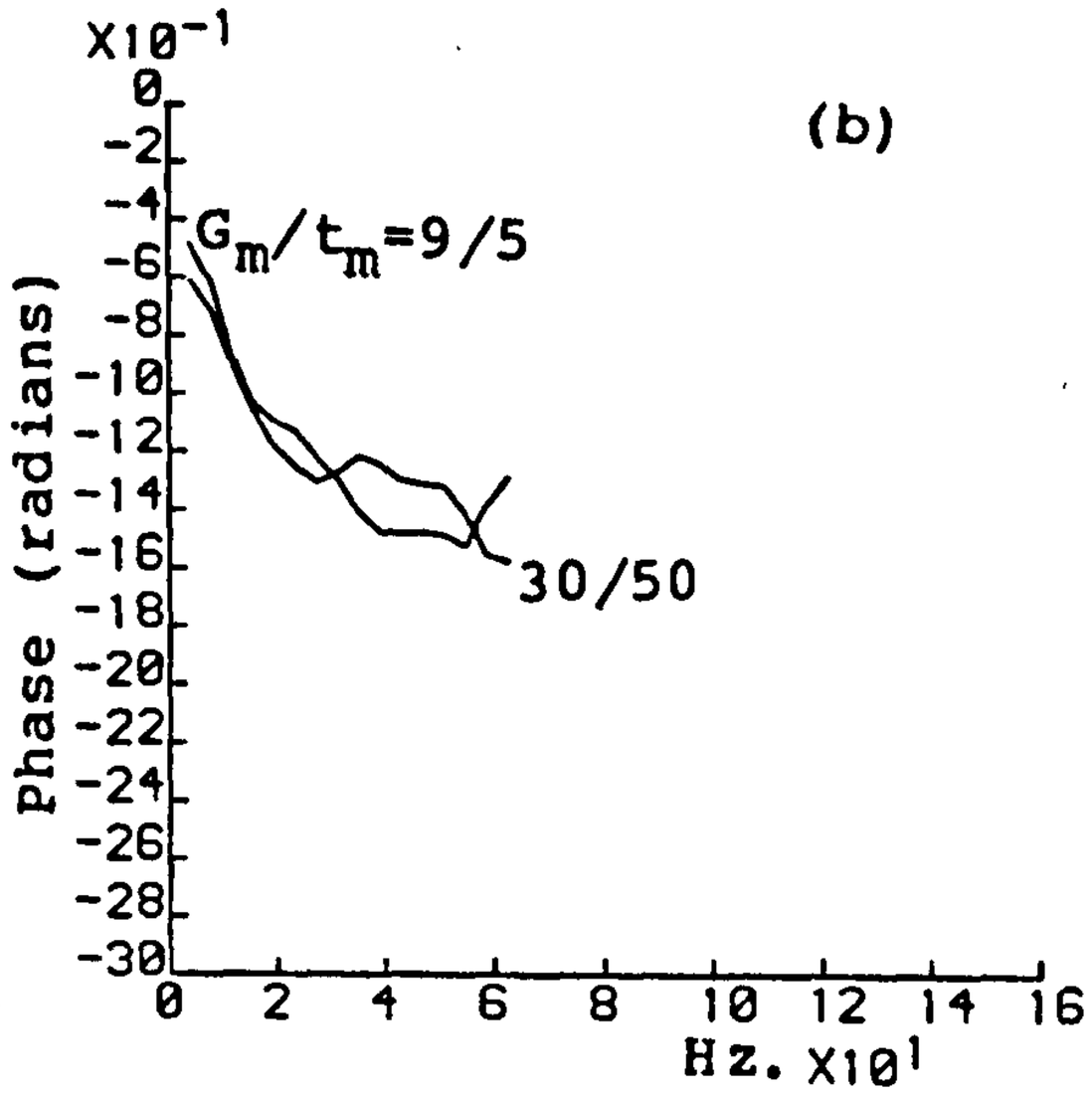

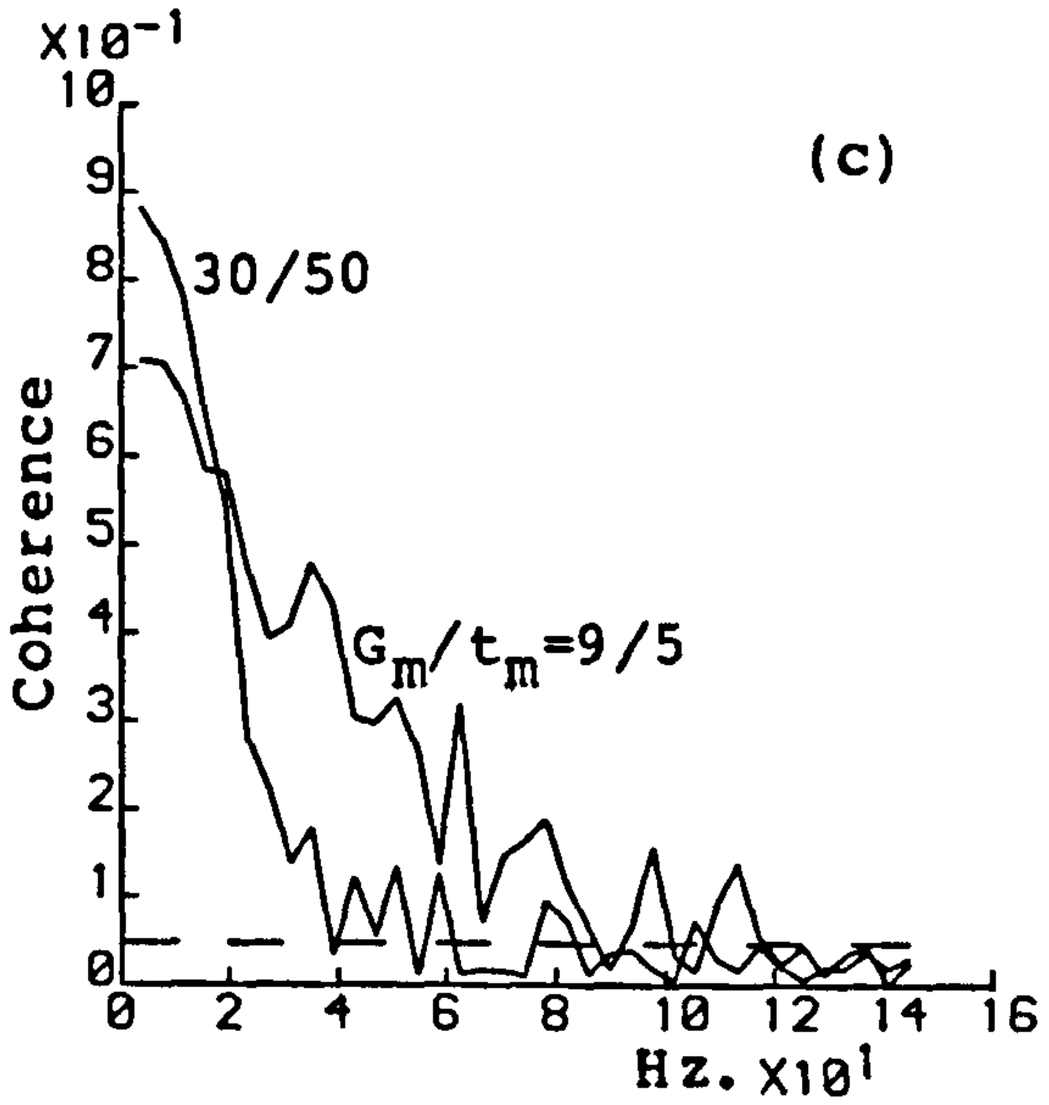

Fig. 2.9.6 (a) Estimates of gain and

(b) Phase of $S_1(\lambda)$, and

(c) Coherence estimates for simulated data with t_d=25msec., and varying modulator gain and time constant (G_m/t_m=9/5 and 30/50). Dashed line in (c) indicates the approximate 95% confidence limit.

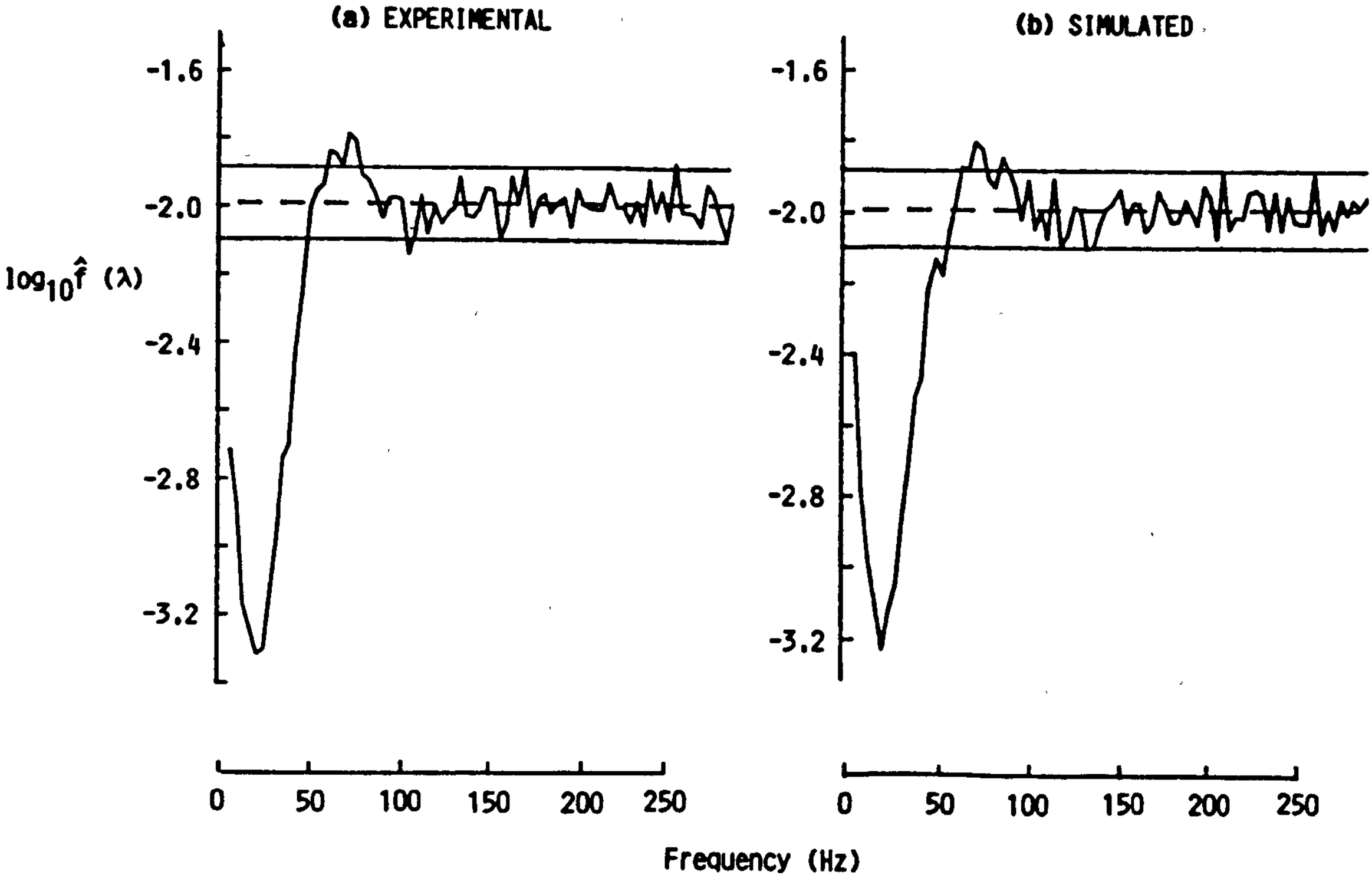

Fig. 2.9.7 Comparison of :

(a) experimental auto spectrum estimate (2.3.29), with T=256, with

(b) auto spectrum estimate of simulated data, with t_d=50msec.

Dashed lines shows estimate of asymptotic distribution, solid lines indicate the approximate 95% confidence limits.

autospectral estimates for this type of point-process system. This is illustrated in figure 2.9.8 showing autospectral estimates for values of t_d of 5, 10, and 20 msec.. The changes in the range and magnitude of the reduction of spectral power at low frequencies can be seen, and other values of t_d have been found to be consistent with these findings. The estimate in figure 2.9.8d is that of another fusimotor experiment on a different spindle. Comparing this with the other three estimates in figure 2.9.8 sugests an equivalent linear time constant of around 10 msec. in the simulation.

Although no formal interpretation for the autospectrum of a point-process has been given, this does not mean that autospectral estimates are not valid or useful. The Finite Fourier Transform , $d_M^{(T)}(\lambda)$, of the process M (2.2.24) can also be considered as the correlation, over the interval (0,T], of sinusoids of frequency λ with the differential increments dM(t). The differential increments will in practice be either zero or one, and correlation with a sinusoid of frequency λ will give an indication of the presence of a periodicity of this frequency in the interval (0,T]. Comparison of autospectral estimates from different experiments shows up any changes that may have occurred in the Ia discharge. A useful starting point in determining what changes in Ia activity have occurred from autospectral estimates has been the results from the simulation. In particular changing the value of t_d in the simulation can account for the wide range of autospectral estimates obtained from random fusimotor experiments, as shown by figures 2.9.7 and 2.9.8.

Altering the gain and time constant in the modulator also has an effect on autospectral estimates. Increasing the gain in

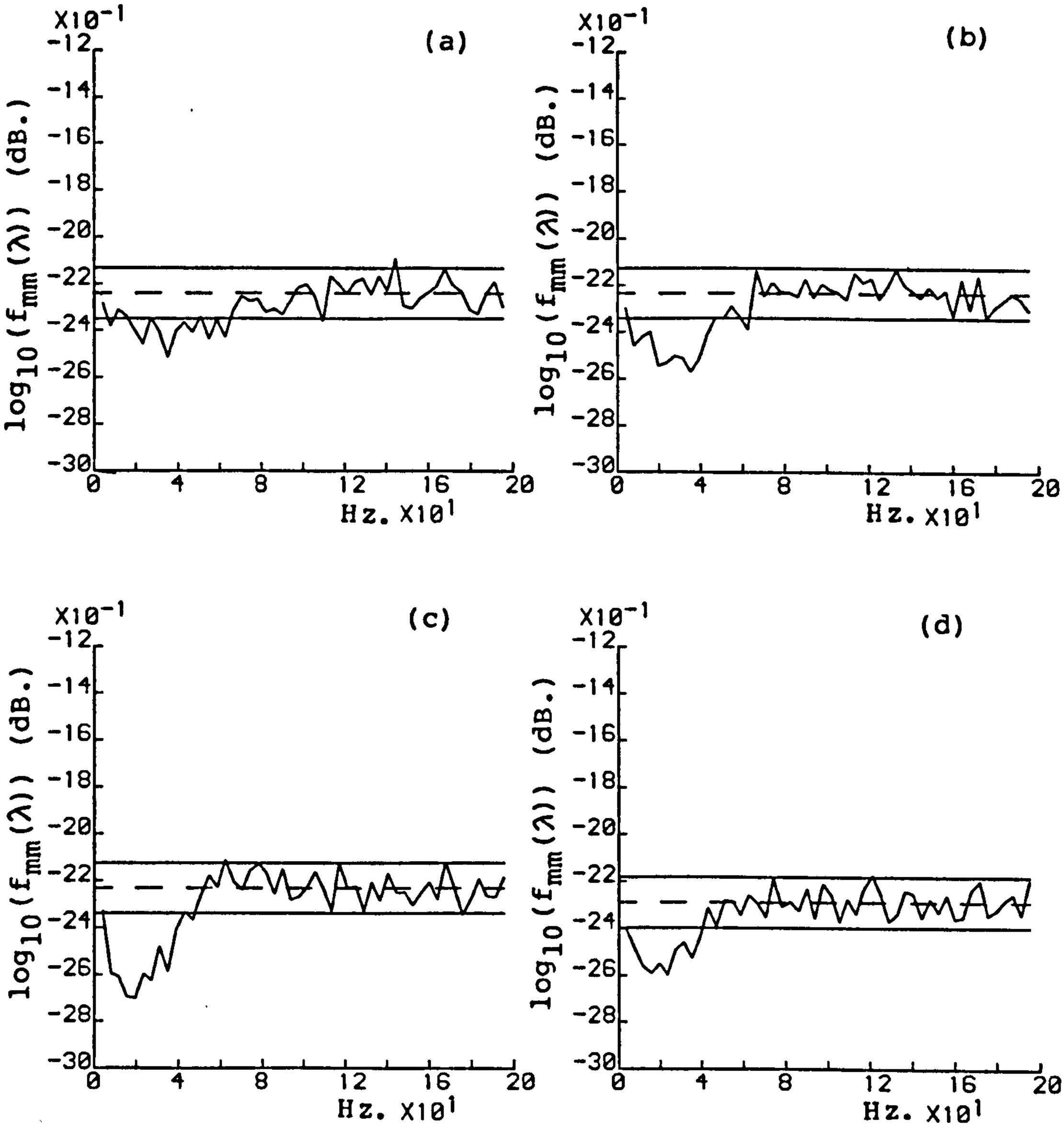

Fig. 2.9.8 Estimates of auto spectrum for simulated data with G_m=20 and t_m=50msec., and

(a) t_d=5msec.,

(b) t_d=10msec. and

(c) t_d=20 msec.

(d) Estimate of auto spectrum of primary discharge for random fusimotor experiment. Dashed lines show estimate of asymptotic distribution, solid lines indicate approximate 95% confidence limits.

the modulator increases both the width and the magnitude of the dip in the auto spectrum. This is illustrated in figure 2.9.9 showing autospectral estimates for three gain values of 20,30 and 50 in the modulator, with t_m=50msec., and t_d=10msec.. This effect is slightly different from that observed in the results in figure 2.9.8, in that increasing the modulator gain increases both the width and the magnitude of the dip in the autospectrum, whereas the increase in magnitude of the dip caused by increasing t_d is accompanied by a corresponding decrease in the width of the dip.

The effect of varying the time constant in the modulator also has a consistent and again slightly different effect on autospectral estimates. As previously explained the gain in the modulator was also adjusted to keep the ratio of output to input spikes close to unity. Figure 2.9.10 shows three autospectral estimates for t_d=10msec. and three G_m/t_m pairs 9/5, 12/10 and 21/25msec.. The effect of decreasing G_m/t_m is to increase the width of the dip in the autospectrum, with the magnitude remaining fairly constant. This increase in width is accompanied by a shift of the position of this dip to lower frequencies, and an increase in spectral power at the lowest frequencies.

As well as changing t_d in the simulation to account for the range of experimental results obtained, the effects of altering the modulator parameters can also be used to provide a more accurate match between simulated data and experimental spindle data. Going back to the experimental autospectral estimate in figure 2.9.8d, the position of the dip at low frequencies and the lack of any spectral components above the asymptotic distribution at the lowest frequencies, suggests an equivalent time constant in the modulator of around 50msec. This is in agreement with the findings of previous studies (Angers and Delilse, 1971; Kroin,

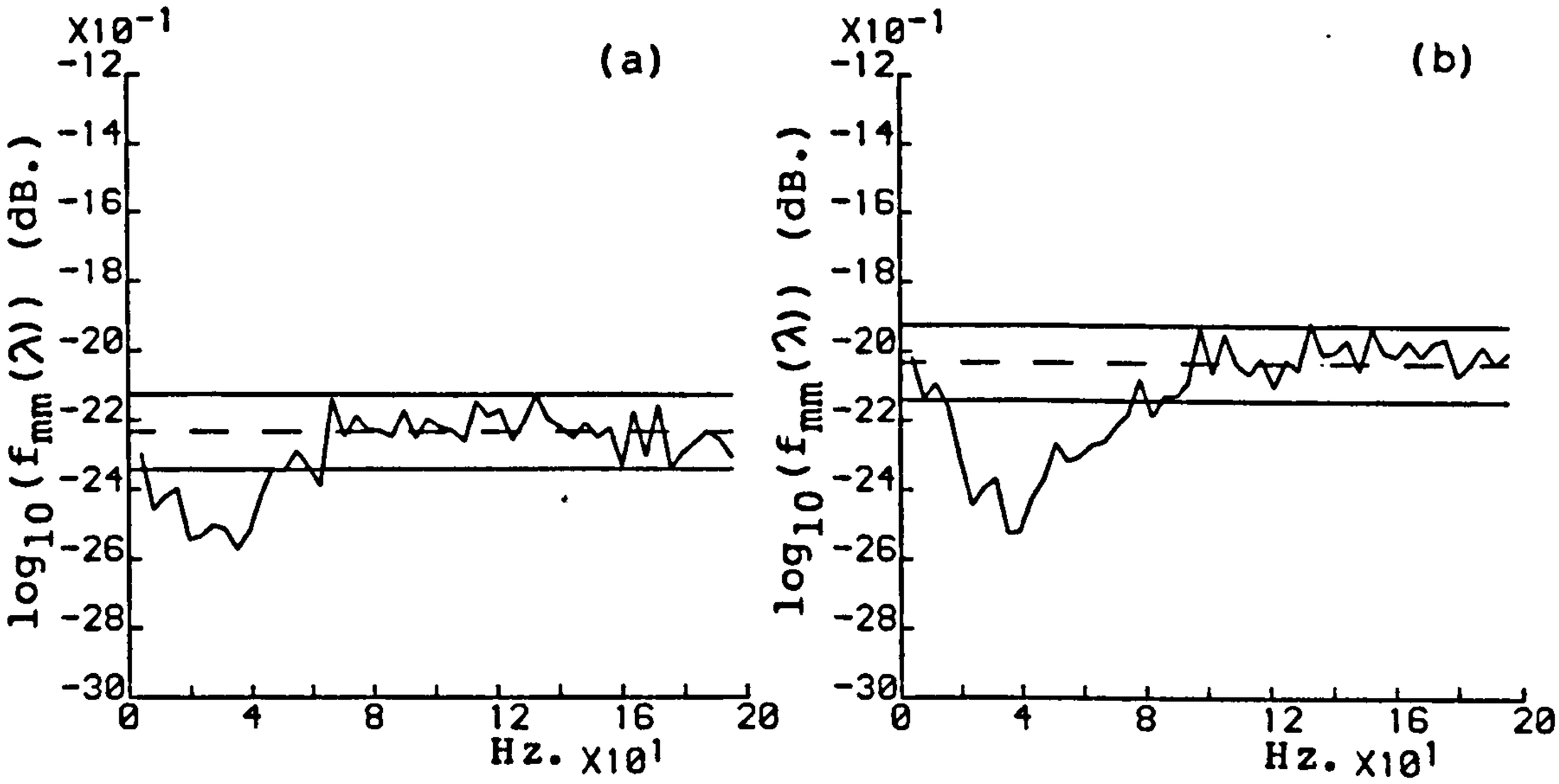

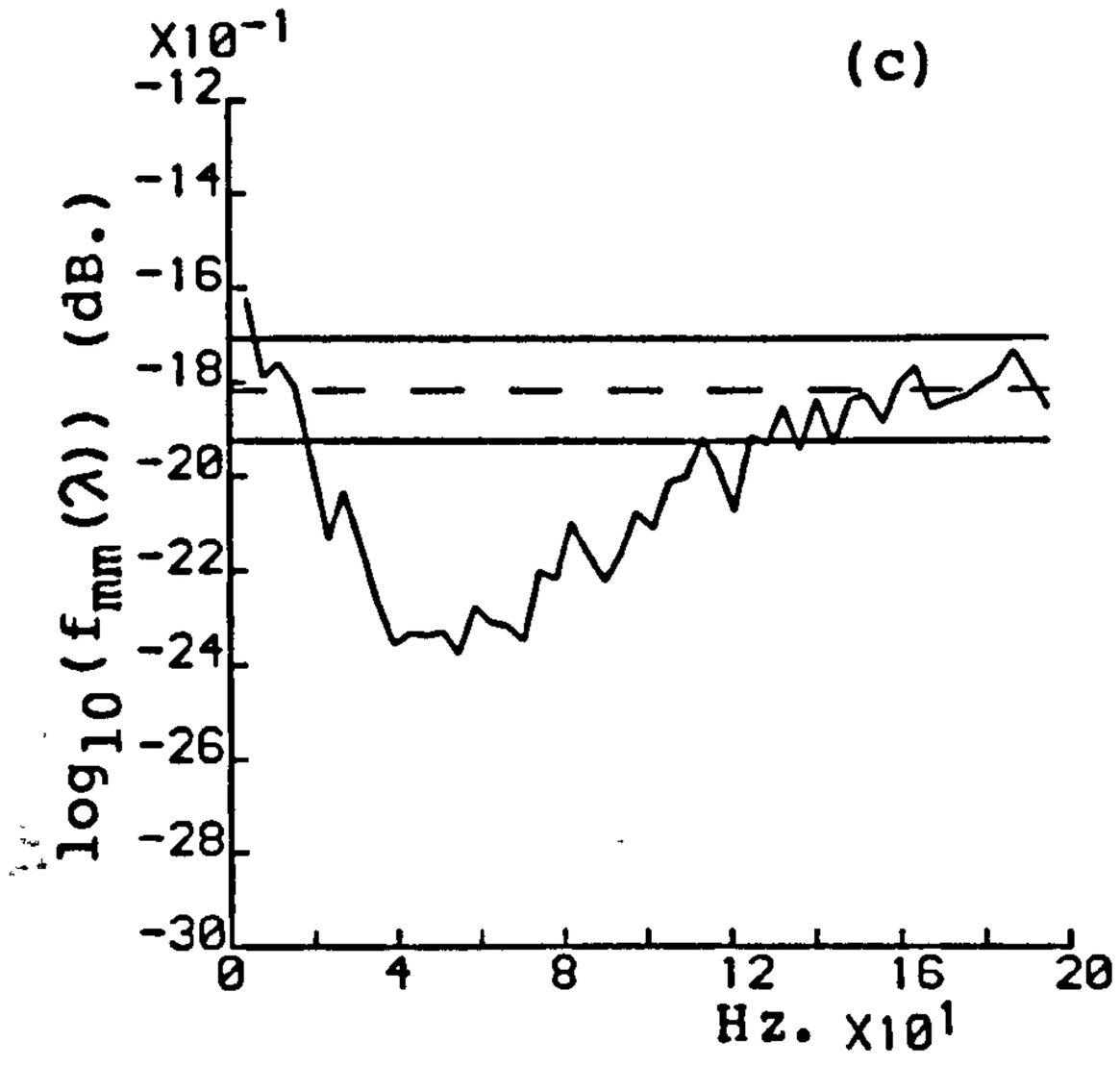

Fig. 2.9.9 Estimates of auto spectrum for simulated data with t_d=10msec., t_m=50msec. and

(a) G_m=20,

(b) G_m=30 and

(c) G_m=50.

Dashed lines show estimate of asymptotic distribution, solid lines indicate approximate 95% confidence limits.

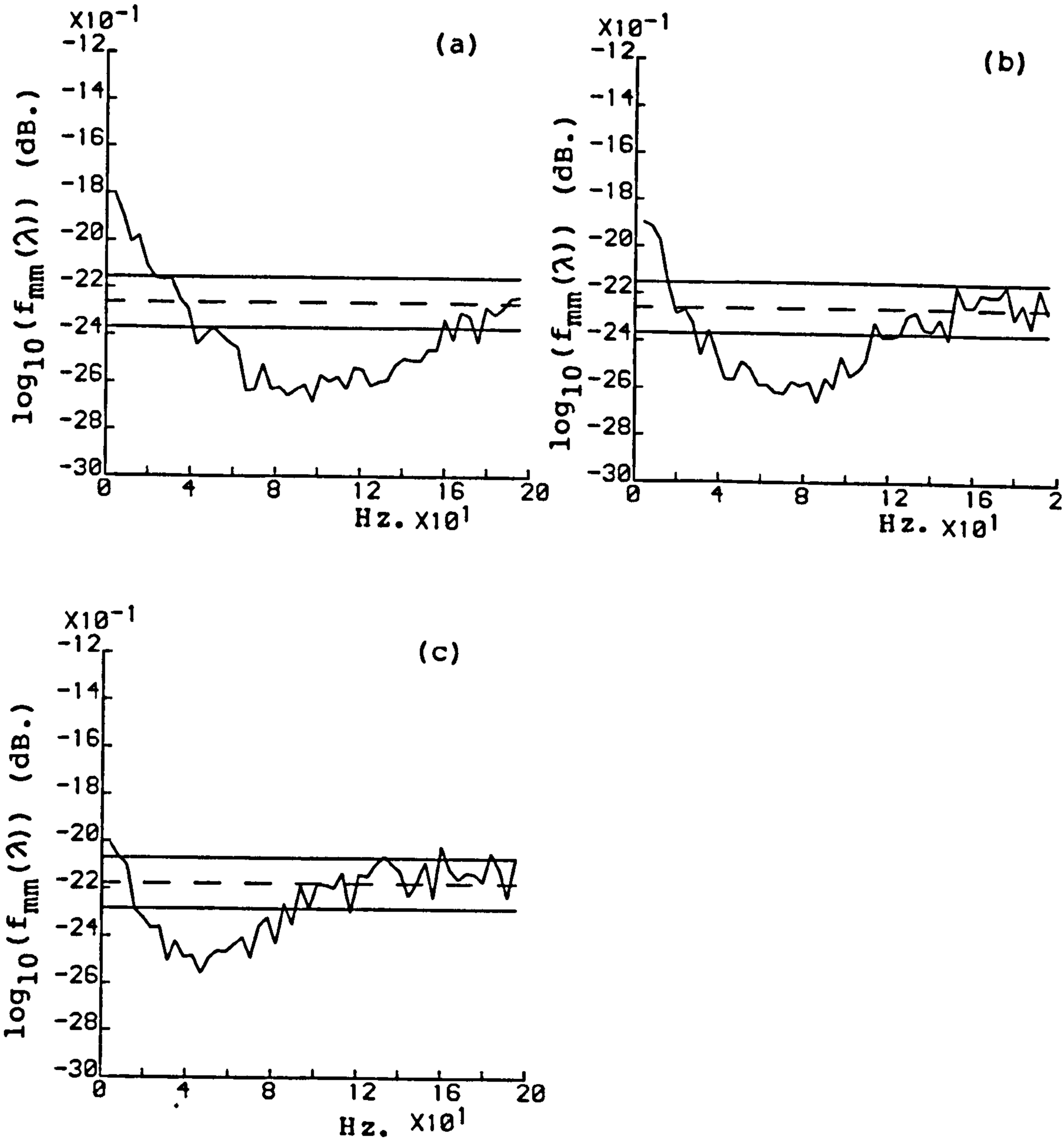

Fig. 2.9.10 Estimates of auto spectrum for simulated data with t_d=10 msec., and

(a) G_m/t_m=9/5,

(b) G_m/t_m=12/10 and

(c) G_m/t_m=21/25msec..

Dashed lines show estimate of asymptotic distribution, solid lines show approximate 95% confidence limits.

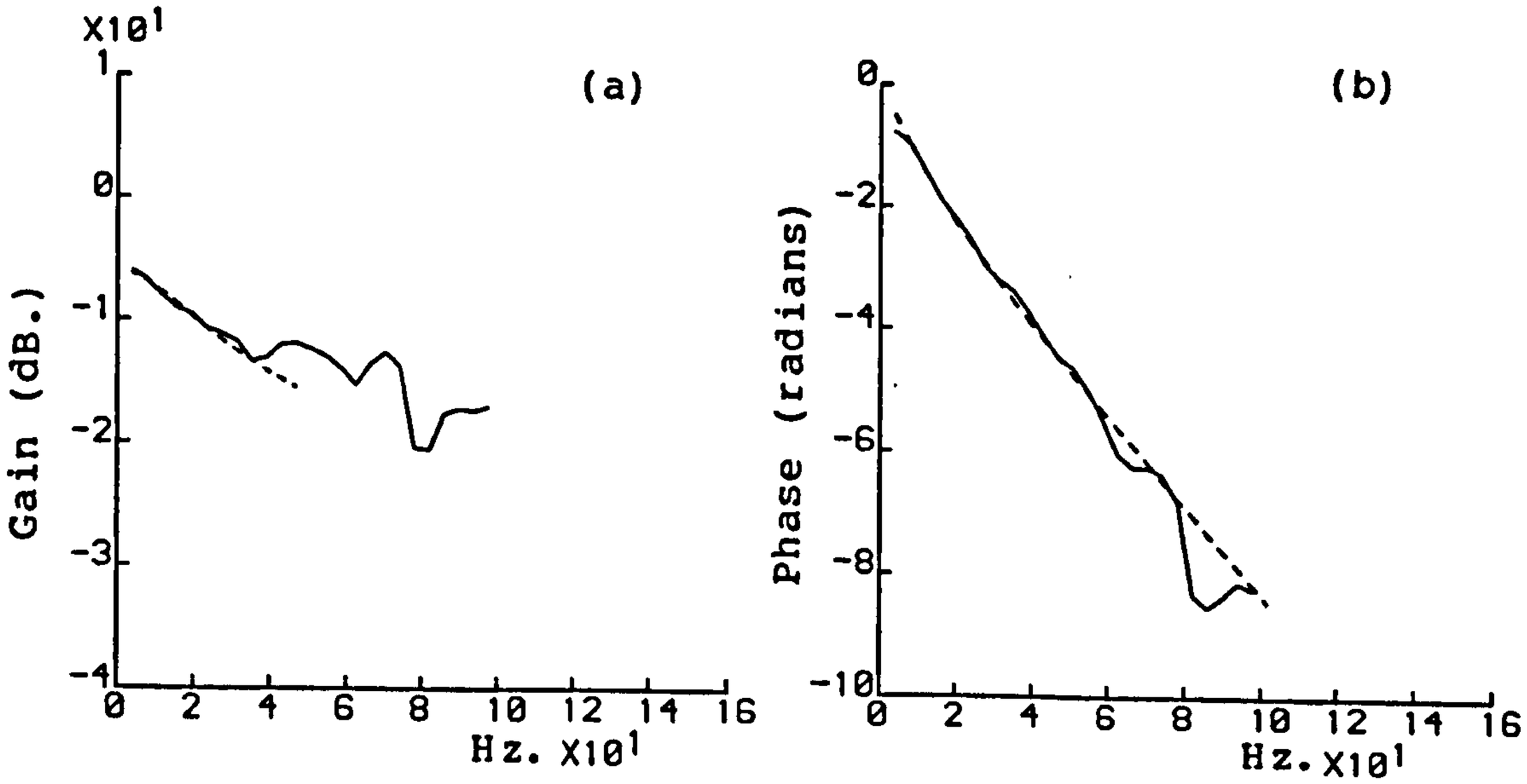

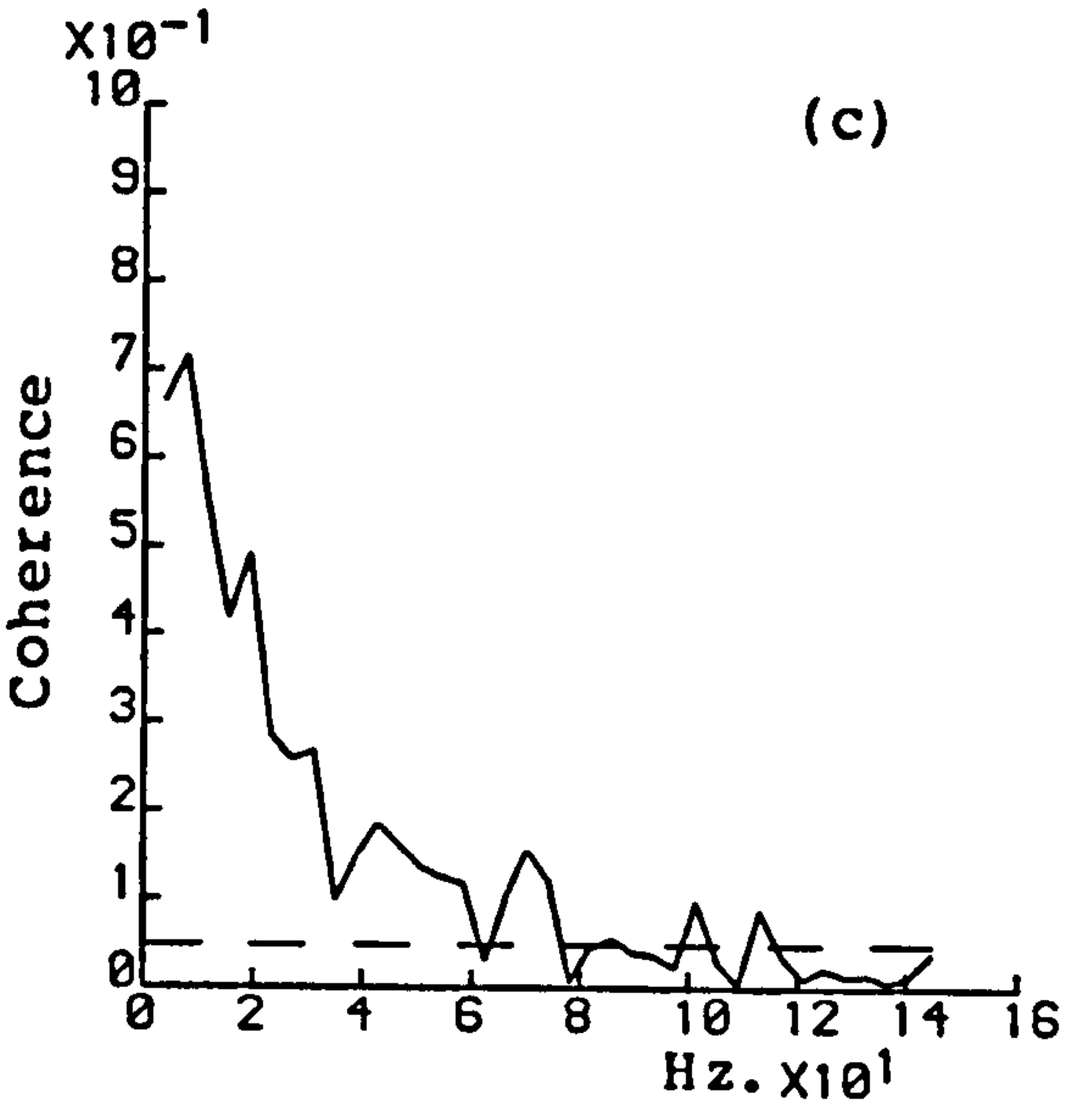

Fig. 2.9.11 (a) Gain and

(b) Phase of estimate of $S_1(\lambda)$ and

(c) Coherence estimate for static fusimotor input and primary discharge at fixed muscle length.

Dashed lines in (a) and (b) show theoretical response for K=0.5, γ=9.5msec., and a delay of 11msec.. Dashed line in (c) indicates approximate 95% confidence limits.

1974). For this experimental data set the numbers of spikes for the input and output processes were 1010 and 512 respectively, giving a ratio of 0.51. In the simulation, using a time constant in the modulator of 50msec., this ratio is rouqhly the same as that obtained by setting the gain in the modulator to 20. Therefore for this experimental data set the equivalent simulation parameters would appear to be t_d in the region of 10 msec., and G_m/t_m=20/50. These are the values for the estimate in figure 2.9.8b and comparison of the two estimates shows them in fact to be very similar in the region outside the confidence band. Figure 2.9.11 shows the gain phase and coherence estimates for this experimental data set. The dashed line is the theoretical response of the transfer function (2.7.1) with K=0.50, τ=9.5msec and a delay of σ=11msec. This value of τ is roughly in agreement with the value estimated from the autospectrum.

2.10 SUMMARY

The application of point-process system identification techniques to muscle spindle data has allowed a linear transfer function description of a fusimotor subsystem to be determined. Time and frequency domain representations of this transfer function can be used to relate activity in the primary discharge to the fusimotor input.

This transfer function description has been used as the basis of simulation studies which have provided further insight into the interpretation of experimental results. The results from this simulation have shown how varying the gain and time constant parameters in the mathematical model of the simulation may be

able to explain the variety of different experimental results obtained.

CHAPTER THREE

3.1 INTRODUCTION

As well as treatment of neuronal spike-trains as point-processes, several older and more accepted methods of spike-train analysis exist. These generally involve some form of pre-processing of the spike-train based on the interspike interval, or some function of this interval. This is currently regarded as one type of mechanism by which information is transmitted in nervous systems (see for example Stein, 1970). This chapter will look briefly at the use of the instantaneous frequency measure, and will then consider a technique where the spike-train is filtered to give a continuous signal which can be analysed using conventional time-series analysis. Comparison with point-process spectra will be made in the latter case.

One commonly used method of analysis is the instantaneous frequency of the spike-train, where the time interval between a spike and a preceeding spike is inverted to give a continuous signal which changes value at the time of occurrence of each spike. This method is easy to implement, and has been used to study spindle responses to ramp stretches (Hasan and Houk, 1972; Maclaine et al, 1977). The results in figures 1.3.2 and 1.3.3 have been obtained using this method. However the instantaneous frequency method can only be used for small perturbations at the input, and if periodic stimuli are used then only low frequency signals can be used. At higher frequencies the number of spikes per input cycle may be insufficient to obtain any useful information. For an irregular spike-train with large deviations in frequency about the mean value no simple relationship exists for the fluctuations about the mean interval and the resulting instantaneous frequency. Since it is not certain that the information in a spike-train is coded as the instantaneous

frequency, care must be exercised if using instantaneous frequency results derived from an irregular spike-train in system identification studies.

3.2 ANALYSIS BASED ON THE LINEAR TRANSFORMATION OF SPIKE-TRAINS

Conventional spectral analysis requires a sampled-data time domain signal with equispaced samples as the input, whereas a point-process representation is defined as a series of events with unequal spacing. Priestly (1963) suggested a pre-processing technique using a linear transformation or filtering of the point-process to provide a continuous signal suitable for conventional spectral analysis. He also recommended the use of a low-pass filter as the transformation, which would remove unwanted frequency components present in the point-process and allow the periodogram of the spike-train to be calculated for the frequency range of interest.

French and Holden (1971) extended this approach and chose SIN(x)/x as the transformation, this being the time domain response of an ideal phaseless low pass filter. The impulse response of an ideal low pass filter of cut off frequency F_c is given by :

$$2 F_c \frac{SIN(2\pi F_c(t - t_i))}{2\pi F_c(t - t_i)}, \qquad (3.2.1)$$

where t_i is the time of occurrence of the i^{th} spike. If each spike at time t_i is considered as a delta function and convolved with expression (3.2.1), then this will give its contribution to the output of the filter. Summation of (3.2.1) over all the spikes in the train will give a continuous signal representing

the linear transformation of the spike-train. This can then be sampled at regular intervals and used as a conventional sampled-data signal for spectral analysis.

The sinc function, (3.2.1), is in practice non-realisable since it extends from $-\infty$ to $+\infty$, however French and Holden overcome this problem by multiplying this infinite time series by a rectangular data window of unity height which extends from t=0 to t=R, where R is the length of the spike-train. This operation convolves each spectral component with the sinc function R Sa(πfR), but this will not affect spectral estimates since the initial selection of a record of length R also convolves each spectral component with the same sinc function. The summation of expression (3.2.1) is then of finite extent and can be implemented on a digital computer.

The expression for the implementation of the French-Holden algorithm is given by:

$$f(j\ T_f) = \frac{2\ F_c}{\pi} \sum_{i=1}^{N} \frac{(-1)^{(j+1)}\ SIN(2\pi F_c\ t_i)}{(j - 2\ F_c\ t_i)}, \qquad (3.2.2)$$

where T_f is the French-Holden sampling interval for the filter output and is related to F_c by :

$$T_f = 1 / 2F_c, \qquad (3.2.3)$$

where Fc is the cutoff frequency of the low pass filter, N is the total number of spikes in the spike-train, t_i is the time of occurrence of the i^{th} spike, and j is the number of the sample being calculated.

Equation (3.2.2) is given in a paper by Peterka et al (1974) concerned with practical considerations in the implementation of the French-Holden algorithm to the analysis of regularly firing

spike-trains. The effect of record length and cutoff frequency on aliasing are studied and they conclude that F_c should be chosen to avoid a major spectral component. Increasing the record length was found to reduce spectral components outside the cutoff frequency, and rejecting the highest ten frequency components was recommended since they may contain aliasing and distortion errors.

Several practical considerations have to be taken into account for successful implementation of the French-Holden algorithm. Once the value of F_c is chosen it then effectively becomes a constant. Therefore $SIN(2\pi F_c\ t_i)$ and $(2\ F_c\ t_i)$ need only be calculated once for each spike. Two arrays containing the values of these two expressions for each spike will reduce the calculations involved. If T_f is chosen according to equation (3.2.3) then the period of oscillation of the sinc function is also T_f, and this helps to simplify the expansion of expression (3.2.1)

Since the magnitude of the central lobe of a sinc function is much greater than the magnitude of the side lobes, the contribution to a sample from a given spike will decrease with increasing distance from this sample. Consequently considerable savings in calculation time can be made if not all the spikes in the spike-train are summed for each sample.

Two different versions of this modification were successfully implemented. Both methods first determine the nearest spike to the French-Holden sample being calculated, the first algorithm then adds the contributions to this sample from a user specified number of spikes on either side of this spike. A typical value for implementing this method is between 10 and 20

spikes on each side of the nearest spike.

The second shortened implementation adds contributions to the French-Holden sample from alternate positive and negative spikes until the current contribution falls below a user specified percentage of the initial contribution from the nearest spike. A typical value for this method is 1%. Comparing results from these two implementations showed a negligible difference in spectral estimates for a considerable saving in calculation time. The full implementation (summing all spikes for each filter sample) took approximately 30 to 40 times longer than the corresponding point-process analysis, whereas these two shortened French-Holden algorithms typically took 2 to 3 times longer. Unless stated otherwise, all results presented have been calculated by one of the two shortened methods.

The general form of the linear transformation of N(t) can be expressed as :

$$y(t) = \int_{-\infty}^{\infty} w(t-u)\ dN(u)\ , \qquad (3.2.4)$$

where w(t) is the filter function. This can then be sampled to give regularly spaced samples, y_t, and allows the periodogram of the process, $I(\lambda)$, to be defined as :

$$I(\lambda) = 1/2\pi n \sum_{t=0}^{n-1} \left| y_t\ e^{-i\lambda t} \right|^2\ , \qquad (3.2.5)$$

where n is the total number of samples. By splitting the filter output into sections and averaging the periodogram of each section as described for the estimate of the auto spectrum of a point-process (2.3.29), allows an estimate for the auto spectrum of the filtered spike-train to be constructed, and this is given in (3.2.6).

$$f(\lambda) = 1/K \sum_{i=1}^{K} I^{(i)}(\lambda), \qquad (3.2.6)$$

where $I^{(i)}(\lambda)$ is the periodogram of the i^{th} disjoint section of the filter output. Direct comparison of the auto spectrum estimate using point-process and French-Holden methods can be made if the number of samples and the sampling interval in each periodogram segment are equated for the two different methods The spectral resolution will then be the same for each method.

3.3 EXAMPLES OF SPECTRA OF FILTERED SPIKE-TRAINS AND COMPARISON WITH POINT-PROCESS SPECTRA

Figure 3.3.1 shows the estimate (3.2.6) of the output auto spectrum of the same experiment used in figure 2.6.3a (random fusimotor stimulus with muscle held at fixed length). Figure 3.3.1a is the French-Holden estimate, while Figure 3.3.1b is the point-process estimate shown again for comparison. For the point-process analysis use of 1msec. time increments gives an equivalent Nyquist frequency of 500Hz.. The frequency F_c for the filter was chosen to be 499 Hz.. The reason for not choosing 500Hz. will be explained below. Figure 3.3.1 shows that the two spectra are almost identical.

The statistical properties of the point-process representation are known for spike-trains with a Poisson distribution, and this allows the asymptotic distribution for the autospectral estimates to be determined as shown in section 2.3. The effect of the French-Holden transformation on these properties is not known, thus the asymptotic distribution cannot be estimated from the statistical properties.

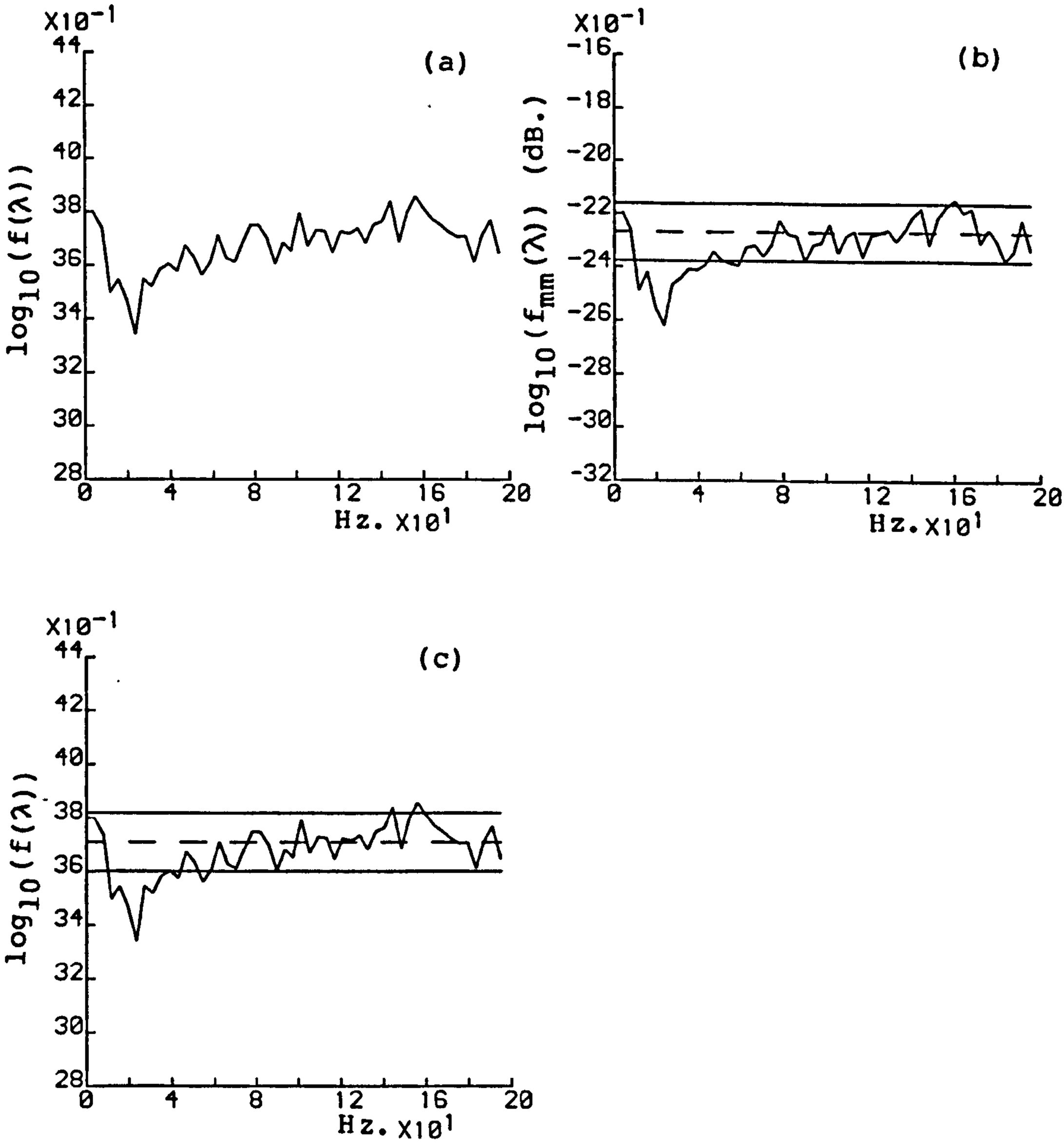

Fig. 3.3.1 (a) Estimate of output auto spectrum (3.2.6) for filtered spike-train from random fusimotor input experiment. F_c=499Hz.

(b) Corresponding point-process estimate (2.3.29), T=256, with asymptotic distribution and confidence band.

(c) Figure 3.3.1a with estimate of asymptotic distribution using Olhsen's method. Solid lines indicate 95% confidence band

Olhsen (1967) gives a general method where the expected value of a periodogram may be determined and states the condition for convergence of $I(\lambda)$ to this value, thus allowing the asymptotic distribution to be determined. This method involves taking the average of the periodogram ordinates after the filter output has been transformed to the frequency domain. Since this method of determining the asymptotic distribution of the spectra is based on averaging of the periodogram ordinates, it is only of use when small deviations from the mean value occur. This is what happens in figure 3.3.1. However in other examples, especially with lower values of F_c, where significant deviation from the mean value occurs over a wider range of frequencies, then this method has been found to give innaccurate estimates of the asymptotic distribution. This procedure should therefore be used with caution, but in figure 3.3.1 it does help with interpretation and comparison of the different methods of estimating the auto spectrum. Figure 3.3.1c shows the auto spectrum of figure 3.3.1a with this new value plotted and also with the 95% confidence limits, which are determined, as in section 2.3, by the smoothing weights used in the periodogram.

Figure's 3.3.1b and 3.3.1c show the two estimates to be almost identical, illustrating the equivalence of the two methods if the correct parameters are chosen for the French-Holden filter. Figure 3.3.2a shows the actual filter output for a section of the spike-train. Figure 3.3.2b shows the filter output for this section when F_c=249 Hz.. The shape of the sinc function can clearly be seen in both examples with the period of oscillation of the sinc function in figure 3.3.2b being twice that of figure 3.3.2a.

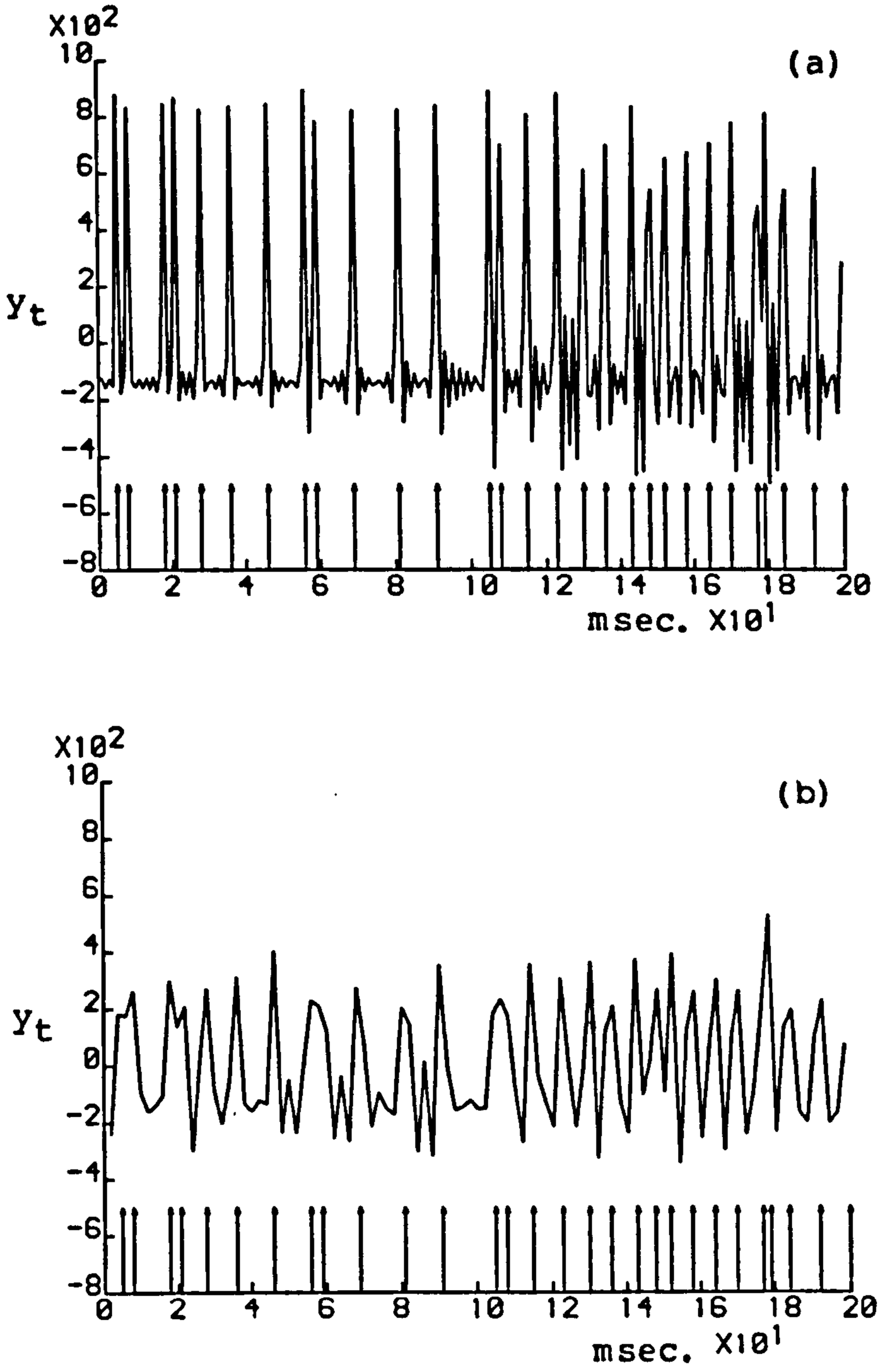

Fig. 3.3.2 (a) Section of French-Holden filter output with F_c=499 Hz. for a section of the primary discharge. Ia spike-train shown inset.

(b) Filter output for same section with F_c=249 Hz.. Ia spike-train shown inset.

Altering the value of F_c will also change the value of T_f, according to equation (3.2.3). The chosen value of F_c should be less than the Nyquist frequency of the original data set, since a higher value would result in the re-sampling of this data using a smaller interval than was originally used. Values of F_c should therefore be chosen to be higher than any major spectral components in the data set, but below the Nyquist frequency of the original sampling period. If T_s is the original sampling period then this frequency is given by :

$$F_n = 1 / 2T_s \quad . \tag{3.3.1}$$

The total number of valid samples which the filtering algorithm can generate is related to the filter sampling period T_f. For a spike-train of length R only R/T_f filter samples should be calculated using the algorithm. This number will always be less than the original number of samples in the spike-train (T/T_s). For good spectral estimates the maximum number of filter samples possible should be used.

The value of filter sampling interval, T_f, along with the number of periodogram samples will define the resolution of the spectral estimates. Figures 3.3.3.a and 3.3.3b show estimates of the output auto-spectrum of the example of figure 2.6.3c (random fusimotor input and random length stimulus). Figure 3.3.3a is the point process estimate with the periodogram length doubled to T=512, giving a spectral resolution of approximately 2 Hz.. A value of Fc of 250 Hz. will allow direct comparison of the two methods. As in figure 3.3.1 the similarity of the two estimates is apparent, showing that the two methods are equivalent for the parameters chosen.

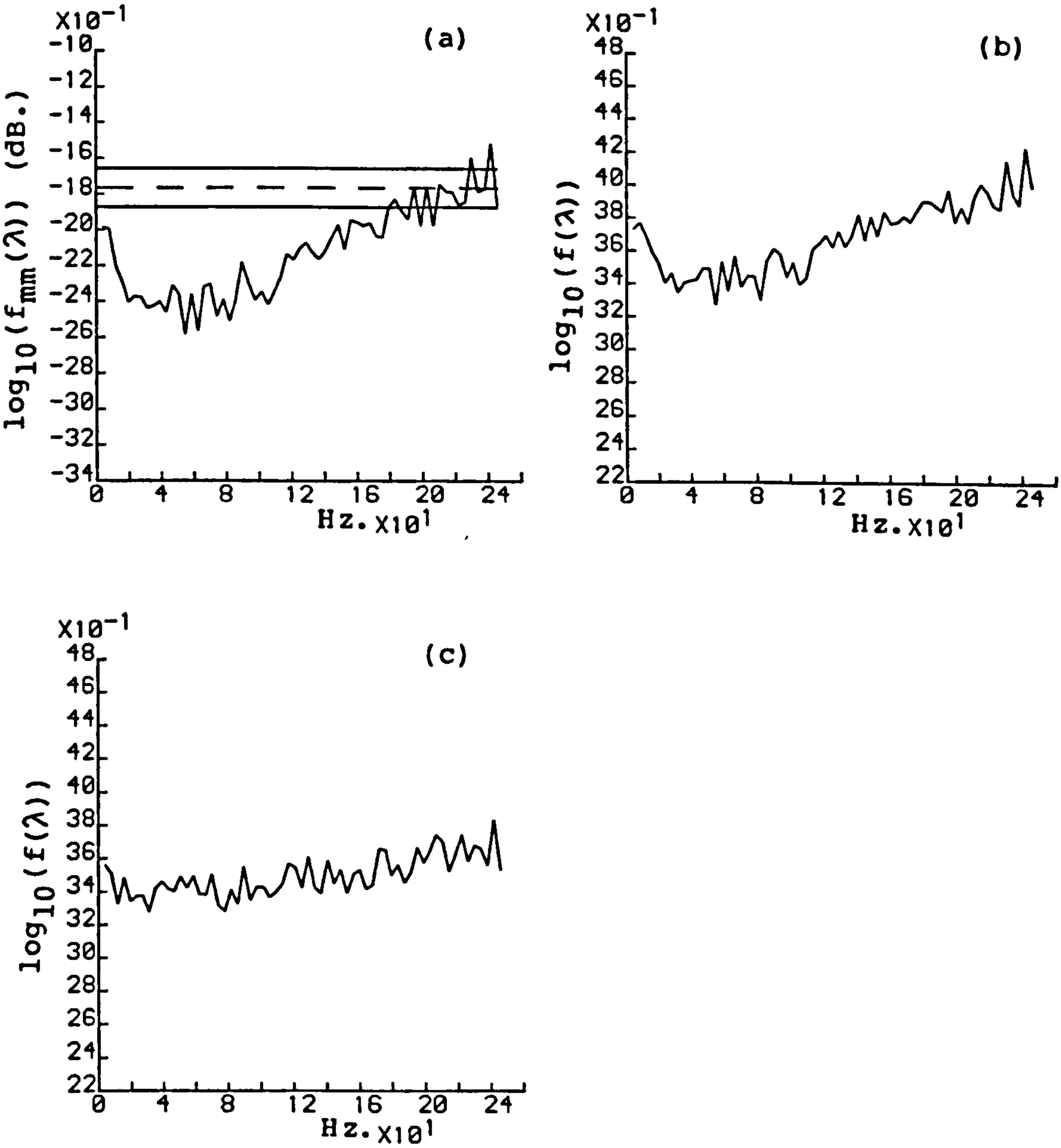

Fig. 3.3.3 (a) Point-process spectral estimate (2.3.29), T=512, for primary discharge with random fusimotor stimulation and random length disturbance applied.

(b) Estimate of autospectrum (3.2.6) for filtered spike-train with F_c=249 Hz..

(c) Estimate of autospectrum (3.2.6) for filtered spike-train with F_c=250 Hz..

3.4 SENSITIVITY OF FRENCH-HOLDEN FILTER TO CUT-OFF FREQUENCY

The value of F_c used for the estimate in figure 3.3.3b was not 250Hz. as suggested above, but was chosen as 249Hz.. Figure 3.3.3c shows the autospectrum estimate obtained when a value of 250Hz. is used in the filter. This estimate is almost completely flat and does not shows the expected deviation from its mean at lower frequencies. The reason for this can be explained by considering the French-Holden algorithm. Firstly we consider the result of equation (3.2.2) when the French-Holden filter sample occurs at the same time as a spike. Since the spike time is specified by an integer number of a sampling period, T_s, then :

$$t_i = j\,T_f = k\,T_s\ , \qquad (3.4.1)$$

where j is the number of the French-Holden sample being calculated and k is an integer specifying the spike time. Considering the two terms in (3.2.2) along with (3.2.3) gives :

$$2\,F_c\,t_i = j, \qquad (3.4.2)$$

$$SIN(2\pi F_c\,t_i) = SIN(j\pi) = 0 \text{ and} \qquad (3.4.3)$$

$$j-2\,F_c\,t_i = 0. \qquad (3.4.4)$$

Therefore whenever a French-Holden filter sample occurs at the same time as a spike then the contribution from this spike to that filter sample cannot be determined. Since the period of oscillation of the sinc function is the same as the filter sampling interval then this spike will also have zero contribution to any other sample in the filter. More generally if the relationship between T_f and T_s can be written as :

$$T_f = m/n\,T_s \quad \text{or alternatively} \quad F_c = n/m\,F_n, \qquad (3.4.5)$$

where m and n are both integers and F_n is the Nyquist frequency of the original data set, then from (3.2.3) and (3.4.2) :

$$SIN(2\pi F_c\ t_i) = SIN(\pi nk/m), \qquad (3.4.6)$$

where k is the integer specifying the time of the i^{th} spike. If nk/m is an integer then equation (3.4.6) equates to zero and it can be deduced that the filter sample has coincided with a spike and therefore its contribution to the filter output cannot be evaluated. If this particular condition occurs frequently enough while filtering a spike-train, then the filter output will not accurately represent the data set and this will be reflected in any spectral estimates as shown by figure 3.3.3c.

The example in figure 3.3.3c is a particular case of equation (3.4.5) where n=1 and m=2, giving $SIN(2\pi F_c\ t_i)$ $=SIN(\pi k/2)$. Therefore if k is even this expression equals zero and the contribution from this spike to the filter output will be lost. For the data sets being used here, which have a Poisson distribution of spike times, then the probability of k being even will be approximately 1/2. Therefore roughly 1/2 the spikes will not be correctly filtered and this is reflected in the spectral estimate shown in figure 3.3.3.c.

One reason for this problem may be that although each spike is specified as a multiple of a sampling period, T_s, it is treated as a delta function at the start of the interval by the algorithm. Any filter sample which then occurs in this sampling bin, because of this delta function, cannot be evaluated. This may be overcome by reducing the original sampling interval, Ts, but the digitised spike-train will always be specified as an integer multiple of some sampling period. Reduction of T_s may not

always be possible and if it is reduced sufficiently so that it is smaller than the width of the action-potentials being digitised then the shape of these spikes may affect spectral estimates. Since the point-process analysis is based on differential increments dN(t), the above problem is not encountered, and 1msec. sampling when digitising neuromuscular data has been found to provide satisfactory results for the point-process case. Priestly (1963) suggests that a point-process has an infinite frequency range, but in practice a finite sampling period is used to digitise a spike-train. If this interval is chosen so that not more than one spike occurs in each bin, then no aliasing will be present, and the digitised spike-train will now have a finite Nyquist frequency as defined in equation (3.3.1).

By careful choice of F_c, this problem in the French-Holden algorithm may be overcome as shown by the example in figure 3.3.3. For an F_c of 250Hz. then every spike which has an even value of k will not be correctly filtered, however if F_c is reduced to 249Hz. then only those spikes where k is a multiple of 250 will not be filtered. This represents less than 3% of all spikes in a typical data set and as can be seen from figure 3.3.3b this effect can be considered as negligible.

3.5 AN ALTERNATIVE METHOD OF FILTERING A SPIKE-TRAIN

Christakos et al (1984) suggest use of a low pass filter where the new sampling interval is always an integer multiple of the original sampling interval. Equation (3.2.3) can then be extended to $F_c=1/2mT_s$ where $T_f=mT_s$. The implementation suggested by Christakos et al is slightly different from the French-Holden algorithm. The sinc function which is convolved with each spike

and does the filtering is calculated once at multiples of T_s and stored in an array. Each time sample will fall on one of these sinc samples at T_s. This method is a special case of the more general method suggested by French and Holden. It may be useful if the condition above, where the new sampling interval is an exact multiple of the original interval, has to be satisfied because this condition can lead to problems in the French-Holden implementation. This method must always use a truncated sinc function, due to storage limitations. The effects of this truncation on spectral estimates are not known. This problem is not present if the full French-Holden implementation is used.

3.6 CONCLUSIONS AND RECOMMENDATIONS

Peterka et al (1974) consider aliasing for periodic spike-trains and recommend the rejection of the ten highest spectral components. The effect of varying F_c for the broad-band spectral estimates being considered here is shown in figure 3.6.1. The same data set as was used in figure 3.3.3 is used here with cutoff frequencies of 249, 149, and 49 Hz. used, the latter being within the area where the system still has an effect on the output. To achieve these results T_f is held constant and F_c varied independently. This requires the full implementation using both COS and SIN terms in the expansion of expression (3.2.1). Figure 3.6.1a demonstrates the very sharp cut-off obtained when using the French-Holden low pass filter, and shows also that the final residual asymptotic value is reached within a few ordinates of the cut-off frequency. Comparing the ratios of the final asymptotic values with that for F_c=249 Hz. gives values of 1/4000 and 1/100 respectively. Figure 3.6.1b is an expanded diagram of

the area of interest. Although the value of F_c is different the three traces are very similar in spectral content, showing that varying Fc does not introduce any distortion into these estimates. The two recommendations made by Peterka et al about the choice of F_c near a spectral component and rejection of the ten highest spectral ordinates would appear, from figure 3.6.1, not to be relevant in the case of broad-band spectra.

F_c should be chosen to be above any frequency components of interest and below the Nyquist frequency of the original data set. However figure 3.6.1 indicates that aliasing should not be a problem if Fc is chosen within the spectral range of the system. Any proposed choice of F_c (and thus T_f) should therefore be related to the original sampling period T_s, since it has been shown how poor results can be obtained if this point is neglected.

The output of the French-Holden filter is a series of equispaced samples which can be considered as a conventional time-series. Thus the periodogram of this series (3.2.5) at a frequency λ can be interpreted as being proportional to the squared amplitude of a sinusoidal component of the same frequency in the filtered spike-train. The similarity between the spectral estimates in figures 3.3.1a and 3.3.1b and figures 3.3.3a and 3.3.3b show that, apart from a constant term, the distribution of the spectral power is the same over the range of interest in each example. This constant offset may be due to the transfer function of the French-Holden filter, which in the frequency domain will be a constant rectangular function. The periodogram of a point-process representation of a spike-train and the periodogram of a filtered spike train extract similar information from the data, illustrating the equivalence of the two methods if

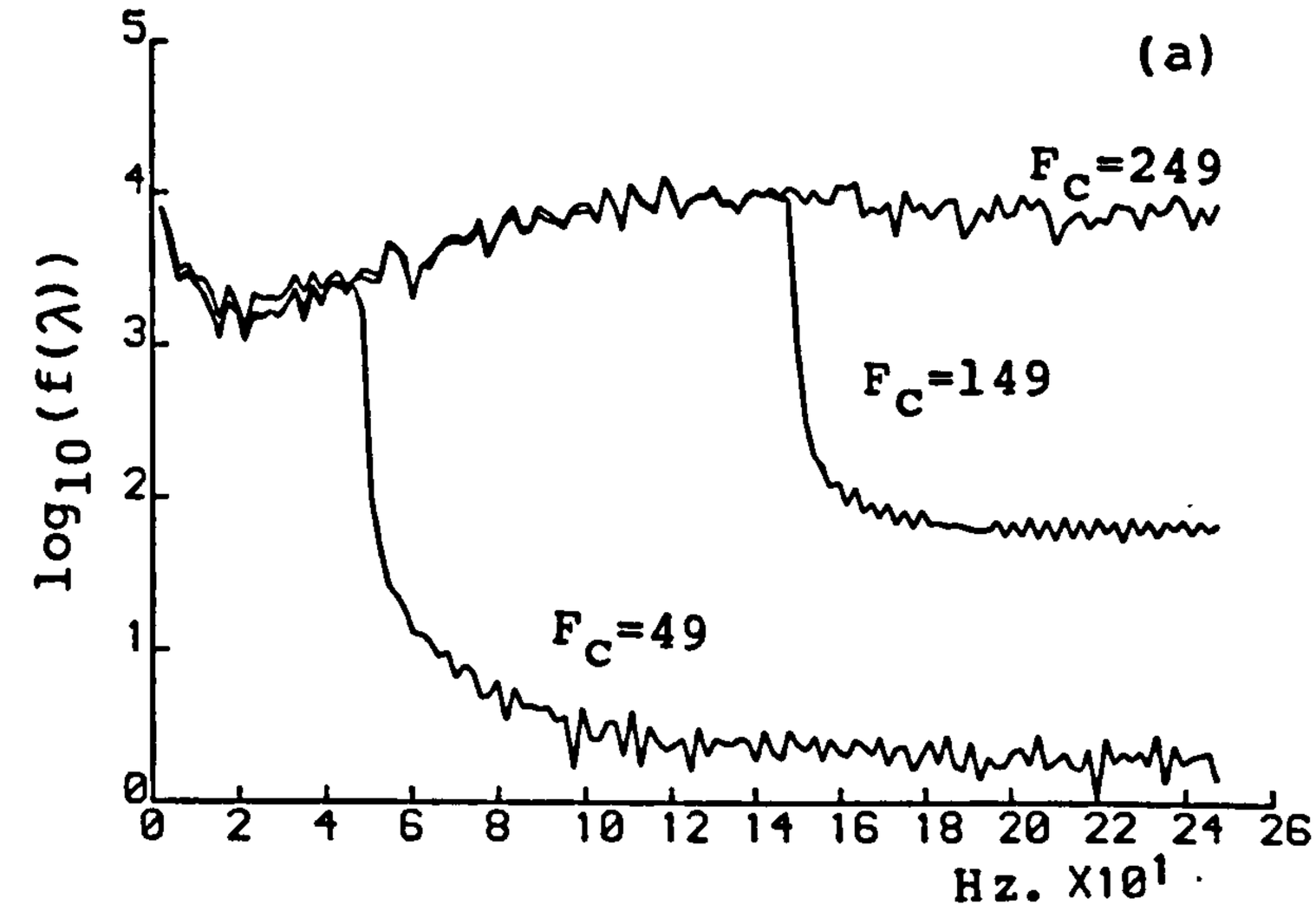

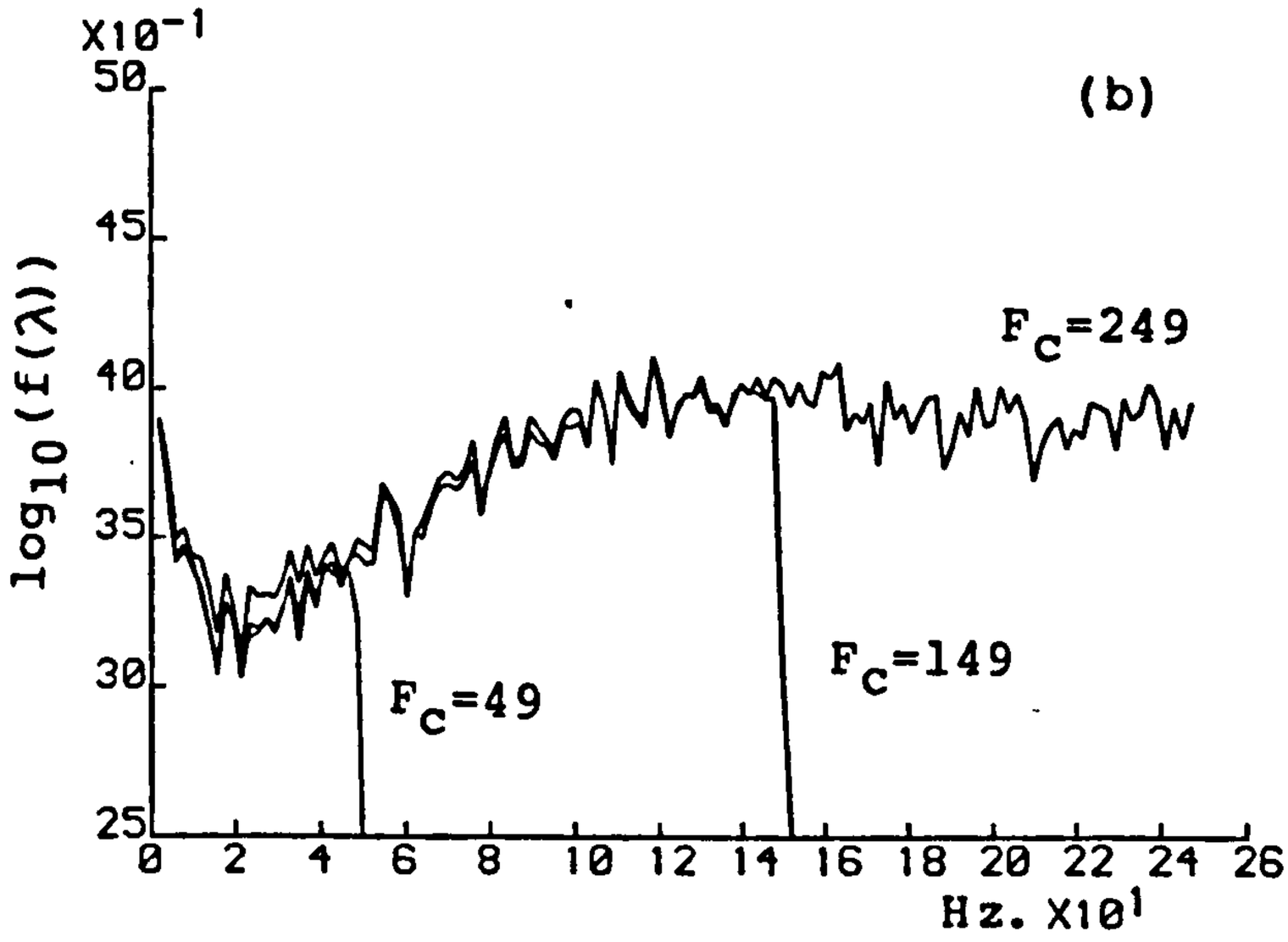

Fig. 3.6.1 (a) Effect of varying filter cut-off frequency on autospectral estimates of filtered spike-train for random fusimotor and random length disturbance. F_c=249, 149 and 49 Hz.

(b) Enlargement of 3.6.1(a)

the spike-train is correctly filtered.

The French-Holden algorithm can be used to reconstruct a data set by filtering and using a larger sampling interval. This will give increased frequency resolution at a cost of less data points available for the analysis, and this in turn will lead to more noisy spectral estimates due to having fewer periodograms to average. A similar effect can be obtained with the point-process analysis by increasing the length of each periodogram in the estimate. Thus an increase in the length of the data set is required to increase the frequency resolution without degrading the quality of the spectral estimates in both the point-process and French-Holden analysis.

The computational time to implement the full French-Holden algorithm (summing every spike for each sample) is very long when compared with the point-process spectral estimates. If only the most relevant spikes for each sample are used, large savings can be made in computational time. Even this would make it a difficult process to implement on-line, requiring low spike rates and a small number of filter samples. The effect on spectral estimates of not summing all the spikes is not known, but from comparisons made with point-process spectra, differences appear to be very small and occur only at frequencies above 450Hz. which is outside the area of interest.

Initial studies using periodic data showed that French-Holden filtering is a useful technique for regularly firing spike-trains and data sets with strong periodicities, providing a useful means of data compression. Fewer filter samples are required to give good autospectral estimates and in some cases the method can be quicker than the corresponding point-process analysis. However this is only true for periodic spike-trains,

the more general broad-band nature of other data sets requiring the maximum possible number of filter samples to achieve comparable results with point-process spectra.

The French-Holden spectral estimates do not appear to yield any more information when compared with the point-process estimates. This factor, when combined with the extra computational load, the sensitivity to the choice of F_c, and the lack of simple statistical properties for the French-Holden method recommends the point-process approach for spectral estimates of neuronal spike-trains.

CHAPTER FOUR

4.1 INTRODUCTION

Having shown in chapter three the advantage of the point-process approach, in terms of computational load and statistical properties, over the more conventional filtering and sampled data techniques, in the analysis of spike-train data, other uses of stochastic point-process parameters will now be studied. As well as the specific case of system identification, point-process parameters can also be used in the analysis of general neurophysiological spike-train data. In particular the detection of a connection between two neuronal spike-trains will be discussed, along with the detection of single frequencies in a point-process representation of spike-train data. A method for the study of connections between multiple spike-trains will be introduced. The study of the muscle spindle response to a particular type of fusimotor input will be used to demonstrate the speed with which results can be obtained from a single experiment by probing a point-process system with a Poisson spike-train and using point-process parameters to analyse the results.

4.2 MEASURES OF ASSOCIATION BETWEEN SPIKE-TRAINS

A common problem encountered in physiology is the detection of functional connections between pairs of neurones. This occurs in many different experimental studies and can be considered as the measurement of the degree of association between two point-processes. Unlike the identification procedure introduced in chapter 2, the two spike-trains will not in general be the input and output for a particular element of the neuromuscular system, but will be two neuronal discharges recorded simultaneously during an experiment. The problem is the detection of any

connection between the two neurones and the determination of the strength of this connection. Measures of association have been proposed in both the time and frequency domain.

In the time domain the most commonly used measure of association is the peristimulus time histogram (PSTH) which is widely used by physiologists (see for example, Bryant et al, 1973; Ellaway et al, 1976 and Kirkwood, 1979). For two point-processes M and N this is the same as the histogram estimate $J_{NM}^{T}(u)$ in equation (2.3.8). However this quantity on its own should not be used since, from equation (2.3.9) it is a biased estimate of the second order cross-product density. Comparison between two PSTH estimates with either different record lengths or bin widths will not be possible. Instead of using the PSTH, the normalised estimate (2.3.11) of the cross-intensity function will be used allowing comparison between different estimates. Using the expression (2.3.21) for the variance of the square root of this estimate to construct confidence intervals as explained in section 2.3 will allow any dependence to be shown by deviation outside these limits. Dependence of one process upon another at positive or negative lag values will indicate the direction of the coupling between the neurones.

Two alternative measures of association, one in the frequency domain, and one in the time domain, have also been proposed. In the time domain, the cusum (cumulative sum technique) has been used to detect changes in the mean level of the PSTH which may be obscured by background fluctuations (Ellaway, 1977). The cusum is formed directly from the PSTH as the sum of the deviations of the count in each bin of the estimate $J_{NM}^{T}(u_j)$ from the mean level. This can be expressed as :

$$S_i = \sum_{j=1}^{i} (J_{NM}^{T}(u_j) - \bar{m}), \qquad (4.2.1)$$

where the mean level, $\bar{m}$, can be approximated from the expected value of the estimate $J_{NM}^{T}(u_j)$ in (2.3.9), and asymptotic distribution (2.3.14) as :

$$\bar{m} = \hat{P}_n \; h \; M(R), \qquad (4.2.2)$$

where R is the record length, and h is the bin width. An expression for the variance can be constructed based on the assumption of a Poisson distribution of counts in a control period of n counts (i.e. n negative lag values in $J_{NM}^{T}(u_j)$) and is written as (Ellaway et al, 1983) :

$$\begin{aligned} \text{Var}\{ S_i \} &= i/n \; (i-n) \; m \qquad \text{for } i>n, \\ \text{Var}\{ S_i \} &= i/n \; (n-i) \; m \qquad \text{for } i<n, \end{aligned} \qquad (4.2.3)$$

where m is defined in (4.2.2). This will allow 95% confidence intervals to be constructed for the cusum estimate (4.2.1) by adding ± 1.96 standard deviations to the null value zero. Taking $\bar{m}$ to be equal to the asymptotic distribution of the PSTH gives a cusum of zero slope. Any dependence of one process upon another will be indicated by a change of slope in the cusum leading to a deviation outside the confidence limits. A positive slope will indicate a facilitation effect, a negative slope will indicate an anti-facilitation or inhibitory effect of one process upon another.

In the frequency domain, the coherence can be used to determine if there is a linear dependence of one process upon another (Brillinger et al, 1976). The coherence is defined in (2.4.10), and an estimate is given in (2.5.10). Instead of looking for a broad range of significant values to indicate the

validity of the linear model, a significant coherence value at a single frequency will indicate coupling between the processes at that frequency. The coherence also has the advantage that the strength of coupling can be determined on an absolute scale from zero to one, with zero occurring in the case of independence. Directional information can be obtained from the phase of the cross-spectrum estimate (2.3.31), and this can be used to estimate the time delay between the two processes at each frequency which has a significant coherence value. The coherence, like the cusum, is also derivable from the PSTH if the spectral estimates are considered in terms of the Fourier transform of the auto- and cross-covariance density functions.

These three methods will be applied to the same data set in order to determine the relative merits of each estimate. In particular varying the length of record used will allow the sensitivity of each measure to be determined, along with the minimum record length required to detect coupling between spike-trains. The data set consists of 60 seconds of signals recorded from two spontaneously firing fusimotor neurones. The PSTH, cusum and coherence were estimated for records of length 10, 15, 30 and 60 seconds from this data set. Figures 4.2.1, 4.2.2 and 4.2.3 show the PSTH (normalised to form the cross-intensity function), cusum and coherence estimates for each record length respectively. The cusum is more sensitive than the PSTH, although the coherence is more sensitive than either of these two measures. The coherence can detect coupling with records as short as 10 seconds, whereas the two time domain measures require approximately 60 seconds to detect a connection between the neurones.

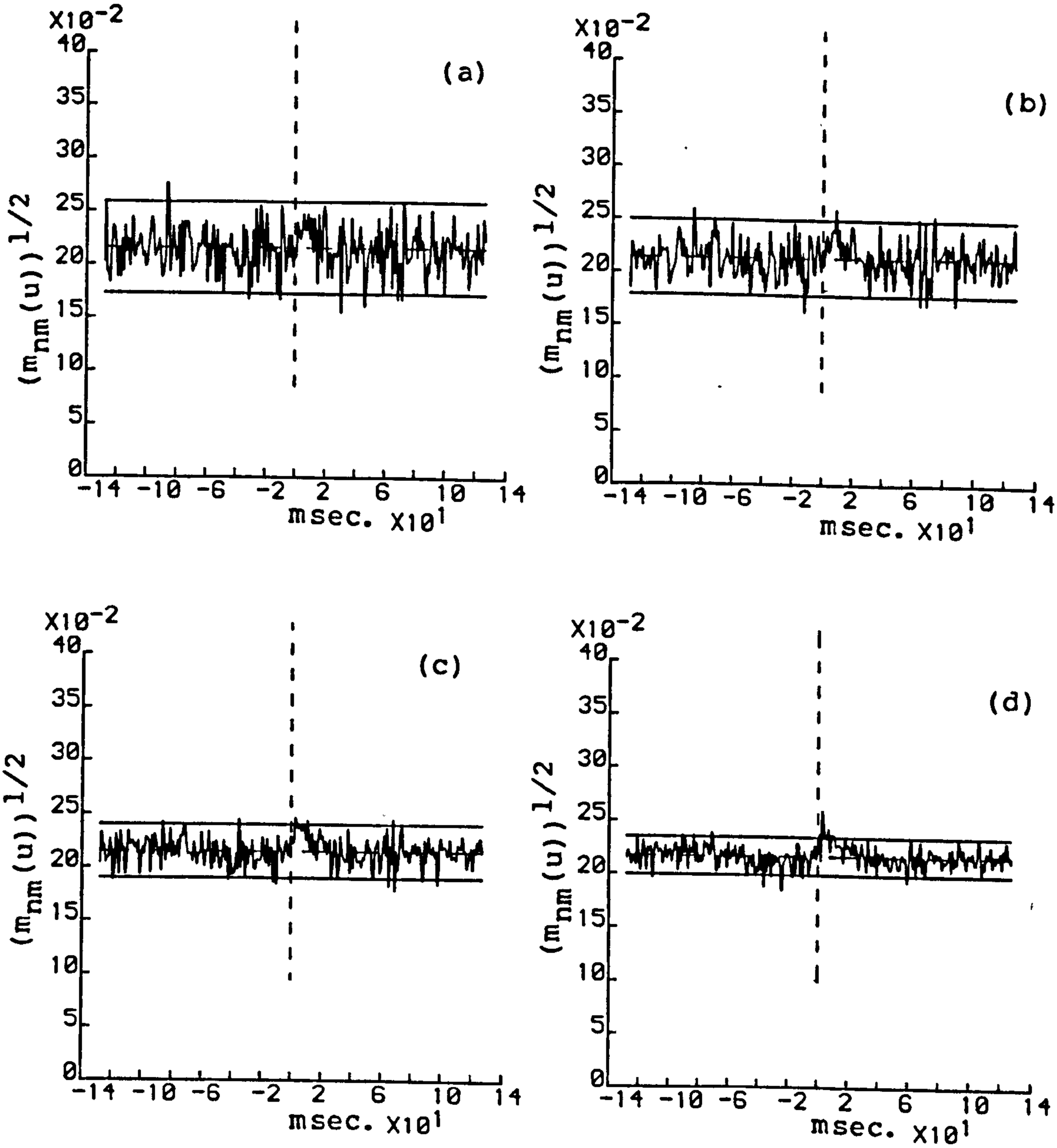

Fig. 4.2.1 Cross-intensity estimate (2.3.11) for two spontaneously firing fusimotor neurones using record length of

(a) 10,

(b) 15,

(c) 30 and

(d) 60 seconds.

Dashed lines show estimate of asymptotic distribution, solid lines indicate approximate 95% confidence band.

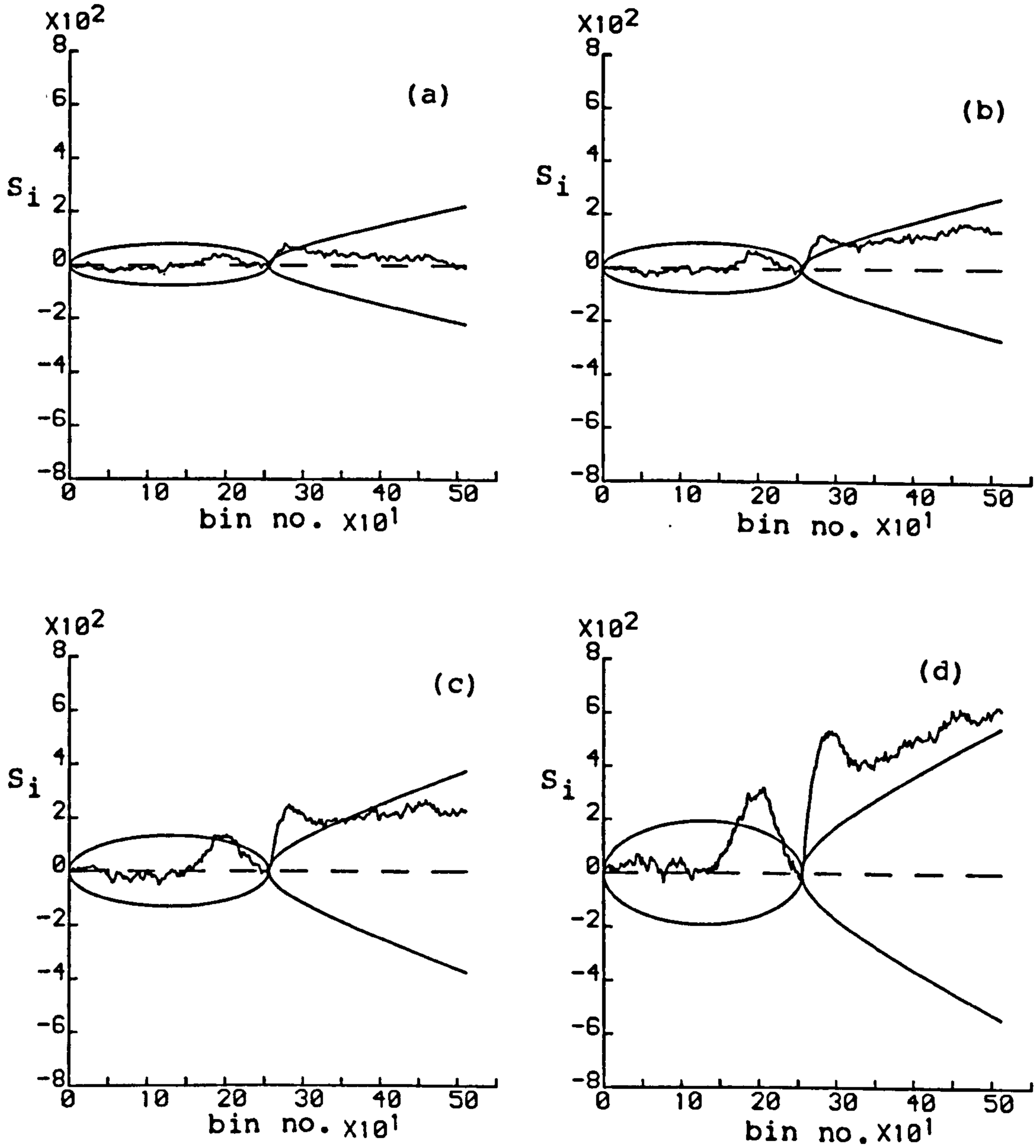

Fig. 4.2.2 Cusum estimate (4.2.1) for two spontaneously firing fusimotor neurones using record length of

(a) 10,

(b) 15,

(c) 30 and

(d) 60 seconds.

Solid lines indicate approximate 95% confidence band.

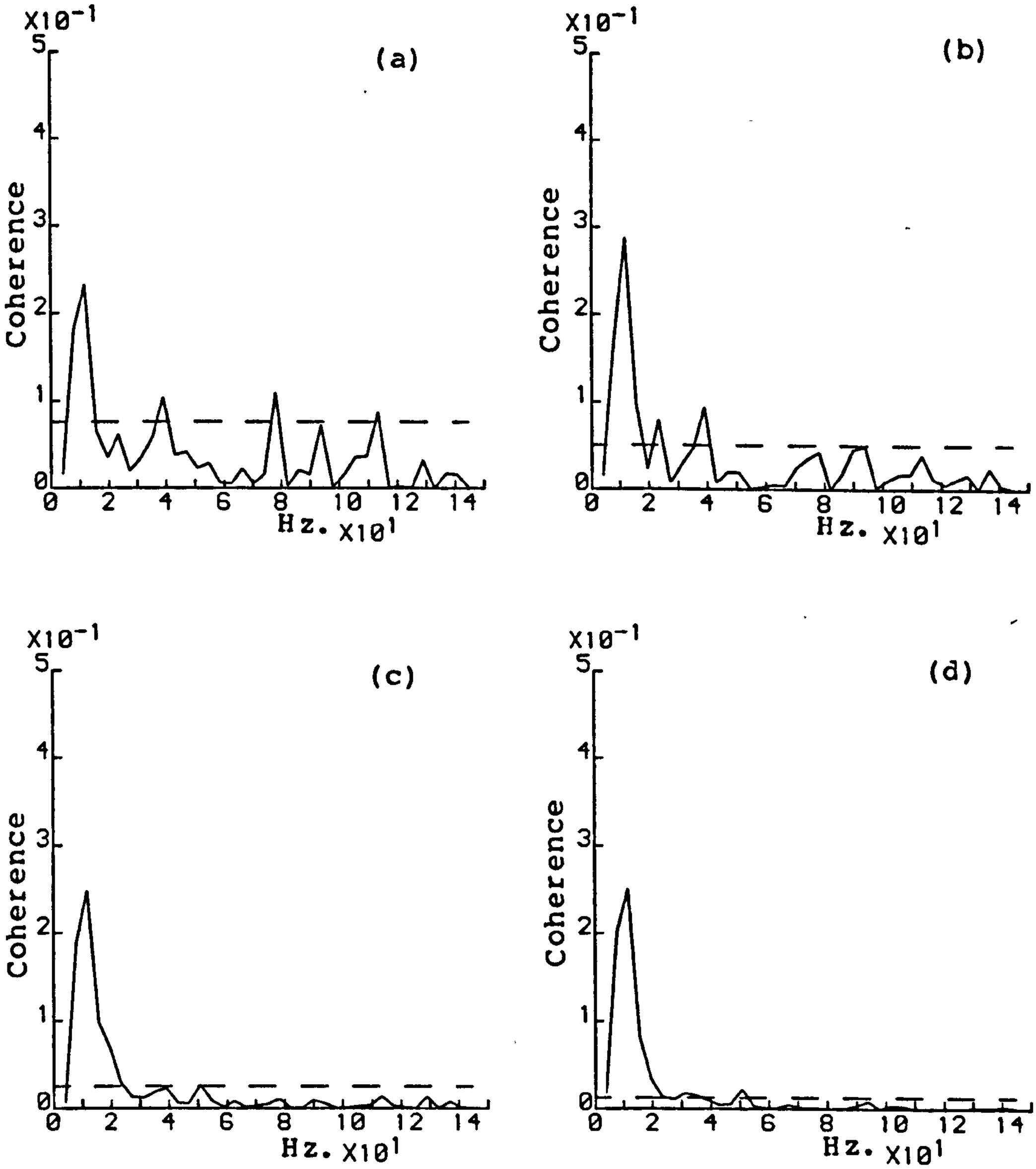

Fig. 4.2.3 Coherence estimate (2.5.10) for two spontaneously firing fusimotor neurones using record length of

(a) 10,

(b) 15,

(c) 30 and

(d) 60 seconds.

Dashed lines indicate approximate 95% confidence limit.

This increased sensitivity is especially useful when dealing with physiological systems, since stationarity is an important consideration, and one method of overcoming this problem is to use shorter record lengths. This can be illustrated with another example using a data set recorded from two different fusimotor neurones and which was subsequently found to contain a non-stationarity. Sixty seconds of data was recorded and split into consecutive 15 second segments. The cusum and coherence for each segment were estimated and are shown in figures 4.2.4 and 4.2.5 respectively. The cusum estimates are all very similar, but the coherence estimates have clear differences in the areas of significance, due to the non-stationarity in the data.

The increased sensitivity, along with the absolute scale of measurement, of the coherence compared to the time domain measures recommends the use of the coherence to determine the presence and strength of any coupling between spike-trains.

4.3 DETECTION OF SINGLE FREQUENCIES IN POINT-PROCESS DATA

As well as the measurement of association between spike-trains, the coherence can also be used to detect coupling at single frequencies. This is particularly useful if an external signal consisting of a single fixed frequency is being applied to the system. The problem then becomes the detection of a single fixed tone in a point-process representation of a spike-train, and since this will be indicated by isolated peaks in the spectral estimates then the question of frequency resolution must be considered. Previous spectral estimates have been based on the periodogram of a point-process (2.3.29) and (2.3.31), and have used a periodogram length of 256 or 512 samples. The minimum frequency which the periodogram can resolve, which is also the

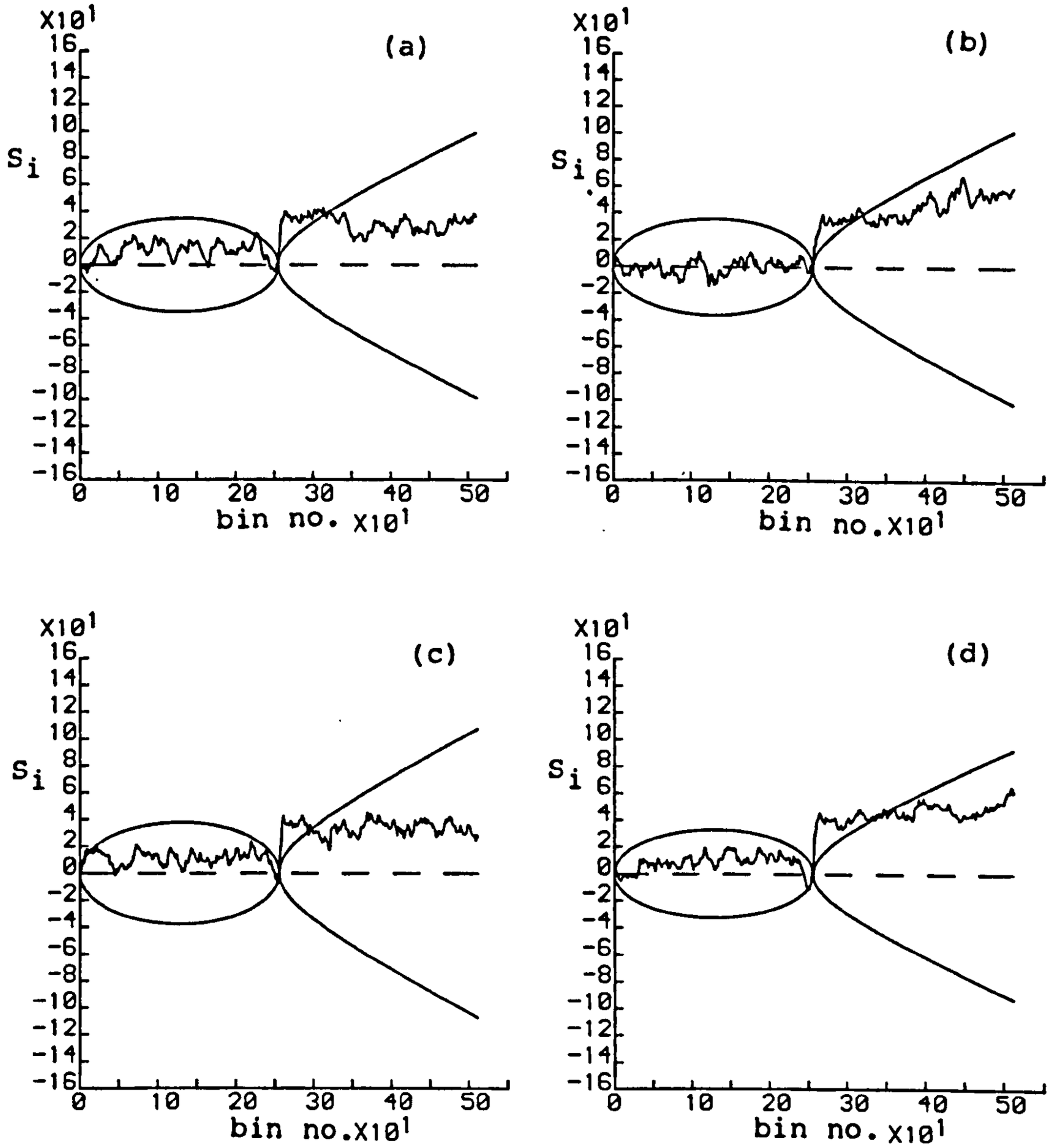

Fig. 4.2.4 Cusum estimate (4.2.1) for two spontaneously firing fusimotor neurones containing non-stationarity and estimated from

(a) 0 to 15,

(b) 15 to 30,

(c) 30 to 45 and

(d) 45 to 60 seconds.

Solid lines indicate approximate 95% confidence band.

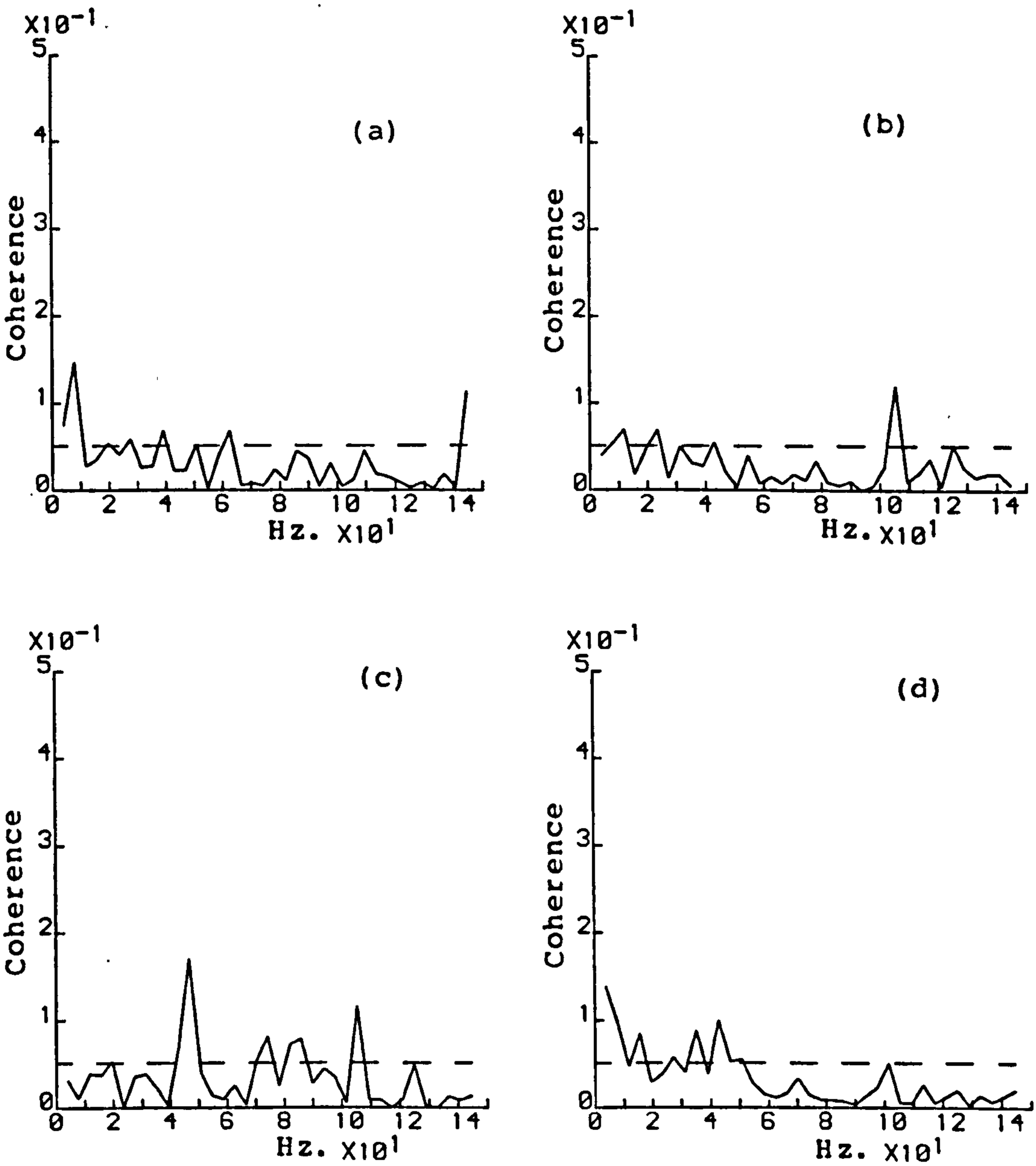

Fig. 4.2.5 Coherence estimate (2.5.10) for two spontaneously firing fusimotor neurones containing non-stationarity and estimated from

(a) 0 to 15,

(b) 15 to 30,

(c) 30 to 45 and

(d) 45 to 60 seconds.

Dashed lines indicate approximate 95% confidence limit.

frequency resolution of the estimate, is given by :

$$f_r = 1/T\ T_s, \qquad (4.3.1)$$

where T is the number of samples in the periodogram and T_s is the sampling interval used to convert the spike-train to a point-process, 1msec.. Using these values gives a frequency resolution of 3.9 Hz. for T=256. The frequency resolution can be altered by changing the periodogram length in the estimates (2.3.29) and (2.3.31), and the resolution will change according to (4.3.1).

To study the effect of resolution on point-process spectral estimates a data set has been analysed at different values of resolution. The data consists of 60 seconds of signals recorded from two spontaneously discharging neurones, with a mechanical vibration signal of approximately 30 Hz. applied externally to the skin close to the region where the recording was made. The objectives here were to determine if the vibration signal could be detected in the spectral estimates, and if the single frequency of the vibration could be resolved. Figure 4.3.1 shows coherence estimates for the two spike-trains using periodogram lengths of 256, 512, and 1024 in the spectral estimates (2.3.29) and (2.3.31). This gives a spectral resolution of 3.9, 2.0 and 1.0 Hz. respectively. The coherence estimates in figures 4.3.1a and 4.3.1b do indicate coupling in the region of 30 Hz., but the nature of these peaks does not suggest that this is due to coupling at a single frequency. The estimate in figure 4.3.1c has a sharp peak indicating significant coupling between the neurones at this single frequency, as well as weaker coupling over a broader range of lower frequencies. The frequency of this coupling is 32 Hz., and this can also be detected in the autospectra of the individual spike-trains. Figure 4.3.1d shows

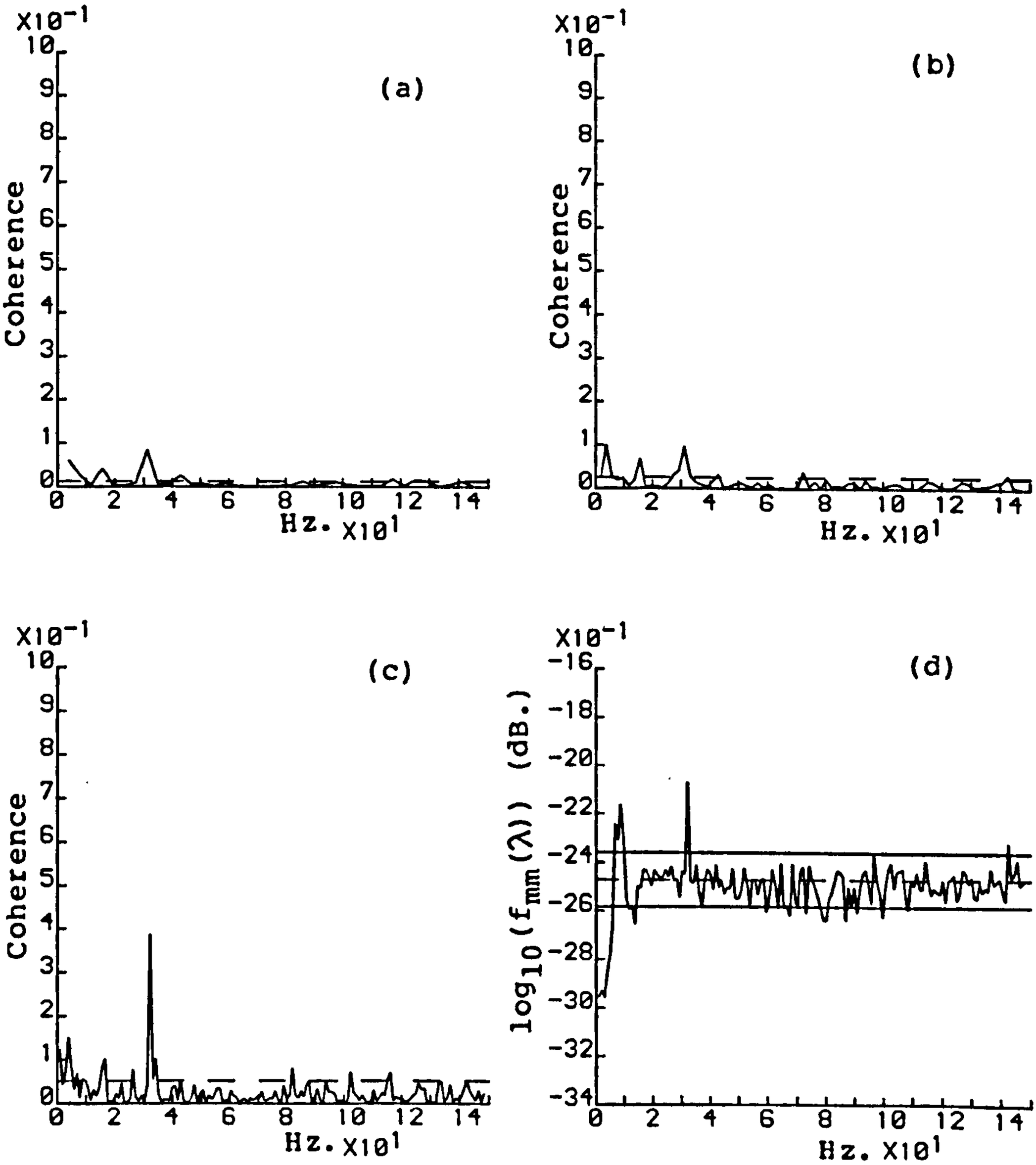

Fig. 4.3.1 Coherence estimate (2.5.10) for two spontaneously firing neuronal discharges subject to mechanical vibration with R=60000, and (a) T=256,

(b) T=512 and

(c) T=1024 in spectral estimates (2.3.29) and (2.3.31). Dashed lines indicate approximate 95% confidence limit.

(d) autospectral estimate (2.3.29) with T=1024. Dashed line indicates asymptotic distribution, solid lines 95% confidence band.

the autospectral estimate of one of the discharges and again the peak at 32 Hz. can be seen indicating the presence of a strong periodicity at this frequency.

This example illustrates that detetction of single tones in point-process spectral estimates requires a frequency resolution of around 1.0 Hz.. As a consequence of increasing the periodogram length, the value of K in equation (2.3.28) decreases resulting in fewer periodograms to average to form spectral estimates and leading to larger variances and noisier estimates. Shorter record lengths also lead to smaller values of K, and for a periodogram length of 1024 samples approximately 60 seconds of data is needed to produce sufficient smoothing in the spectral estimates. If the data set is shorter than this, then other forms of smoothing, such as Hanning, may be required, but these tend to decrease the ability to resolve single frequencies out of the spectral estimates.

Although the coherence can detect coupling, it does not give any indication of whether this coupling is due to the effect of a common input, which is the case here. To determine whether apparent coupling between neurones is due to an actual connection, or due to the effect of a common input, a measure called the Partial Coherence must be used.

4.4 PARTIAL COHERENCE

Partial Coherence deals with three simultaneously recorded spike-trains, A, B and C (Brillinger 1975b, c; Brillinger et al 1976). If the normal coherence estimates show that there is a connection between A and B, A and C and between B and C, then in some circumstances it may be of physiological significance to

determine if B and C are truly connected by some mechanism, or whether the observed connection is due wholly or in part to the common influence of spike-train A. Using N_b and N_c to denote the differential counting increments of processes B and C respectively, this relationship between A, B and C can be written as :

$$\begin{aligned} N_b &= N_{bb} + N_{ba} \\ N_c &= N_{cc} + N_{ca} \quad , \end{aligned} \tag{4.4.1}$$

where the increments N_{ba} in process B and N_{ca} in process C have a common dependence on the process A, and the pair N_{bb} and N_{cc} are independent of the increments N_{ba} and N_{ca} and of the process A. The coherence between the increments N_{bb} and N_{cc} is defined as (Brillinger, 1975b) :

$$\left| R_{ab.c}(\lambda) \right|^2 = \frac{\left(R_{bc} - R_{ab}\, R_{ac} \right)^2}{\left(1 - \left| R_{ab} \right|^2 \right)\left(1 - \left| R_{ac} \right|^2 \right)} \quad , \tag{4.4.2}$$

this is also known as the partial coherence between the processes B and C, which statistically subtracts out any common effect due to process A. The frequency index in the R.H.S. of (4.4.2) has been missed out, and all the terms are formed by combinations of the normal coherence estimates, or the square root of these estimates, between the processes A, B and C. The partial coherence is estimated by substituting estimates (2.5.10) of the normal coherence into expression (4.4.2).

The partial coherence, like the normal coherence, has values between zero and one, with zero occurring when the apparent connection between processes B and C is through the increments N_{ba} and N_{ca}. Partial coherence provides a powerful tool for the analysis of multiple spike-trains, since it allows models of

interconnectivity within elements of the neuromuscular system to be built up. This leads to a greater understanding of how communications pathways are formed. Several data sets will be used to demonstrate the use of the partial coherence function.

The first example uses two data sets recorded from discharging neurones in the common leech (Hirudo Medicinalis). Three neurones in close proximity were isolated and two recordings made. The first of these is a record of the spontaneous activity, the second record is of the discharges when random pulses were injected into the nerve cell body. These records are 30 and 60 seconds long respectively giving three and four spike-trains to analyse using coherence and partial coherence techniques. The three outputs will be called processes 1, 2 and 3, and the input in the second record will be called process 0. Figure 4.4.1 shows estimates of the coherence between each of the three spontaneous spike-trains. Clearly from this figure no connection exists between any of these neurones, so partial coherence analysis is not required in this case.

Stimulation with the random input pulses changes this situation however, as the three plots in figure 4.4.2 illustrate. These are the coherence estimates for the same three pairs, and all now exhibit a weak coupling at low frequencies, showing that the current pulses have an effect on the three discharges. Since there is now an apparent connection between the outputs, it might be assumed that there will now be some coupling between the input and the three outputs. The coherence estimates for the three possible connections between the input and each of the outputs are shown in figure 4.4.3. These estimates show that there is no connection between the input and any of the outputs. Thus it can

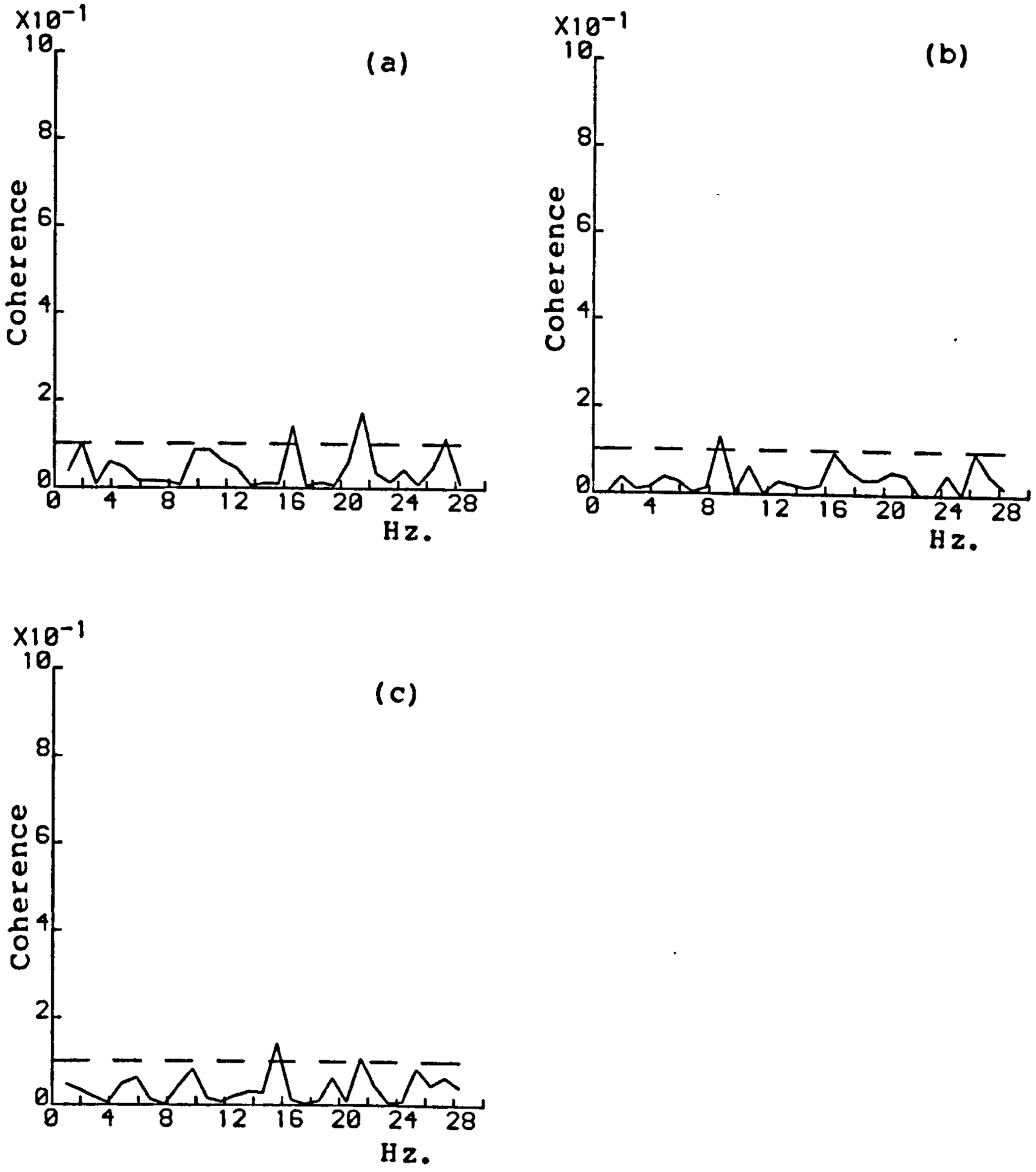

Fig. 4.4.1 Coherence estimates (2.5.10) for three spontaneously discharging neurones (processes 1, 2 and 3). R=30000, T=512 in (2.3.29) and (2.3.31).

(a) Coherence estimate between processes 1 and 2,

(b) 1 and 3 and

(c) 2 and 3.

Dashed line indicates approximate 95% confidence limit.

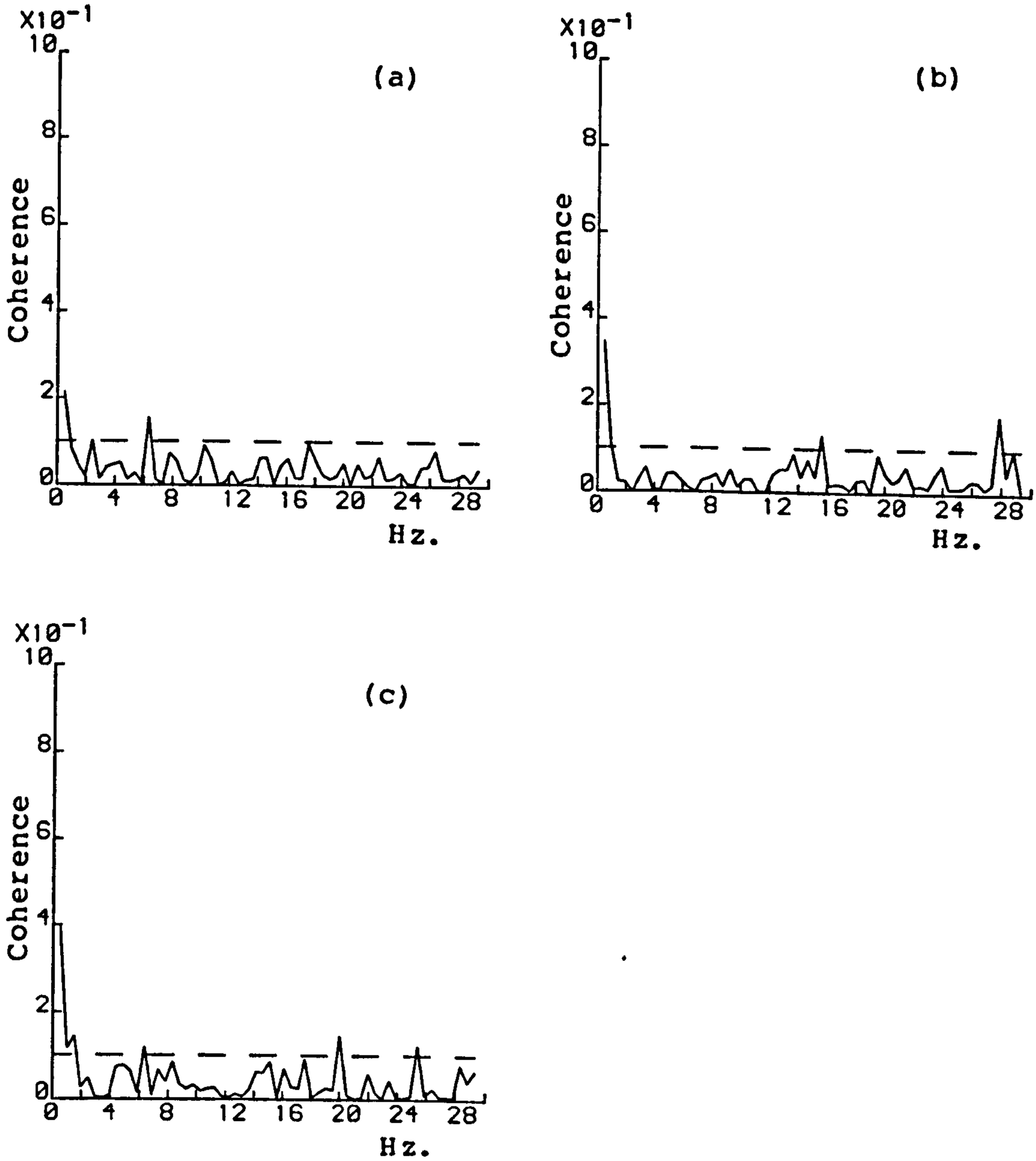

Fig. 4.4.2 Coherence estimates (2.5.10) for three spontaneously discharging neurones (processes 1, 2 and 3) in presence of random input (process 0). R=60000, T=1024 in (2.3.29) and (2.3.31).

(a) Coherence estimate between processes 1 and 2,

(b) 1 and 3 and

(c) 2 and 3.

Dashed line indicates approximate 95% confidence limit.

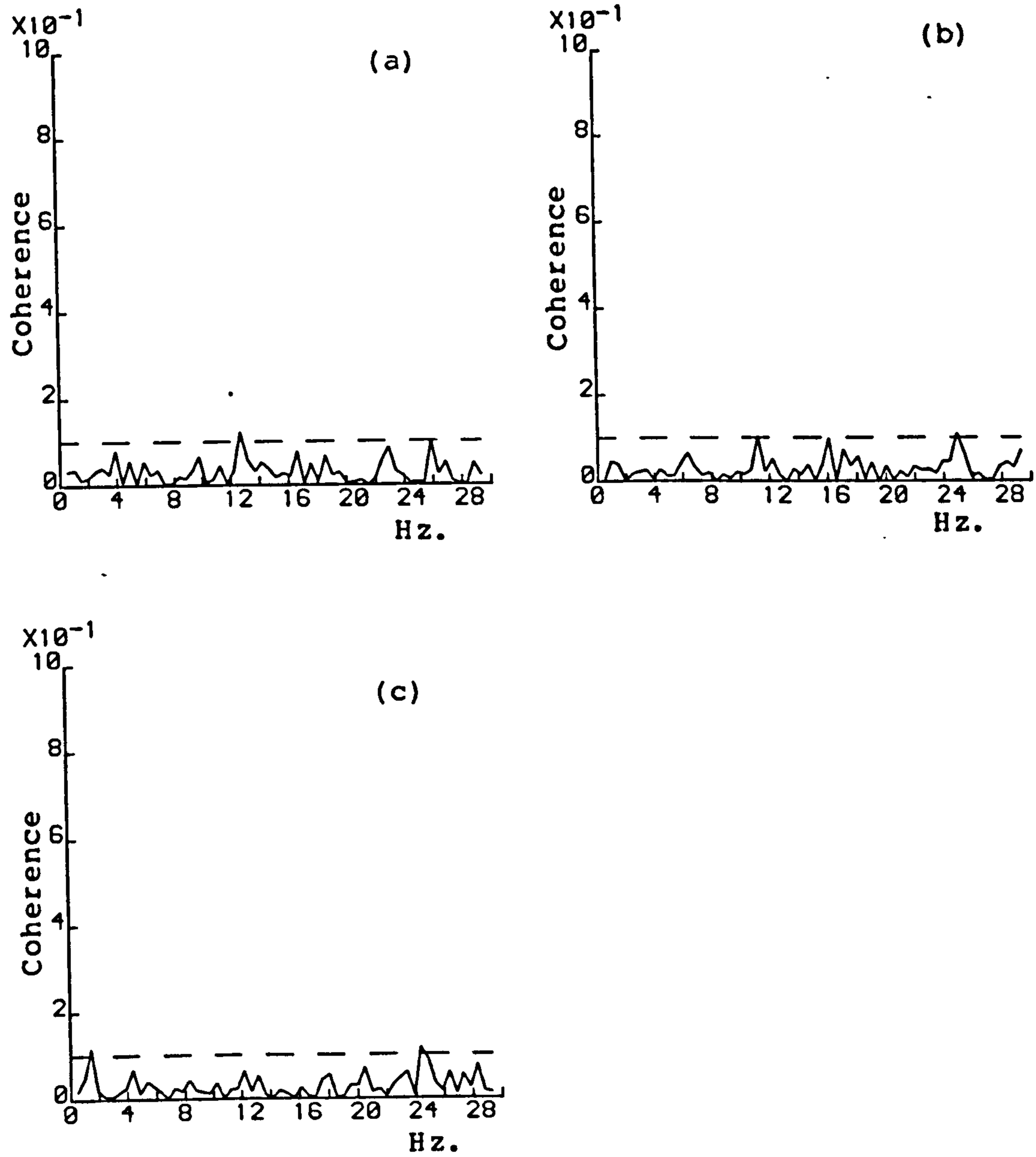

Fig. 4.4.3 Coherence estimates (2.5.10) for three spontaneously discharging neurones (processes 1, 2 and 3) in presence of random input (process 0). R=60000, T=1024 in (2.3.29) and (2.3.31).

(a) Coherence estimate between processes 0 and 1,

(b) 0 and 2 and

(c) 0 and 3.

Dashed line indicates approximate 95% confidence limit.

be concluded that the effect of the input is to form a connection between each of the three output pairs of neurones. This is as far as the analysis can be taken using conventional coherence techniques, any further analysis of the connections between the three neurones requires the use of partial coherence estimates.

There are two sets of partial coherence estimates that could be considered here. These are the partial coherences between each of the three possible pairs of outputs treating either the input or the third output as the common factor in each case. Since there is no connection between the input and any of the outputs, then it would be surprising if the partial coherence estimates which treat the input as the common influence are different from the three coherence estimates in figure 4.4.3. This was found to be the case, and each of the three partial coherence estimates $|R_{12.0}|^2$, $|R_{13.0}|^2$ and $|R_{23.0}|^2$ are identical to the corresponding coherence estimates in figure 4.4.3 indicating that the coupling between each of the output pairs is not due to the common influence of the input.

The other set of partial coherence estimates are shown in figure 4.4.4, and from these it can be concluded that, in the presence of the input, the coupling between processes 1 and 2 is entirely due to the common effect of process 3, and the coupling between processes 1 and 3 and processes 2 and 3 is due only in part to the common effect of process 2 and process 1 respectively.

Although no direct connection is formed between the input and the outputs, in the presence of the input, connections are formed between all of the three output process pairs. These connections can be accounted for in part by the common effect of the third output in two of the three cases, in the third case the

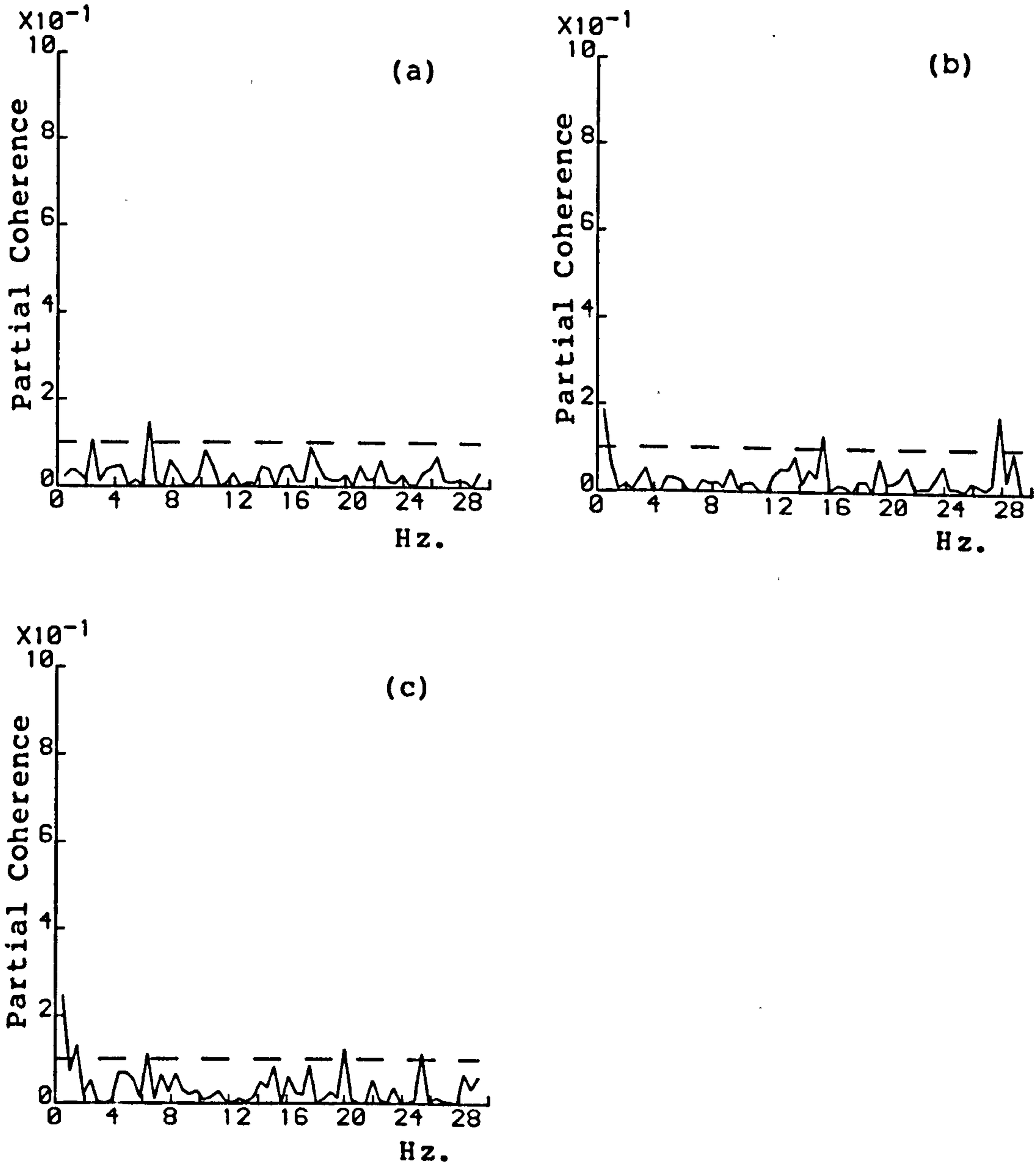

Fig. 4.4.4 Partial coherence estimates (4.4.2) for three spontaneously discharging neurones (processes 1, 2 and 3) in presence of random input (process 0). R=60000, T=1024 in (2.3.29) and (2.3.31).

(a) Partial Coherence estimate between processes 1 and 2 / (3),

(b) 1 and 3 / (2) and

(c) 2 and 3 / (1).

Dashed line indicates approximate 95% confidence limit.

apparent connection is due entirely to the common influence of the third output spike-train. These conclusions could not have been reached without the use of partial coherence functions.

The second example illustrating the use of partial coherence uses a data set from a single muscle spindle, where both the primary and secondary discharges were available. The spontaneous activity in each neurone was recorded, and then a random fusimotor input applied and the resultant primary and secondary responses recorded. No connection between the primary and secondary existed during the spontaneous activity as revealed by the coherence. Applying the fusimotor input showed that there were connections between that input and primary, between that input and secondary and between primary and secondary. The coherence estimates for these are shown in figure 4.4.5. Further analysis of these apparent connections requires the use of partial coherence, and the relevant estimates are shown in figure 4.4.6. From these it can be deduced that a connection exists between the fusimotor and the primary, however the apparent coupling between input and secondary is due almost entirely to the common effect of the primary. This is surprising, since it indicates that the apparent coupling between the input and one output is due to the common effect of the second output. The third partial coherence estimate in figure 4.4.6c shows that the coupling between primary and secondary is partly due to the common effect of the fusimotor input, and partly due to a weak connection between the two outputs. This weak connection is caused by the application of the fusimotor input, but is not due to the common effect of this input.

The conclusions reached about these two examples could not have been obtained without the use of partial coherence

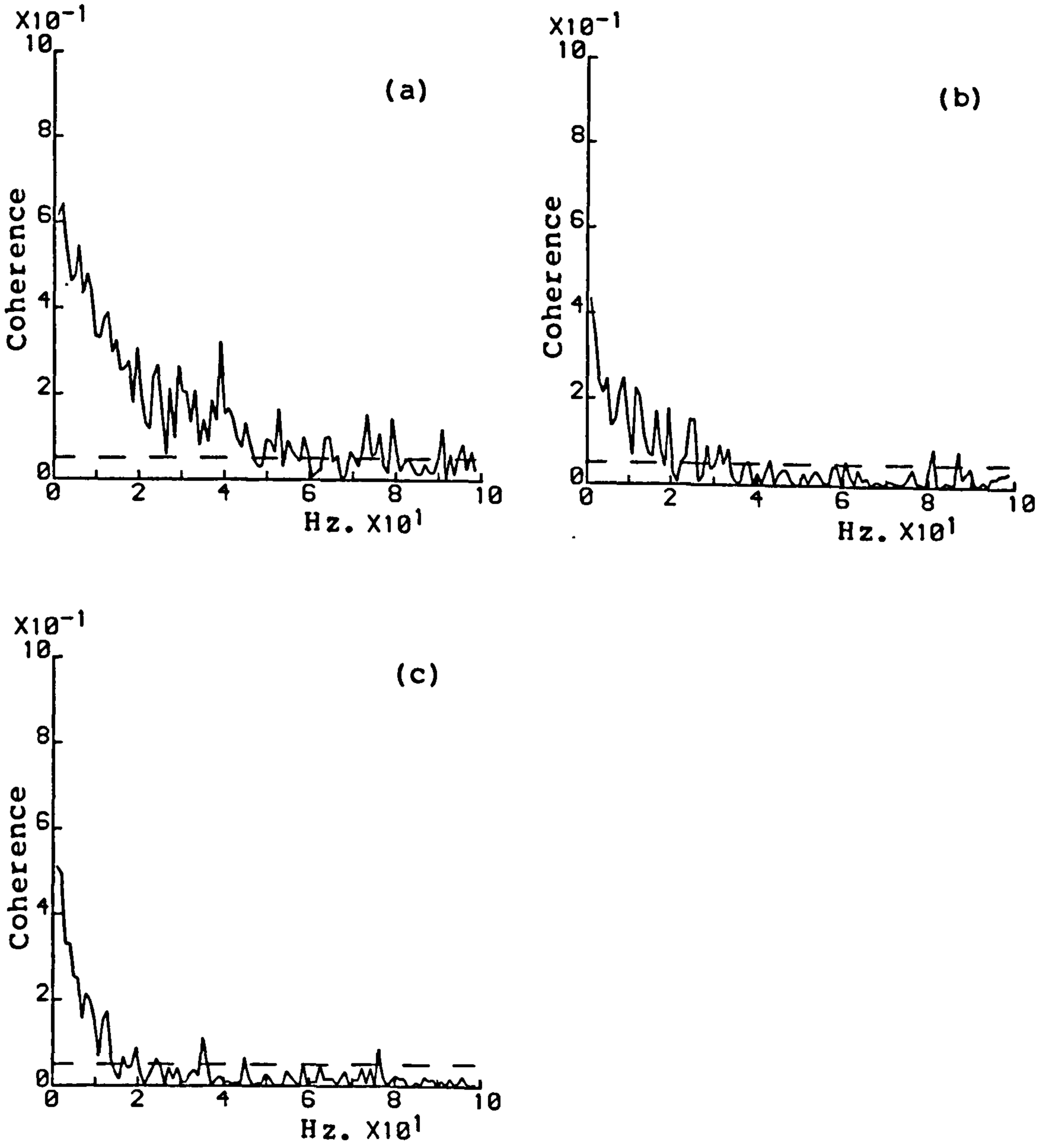

Fig. 4.4.5 Coherence estimates (2.5.10) for primary and secondary spindle response to random fusimotor stimulation. R=60000, and T=1024 in (2.3.29) and (2.3.31).

(a) Coherence estimate between gamma and Ia,

(b) gamma and II and

(c) Ia and II.

Dashed line indicates approximate 95% confidence limit.

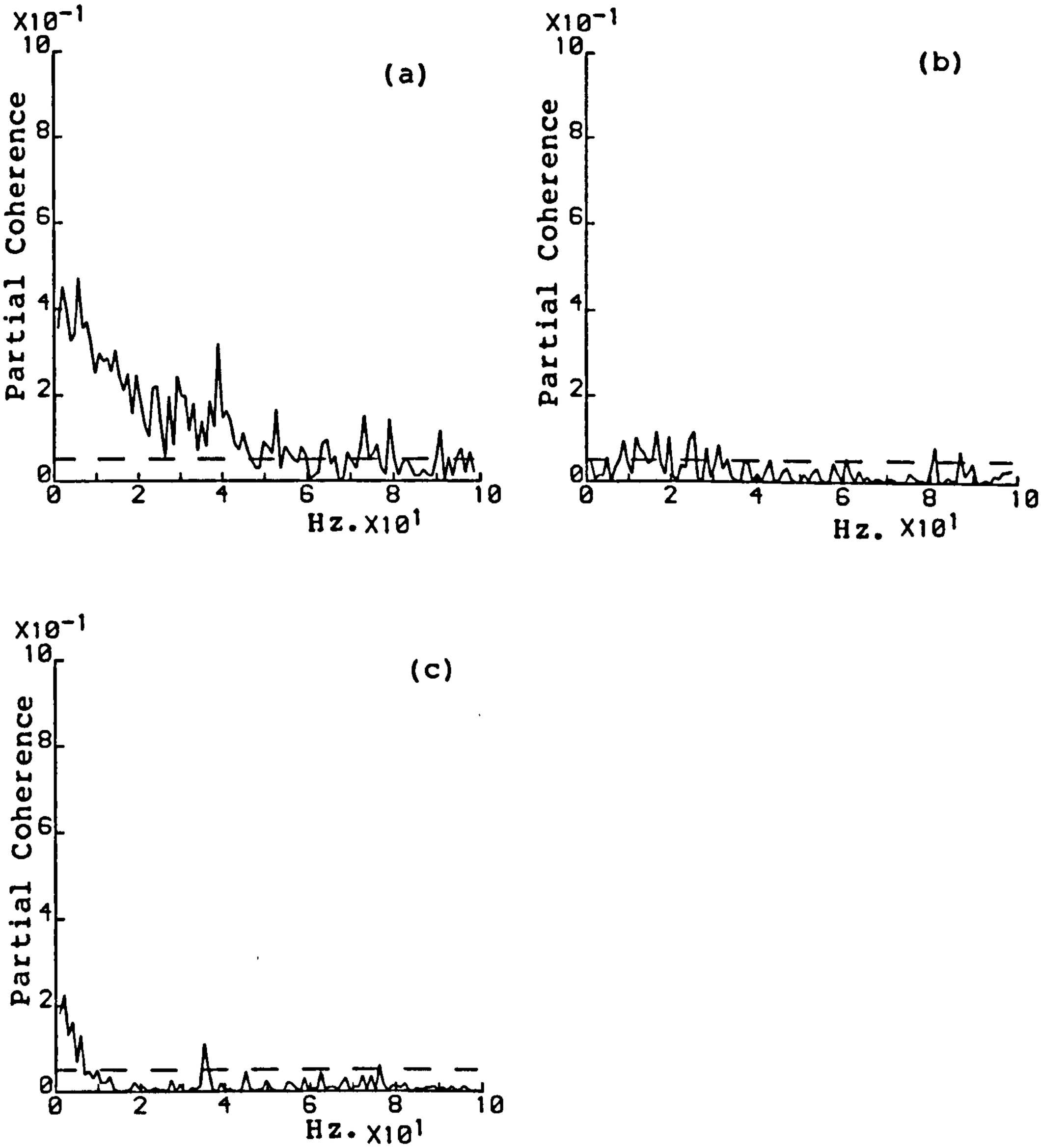

Fig. 4.4.6 Partial coherence estimates (4.4.2) for primary and secondary spindle response to random fusimotor stimulation. R=60000, and T=1024 in (2.3.29) and (2.3.31).

(a) Partial coherence estimate between gamma and Ia / (II),

(b) gamma and II / (Ia) and

(c) Ia and II/ (gamma).

Dashed line indicates approximate 95% confidence limit.

functions, and both clearly illustrate the usefulness of this technique in the analysis of multiple spike-trains.

4.5 PHASE-LOCKING OF MUSCLE SPINDLES

One important feature of the spindle response to a fusimotor input is a phase-locking type phenomenon (Brown et al, 1965). This occurs when a periodic spike-train stimulus is applied, and in certain cases a fixed relationship between the pulse frequency of the fusimotor input and the primary discharge exists. This effect is known as driving and the simplest case of this occurs when each input pulse produces one output pulse, and a slight change in input pulse frequency results in the output following this change. This particular case is known as one-to-one driving. Driving has been found to be dependent on the type of fusimotor input, and the muscle length (Boyd et al, 1977; Dutia et al 1977). In general dynamic gamma inputs do not drive, whereas static gamma fusimotor inputs may produce driving in the primary discharge.

A block diagram of the fusimotor innervation of a single spindle is illustrated in figure 4.5.1a. The situation being considered here is that of a single gamma static input and the primary output with the parent muscle held at fixed length. The input stimulus used to test for driving is a frequency ramp, where a spike-train of linearly increasing instantaneous frequency is applied to the fusimotor input. The frequency plot of a typical ramp input is shown in figure 4.5.1b. Figure 4.5.2 shows this ramp input with the expected response for two different fusimotor inputs superimposed. These are represented by the broken lines and the range over which one-to-one driving occurs is shown by the region where the instantaneous frequency

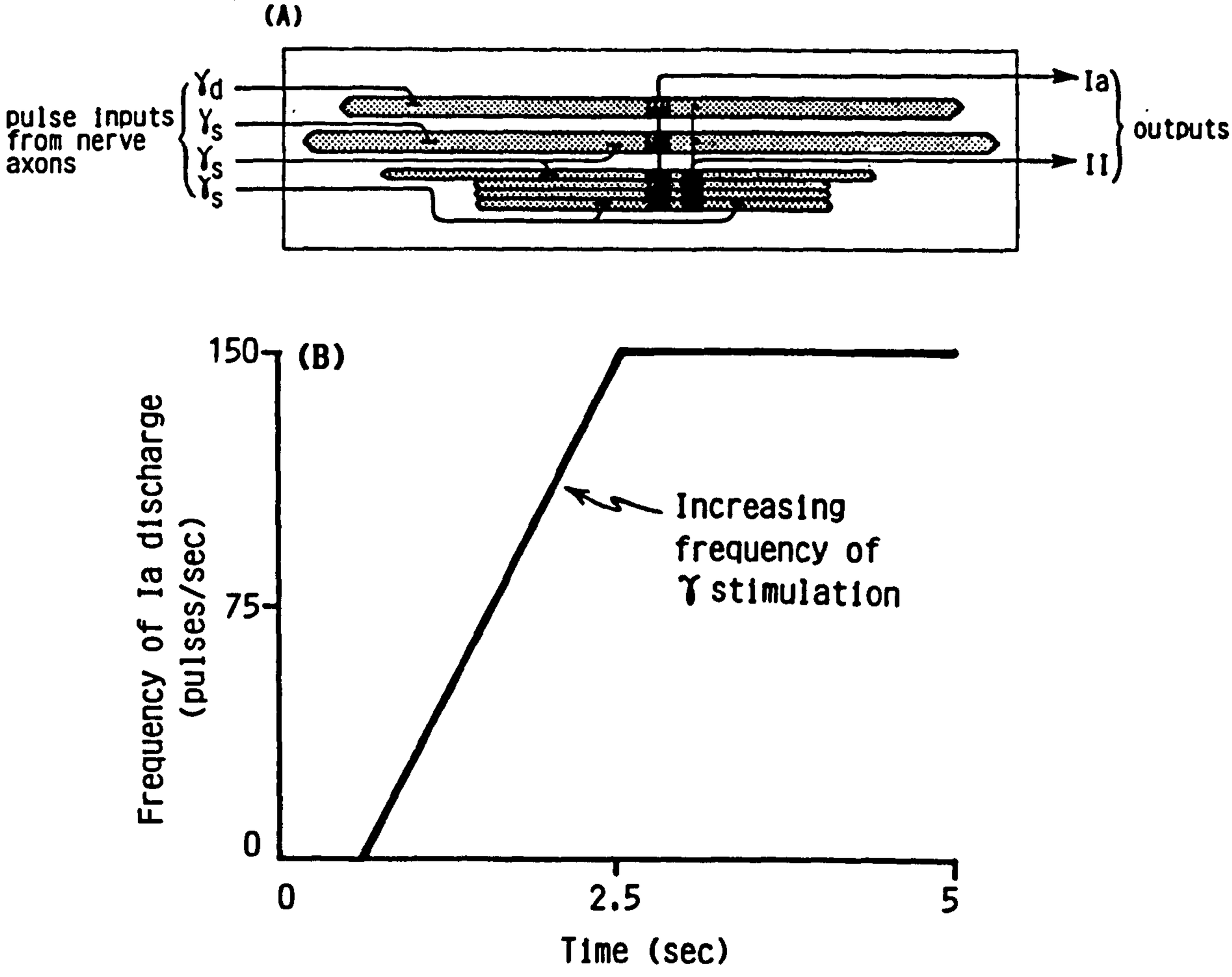

Fig. 4.5.1

(a) Block diagram of muscle spindle innervation.

(b) Fusimotor ramp input used to test for driving effects.

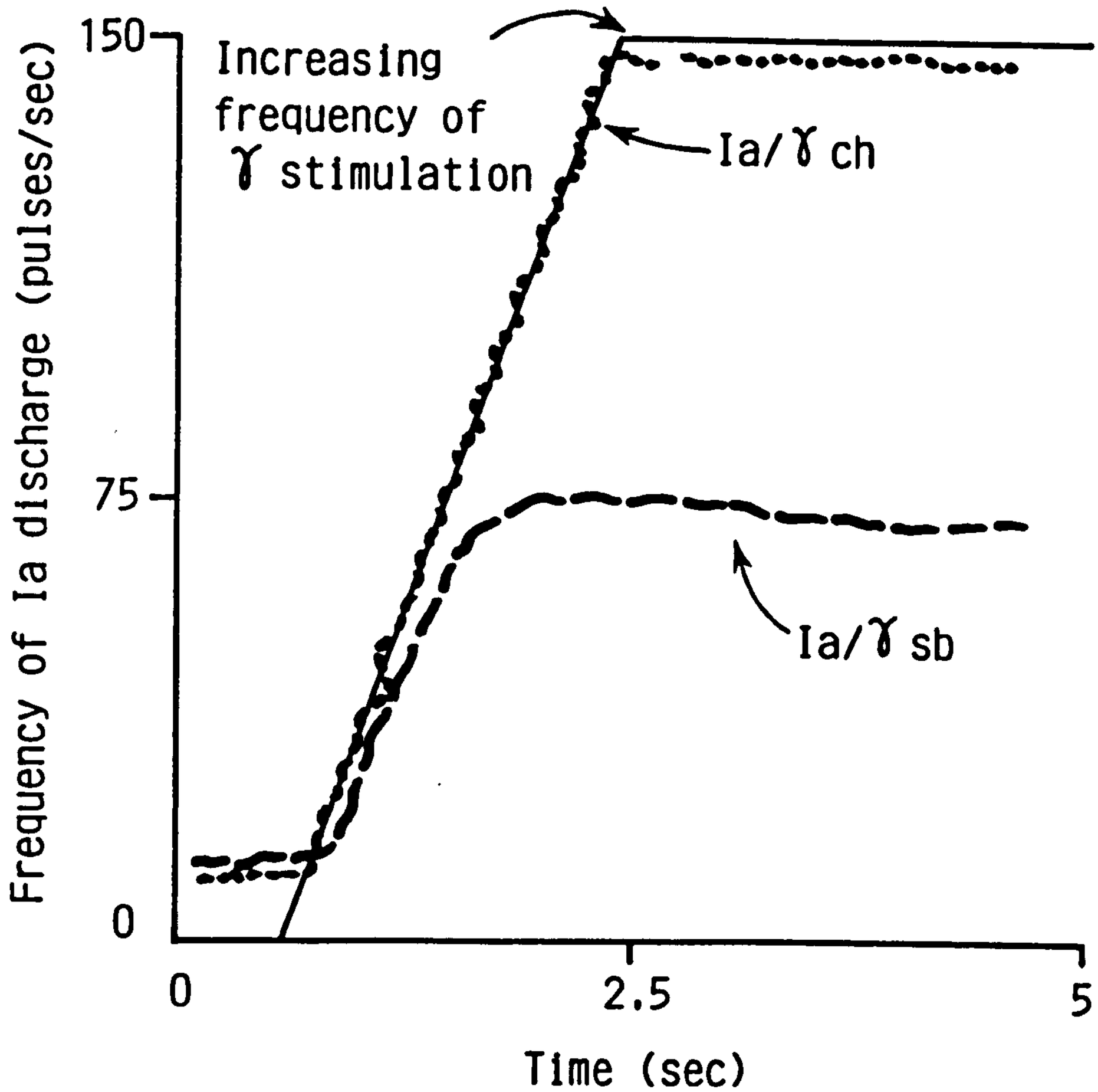

Fig. 4.5.2 Typical expected primary response to ramp input applied to two different fusimotor fibres

of the primary follows the ramp input. The typical chain fibre response exhibits driving over a much wider range of pulse frequencies than the static bag fibre, and it is thought that this may be due to the different mechanical properties of these intrafusal fibres.

The simulation introduced in section 2.8 has also been tested with a ramp input for the presence of driving. Different values of time constant were tried in the linear dynamics as well as different modulator parameters. Both of these were found to affect the ability of the simulation to exhibit one-to-one driving, and the range of frequencies of this driving.

If the time constant in the linear dynamics, t_d, is chosen so that the simulation exhibits one-to-one driving over a particular range of frequencies, then the effect of increasing t_d is to decrease the range of frequencies over which driving will occur. This effect can be seen in figure 4.5.3 which plots the upper and lower limits of the one-to-one driving range in pulses per second against the value of t_d in the simulation. These limits are plotted for four values of modulator gain (G_m), 29 to 32, with the modulator time constant (t_m) fixed at 50 msec. As t_d increases the upper and lower limits become closer to each other indicating a reduced range of driving. For the two gain values 29 and 30 the upper and lower limits merge with each other, this point represents the maximum value of t_d which will allow one-to-one driving for these values of G_m. This value is approximately 5/6 msec. for G_m=29, and 21/22 msec. for G_m=30. These values, do however, depend on other factors such as the value of t_m and the bias added to the encoder to represent the constant length signal.

In these simulations no bias was used. The effect of adding

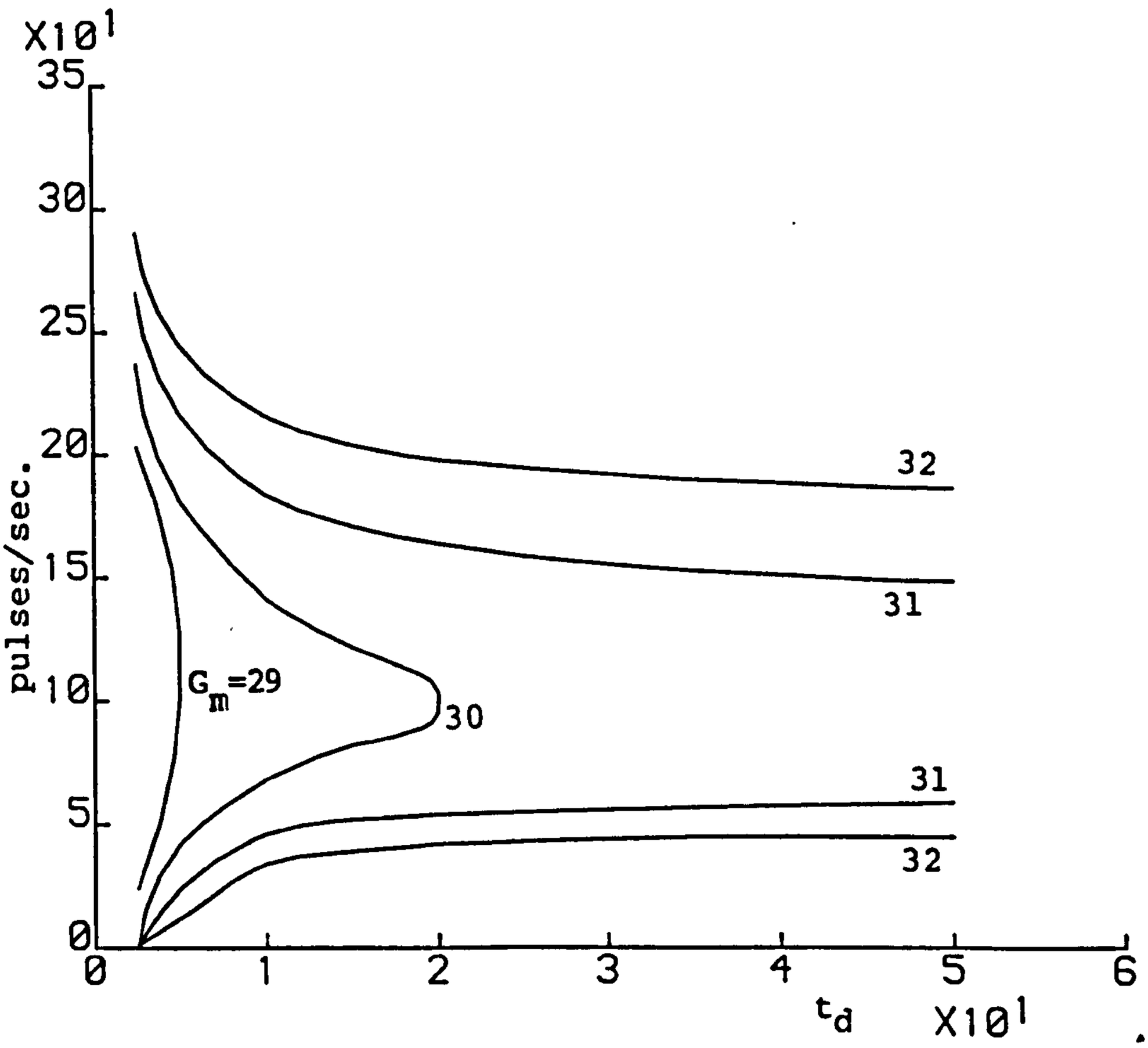

Fig. 4.5.3 Range of one-to-one driving measured on simulation and plotted as a function of time constant in linear dynamics for modulator gains of 29, 30, 31 and 32. Modulator time constant fixed at 50 msec..

a bias to the encoder is to lower the gain required for driving to occur over the same range, for fixed t_d and t_m. The results in figure 4.5.3 suggest that the range of driving is very sensitive to the gain used in the encoder section. This sensitivity can be seen in the figure 4.5.4 showing the upper and lower limits of the range of one-to-one driving against the value of G_m. Three values of t_d were used, 5, 10 and 15 msec. and the results are plotted for two values of t_m, 25 and 50 msec.. The range of driving is given by the range of frequencies enclosed to the right of each curve, the region to the left indicates the gain values over which no driving occurs. A small increase in gain leads to a large increase in the range of driving showing the sensitivity of driving to modulator gain. The effect of decreasing t_m is to shift the set of curves to lower gain values, and this is similar to the effect of introducing a bias into the encoder. These results show that one-to-one driving is in fact a property of this particular pulse frequency modulation system, and that driving is not a phenomenon peculiar to the physiological system being studied.

Adjusting the simulation parameters allows the simulation to exhibit one-to-one driving over a similar range to that measured experimentally using a static fusimotor input. Figure 4.5.5 compares the simulation response with that of a typical spindle response to the same fusimotor ramp input. A bias was added to the encoder input giving a spontaneous rate of 19 pulses/sec.. The modulator parameters were t_m=25msec., and G_m=10, with t_d=5msec.. The simulation exhibits driving over a similarily limited range as the experimental response.

Although driving is thought to be closely associated with the properties of the non-linear encoder (Downie and Murray-

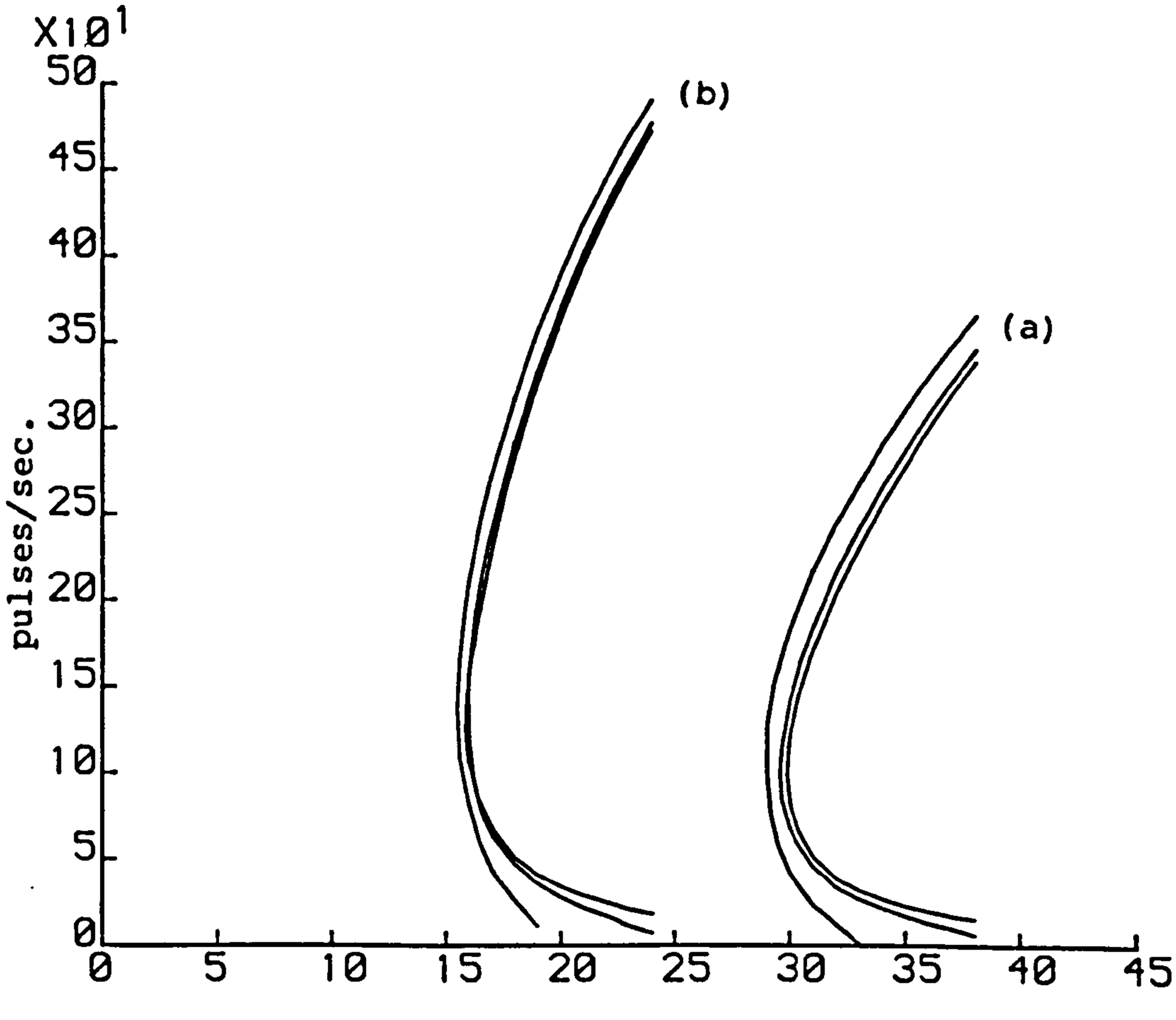

Fig. 4.5.4 Range of one-to-one driving measured on simulation and plotted as a function of gain in modulator for time constants of 5, 10 and 15 msec. in linear dynamics. Modulator time constant fixed at

(a) 50 msec. and

(b) 25 msec..

Smith, 1981), these simulation results show that altering the time constant in the linear dynamics also has a significant effect on the ability of the simulation to drive. The linear point-process model, (2.4.6), is also greatly influenced by this parameter, and driving effects can be detected in the linear point-process model parameters.

Using the same simulation which produced the results in figure 4.5.5b, the response of this simulation to a random spike-train input was recorded. The first order filter in the encoder was replaced by a pure integrator, since it has been shown that integral pulse frequency modulators (I.P.F.M) do not exhibit any driving effects (Downie and Murray-Smith, 1981). The gain in the integrator was adjusted to give a comparable number of output spikes in response to the random input.

The coherence function was estimated for each simulation, and the two estimates are shown in figure 4.5.6. The range of driving for the first simulation is from 51 to 94 pulses/sec.. The correspnding frequencies in cycles/sec. are marked by arrows in the plot. The estimate for the sigma P.F.M. simulation has higher coherence values over this range than the corresponding I.P.F.M simulation. The two estimates are similar in nature outside this frequency range and this suggests that it is the driving effects of the sigma P.F.M simulation which is causing the increased dependence of the output spike-train upon the input over this frequency range. The results in figure 4.5.6 show how the linear point-process model can account accurately for the spindle response to a fusimotor input over a wide range of frequencies, including effects which were previously thought to be due to the non-linear behaviour of the encoder.

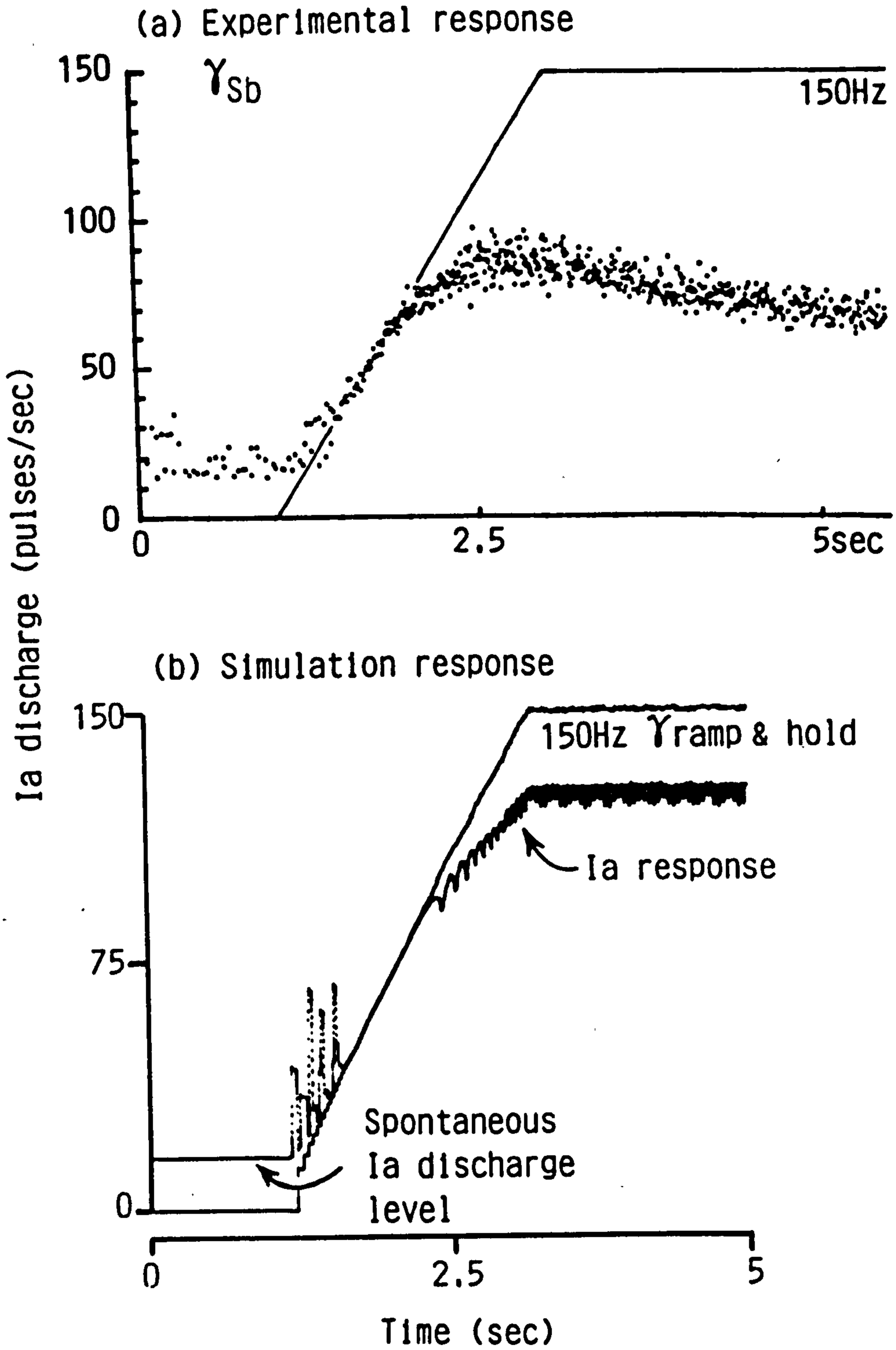

Fig. 4.5.5 Comparison of

(a) Experimentally measured primary response and

(b) Simulated primary response

to the same fusimotor ramp input.

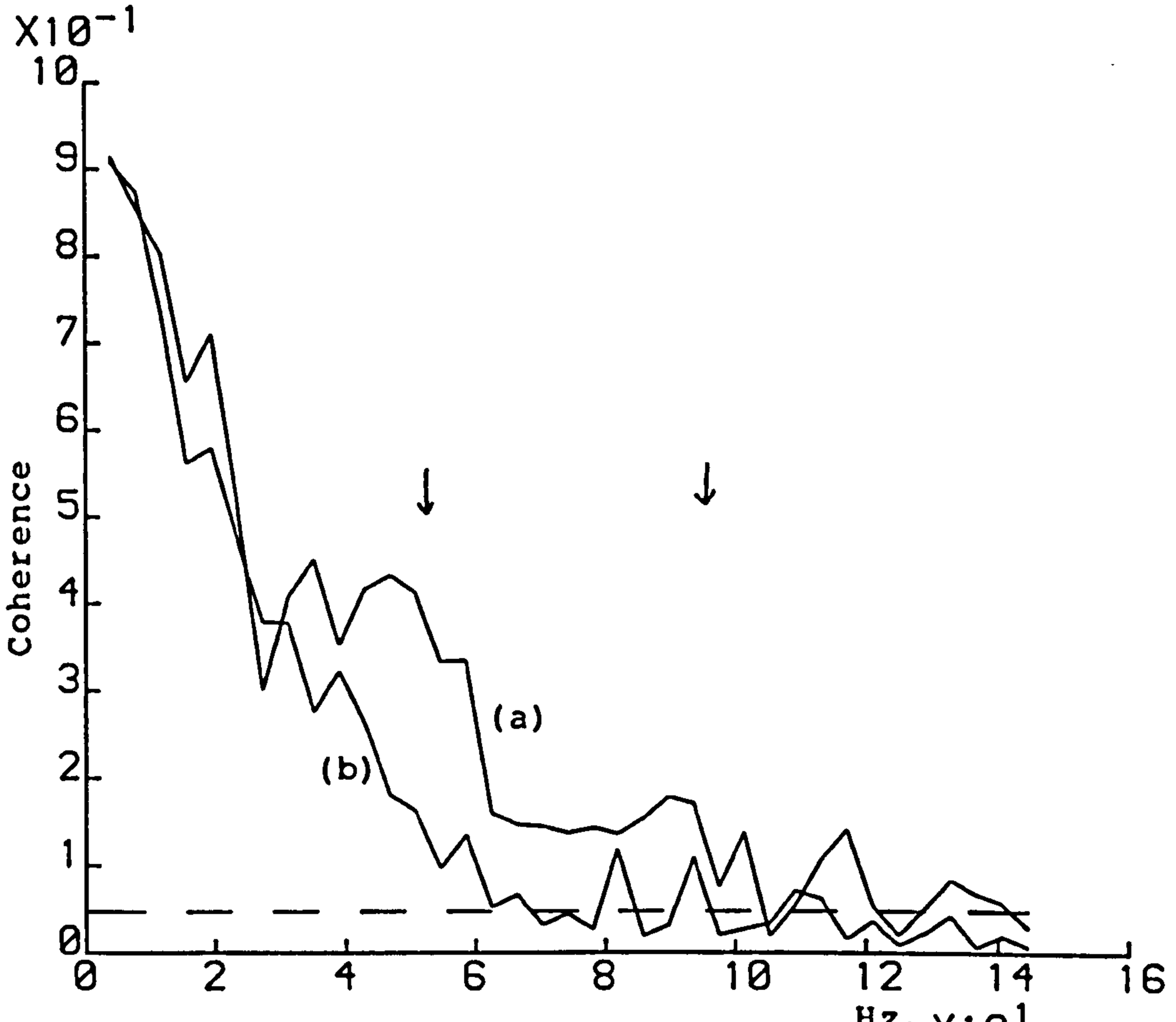

Fig. 4.5.6 Coherence estimates (2.5.10) for simulated primary response to random fusimotor input, R=15872, and T=256 in (2.3.29) and (2.3.31), for simulation

(a) with time constant in modulator and

(b) without time constant in modulator.

4.6 SUMMARY

In this chapter it has been shown that the use of the point-process parameters introduced in chapter two is not restricted purely to system identification techniques, but may also be used in the analysis of more general neurophysiological spike-train data. In section 4.2 the increased sensitivity of the coherence function compared with more conventional time domain measures was demonstrated when detecting connections between neurones, and section 4.3 illustrated the ability of the coherence concept to resolve individual harmonic components in spike-trains. The extension of the coherence to deal with multiple spike-trains in section 4.4 indicates that the point-process approach is a very powerful technique in the analysis of several simultaneous spike-trains allowing a model of the connections formed between discharging neurones to be built up. This may be used to provide information about how communications pathways are formed within nervous systems.

Finally, the analysis of driving effects in section 4.5 showed the value of using the coherence functions. By probing the simulation with a Poisson spike-train the range of one-to-one driving was detected from two 16 second experiments, as opposed to a fixed frequency trial and error approach, requiring many repetitions, to determine the range of one-to-one driving.

CHAPTER FIVE

5.1 INTRODUCTION

The definitions of stochastic point-process parameters in chapter two can all be extended to include higher order parameters. These allow non-linear effects due to interactions between two or more spikes in the time domain, or two or more periodicities in the frequency domain, to be looked at. The quadratic point-process model can be solved in terms of these parameters allowing the second kernel to be estimated.

This chapter will give definitions and estimates for higher order point-process parameters. The quadratic point-process model will be defined for one and two spike-train inputs, along with estimates in the time and frequency domain for the second kernel. These estimates will be applied to data sets obtained from the muscle spindle using stimulation of one and two fusimotor inputs. In this way the linear model introduced in chapter two will be extended to look at interactive effects within the muscle spindle.

5.2 HIGHER ORDER POINT-PROCESS PARAMETERS

5.2a Time Domain parameters

In the time domain, expressions for the third order product density, conditional intensity, and cumulant density functions can be obtained by extending the definitions in section 2.2a (Brillinger, 1972, 1975b). The third order product density $P_{nmm}(u,v)$ for the orderly bivariate point-processes M and N is defined as :

$$E\{\, dN(t+u)\; dM(t+v)\; dM(t)\,\} = P_{nmm}(u,v)\; du\; dv\; dt, \qquad (5.2.1)$$

and this may be interpreted as the probability of :

{ N pt in (t+u,t+u+du], M pt in (t+v,t+v+dv] & M pt in (t,t+dt] }

(5.2.2)

giving a probabalistic measure of the occurrence of an N event u and u-v time units after two previous M events. This situation is shown diagramatically in figure 5.2.1.

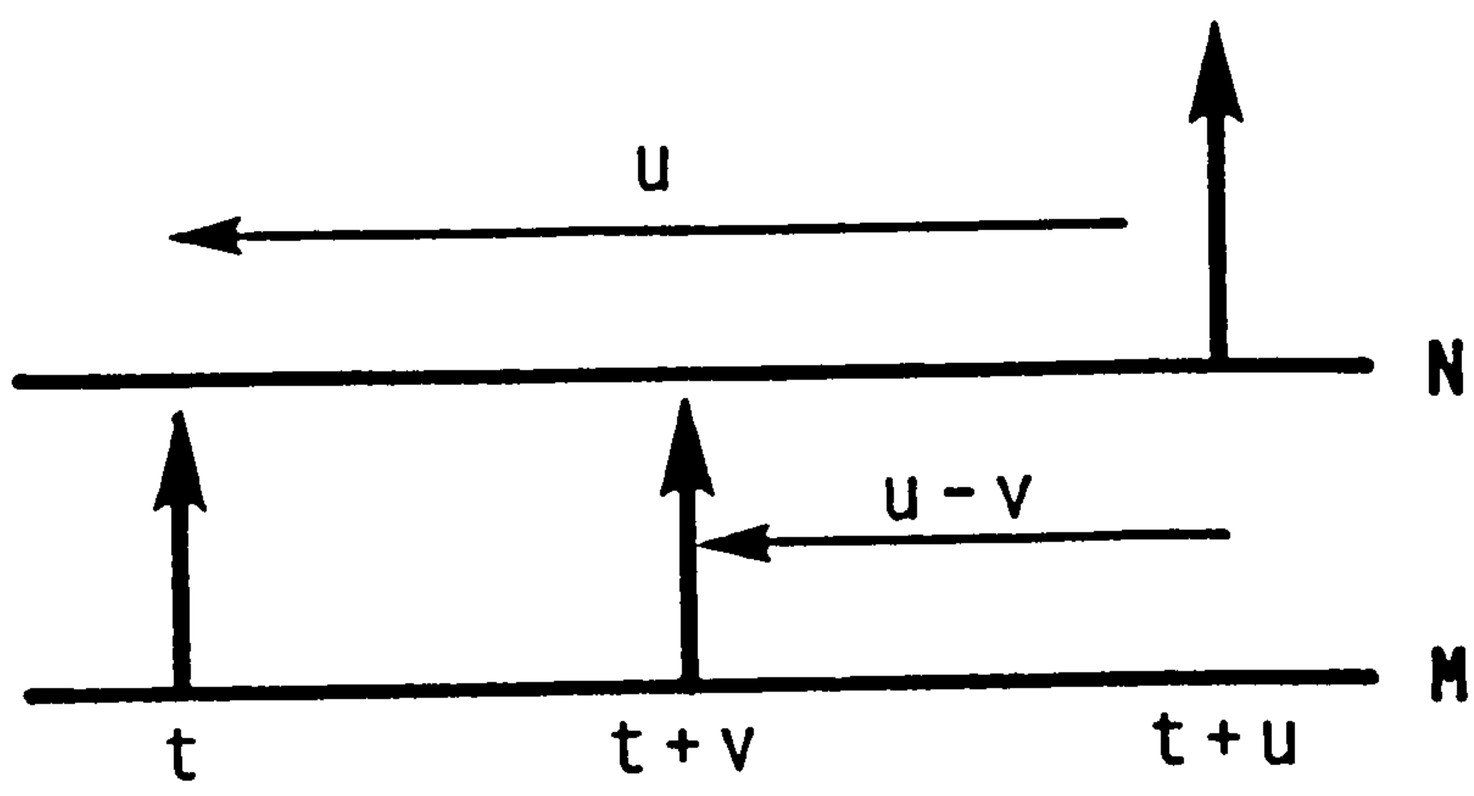

Fig. 5.2.1 Diagramatic representation of $P_{nmm}(u,v)$.

The third order product density for the univariate process M can be defined and interpreted by equating the processes M and N in (5.2.1) and (5.2.2). For three stationary and orderly processes A, B and C, $P_{abc}(u,v)$ is defined as in (5.2.1) by considering the expected value of the product of the increments dA(t+u), dB(t+v) and dC(t). The interpretation of $P_{abc}(u,v)$ is similar to (5.2.2) except that the events at time t and t+u are from different processes. This product density can be used to look at the interactive effects of two point-processes B and C upon a third process A.

The mixing condition allows an asymptotic distribution for $P_{abc}(u,v)$ to be defined as (Brillinger, 1975d) :

$$\lim_{u\to\infty} P_{abc}(u,v) = P_a\, P_{bc}(v). \qquad (5.2.3)$$

Expression (5.2.1) can be extended to define the k^{th} order

product density $P_{a1...ak}(u_1,...,u_{k-1})$ between processes $A_1...A_k$ as (Brillinger, 1975d) :

$$E\{ dA_1(t+u_1) \ldots dA_{k-1}(t+u_{k-1})\, dA_k(t) \}$$
$$= P_{a1...ak}(u_1,...,u_{k-1})\, du_1...du_{k-1}\, dt. \qquad (5.2.4)$$

The interpretation of this expression can be obtained by the expansion of (5.2.2), and allows the interactive effects of k-1 processes upon another process to be studied.

The third order conditional intensity between processes M and N, $m_{nmm}(u,v)$, is defined as (Rigas, 1983, ch4) :

$$E\{ dN(t+u) \mid M(t)=1 \text{ and } M(t+v)=1 \} = m_{nmm}(u,v)\, du, \qquad (5.2.5)$$

and using the rules of conditional probability this may be written as :

$$m_{nmm}(u,v) = P_{nmm}(u,v) \;/\; m_{mm}(u-v)\; P_m. \qquad (5.2.6)$$

If M is a Poisson process then this expression can be simplified to (Rigas, 1983, ch4) :

$$m_{nmm}(u,v) = P_{nmm}(u,v) \;/\; P_m^{\,2}. \qquad (5.2.7)$$

An interpretation is given in (5.2.8), and figure 5.2.1 can be referred to for a diagramatic interpretation.

$$\text{Prob}\{ \text{N pt in } (t+u, t+u+du] \mid \text{M events at t and t+v} \} \qquad (5.2.8)$$

Here we are considering the conditional probability of an N event occurring at time t+u given that two M events have occurred at times t and t+v. Depending on the number of point-processes being considered then (5.2.5) and (5.2.8) can also be defined for the univariate and trivariate cases. An expression for the asymptotic

distribution of (5.2.7) follows directly from (5.2.3) and is :

$$\lim_{u\to\infty} m_{nmm}(u,v) = m_{nm}(v). \qquad (5.2.9)$$

If M and N are the input and output of a point-process system respectively, then this conditional intensity function can be used to determine the interactive effects of two input events at times t and t+v on the rate of the output process N at time t+u.

A different conditional intensity function may be used to look at the interactive effects of one output and one input event on the rate of the output process. This is provided by $m_{nnm}(u,v)$, which considers the effect of an M spike at time t and and N spike at time t+v upon subsequent output events in process N at time t+u.

The third order cumulant density function, $q_{nmm}(u,v)$, is defined as (Brillinger, 1975b) :

$$\text{cum}\{\, dN(t+u),\, dM(t+v),\, dM(t)\,\} = q_{nmm}(u,v)\, du\, dv\, dt. \qquad (5.2.10)$$

This measures the statistical dependence of the increments dM(t), dM(t+v) and dN(t+u) and $q_{nmm}(u,v)$ can be defined in terms of product density functions as (Brillinger, 1975d) :

$$q_{nmm}(u,v) = P_{nmm}(u,v) - P_{nm}(u-v)P_m - P_{nm}(u)P_m - P_{mm}(v)P_n + 2P_nP_m^2. \qquad (5.2.11)$$

The mixing condition can be used to define the asymptotic distribution of (5.2.11) and gives (Brillinger, 1975d) :

$$\lim_{v\to\infty} q_{nmm}(u,v) = 0. \qquad (5.2.12)$$

The general expression for the cumulant function of order k, $q_{a1\ldots ak}(u_1,\ldots,u_{k-1})$, can be written in a manner similar to (5.2.10) as (Brillinger, 1975d) :

$$\text{cum}\{\, dA_1(t+u_1),\ \ldots,\ dA_{k-1}(t+u_{k-1}),\ dA_k(t)\,\}$$

$$= E\{\, [dA_1(t+u_1)-P_{a1}du_1]\ \ldots\ [dA_k(t)-P_{ak}dt]\,\}$$

$$= q_{a1\ldots ak}(u_1,\ldots,u_{k-1})\ du_1\ldots du_{k-1}\ dt. \qquad (5.2.13)$$

This cumulant density can be used to determine if there is a statistical dependence between k differential increments and (5.2.13) subtracts out lower order effects by considering the expected value of the product of the k increments with the mean rate of each process subtracted from each increment. If one of the k differential increments is not dependent on the k-1 other increments then the cumulant will be zero. For three processes A, B and C the cumulant density can be expressed as :

$$q_{abc}(u,v) = P_{abc}(u,v)-P_{ab}(u-v)P_c-P_{ac}(u)P_b-P_{bc}(v)P_a+2P_aP_bP_c, \qquad (5.2.14)$$

and in the reverse direction as :

$$P_{abc}(u,v) = q_{abc}(u,v)+q_{ab}(u-v)q_c+q_{ac}(u)q_b+q_{bc}(v)q_a+q_aq_bq_c. \qquad (5.2.15)$$

Expressions for the relationship between cumulant density and product density functions of order k are given in Kuznetsov and Stratonovich (1965), and Brillinger (1972). Kuznetsov et al (1965) describe the relationship between moment functions and correlation functions for random functions. For stochastic point-processes, product density functions can be considered analogous to moment functions and cumulative density functions analogous to correlation functions. Cumulant density functions are useful measures on their own since they provide a measure of joint statistical dependence between point-processes.

5.2b Frequency Domain Parameters

As in the second order case all higher order point-process

spectra can be defined indirectly in terms of the Fourier transform of the cumulant density functions, or directly in terms of the higher order periodogram which is based upon the finite Fourier transform of the differential increments of a segment of the process.

Considering the indirect method first, the third order cumulant spectrum of the process M, $f_{mmm}(\lambda,\mu)$, is defined as :

$$(2\pi)^2 f_{mmm}(\lambda,\mu) = q_m + \int e^{-i\lambda u} q_{mm}(u)\,du + \int e^{-i\mu u} q_{mm}(u)\,du$$
$$+ \int e^{-i(\lambda+\mu)u} q_{mm}(u)\,du + \iint e^{-i(\lambda u+\mu v)} q_{mmm}(u,v)\,du\,dv. \quad (5.2.16)$$

For two time series X and Y, a useful measure of quadratic non-linear dependence is the Cross Bi-Spectrum $f_{xxy}(\lambda,\mu)$ (Tick, 1961). The analogy of this in the bivariate point-process case is the quantity $f_{mmn}(\lambda,\mu)$, and this is defined as :

$$(2\pi)^2 f_{mmn}(\lambda,\mu) = \int e^{-i(\lambda+\mu)u} q_{mn}(u)\,du + \iint e^{-i(\lambda u+\mu v)} q_{mmn}(u,v)\,du\,dv, \quad (5.2.17)$$

and gives a measure of quadratic non-linear dependence of the process N upon the process M at frequencies λ and μ. If the third order cumulant point-process spectrum is defined for three separate processes A, B and C, then (5.2.17) can be further simplified to :

$$(2\pi)^2 f_{abc}(\lambda,\mu) = \iint e^{-i(\lambda u+\mu v)} q_{abc}(u,v)\,du\,dv. \quad (5.2.18)$$

Expressions (5.2.16), (5.2.17) and (5.2.18) can be found in Brillinger (1975d), along with the inverse relationships which define the cumulant density functions in terms of the inverse Fourier transforms of the cumulant spectra. The general relationship between cumulant density functions of order k and cumulant spectra of order k can be found in Brillinger (1972).

If the process M is Poisson then expression (5.2.16) simplifies to $(2\pi)^2 f_{mmm}(\lambda,\mu) = q_m$. This can be used to construct an asymptotic distribution for (5.2.16) of:

$$\lim_{\lambda,\mu\to\infty} f_{mmm}(\lambda,\mu) = P_m / (2\pi)^2. \qquad (5.2.19)$$

A deviation from this value will indicate non-linear effects due to a non-Poisson process.

Higher order point-process spectra can also be defined directly by forming complex products of the finite Fourier transform of the differential increments. For a segment of the process M of length T this is termed $d_M^{(T)}(\lambda)$, and is defined in (2.2.24). The third order periodogram of the process M is then defined as (Brillinger, 1972) :

$$I_{MMM}^{(T)}(\lambda,\mu) = 1/(2\pi)^2 T\, d_M^{(T)}(\lambda)\, d_M^{(T)}(\mu)\, \overline{d_M^{(T)}(\lambda+\mu)}, \qquad (5.2.20)$$

where the overbar indicates a complex conjugate quantity. Expression (5.2.20) is analogous to the higher order periodograms considered in Brillinger and Rosenblatt (1967a, b) for ordinary time-series. The corresponding definition for the periodogram of order k of a point-process can be found in Brillinger (1972) and is written as :

$$I_{a1\ldots ak}^{(T)}(\lambda_1,\ldots,\lambda_k) = (2\pi)^{-k+1} T^{-1} \prod_{j=1}^{k} da_j^{(T)}(\lambda_j), \qquad (5.2.21)$$

where $\sum_1^k \lambda_j = 0$.

For the bivariate case the third order periodogram between processes M and N can be defined as :

$$I_{MMN}^{(T)}(\lambda,\mu) = 1/(2\pi)^2 T\, d_M^{(T)}(\lambda)\, d_M^{(T)}(\mu)\, \overline{d_N^{(T)}(\lambda+\mu)}. \qquad (5.2.22)$$

The third order periodogram can be defined for three separate

point-processes by direct extension of (5.2.20) and (5.2.22). As in the second order case, in general the k^{th} order periodogram will not provide a consistent estimate of the k^{th} order spectrum and will require further smoothing (Brillinger and Rosenblatt, 1967a, b; Brillinger 1972).

5.3 ESTIMATES OF HIGHER ORDER POINT-PROCESS PARAMETERS

This section will consider estimates of the higher order parameters defined in section 5.2.

5.3a Estimates of time domain parameters

Estimates of third order intensity and density functions are all based on a histogram like counting variate similar to that defined in (2.3.8) for the second order case. For three point-processes A, B and C this is called $J_{ABC}^{T}(u,v)$ and is defined as :

$$J_{ABC}^{T}(u,v) =$$

$$\#\{ (i,k,l): u-h/2 < r_i-t_k < u+h/2 \text{ and } v-h/2 < s_l-t_k < u+h/2 \} \qquad (5.3.1)$$

where r_i denote the times of the A events, s_l the B events and t_k the C events respectively, $(i,k,l = 1,2,...)$, h is the bin width, and T the record length. In discrete form this can be written as $J_{ABC}^{T}(u_{j1},v_{j2})$, where $u_{j1}=j1\ h$ and $v_{j2}=j2\ h$, $(j1,j2 = ...,-2,-1,0,1,2,...)$. The situation being studied is shown diagramatically in figure 5.3.1.

This variate counts the number of occurrences of an A event inside a bin of width h which is u time units away from a C event, and a B event inside a bin of width h which is v time units away from the same C event. The expected value of this variate can be shown to be (Brillinger, 1975d) :

$$E\{ J^{T}_{ABC}(u,v) \} = h^2 \, T \, P_{abc}(u,v), \qquad (5.3.2)$$

where h is the bin width and T is the record length used in the estimate.

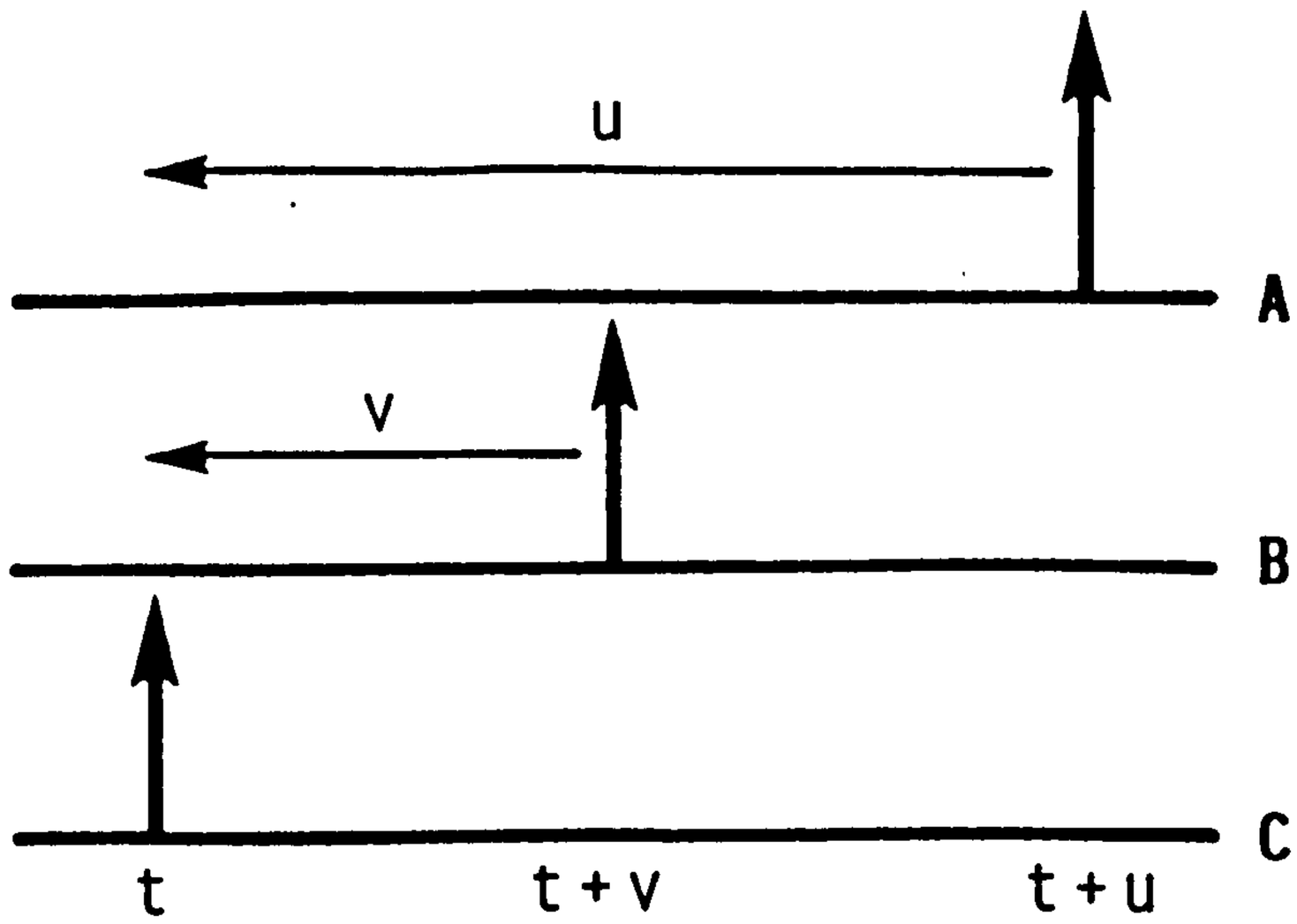

Fig. 5.3.1 Diagramatic representation of $J^{T}_{ABC}(u,v)$.

An estimate of the third order product density can be constructed as (Brillinger, 1975d) :

$$\hat{P}_{abc}(u,v) = J^{T}_{ABC}(u,v) \; / \; h^2 \, T. \qquad (5.3.3)$$

To estimate the third order product density in the bivariate case for the processes M and N the processes A, B, and C are equated to M or N respectively in (5.3.1) and (5.3.3). Thus to estimate $P_{nmm}(u,v)$, the variate $J^{T}_{NMM}(u,v)$ is formed according to (5.3.1) by equating A to N and B and C to M and forming :

$$\hat{P}_{nmm}(u,v) = J^{T}_{NMM}(u,v) \; / \; h^2 \, T. \qquad (5.3.4)$$

If the process M is Poisson, then the third order conditional intensity function $m_{nmm}(u,v)$ can be estimated as :

$$\hat{m}_{nmm}(u,v) = J^{T}_{NMM}(u,v) \; / \; h^2 \, M(T) \; \hat{P}_{m}, \qquad (5.3.5)$$

this follows directly from (5.2.7). For the univariate case the third order product density $P_{mmm}(u,v)$ can be estimated by equating A, B and C to the process M in (5.3.1) and (5.3.3).

The computation of the variate $J^{T}_{ABC}(u,v)$ can be exceedingly time consuming. Several authors (see Brillinger 1975d, 1976a; Rigas, 1983, ch4) have suggested a technique where the spike times are arranged in one series of ordered values with a corresponding series of flags to indicate which type of event has occurred. This allows the estimate to be calculated with one pass through the data and also restricts the number of triplets which are searched through. This method is also very time consuming since the remaining record after each current spike is searched for relevant lag values. The record length used here is 15872 msec. and if the area of interest is within 50 msec. of each spike, then this is a very inefficient method.

To overcome this problem a new technique was developed where the processes A, B and C are stored in three separate arrays in order of increasing time of occurrence. In practice this is the same as the output from the digitising program. From figure 5.3.1, to calculate $J^{T}_{ABC}(u,v)$ the C spike is common to both the u and v lags and the routine uses each C spike as a reference. Firstly a two dimensional array to represent the variate $J^{T}_{ABC}(u,v)$ is initialised to zero and two counters for the B and A processes are initialised to one (i.e. the first spike). The routine then calculates $J^{T}_{ABC}(u,v)$ with one pass through all the C spikes as follows.

For each C spike the B counter is updated until the first B spike which is within the lag range is reached. The B counter is retained, and for each successive B spike, starting with the one

which the B counter now points to, the lag value representing v is calculated. These are stored in a separate array for future use. Once the first B spike which is out of the lag range is reached the process stops, since the spikes are ordered and all subsequent B spikes will be out of range. The algorithm then goes on to the A spikes and updates the A spike counter until the first A spike within the range of lags is reached. The A counter is retained and starting with the spike that it now points to the u lag values are calculated for successive A spikes. For each such u lag obtained all the previous v lags are used to update the count in the two dimensional array representing $J^{T}_{ABC}(u,v)$. When the first A spike which is outside the lag range is reached this process stops. The algorithm then proceeds on to the next C spike, using the values for the B and A counters which were retained from the previous C spike as the starting point to search for the next B and A spikes within the lag range. In this way only those relevant spikes within the lag range are searched and the computational load is very much reduced. In practice it was found that computational times were reduced from 9000 seconds using the old method to around 5 seconds using this new algorithm. This allows estimates of higher order time domain parameters to be formed very rapidly.

Several authors (see French and Butz, 1973; Brillinger, 1975d and Rigas, 1983) have suggested that it may be quicker to generate higher order time domain parameters by first estimating directly the higher order cumulant spectra and then doing an inverse multi-dimensional Fourier transform. Using this new algorithm it is now much quicker to estimate higher order time domain parameters directly. The algorithm has also been

simplified to the second order case and used to form rapid estimates of second order time domain parameters.

An estimate of the third order cumulant function is formed by direct substitution of second and third order product densities into (5.2.14) giving :

$$\hat{q}_{abc}(u,v) = \hat{P}_{abc}(u,v) - \hat{P}_{ab}(u-v)\hat{P}_{c} - \hat{P}_{ac}(u)\hat{P}_{b} - \hat{P}_{bc}(v)\hat{P}_{a} - 2\hat{P}_{a}\hat{P}_{b}\hat{P}_{c}. \tag{5.3.6}$$

Estimates of the first and second order product densities are given in section 2.3. As with the product density function, the third order cumulant density of the bivariate processes M and N, $q_{nmm}(u,v)$, is estimated according to (5.3.6) by equating A to N and B and C to M. For the univariate process M, $q_{mmm}(u,v)$ can be estimated by equating A, B and C to M in (5.3.6). The asymptotic distribution of (5.3.6) can be estimated as :

$$\lim_{v\to\infty} \hat{q}_{abc}(u,v) = 0. \tag{5.3.7}$$

This result follows from (5.2.12). The large sample properties of the estimates (5.3.3) and (5.3.5) of the third order product density and third order intensity function are similar to those of the corresponding second order estimates (Brillinger, 1975c; Brillinger et al, 1976; Rigas, 1983, ch4). Thus $\hat{P}_{abc}(u,v)$ is asymptotically normal with mean $P_{abc}(u,v)$ and variance $(h^2T)^{-1}P_{abc}(u,v)$, this again suggests the use of a square root transform. The estimate $(\hat{P}_{abc}(u,v))^{1/2}$ is normally distributed with mean $(P_{abc}(u,v))^{1/2}$ and variance $(4h^2T)^{-1}$.

5.3b Estimates of frequency domain parameters

Firstly we consider indirect estimates for higher order spectra based on the Fourier transform of cumulant density functions. The definitions for the third order spectrum between

one, two and three point-processes are given in section 5.2b. These are all special cases of the general formula given in Brillinger (1972, Theorem 3.3) for the cumulant spectra of order k. For the third order spectral estimates being considered here this can be written as :

$$f_{a1a2a3}(\lambda_1,\lambda_2,\lambda_3) = 1/(2\pi)^2$$
$$\sum_{i=1}^{3} [\prod_{j\in v1} \delta(x-a_j)] [\prod_{j\in v2} \delta(y-a_j)] [\prod_{j\in v3} \delta(z-a_j)] g_{xyz}(\sum_{j\in v1}\lambda_j, \sum_{j\in v2}\lambda_j, \sum_{j\in v3}\lambda_j) \tag{5.3.8}$$

with the summation extending over all the three possible partitions (v1 ... vi) of (1,2,3). Since a necessary condition for the definition of higher order spectra is :

$$\sum_{j=1}^{k} \lambda_j = 0, \tag{5.3.9}$$

then $f_{a1a2a3}(\lambda_1,\lambda_2,\lambda_3)$ depends only on two arguments, since $\lambda_3=-\lambda_1-\lambda_2$, and can be simplified to $f_{a1a2a3}(\lambda_1,\lambda_2)$. The same argument applies to the spectra $g_{xyz}(\lambda_i,\lambda_j,\lambda_k)$ and the third frequency index λ_k can be neglected. Similarily in the time domain the cumulant density of order k depends only on k-1 arguments due to stationarity. The spectra g_x, $g_{xy}(\lambda)$ and $g_{xyz}(\lambda,\mu)$ are the Fourier transform of the individual cumulant density functions q_x, $q_{xy}(u)$ and $q_{xyz}(u,v)$.

In the expansion of the summation in (5.3.8) there will be terms for i=1,2 and 3. The index i gives the number of elements that exists in each partition of (1,2,3). Considering this expansion in more detail, i=1 results in 1 partition per element giving the term :

$$\delta(x-a_1)\delta(y-a_2)\delta(z-a_3)\ g_{xyz}(\lambda_1,\lambda_2,\lambda_3).$$

For i=2, there are 3 possible combinations with one element in the first partition and two elements in the second giving the three terms :

$$\delta(x-a_1)\delta(y-a_2)\delta(y-a_3)\ g_{xy}(\lambda_1,\lambda_2+\lambda_3)$$

$$\delta(x-a_2)\delta(y-a_1)\delta(y-a_3)\ g_{xy}(\lambda_2,\lambda_1+\lambda_3)$$

$$\delta(x-a_3)\delta(y-a_1)\delta(y-a_2)\ g_{xy}(\lambda_3,\lambda_1+\lambda_2),$$

and finally i=3 results in three elements in 1 partition giving the term :

$$\delta(x-a_1)\delta(x-a_2)\delta(x-a_3)\ g_x(\lambda_1+\lambda_2+\lambda_3).$$

Neglecting the highest frequency component and using (5.3.9) results in the expansions given in section 5.2b for one, two and three point-processes. The delta functions in the above expressions incorporate the singularities into the third order spectrum which are present for univariate and bivariate processes. Expression (2.3.23) for the estimation of the second order spectrum of the process M is also a special case of (5.3.8) for k=2. The two dimensional spectrum $g_{xyz}(\lambda,\mu)$ can be estimated by :

$$\hat{g}_{xyz}(\lambda,\mu) = 1/(2\pi)^2 \sum_i \sum_j \hat{q}_{xyz}(u_i,v_j)K_{TT}(u_i,v_j)e^{-i(\lambda u_i+\mu v_j)}\ , \qquad (5.3.10)$$

where $\hat{q}_{xyz}(u,v)$ is an estimate of the third order cumulant density, and $u_i=hi$, $v_j=hj$ (i,j = ...,-2,-1,0,1,2,...). $K_{TT}(u,v)$ is a convergence factor (Brillinger, 1975c; Harris, 1978) which improves the convergence properties of the estimate (5.3.10). Expressions for estimating the lower order terms in (5.3.8) are given in section 2.3b.

The direct method of estimating third order spectra is based on the periodogram. For the process M, an estimate of the finite Fourier transform of a section of length T, $d_M^{(T)}(\lambda_j)$, is given

in (2.3.26). For the processes A, B and C the third order periodogram is given by :

$$I_{ABC}^{(T)}(\lambda_i,\mu_j) = 1/(2\pi)^2 T \; d_A^{(T)}(\lambda_i)\, d_B^{(T)}(\mu_j)\, \overline{d_C^{(T)}(\lambda_i+\mu_j)}. \tag{5.3.11}$$

This is not a consistent estimate of the third order spectrum and requires further smoothing. Averaging over disjoint sections can also be used in the higher order case. For a record of length R consisting of K disjoint sections of length T then an estimate of the third order spectrum for the univariate process M can be formed as :

$$\hat{f}_{mmm}(\lambda_i,\mu_j) = 1/K \sum_{k=1}^{K} I_{MMM}^{(Tk)}(\lambda_i,\mu_j), \tag{5.3.12}$$

where $I_{MMM}^{(Tk)}(\lambda_i,\mu_j)$ is the periodogram of the k^{th} disjoint section and is formed by equating A, B and C to M in (5.3.11). Similarily the cross bi-spectrum between process M and N, $f_{mmn}(\lambda,\mu)$, can be estimated by :

$$\hat{f}_{mmn}(\lambda_i,\mu_j) = 1/K \sum_{k=1}^{K} I_{MMN}^{(Tk)}(\lambda_i,\mu_j), \tag{5.3.13}$$

where $I_{MMN}^{(Tk)}(\lambda_i,\mu_j)$ is the periodogram of the k^{th} disjoint section and is formed by equating A and B to M and C to N in (5.3.11). The resolution of these estimates will be the same as that for the second order spectral estimates formed in this manner, and is given in section 2.3.

Unless stated otherwise, all third order spectral estimates will be based on the periodogram estimates (5.3.12) and (5.3.13).

5.4 THE QUADRATIC POINT-PROCESS MODEL

Considering the model (2.4.2) introduced in section 2.4 for

a bivariate process with input M and output N, then the quadratic model is given by :

$$x_M(t) = s_o + \int s_1(t-u)\ dM(u) + \iint_{u\neq v} s_2(t-u,t-v)\ dM(u)dM(v) \qquad (5.4.1)$$

The function $s_2(u,v)$ is the kernel of order two whose arguments are the times to two distinct input spikes. This kernel gives a measure of the interactive effect of two spikes at times t-u and t-v upon the output at time t.

For time-series analysis, Tick (1961) defines a quadratic coherence function for a noise free system probed with a zero mean Gaussian series. This function gives a measure in the frequency domain of the dependence of the quadratic model upon the second kernel. It is not presently clear how to extend this approach to the point-process case.

As well as looking at non-linear terms for a single input, the quadratic model (5.4.1) can also be used to look at the effects of several inputs. The two input quadratic model contains terms which look at the linear and non-linear effects of each input on its own plus a term relating to non-linear interactive effects from both inputs. For two point process inputs, M_1 and M_2, and one output then (5.4.1) can be extended to :

$$\begin{aligned} x_M(t) = s_o &+ \int s_1(t-u)\ dM_1(u) + \int s_2(t-u)\ dM_2(u) \\ &+ \iint s_{11}(t-u,t-v)\ dM_1(u)dM_1(v) + \iint s_{22}(t-u,t-v)\ dM_2(u)dM_2(v) \\ &+ \iint s_{12}(t-u,t-v)\ dM_1(u)dM_2(v) \end{aligned} \qquad (5.4.3)$$

where $s_1(u)$ and $s_2(u)$ are the first order kernels for the two inputs M_1 and M_2, and $s_{11}(u,v)$ and $s_{22}(u,v)$ are the quadratic kernels. The function $s_{12}(u,v)$ is an interactive kernel which looks at the effect upon the output of a spike from process M_1 at

time t-u interacting with a spike from process M_2 at time t-v.

For the case of conventional time series, the kernel approach was suggested by Wiener (1958), and reviews can be found in Harris and Lapidus (1967), Hung and Stark (1977) and Schetzen (1981). Various methods of estimating Wiener kernels are detailed in Lee and Schetzen (1965) and French and Butz (1973, 1974). Applications of this approach to biological systems are given in Marmarelis and Marmarelis (1978), and Hung et al (1979).

5.5 ESTIMATES OF THE QUADRATIC MODEL PARAMETERS

The solution of the quadratic model (5.4.1) can be found in Brillinger (1975b) for the case of a zero mean point process M'. This is achieved by subtracting the value P_m from each of the differential increments in (5.4.1) giving $dM'(u)=dM(u)-P_m\,du$. A general solution of the quadratic model in terms of the previously defined point-process parameters including a solution for the second kernel in both the time and frequency domain can be found in Rigas (1983, App. III). The quadratic kernel can only easily be identified directly for a Poisson input process M and, assuming $s_2(u,v)=s_2(v,u)$, is given by Brillinger (1975b) as:

$$s_2(u,v) = q_{mmm}(u,u-v) \;/\; 2\,P_m^{\,2}. \qquad (5.5.1)$$

This can be estimated by substituting the estimates $\hat{q}_{nmm}(u,u-v)$ and $\hat{P}_m$ into (5.5.1). The third order cumulant $q_{nmm}(u,u-v)$ can be estimated by :

$$\hat{q}_{mmm}(u,u-v) = \hat{P}_{mmm}(u,u-v)-\hat{P}_{mm}(v)\hat{P}_m-\hat{P}_{mm}(u)\hat{P}_m-\hat{P}_{mm}(u-v)\hat{P}_n+2\hat{P}_n\hat{P}_m^{\,2}. \qquad (5.5.2)$$

This is slightly different from the expression given for the third order cumulant $q_{nmm}(u,v)$ in (5.2.11) since we are now

interested in the cumulant with arguments u and u-v time units. This requires the estimation of the third order product density $P_{nmm}(u,u-v)$, which is based upon the variate $J^{T}_{NMM}(u,u-v)$. A diagramatic representation of this is shown in figure 5.5.1.

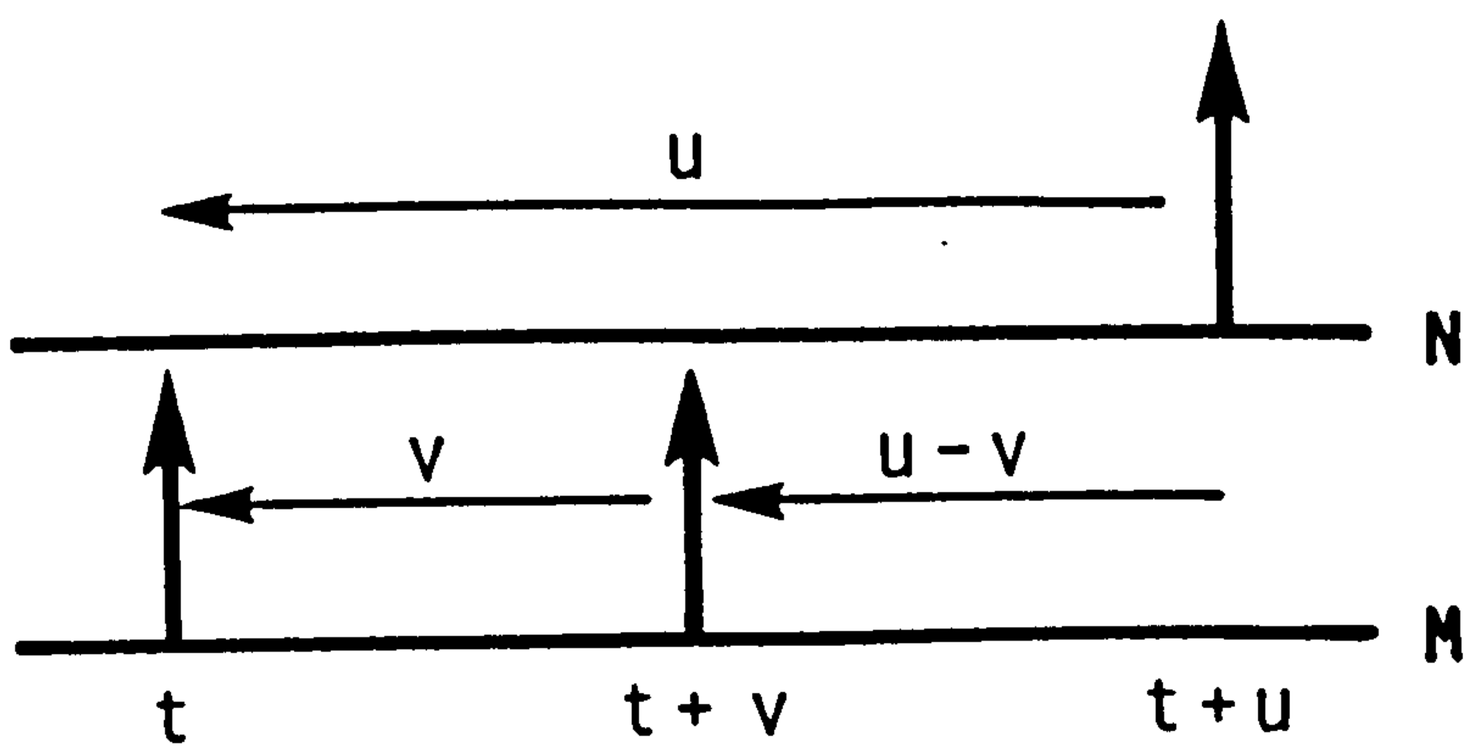

Fig. 5.5.1 Diagramatic representation of $J^{T}_{NMM}(u,u-v)$.

This variate is very similar to $J^{T}_{ABC}(u,v)$ defined in (5.3.1) except that the common spike is now at time t+u instead of at time t.

The second order kernel also has a frequency domain representation, $S_2(\lambda,\mu)$, and can be estimated in the frequency domain using the third order cross bi-spectrum estimate in (5.3.13). For the case of ordinary time series an expression for the estimation of the quadratic kernel in the frequency domain can be found in Tick (1961). For a system being probed with a stationary Gaussian series, x, this can be written as :

$$S_2(\lambda,\mu) = f_{xxy}(\lambda,\mu) \;/\; 2\, f_{xx}(\lambda)\; f_{xx}(\mu)\;, \qquad (5.5.3)$$

where y is the output series. Brillinger (1970) gives an expression for the estimation in the frequency domain of the kernel of order k for a polynomial system probed with a zero mean Gaussian series. This is a direct extension of (5.5.3) and

involves the estimation of the cumulant spectra $f_{x\ldots xy}(\lambda_1,\ldots,\lambda_k)$, of order k+1. By analogy with (5.5.3) the second order kernel $S_2(\lambda,\mu)$ of the bivariate point-process system with Poisson input M and output N can be estimated as :

$$\hat{S}_2(\lambda,\mu) = \hat{f}_{mmn}(\lambda,\mu) \;/\; 2\,\hat{f}_{mm}(\lambda)\;\hat{f}_{mm}(\mu)\;, \qquad (5.5.4)$$

and the functions $s_2(u,v)$ and $S_2(\lambda,\mu)$ will form a Fourier transform pair (Rigas, 1983, App. III). The estimate (5.5.4) like (5.5.1) is only applicable if M is a Poisson process, and $S_2(\lambda,\mu)$ is a complex quantity having gain and phase components.

5.6 THE TWO INPUT LINEAR MODEL

The simplest extension of the linear point-process model (2.4.6) is to consider the two input model (5.4.3) without the quadratic terms. This model can be written :

$$x_M(t) = s_o + \int s_1(t-u)\; dM_1(u) + \int s_2(t-u)\; dM_2(u), \qquad (5.6.1)$$

where M_1 and M_2 are the two inputs and $s_1(u)$ and $s_2(u)$ are the first order kernels associated with each input. This model has the advantage that it requires only the estimation of the linear model parameters described in chapter 2. When considering multi-input models an indication of the effect of an additional input may be obtained by comparing the kernel and coherence estimates in the absence and then in the presence of this particular input. Thus for each of the two point-process inputs M_1 and M_2, the effect of the second input upon the existing input can be investigated by comparing the coherence estimate between the input and output in the absence and then in the presence of the second input

The multiple coherence between several inputs and an output

is defined in Brillinger (1975a, ch8) and Bloomfield (1976, pp237-240) for the case of ordinary time-series and can be extended directly to the point-process case. Using matrix notation then r different point-process inputs can be written as [**M**(t)]. The r vector valued cumulant densities associated with these r inputs and the output process N can be defined by direct extension of the definitions in section 2.3a to the vector case. This allows the matrix of r vector valued second order spectra $f_{mm}(\lambda)$, $f_{mn}(\lambda)$ and $f_{nm}(\lambda)$ to be defined by extending the definitions in section 2.3b to the vector case. The multiple coherence between the output N and the r inputs [**M**(t)] can then be defined as :

$$\left|R_{nm}(\lambda)\right|^2 = f_{nm}(\lambda)\ f_{mm}(\lambda)^{-1}\ f_{mn}(\lambda)\ /\ f_{nn}(\lambda), \qquad (5.6.2)$$

where $f_{mm}(\lambda)$, $f_{mn}(\lambda)$ and $f_{nm}(\lambda)$ are the r vector valued second order spectra associated with the r inputs and the output, and $f_{nn}(\lambda)$ is the second order spectrum of the output process. Expression (5.6.2) can be estimated by using the estimates in section 2.3b to form the r vector valued matrix of second order spectra and substituting these into (5.6.2). Alternatively, if the linear coherence estimates between the output N and each of the r inputs are already available, then these may be added together to form (5.6.2). When r=1, (5.6.2) simplifies to (2.4.11), the normal coherence function.

This technique will now be applied to the analysis of the muscle spindle to assess the effect of a second random fusimotor input upon the primary discharge. In this experiment two fusimotor inputs to the same spindle were isolated and each in turn was stimulated with a Poisson spike-train, then both

together were simultaneously probed with different Poisson spike-trains, and the primary response recorded. Figures 5.6.1a and 5.6.1b show the coherence estimates (2.5.10) between each of the two fusimotor inputs, gammal and gamma2, and the output when applied separately. Both inputs are coupled to a similar degree with the output, the gammal input exhibiting stronger coupling in the range 15-40 cycles/sec..

The application of both fusimotor inputs simultaneously changes this situation as the coherence estimates in figures 5.6.2a and 5.6.2b illustrate. These are the corresponding coherence estimates in the presence of the second fusimotor input. The gammal input almost totally overrides any dependence of the primary discharge upon the gamma2 input. The multiple coherence between the two inputs and the output is shown in figure 5.6.2c, this is similar to both the separate coherence estimates in figure 5.6.1, perhaps resembling more closely the coherence of the gammal input on its own.

These results show that, for this particular spindle, when two different random fusimotor inputs are applied separately to the same muscle spindle a similar level of linear dependence between the output and each of the inputs exists. However the application of the two inputs simultaneously leads to the linear coupling between the primary discharge and these two inputs being almost completely dominated by one of the fusimotor inputs.

Extending the linear model without considering higher order kernels can provide a powerful tool to look at interactions within multi-input point-process systems.

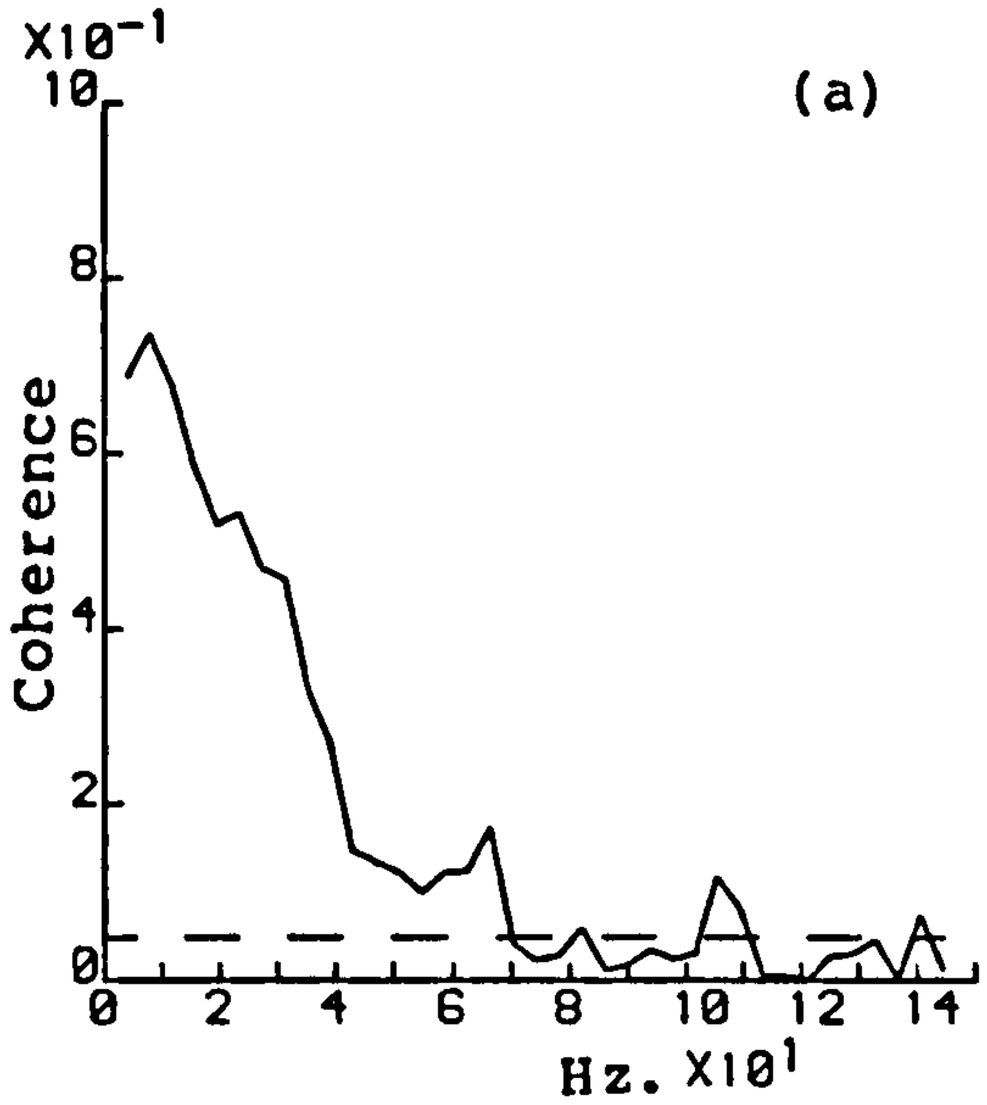

(a)

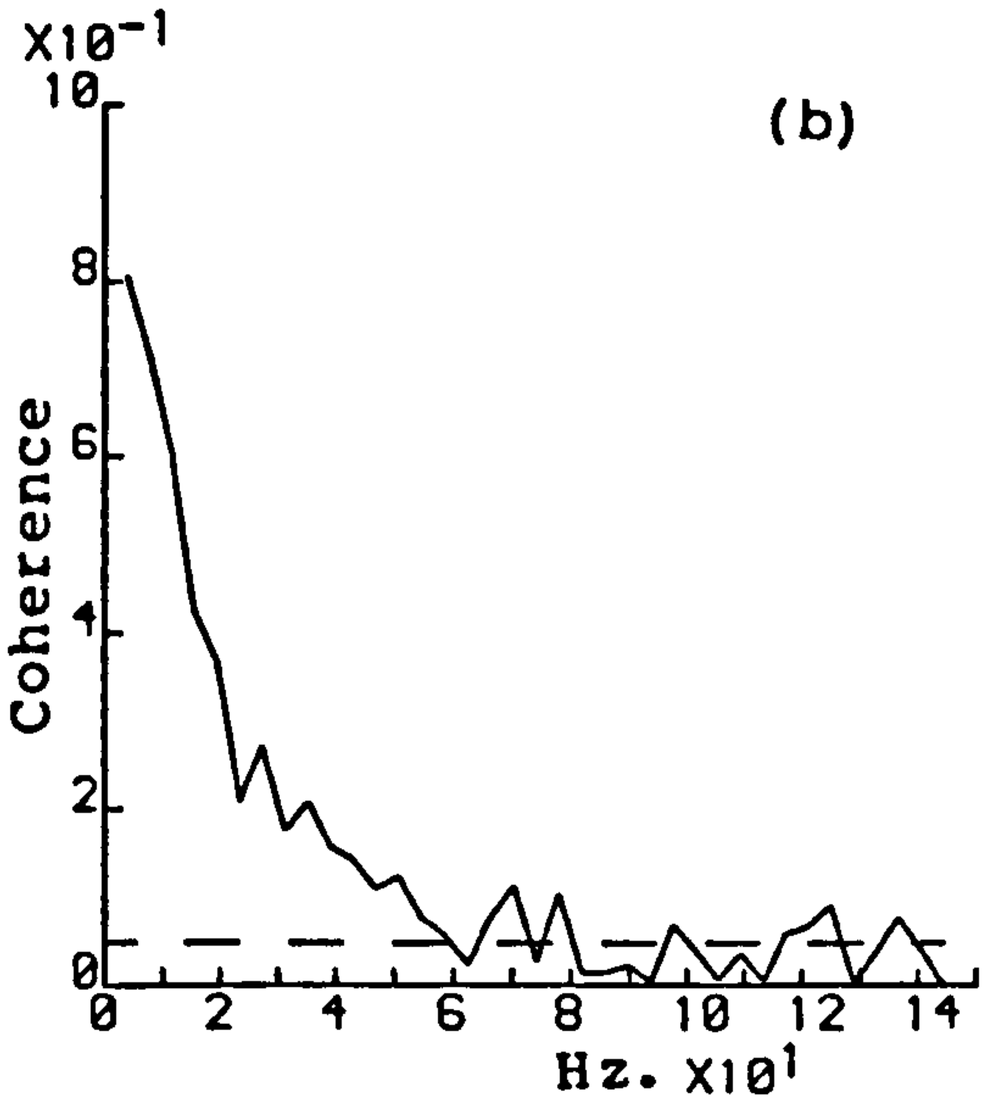

(b)

Fig. 5.6.1 Coherence estimate (2.5.10) between Ia discharge and

(a) gamma1 and

(b) gamma2 fusimotor inputs applied separately.

Dashed line shows approximate 95% confidence level.

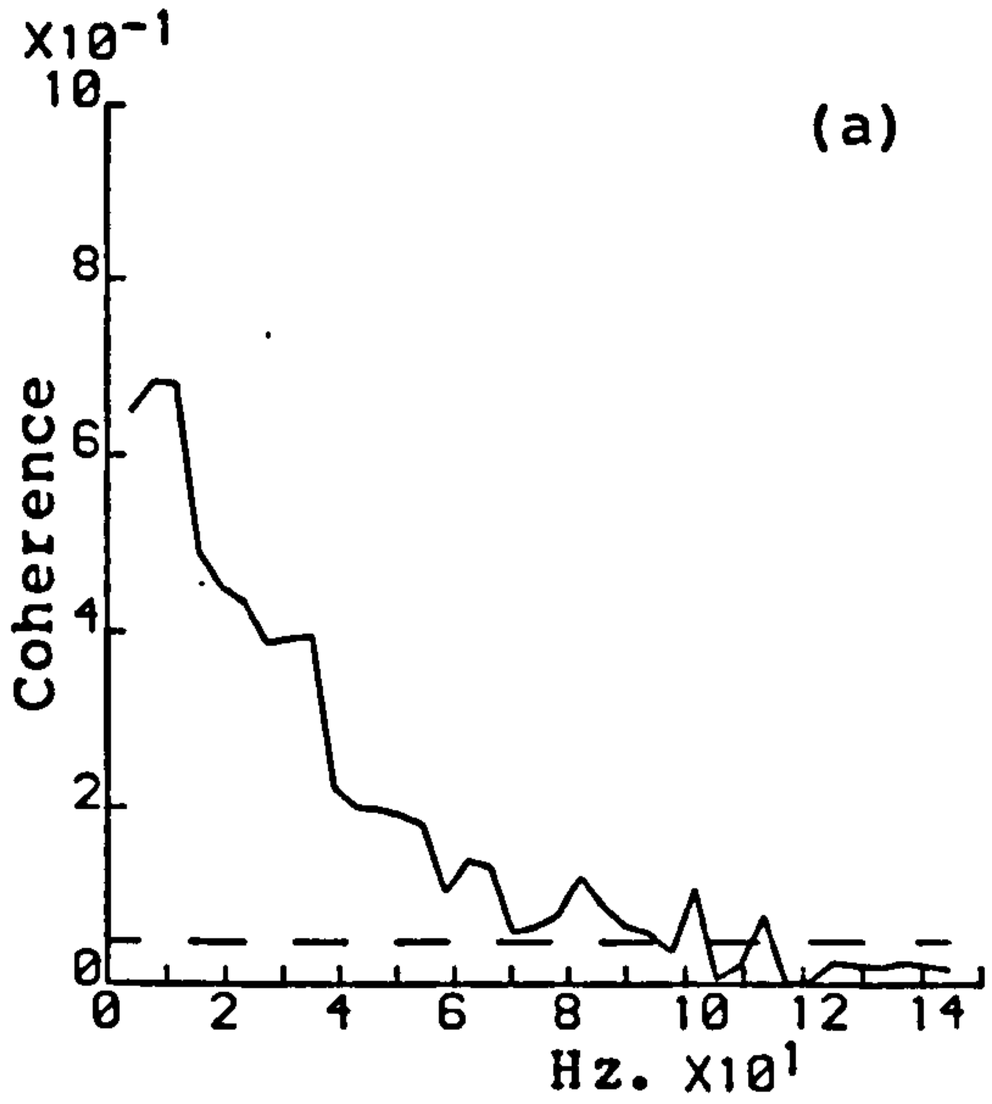

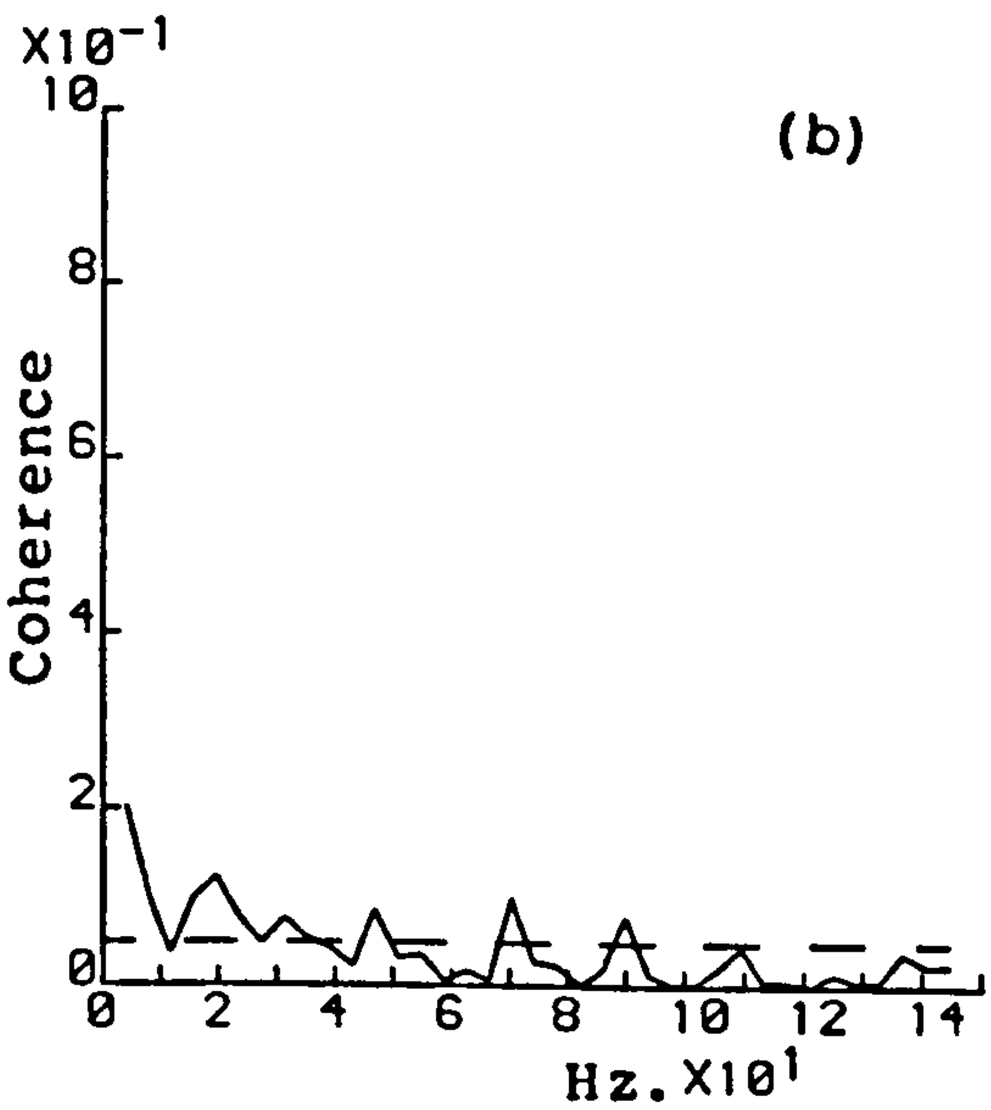

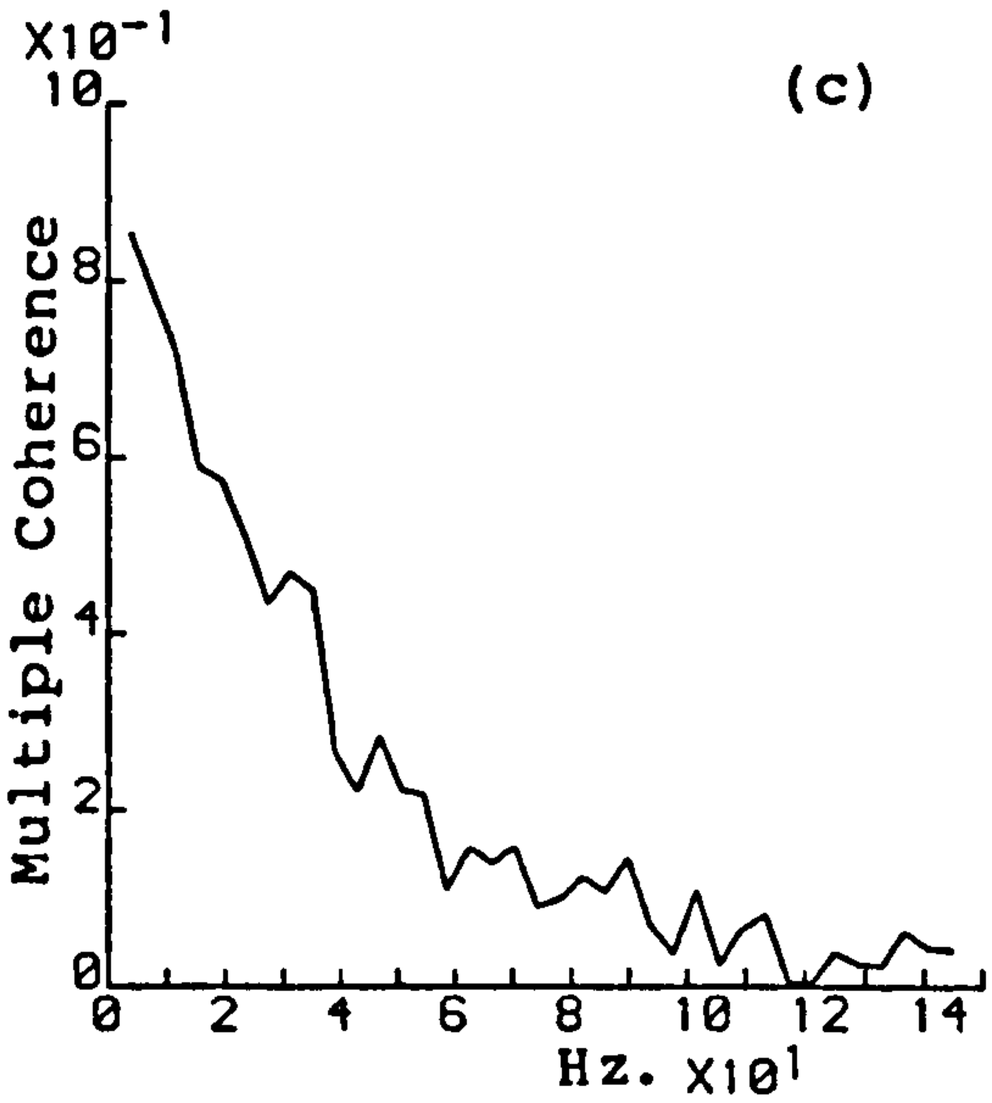

Fig. 5.6.2 Coherence estimate (2.5.10) between Ia discharge and

(a) gammal in presence of gamma2 and

(b) gamma2 in presence of gammal fusimotor input.

Dashed line shows approximate 95% confidence level.

(c) Estimate of multiple coherence (5.6.2) between Ia discharge and both gammal and gamma2 fusimotor inputs.

5.7 THE SINGLE INPUT QUADRATIC MODEL

The investigation of non-linear interactions using the point-process model (2.4.2) requires the calculation of kernels of order two and higher. The simplest form of this is the single input quadratic model :

$$x_M(t) = s_o + \int s_1(t-u)\ dM(u) + \iint_{u \neq v} s_2(t-u,t-v)\ dM(u)dM(v). \qquad (5.7.1)$$

The solution of this model involves estimating the second kernel and this can be done in either the time domain or frequency domain provided the process M is Poisson. In the time domain $s_2(u,v)$ can be estimated according to (5.5.1), and an estimate in the frequency domain of $S_2(\lambda,\mu)$ is given in (5.5.4).

Figure 5.7.1 shows a surface plot of the estimate of $s_2(u,v)$ for a data set derived from the primary response of a muscle spindle to random fusimotor stimulation at fixed muscle length. The estimate is shown for u,v=0 to 50 msec., using a bin width of 1msec. in the second and third order histogram estimates (2.3.3), (2.3.8) and (5.3.1) used to form the product densities. The estimate is further smoothed before graphing by the application of a two dimensional moving average which consists of the equal weighting of a single point plus its eight nearest neighbours in the two dimensional array. Denoting 1 element in the estimate (5.5.1) as x_{ij}, and the corresponding smoothed element as xs_{ij} this smoothing can be written as :

$$xs_{ij} = 1/9 \sum_{i-1}^{i+1} \sum_{j-1}^{j+1} x_{ij}. \qquad (5.7.2)$$

This smoothing is applied twice to obtain the estimate in figure 5.7.1. Figure 5.7.2 is a contour plot of this smoothed estimate

of $s_2(u,v)$. Several features can be isolated in these plots as standing out from the general variations due to the sampling properties of the estimation technique. Before commenting on the relevance of these features to the model (5.7.1) a level of significance must be determined which will account for fluctuations in the plots due to these sampling properties. From (5.3.7) the asymptotic distribution for the estimate (5.5.1) of $s_2(u,v)$ can be written as :

$$\lim_{v\to\infty} s_2(u,v) = 0, \qquad (5.7.3)$$

and since the kernel is assumed symmetrical, then as u and v increase the value of $s_2(u,v)$ will tend to zero. Rigas (1983, ch4) gives an expression for the variance of $q_{nmm}(u,v)$, but it is not presently clear if this approach may be extended to estimate the variance of $s_2(u,v)$. However a rough indication of the variability of the smoothed estimate of (5.5.1) due to sampling fluctuations may be obtained by processing two Poisson spike-trains with equal record length and with the same number of spikes as the data set being studied. For the second order time domain estimates considered in section 2.3a, bivariate processes of equal record length and equal spike numbers have the same variance. On the assumption that this fact also applies to third order product densitiy and subsequent second kernel estimates, the hypothesis that estimates of $s_2(u,v)$ for bivariate processes will have the same variance, if the processes have equal record length and equal number of input and output spikes, appears reasonable. Processing two Poisson spike-trains with the same mean rates as the data set being studied can be used to estimate a 95% confidence band around the assumption of independence. Firstly the variance of the smoothed estimate $s_2(u_i,v_j)$ is

calculated as :

$$\text{var}\{\ s_2(u_i,v_j)\ \} = 1/(n_1n_2-1) \sum_{i=1}^{n_1} \sum_{j=1}^{n_2} (s_2(u_i,v_j)-s)^2, \quad (5.7.4)$$

where s is the average value of $s_2(u_i,v_j)$, and the range of values over which the kernel is estimated is given by $(s_2(u_i,v_j)$: $u_i=ih$, $i=1,\ldots,n_1$ and $v_j=jh$, $j=1,\ldots,n_2)$. Expression (5.7.4) is an extension to two dimensions of the standard technique for estimating the variance of a set of data corresponding to a continuous random variable, see for example Jenkins and Watts (1968, ch3). The confidence band is estimated, as previously by adding ± 1.96 standard deviations to the asymptotic distribution (5.7.3), where the standard deviation is the positive square root of (5.7.4). This data set, whose second order properties and first order kernel are estimated in section 2.7, has M(R)=1010, N(R)=538 and R=15872. Processing a data set comprising of two Poisson spike-trains with the same values of M(R), N(R) and R gives an estimate of $0.65*10^{-5}$ for the variance (5.7.4), and an approximate confidence band of $\pm 0.50*10^{-2}$ for the second kernel.

Using the above hypothesis this value can be used to indicate areas of significance for the smoothed kernel estimate, and regions where the estimate exceeds $50*10^{-4}$ are indicated along with regions where the estimate exceeds $-50*10^{-4}$ in figure 5.7.2. These regions can now be considered as significant contributions from $s_2(u,v)$ to the model (2.4.2). Areas where $s_2(u,v) > 50*10^{-4}$ will indicate a facilitation or speeding up of the instantaneous rate of the primary discharge, and $s_2(u,v) < -50*10^{-4}$ indicates an inhibitory effect or slowing down of the instantaneous rate of the primary discharge. The range of u and v over which these areas extend will give the relative input spike

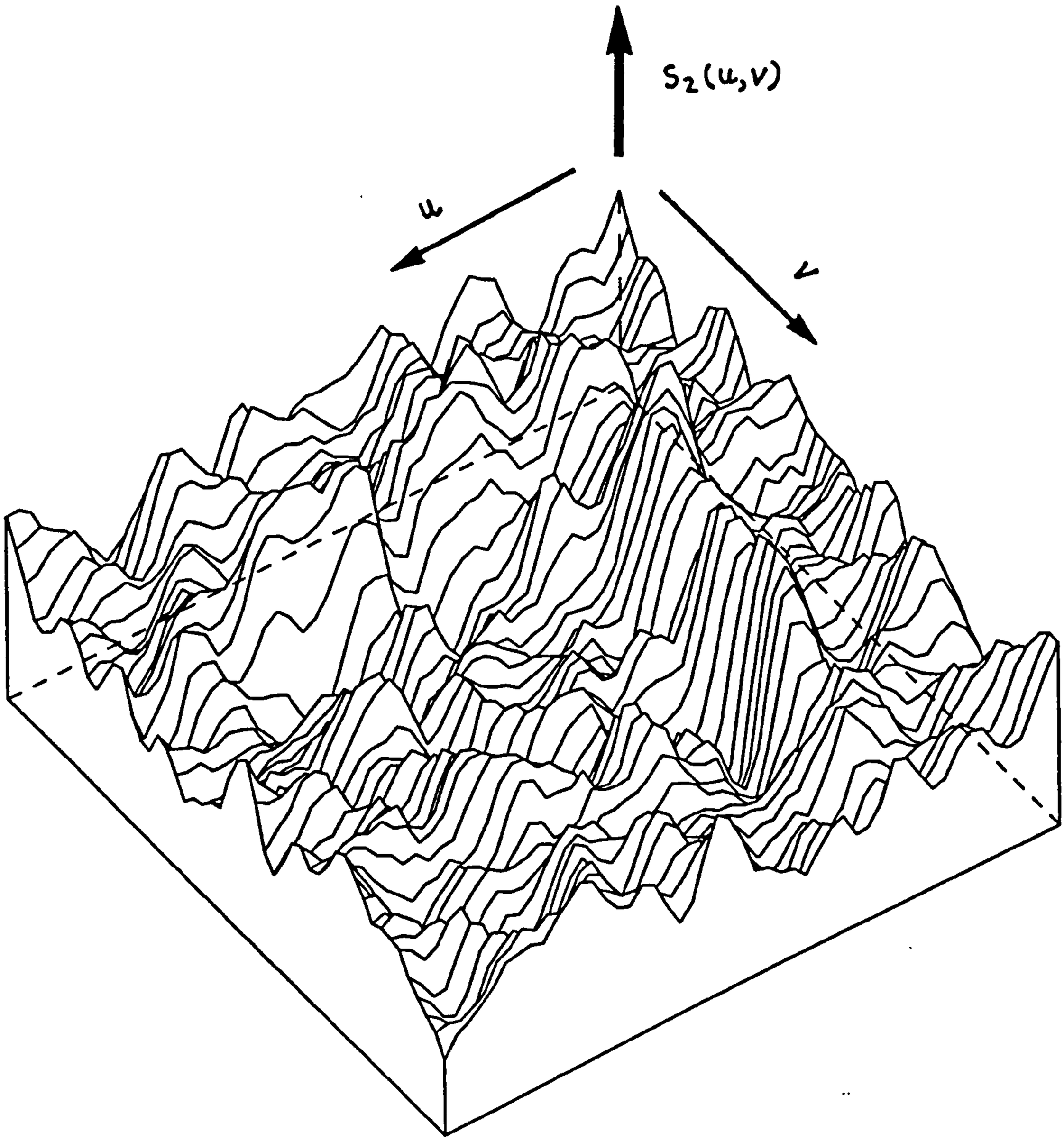

Fig. 5.7.1 Surface plot of smoothed estimate of $s_2(u,v)$ for u,v=0 to 50msec.. Estimated using (5.5.1), with h=1.0 in (2.3.3), (2.3.8) and (5.3.1) and smoothed using 2 applications of (5.7.2).

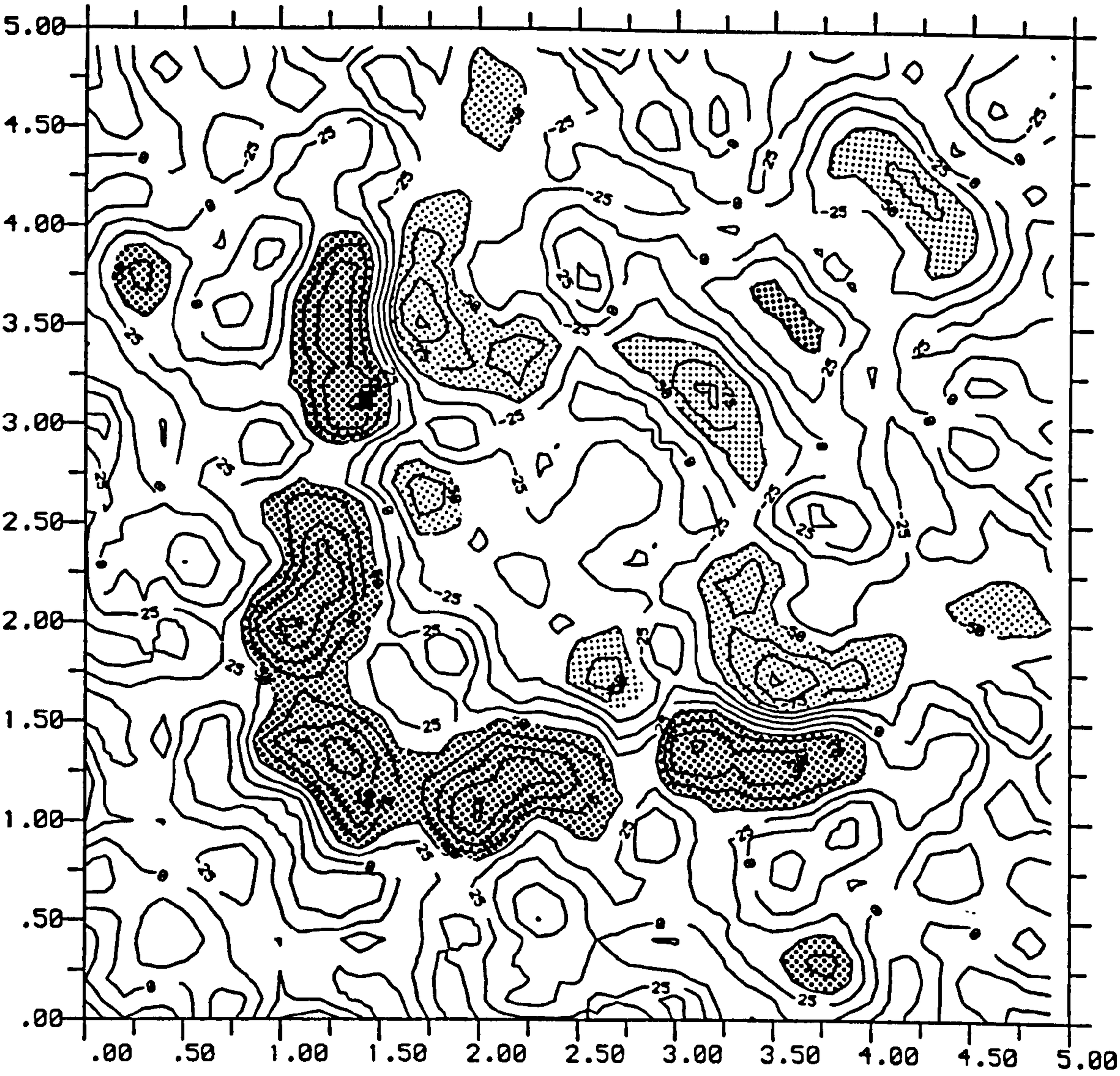

Fig. 5.7.2 Contour plot of smoothed estimate of $s_2(u,v)$ for u,v=0 to 50msec.. Estimated using (5.5.1), with h=1.0 in (2.3.3), (2.3.8) and (5.3.1) and smoothed using 2 applications of (5.7.2). 95% confidence band estimated as $\pm 50*10^{-4}$ using (5.7.4). Areas exceeding $50*10^{-4}$ are marked ▒ and areas exceeding $-50*10^{-4}$ are marked ▒.

pair timings which make a contribution to the quadratic model. A timing diagram for the second kernel is shown in figure 5.7.3, and v here corresponds to u-v in figures 5.3.1 and 5.5.1 in agreement with (5.5.1).

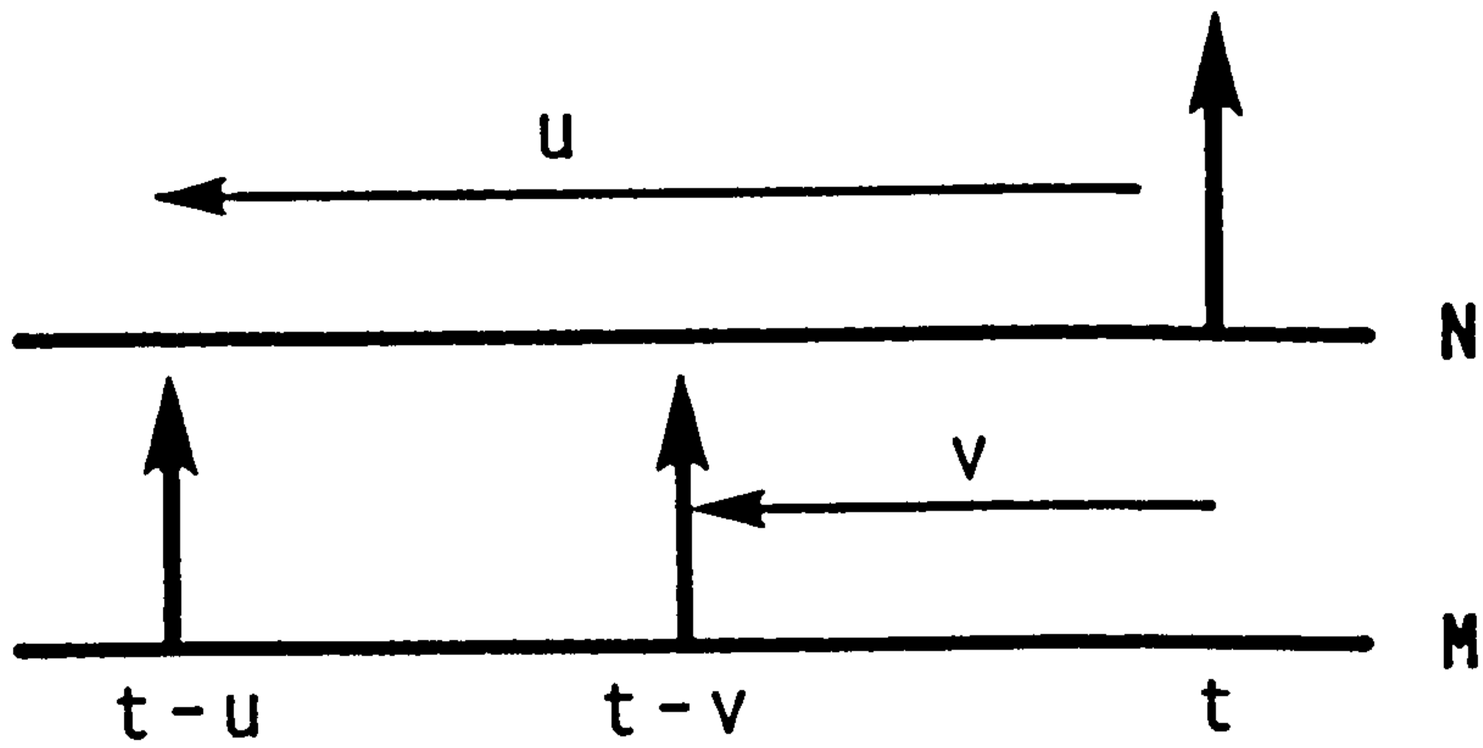

Fig. 5.7.3 Timing diagram for second order kernel $s_2(u,v)$.

Both plots are symmetrical about u=v (v=0 in figure 5.3.1), this corresponds to coincident input spikes, however the model (5.7.1) is not defined for this condition. Due to this symmetry only one half of the estimate need be considered, and the following discussion will concentrate on u>v in $s_2(u,v)$. The same arguments can be applied to v>u by reversing u and v.

The main feature is a large ridge which runs parallel to the u axis. The centre of this ridge is at u=v=13msec., which is the same as the delay present in figure 2.7.3b of the estimate of $s_1(u)$ for this data set. It has been found that data sets which have a negligible delay present in $s_1(u)$ have corresponding second kernel estimates where this ridge feature is centred at values of u and v in $s_2(u,v)$ corresponding to this delay. This point will be discussed further in the next section. The facilitation effect indicated by this ridge extends roughly from u=10msec. to 40msec. and v=10msec. to 15msec.. These point-

process kernels are analogous to the Volterra kernels which can be used to characterize a polynomial system driven by Gaussian white noise in conventional time-series analysis. As such they will give an indication of the memory of the system (Schetzen, 1981) since a Volterra series can be considered as a Taylor series with memory. Therefore the range of timings covered by areas of significance in figure 5.7.2 will indicate how long the effects of one spike will remain within the muscle spindle so that a second spike can interact with the first spike and facilitate or inhibit the rate of the primary discharge. Considering again this ridge, then a u spike which has occurred between 10 and 40 msec. previously to an arbritary time t can interact with a v spike which has occurred in the range 10 to 15msec. previously and produce a quadratic contribution to the probability, (2.4.2), of occurrence of an event at time t.

Another area of significance is a region of inhibition which runs roughly parallel to the u axis. This area is not as extensive as the area of facilitation, but the same arguments can be applied to interpret the contribution of this region to the model (2.4.2). Thus if a u spike occurs between 25 to 28 msec. or between 31 to 40 msec. before an arbritary time t, then a v spike between 15 to 20 msec. or between 15 to 25 msec. before time t will interact with the u spike to produce a quadratic contribution which will lead to a decreased probability of occurrence of an output event at time t. The results in figures 5.7.1 and 5.7.2 indicate that a non-linear interaction between two spikes can facilitate the primary output with input spike intervals as large as 30 msec. Although the results of chapter 2 have indicated that the linear point-process model can accurately account for the primary response to a fusimotor input over a wide

range of input conditions, these results show that non-linear interactive effects can occur even with only moderately fast spike rates in the input spike-train.

As well as these two main features other areas of significance are present in figure 5.7.2. Some of these are concentrated along the main diagonal, and this represents short interspike intervals in the input. Two of these areas are centred on u=v=32msec. and u=v=45msec. and it can be concluded that short interspike intervals of between 1 and 7 msec. in the input spike-train can exert an interactive inhibitory effect up to 45 msec. later on the primary discharge. This indicates that spindle memory effects can last up to 45msec. This may be due to the mechanical time-constants associated with the intrafusal fibres being of similar duration, or it may be due to other, as yet undocumented, effects.

Finally one isolated region of facilitation is present at u=37msec. and v=2msec.. From this it appears that in some circumstances non-linear effects can propagate through the spindle much faster than the mean delay estimated in chapter 2.

In the frequency domain the second kernel $S_2(\lambda,\mu)$ can be estimated by using (5.5.4). Figures 5.7.4 and 5.7.5 show surface and contour plots of the magnitue of $S_2(\lambda,\mu)$ plotted as $20\log_{10}|S_2(\lambda,\mu)|$ in dB.. The estimate is formed according to (5.5.4) and the second and third order spectra are estimated directly using (2.3.29) and (5.3.13) by averaging periodograms of disjoint sections of data, where R=15872 and T=256 in (2.3.28). This is followed by one application of the smoothing algorithm (5.7.2) to the real and imaginary parts to obtain the results shown in figures 5.7.4 and 5.7.5. The estimate of the phase of

$S_2(\lambda,\mu)$ is shown as a surface plot in figure 5.7.6 and as a contour plot in figure 5.7.7, and is plotted in unrestrained form to allow any delay to show up.

The frequency domain representation of the second order kernel has arguments of cycles/sec. which relate to periodicities in the input spike-train which are strongly correlated to sinusoidal components of this frequency. The magnitude of $S_2(\lambda,\mu)$ will indicate the strength of dependence of the output upon interactions between two periodicities of frequencies λ and μ in the input spike-train. The phase can be used to determine the average delay between input spikes which correlate strongly with these periodicities and output spikes using the relationship $\phi(\lambda)/\lambda$ to estimate the delay.

Considering the magnitude of $S_2(\lambda,\mu)$ in figures 5.7.4 and 5.7.5, the dependence of the output upon interactive effects of periodicities in the input spike-train is largest at lower frequencies, being fairly constant for frequencies less than 35 Hz. and in general the magnitude of this contribution drops as λ and μ increase. There is also a region close to each axes where a similar level of interactive dependence occurs between periodicities of low frequency (<5Hz.) with periodicities up to 75Hz.. One other area has a similar magnitude and this is centred about $\lambda=\mu=80$Hz. indicating an interaction between two periodicities close to this frequency.

The phase estimate in figures 5.7.6 and 5.7.7 can be used to indicate the delay between harmonics of frequency λ and μ and the output. In the region at low frequencies where the magnitude plot is at a maximum the general form of this estimate is that of a constantly decreasing phase which is consistent with a time delay. Considering fixed values of λ less than 50Hz., then the

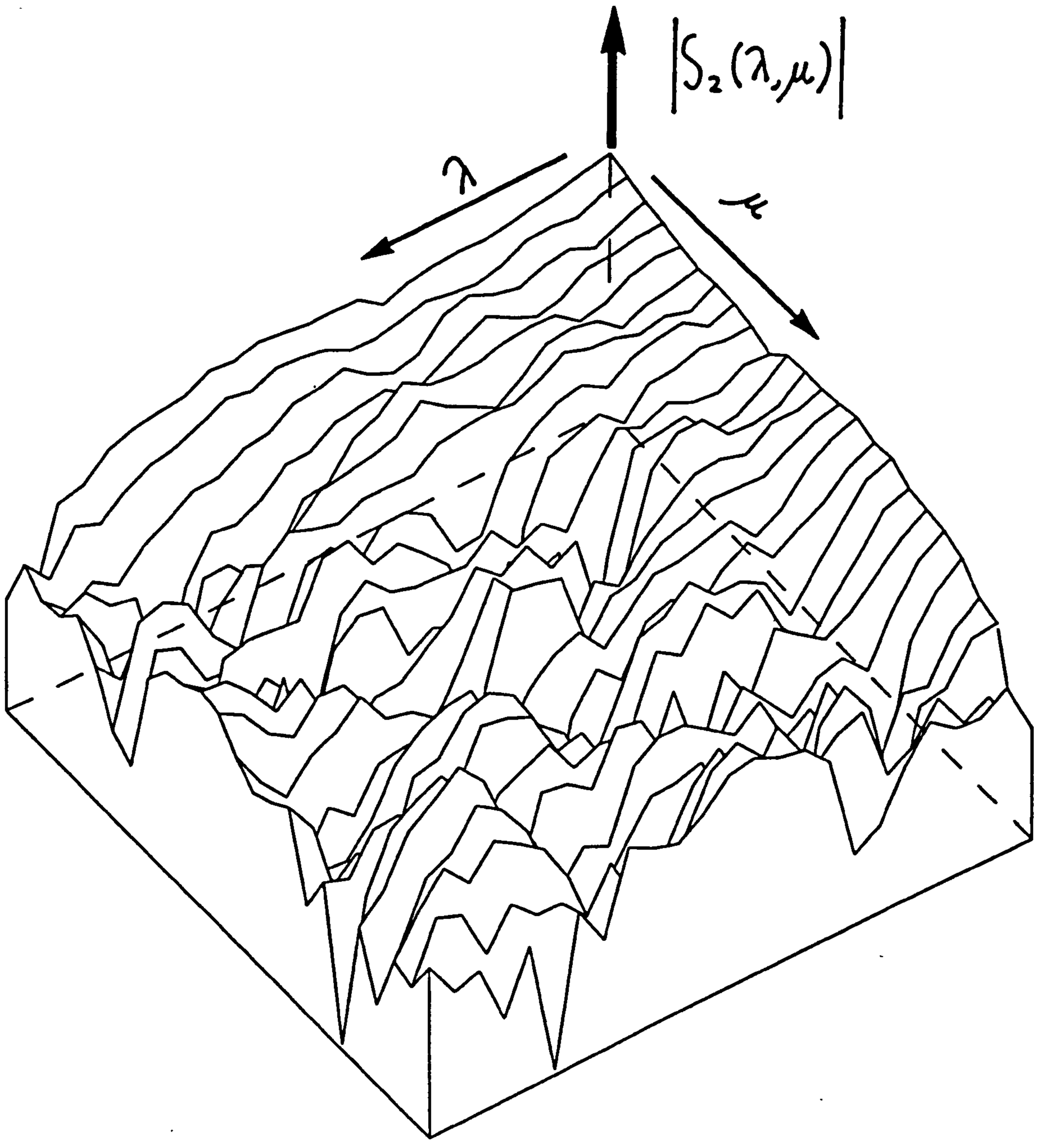

Fig. 5.7.4 Surface plot of magnitude of smoothed estimate of $S_2(\lambda,\mu)$ plotted as $20\ \mathrm{Log}_{10}\ |S_2(\lambda,\mu)|$ for λ,μ =0 to 100Hz.. Estimated using (5.5.4), with T=256 in (2.3.29) and (5.3.13) and smoothed using 1 application of (5.7.2).

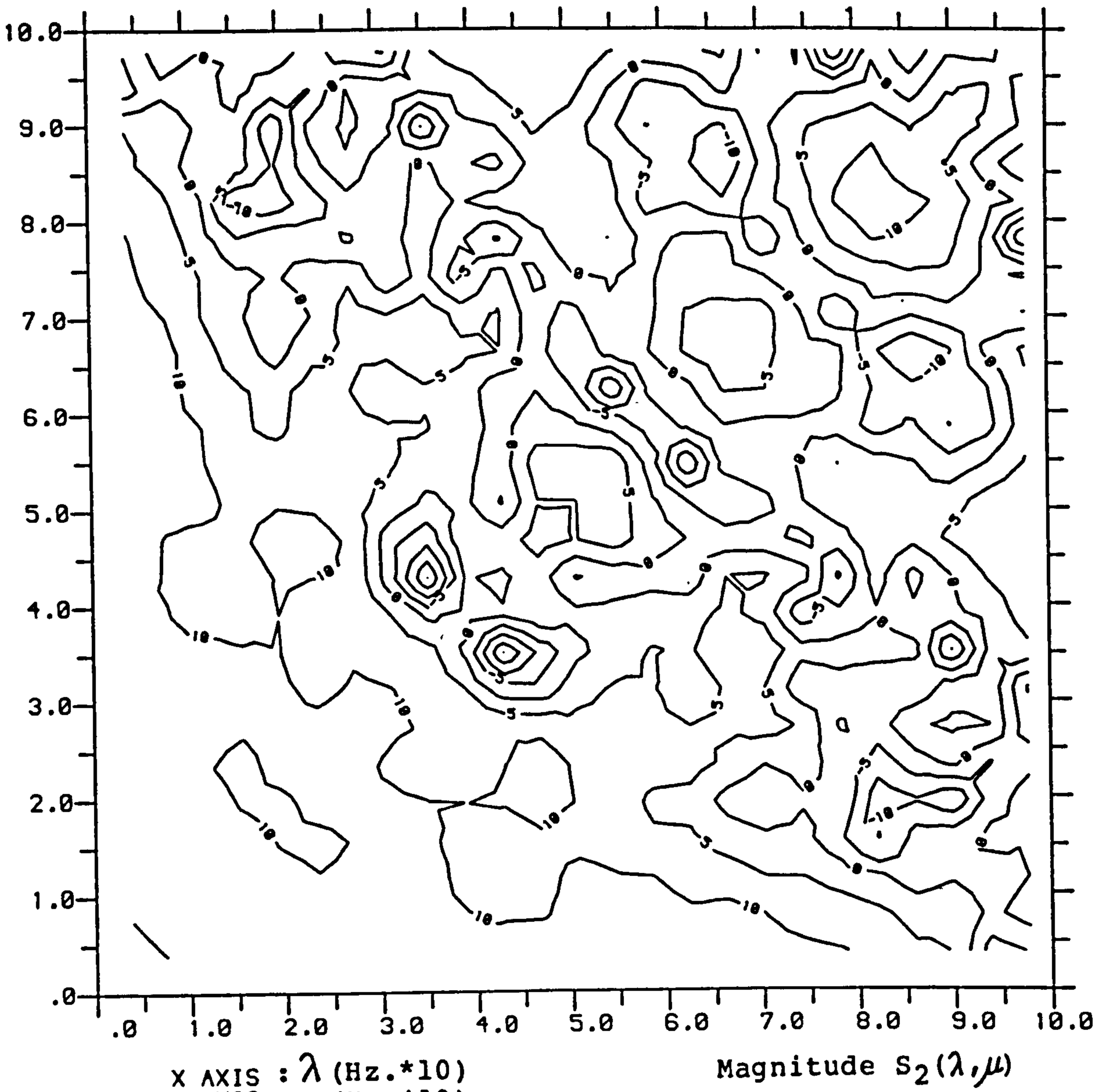

Fig. 5.7.5 Contour plot of magnitude of smoothed estimate of $S_2(\lambda,\mu)$ plotted as $20\ \mathrm{Log}_{10}\left|S_2(\lambda,\mu)\right|$ for λ,μ=0 to 100Hz.. Estimated using (5.5.4), with T=256 in (2.3.29) and (5.3.13) and smoothed using 1 application of (5.7.2).

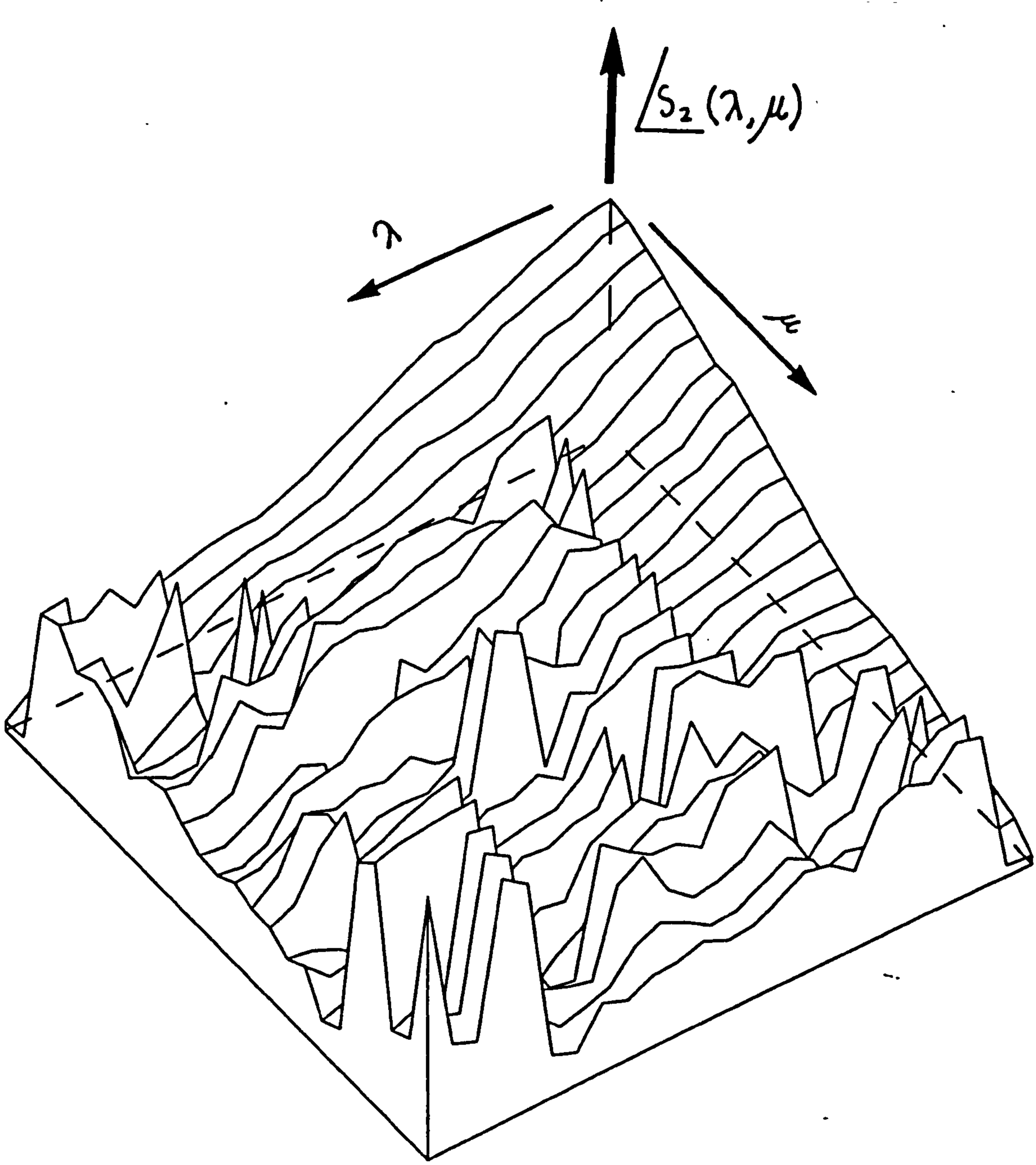

Fig. 5.7.6 Surface plot of unrestrained phase of smoothed estimate of $S_2(\lambda,\mu)$ for λ,μ=0 to 100Hz.. Estimated using (5.5.4), with T=256 in (2.3.29) and (5.3.13) and smoothed using 1 application of (5.7.2).

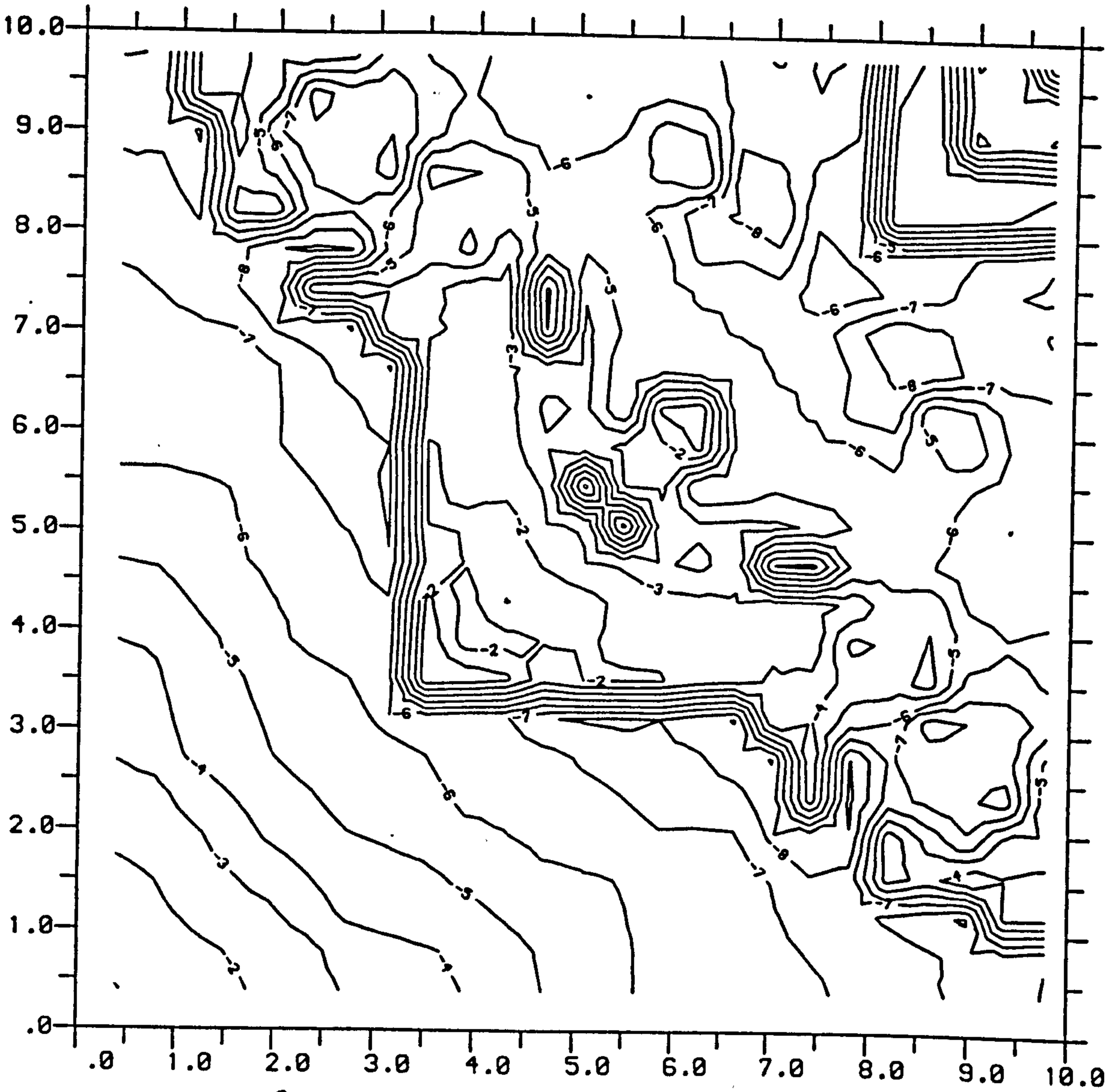

Fig. 5.7.7 Contour plot of unrestrained phase of smoothed estimate of $S_2(\lambda,\mu)$ for λ,μ=0 to 100Hz.. Estimated using (5.5.4), with T=256 in (2.3.29) and (5.3.13) and smoothed using 1 application of (5.7.2).

interactive effect on this fixed periodicity of increasing μ from zero upwards is to increase the phase and thus the time taken for the periodicity of frequency λ in the input spike-train to propagate through the muscle spindle. The phase for the periodicity of increasing frequency μ can be approximated by a straight line which indicates a constant delay, and this leads to estimates of between 13 and 15 msec. for the effects of the periodicity of increasing frequency μ to propagate through the spindle. As an example, for λ=20 Hz. the phase can be approximated by a straight line giving a constant delay of 13 msec. for the periodicity μ over the range 0 to 75 Hz., whereas the delay for the fixed periodicity of 20Hz. increases from 20msec. when μ=4 Hz. to approximately 48 msec. when μ=50 Hz.. The phase surface 5.7.6 can also be approximated by a straight line along its main diagonal, this is in fact the steepest part of the surface and leads to an estimate of a constant delay of 36 msec. when $\lambda = \mu$. Therefore if the frequency of one periodicity in the input spike-train varies so that it tends towards the frequency of a second periodicity which is present, then the net effect of the interaction between these two periodicities is to increase the time for the interactive effects to propagate through the spindle.

Lines of constant phase in figure 5.7.7 indicate variations in λ and μ where periodicities in the input spike-train correlate with the same point on sinusoidal waveforms of frequency λ and μ cycles/sec. In general as λ increases then a decrease in μ will lead to constant phase. One interesting effect can be seen at larger phase lags, and is most noticeable in the -6 radian contour which starts at λ=58Hz., μ=0Hz. As μ increases the phase

remains constant until μ exceeds 19 Hz., and then this contour follows the general trend mentioned above. Consequently a fixed periodicity of frequency 58 Hz. will interact with a periodicity in the range 0 to 19 Hz. in such a manner that on average the input spikes will always correlate with the same point on a sinusoidal waveform, even although the frequency is altering. This constant phase contour parallel to the frequency axes may indicate a type of phase-locking phenomenon, where spike-trains containing periodicities of increasing frequency can interact with a fixed periodicity in the spike-train and produce a constant phase effect between input and output spike-trains.

5.8 QUADRATIC KERNEL ESTIMATES FOR SIMULATED DATA

This section will study the application to simulated muscle spindle data of the techniques developed in section 5.7 for time and frequency domain second kernel estimates. The simulation is introduced in section 2.8, and the range of time constants and gains, along with the corresponding first kernel estimates are described in section 2.9. Comparison between second kernel estimates for simulated data sets with different parameters will be made. This will allow the effects of varying the individual simulation parameters on the second kernel estimates to be determined. These differences can then be related to estimates from real muscle spindle data and comparison between real and simulated data second kernel estimates will provide a more rigorous test of the accuracy with which the simulation can model the behaviour of a fusimotor sub-system, since non-linear effects are now being studied.

In the time domain expression (5.5.1) gives the estimate of the second kernel which is further smoothed according to (5.7.2).

The effect of independently varying the time constant in the linear dynamics (t_d) and the modulator gain and time constant (G_m/t_m) on second kernel estimates will be studied. Figures 5.8.1 and 5.8.2 show surface and contour plots of the smoothed estimate of $s_2(u,v)$ for simulated data with t_d=5msec. and G_m/t_m=11/10msec.. Using expression (5.7.4) a 95% confidence band for this estimate can be constructed and this gives a value $\pm 100*10^{-4}$. Figure 5.7.3 can be referred to for a timing diagram. The main features of this estimate are regions of facilitation and inhibition running parallel to the u and v axes. These are similar to the features present in figures 5.7.4 and 5.7.5, except that these areas are now shifted so that they are centred approximately at the origin. This results from the absence of any delay in the simulation, whereas real data always has propagation delays associated with it, and the effect of this delay is to offset by an amount equal to the delay the effective origin of the main regions of facilitation and inhibition which run parallel to the axes. All the simulated data studied has negligible propagation delays and this results in time domain second kernel estimates where any areas of facilitation and inhibition which run parallel to the axes are centred approximately at the origin.

Altering the simulation parameters has a clear and consistent effect on subsequent second kernel estimates. Four definite trends were detected while independently varying t_d or G_m/t_m. The choice of G_m/t_m pairs used in the simulation is explained in section 2.9. Three of these trends deal with the area covered and the magnitude of any regions of facilitation or inhibition which run parallel to the kernel axes, and the following discussion will concentrate on u>v in the kernels.

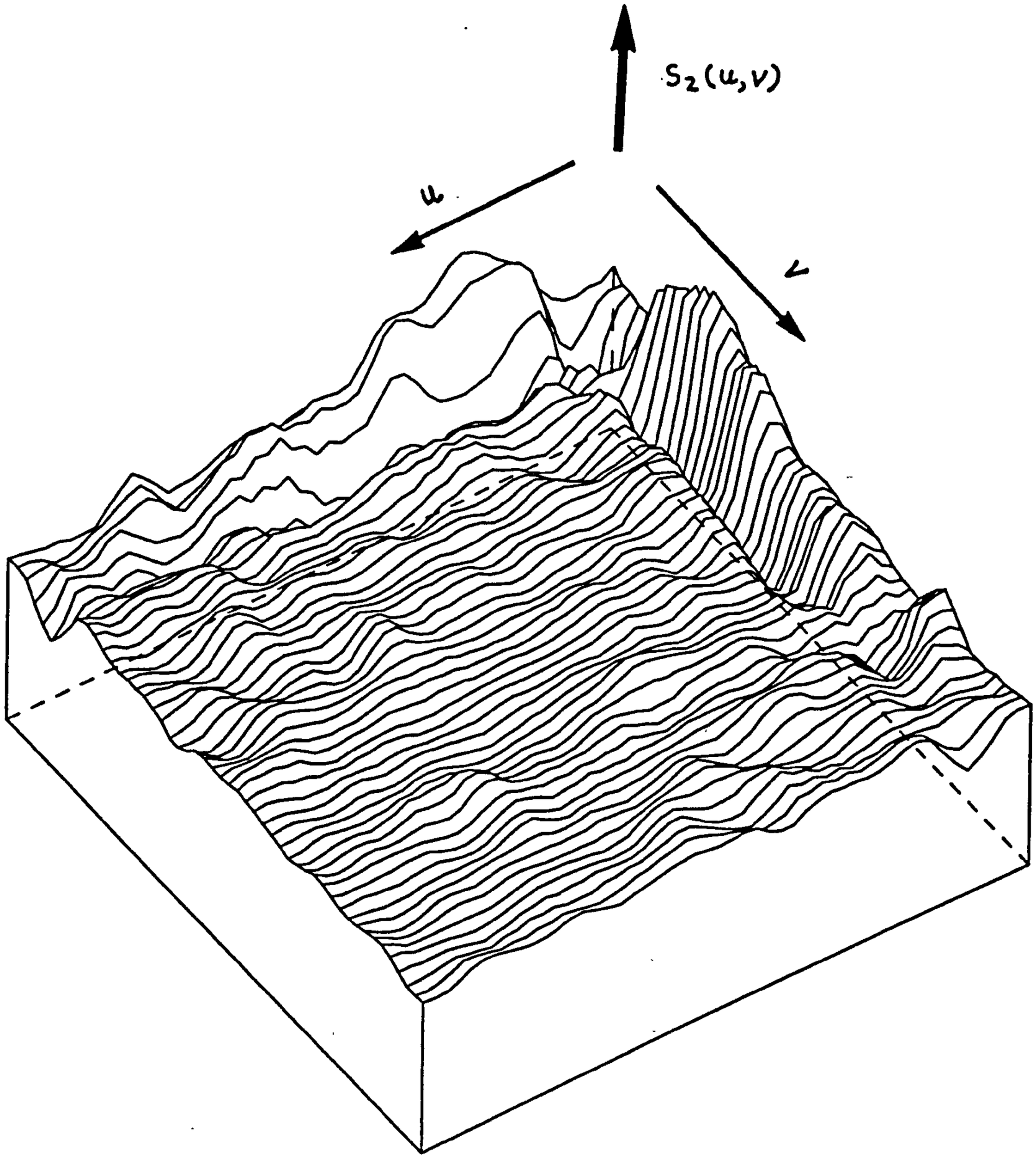

Fig. 5.8.1 Surface plot of smoothed estimate of $s_2(u,v)$ for u,v=0 to 50msec. and using simulated data with t_d=5msec. and G_m/t_m=11/10msec.. Estimated using (5.5.1), with h=1.0 in (2.3.3), (2.3.8) and (5.3.1) and smoothed using 2 applications of (5.7.2).

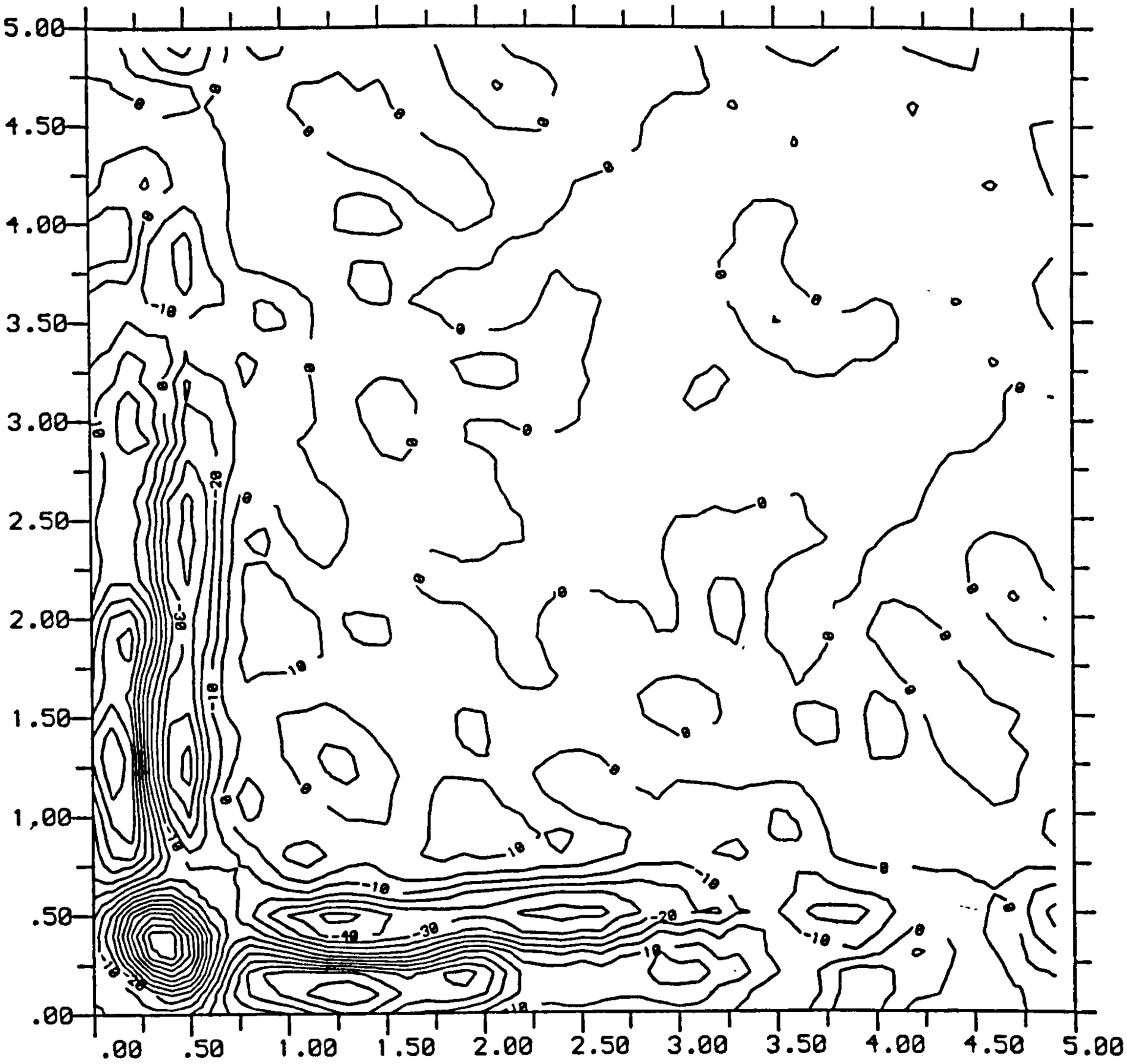

Fig. 5.8.2 Contour plot of smoothed estimate of $s_2(u,v)$ for u,v=0 to 50msec. and using simulated data with t_d=5msec. and G_m/t_m=11/10msec.. Estimated using (5.5.1), with h=1.0 in (2.3.3), (2.3.8) and (5.3.1) and smoothed using 2 applications of (5.7.2). 95% confidence band estimated as $\pm 100*10^{-4}$ using (5.7.4).

As G_m/t_m is increased for fixed t_d the extent of the area covered by the regions of facilitation and inhibition increases in the u direction (i.e. parallel to the axis), with only a slight increase in the v direction (i.e. perpendicular to the axis). Increasing t_d for fixed G_m/t_m has the opposite effect in that the regions over which the facilitation and inhibition extend increase in the v direction, with only a slight increase in the u direction. If either t_d or G_m/t_m are increased independently, or together, then the magnitude of the areas of facilitation and inhibition decreases and the rate of change between areas of facilitation and inhibition decreases, reflecting the longer time constants in the simulation. Finally, increasing t_d from 5 to 50 msec. results in the areas of facilitation and inhibition changing gradually from being parallel to the axes to being parallel to the main diagonal.

Therefore it can be concluded that longer time constants in the linear dynamics and modulator increase the memory effects in the simulation as shown by the increase in range and decrease in magnitude of any areas of facilitation and inhibition. Although longer time constants lead to increased memory effects, the major contribution to the second kernel is made by short interspike intervals in the input spike-train and is indicated by dominant features close to the main diagonal.

Varying the simulation parameters can be used to systematically alter second kernel estimates so that similar kernels to those estimated from muscle spindle data can be obtained. Figures 5.8.3 and 5.8.4 show the second kernel estimate for a simulated data set with t_d=10 msec. and G_m/t_m=14/15 msec.. Apart from the negligible propagation delay associated with the

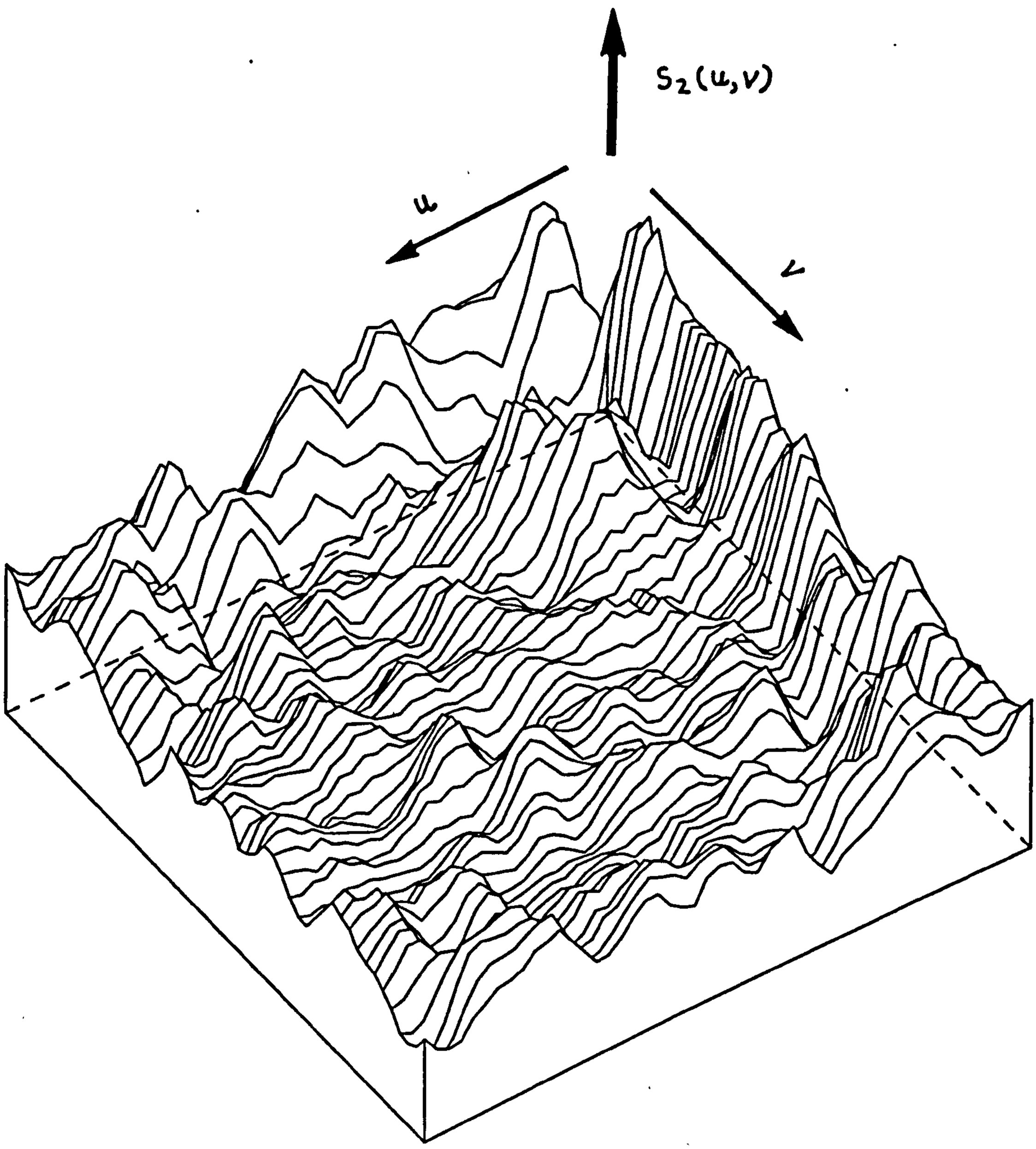

Fig. 5.8.3 Surface plot of smoothed estimate of $s_2(u,v)$ for u,v=0 to 50msec. and using simulated data with t_d=10msec. and G_m/t_m=14/15msec.. Estimated using (5.5.1), with h=1.0 in (2.3.3), (2.3.8) and (5.3.1) and smoothed using 2 applications of (5.7.2).

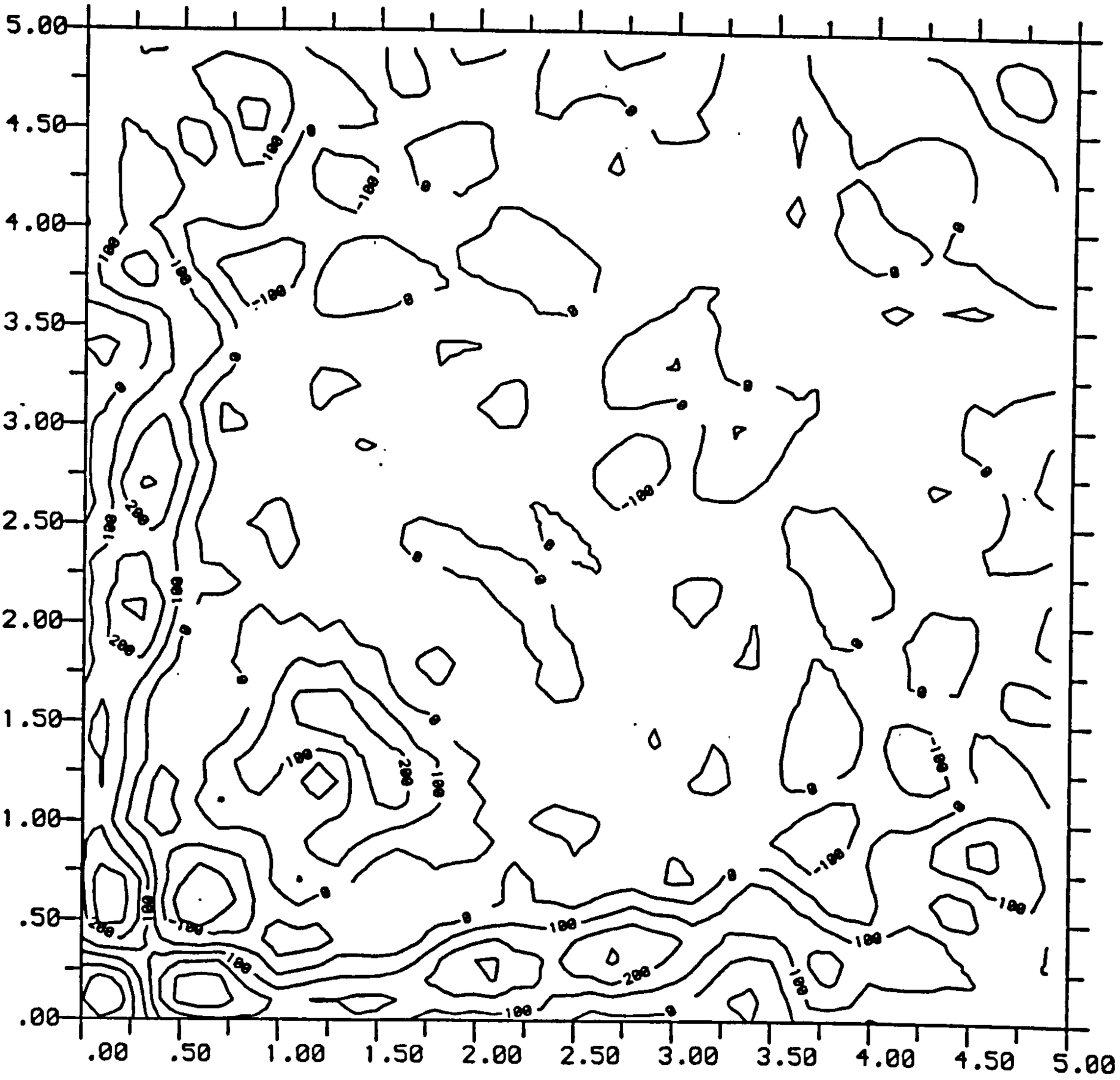

Fig. 5.8.4 Contour plot of smoothed estimate of $s_2(u,v)$ for u,v=0 to 50msec. and using simulated data with t_d=10msec. and G_m/t_m=14/15msec.. Estimated using (5.5.1), with h=1.0 in (2.3.3), (2.3.8) and (5.3.1) and smoothed using 2 applications of (5.7.2). 95% confidence band estimated as $\pm 100*10^{-4}$ using (5.7.4).

kernel estimate in figures 5.7.1 and 5.7.2 for real muscle spindle data. These results show that the simulation described in section 2.8 can model accurately the behaviour of a muscle spindle fusimotor subsystem, even when considering non-linear interactive effects between input spike pairs.

Finally figures 5.8.5 and 5.8.6 show surface and contour plots of the second kernel estimate for a simulated data set with t_d increased to 25 msec. and G_m/t_m=10/5msec.. The diagonal effects mentioned above can clearly be seen in this estimate, along with smaller, but also significant, effects parallel to the axes.

In the frequency domain, the second kernel can be estimated using (5.5.4) followed by one application of the smoothing (5.7.2) as described in section 5.7. As before, the gain (in logarithmic form) and phase will both be considered. Figures 5.8.7 and 5.8.8 show surface and contour plots of the magnitude of the estimate in the frequency domain of the second kernel for the simulated data set dealt with in figures 5.8.1 and 5.8.2. The phase is shown in figures 5.8.9 and 5.8.10. The similarity between frequency domain representations of simulated and real data second kernel estimates is apparent. The magnitude in the simulated case is 7/8 dB. larger, perhaps due to the lack of noise in the simulation, and the phase does not reach such large lag values. This can be explained by the absence of any propagation delay in the simulated data sets. However both real and simulated data have the dependence upon double periodicities in the input spike-train concentrated at lower frequencies, and in this region the gain and phase have similar forms both decreasing as the frequency of periodicity increases. All the

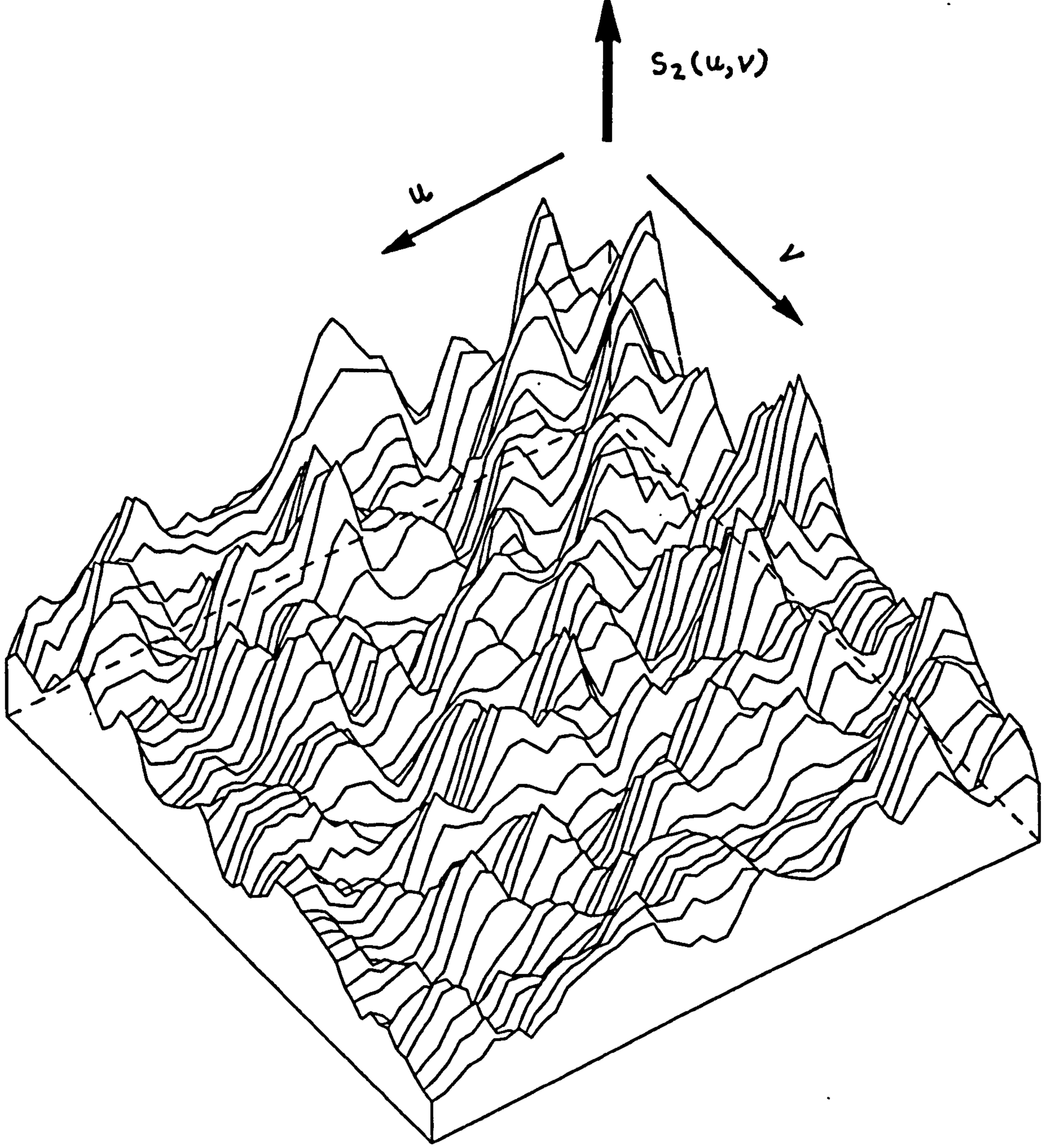

Fig. 5.8.5 Surface plot of smoothed estimate of $s_2(u,v)$ for u,v=0 to 50msec. and using simulated data with t_d=25msec. and G_m/t_m=10/5msec.. Estimated using (5.5.1), with h=1.0 in (2.3.3), (2.3.8) and (5.3.1) and smoothed using 2 applications of (5.7.2).

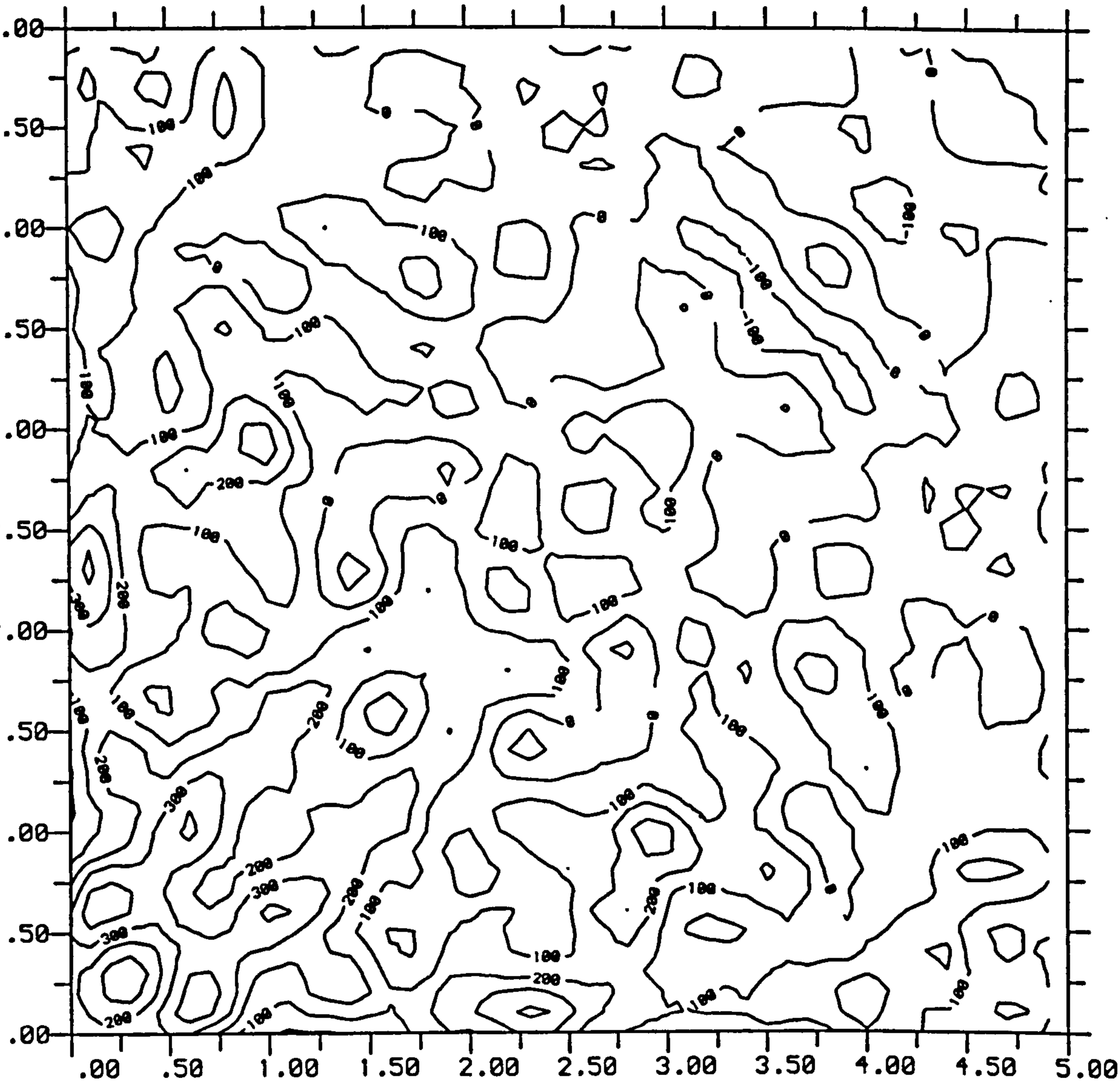

Fig. 5.8.6 Contour plot of smoothed estimate of $s_2(u,v)$ for u,v=0 to 50msec. and using simulated data with t_d=25msec. and G_m/t_m=10/5msec.. Estimated using (5.5.1), with h=1.0 in (2.3.3), (2.3.8) and (5.3.1) and smoothed using 2 applications of (5.7.2). 95% confidence band estimated as $\pm 100*10^{-4}$ using (5.7.4).

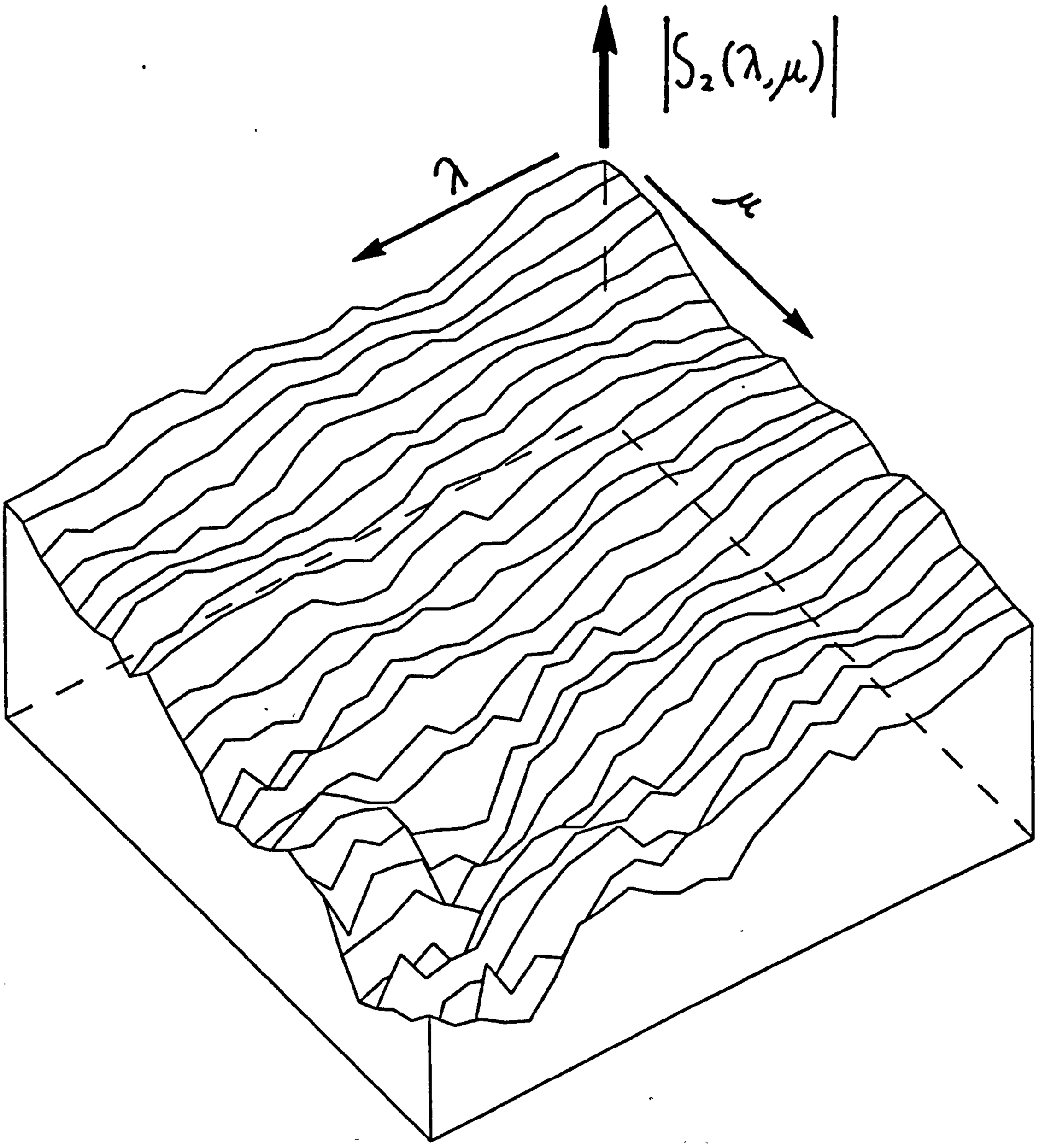

Fig. 5.8.7 Surface plot of magnitude of smoothed estimate of $S_2(\lambda,\mu)$ plotted as 20 $\text{Log}_{10}\left|S_2(\lambda,\mu)\right|$ for λ,μ=0 to 100Hz. and using simulated data with t_d=5msec. and G_m/t_m=11/10msec.. Estimated using (5.5.4), with T=256 in (2.3.29) and (5.3.13) and smoothed using 1 application of (5.7.2).

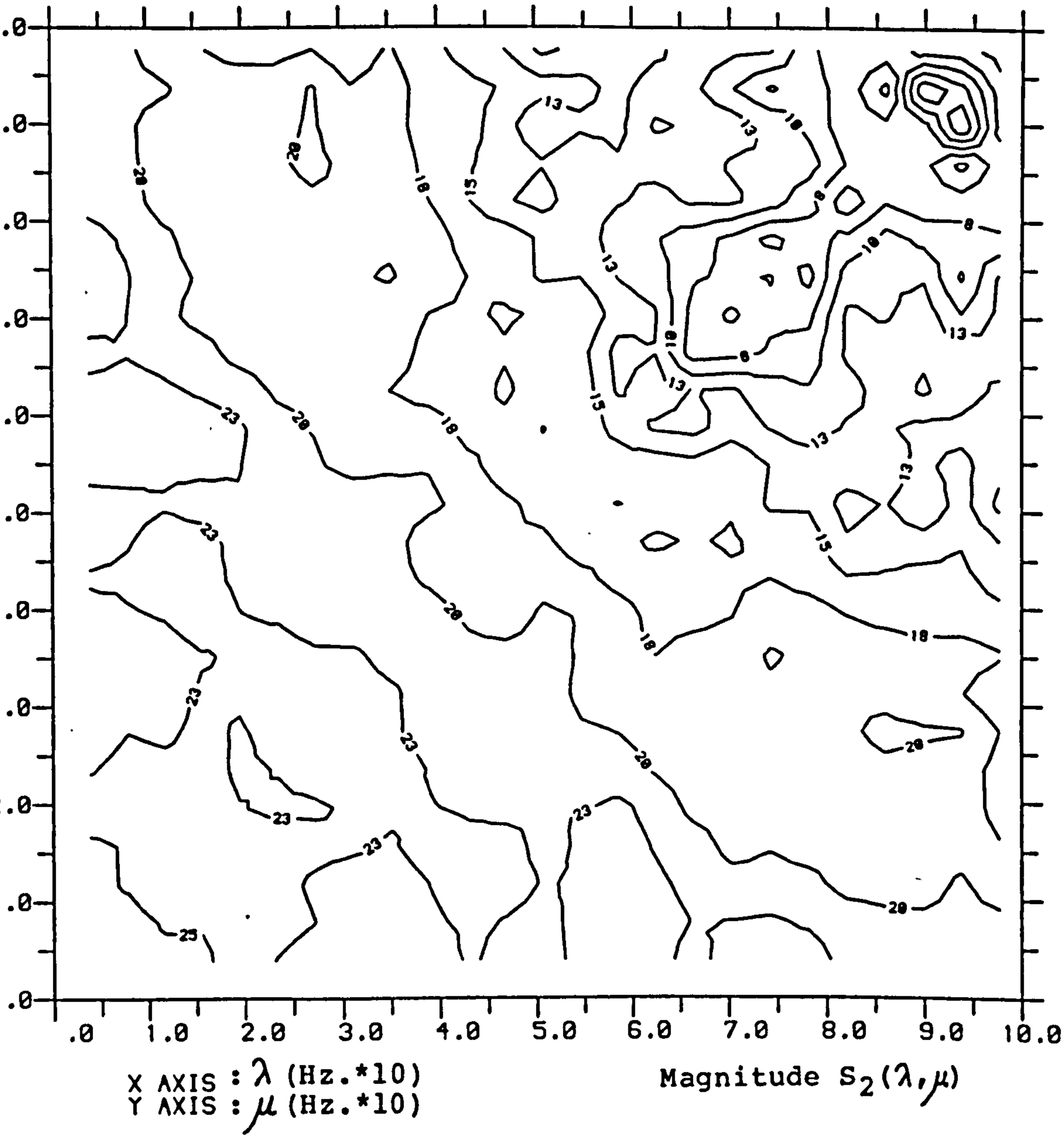

Fig. 5.8.8 Contour plot of magnitude of smoothed estimate of $S_2(\lambda,\mu)$ plotted as 20 $\text{Log}_{10}|S_2(\lambda,\mu)|$ for λ,μ=0 to 100Hz. and using simulated data with t_d=5msec. and G_m/t_m=11/10msec.. Estimated using (5.5.4), with T=256 in (2.3.29) and (5.3.13) and smoothed using 1 application of (5.7.2).

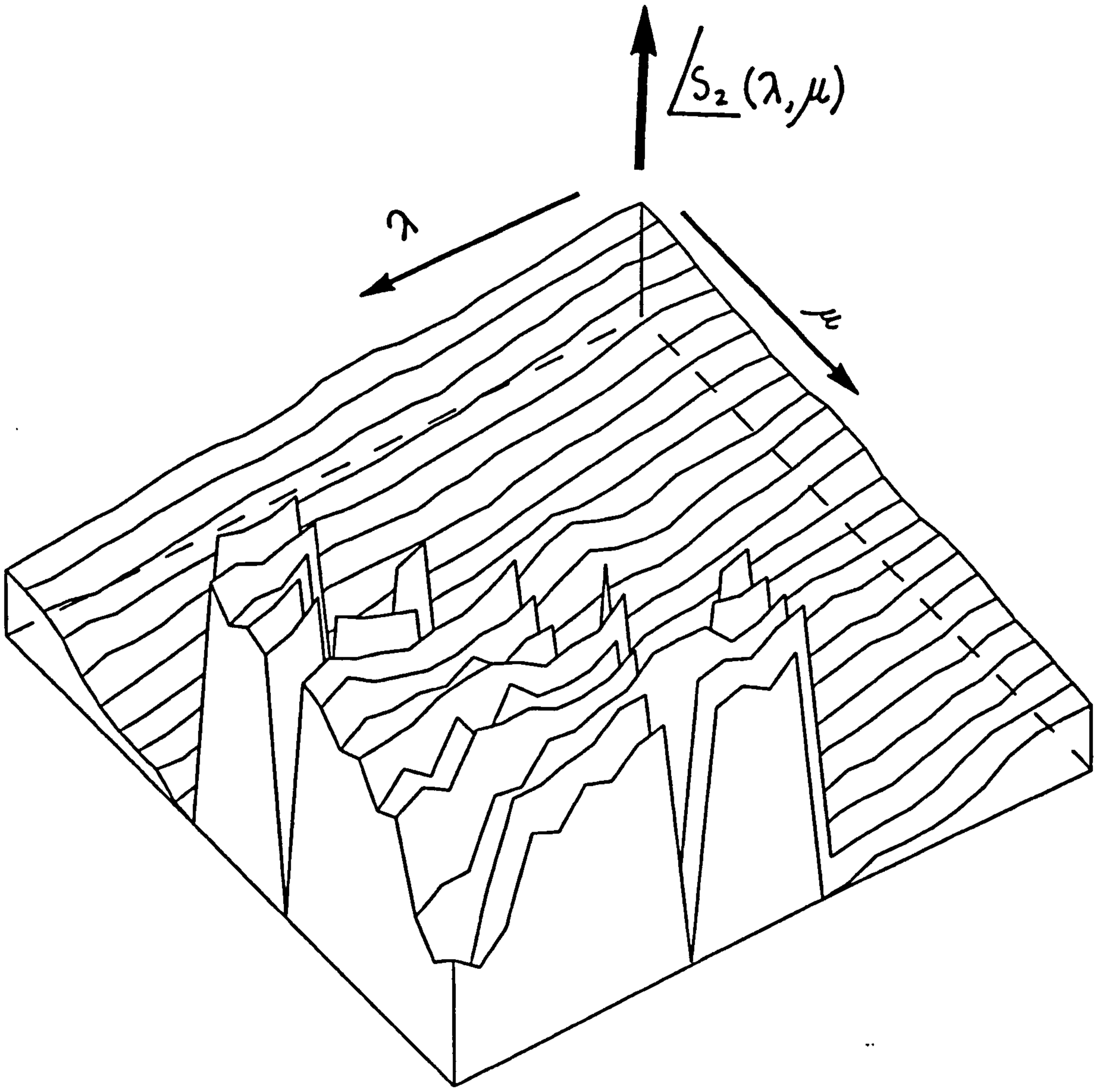

Fig. 5.8.9 Surface plot of restrained phase of smoothed estimate of $S_2(\lambda,\mu)$ for λ,μ=0 to 100Hz. and using simulated data with t_d=5msec. and G_m/t_m=11/10msec.. Estimated using (5.5.4), with T=256 in (2.3.29) and (5.3.13) and smoothed using 1 application of (5.7.2).

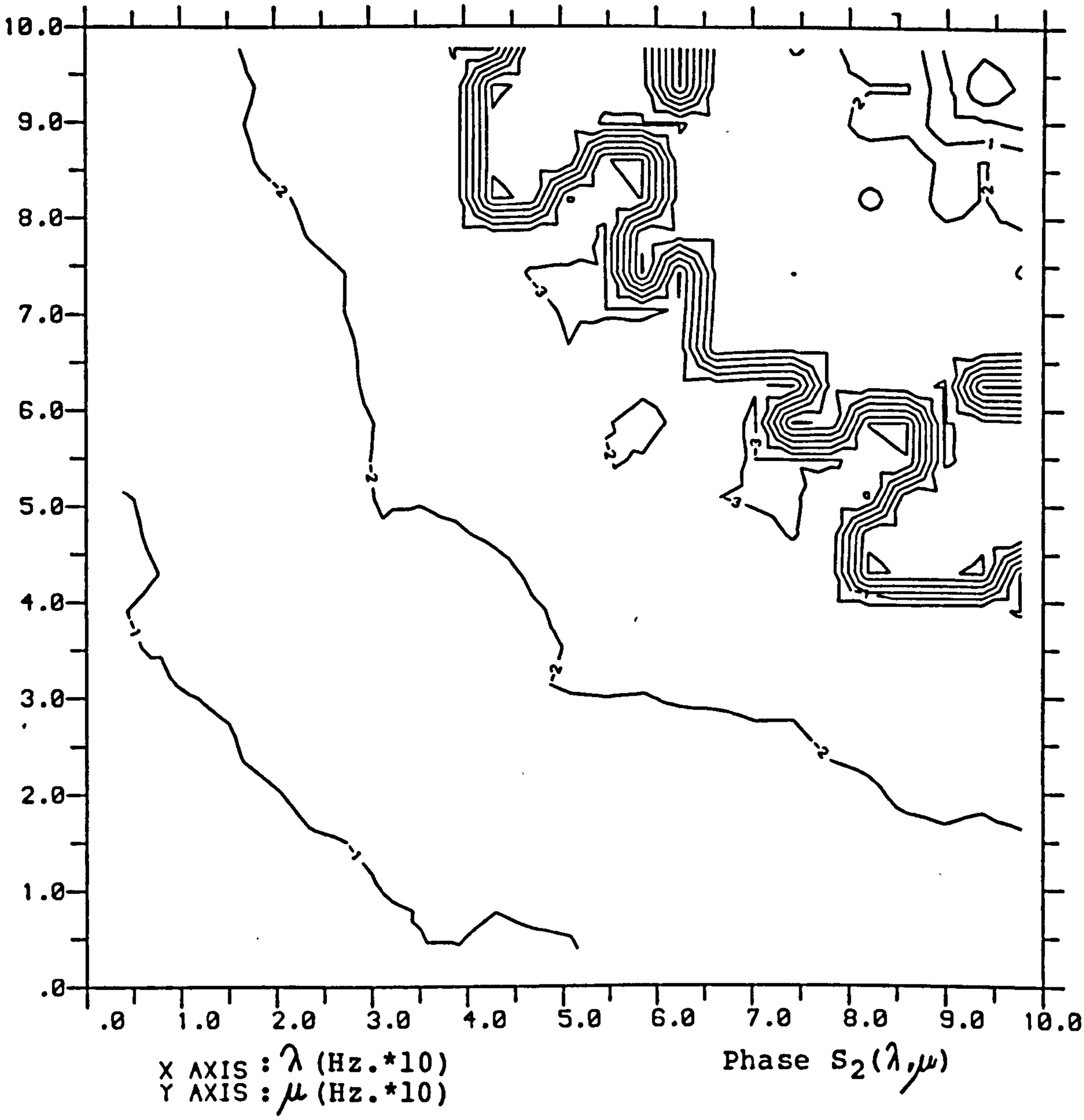

Fig. 5.8.10 Contour plot of restrained phase of smoothed estimate of $S_2(\lambda,\mu)$ for λ,μ=0 to 100Hz. and using simulated data with t_d=5msec. and G_m/t_m=11/10msec.. Estimated using (5.5.4), with T=256 in (2.3.29) and (5.3.13) and smoothed using 1 application of (5.7.2).

simulated data second kernels studied have a form similar to those in figures 5.8.7 to 5.8.10, and varying the simulation parameters has a consistent effect on subsequent frequency domain second kernel estimates.

Three trends were detected in $S_2(\lambda,\mu)$ with varying simulation parameters. Increasing t_d or G_m/t_m will on average lead to slightly lower D.C. magnitude values, and also the area over which the magnitude plot stays within 6dB. of the D.C. value decreases. This decrease in area occurs where the two frequencies are close to each other leaving regions close to the axes which extend out to higher frequency values, and which are still within 6dB. of the D.C. value. Therefore if longer time constants are used in the simulation interactive effects are more likely to occur between periodicities of low and high frequencies than with periodicities of similar frequency. Increasing t_d or G_m/t_m will also lead to larger decay rates in both the magnitude and phase estimates. This may be explained by the greater filtering effect a longer time constant will have, which may result in the sharper cutoff in the magnitude and longer delay observed in the phase of second kernel estimates. Figures 5.8.11 and 5.8.12 show surface and contour plots of the smoothed estimate of the magnitude of $S_2(\lambda,\mu)$ for the simulated data set dealt with in figures 5.8.3 and 5.8.4, with t_d=10 msec. and G_m/t_m=14/15 msec.. The phase estimate is shown in figures 5.8.13 and 5.8.14. These estimates reflect the points mentioned, with a concentration of the magnitude effects within 6 dB. of the D.C. value close to the axes above 30 Hz., and a steeper phase slope at lower frequencies.

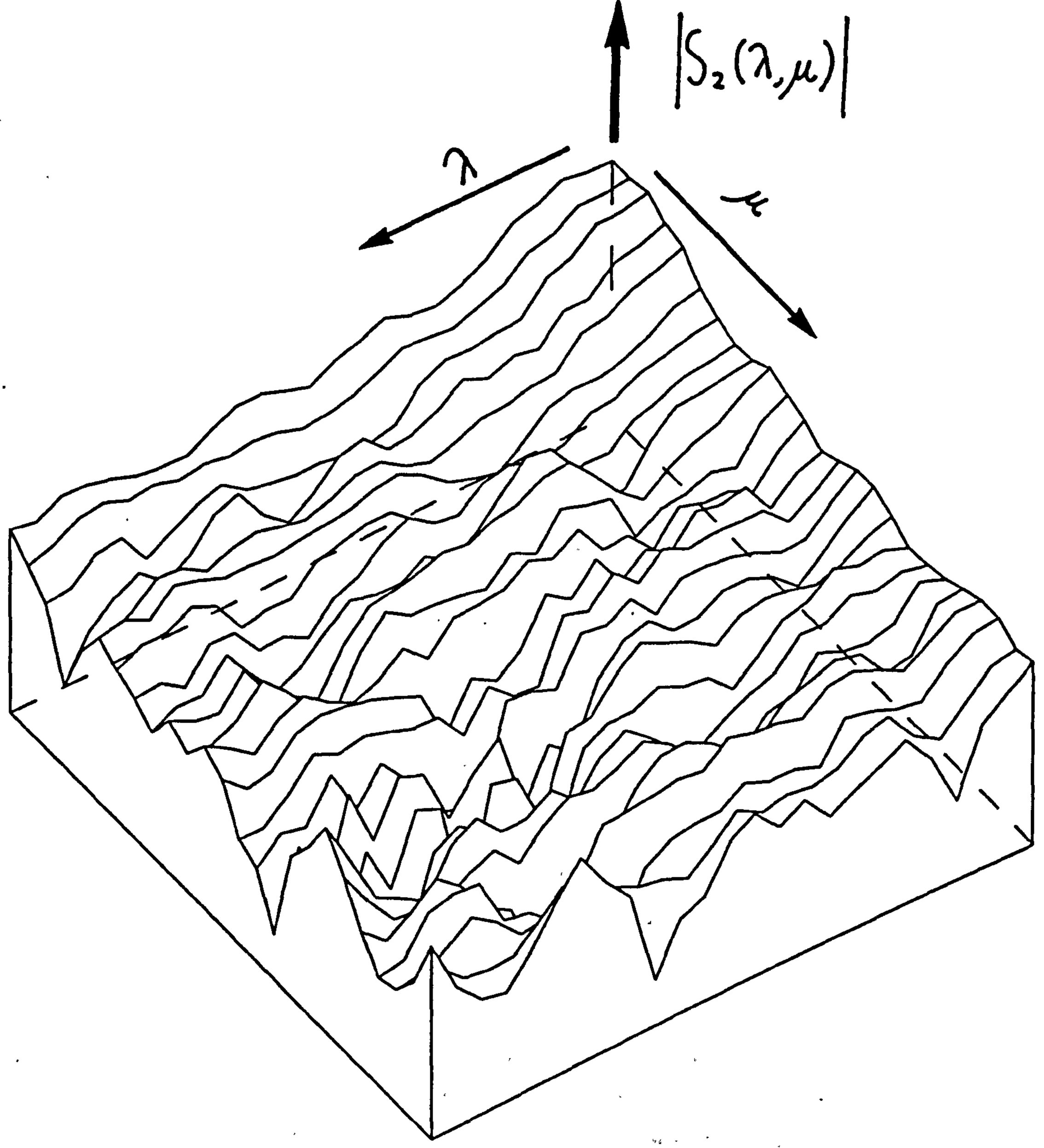

Fig. 5.8.11 Surface plot of magnitude of smoothed estimate of $S_2(\lambda,\mu$ plotted as 20 Log_{10} $|S_2(\lambda,\mu)|$ for λ,μ=0 to 100Hz. and using simulated data with t_d=10msec. and G_m/t_m=14/15msec.. Estimated using (5.5.4), with T=256 in (2.3.29) and (5.3.13) and smoothed using 1 application of (5.7.2).

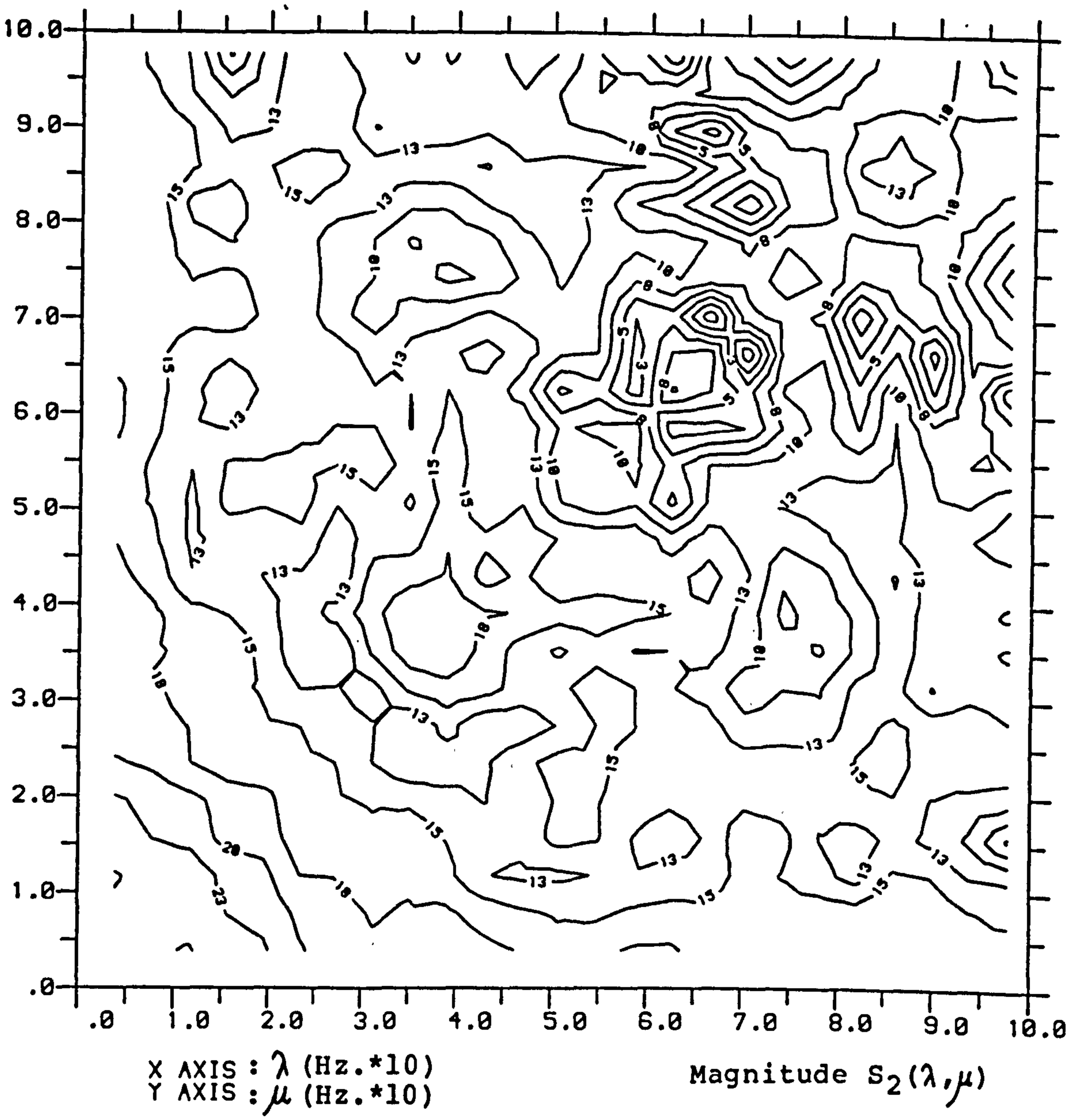

Fig. 5.8.12 Contour plot of magnitude of smoothed estimate of $S_2(\lambda,\mu)$ plotted as $20\ \mathrm{Log}_{10}\left|S_2(\lambda,\mu)\right|$ for λ,μ=0 to 100Hz. and using simulated data with t_d=10msec. and G_m/t_m=14/15msec.. Estimated using (5.5.4), with T=256 in (2.3.29) and (5.3.13) and smoothed using 1 application of (5.7.2).

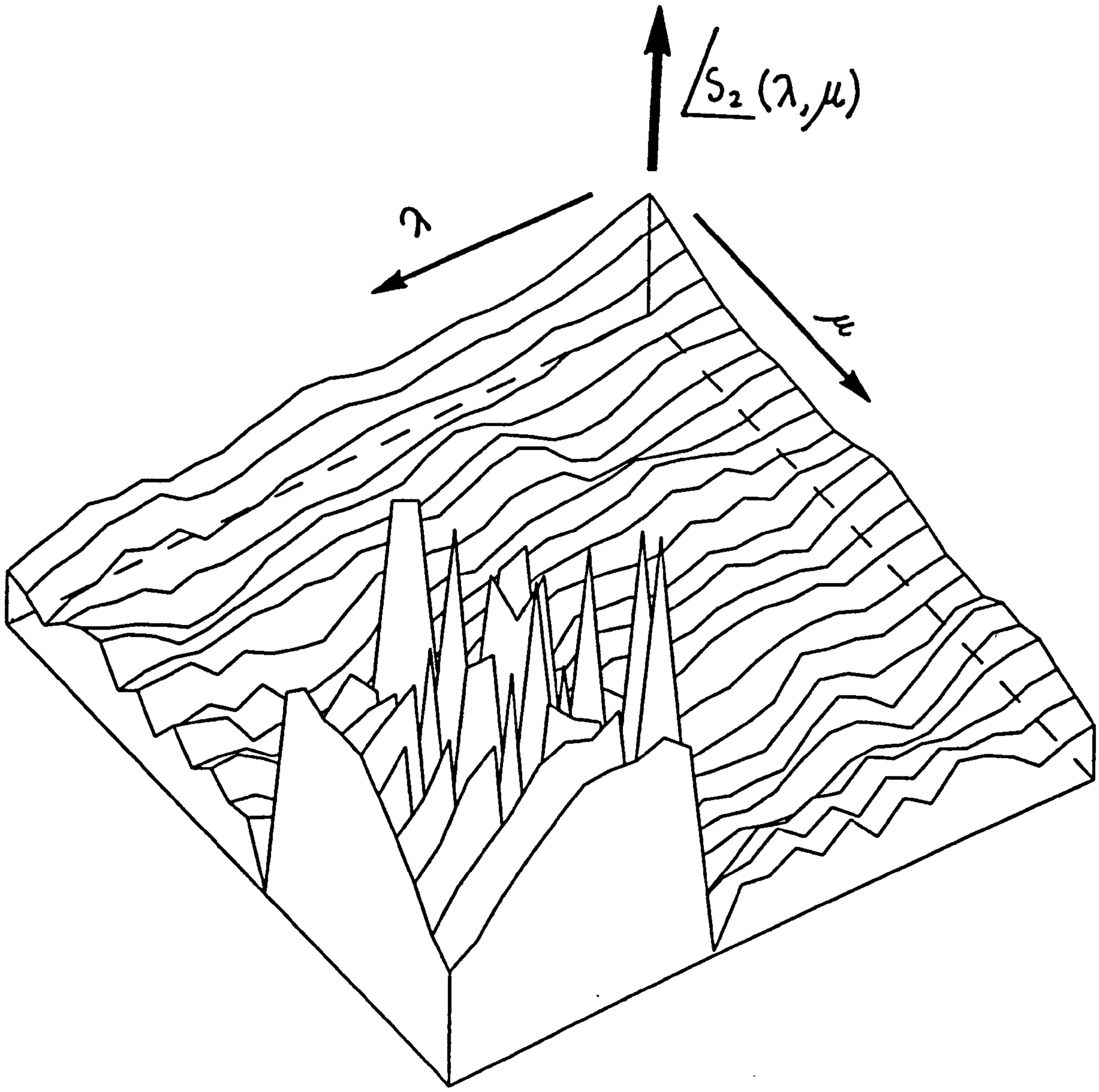

Fig. 5.8.13 Surface plot of restrained phase of smoothed estimate of $S_2(\lambda,\mu)$ for λ,μ=0 to 100Hz. and using simulated data with t_d=10msec. and G_m/t_m=14/15msec.. Estimated using (5.5.4), with T=256 in (2.3.29) and (5.3.13) and smoothed using 1 application of (5.7.2).

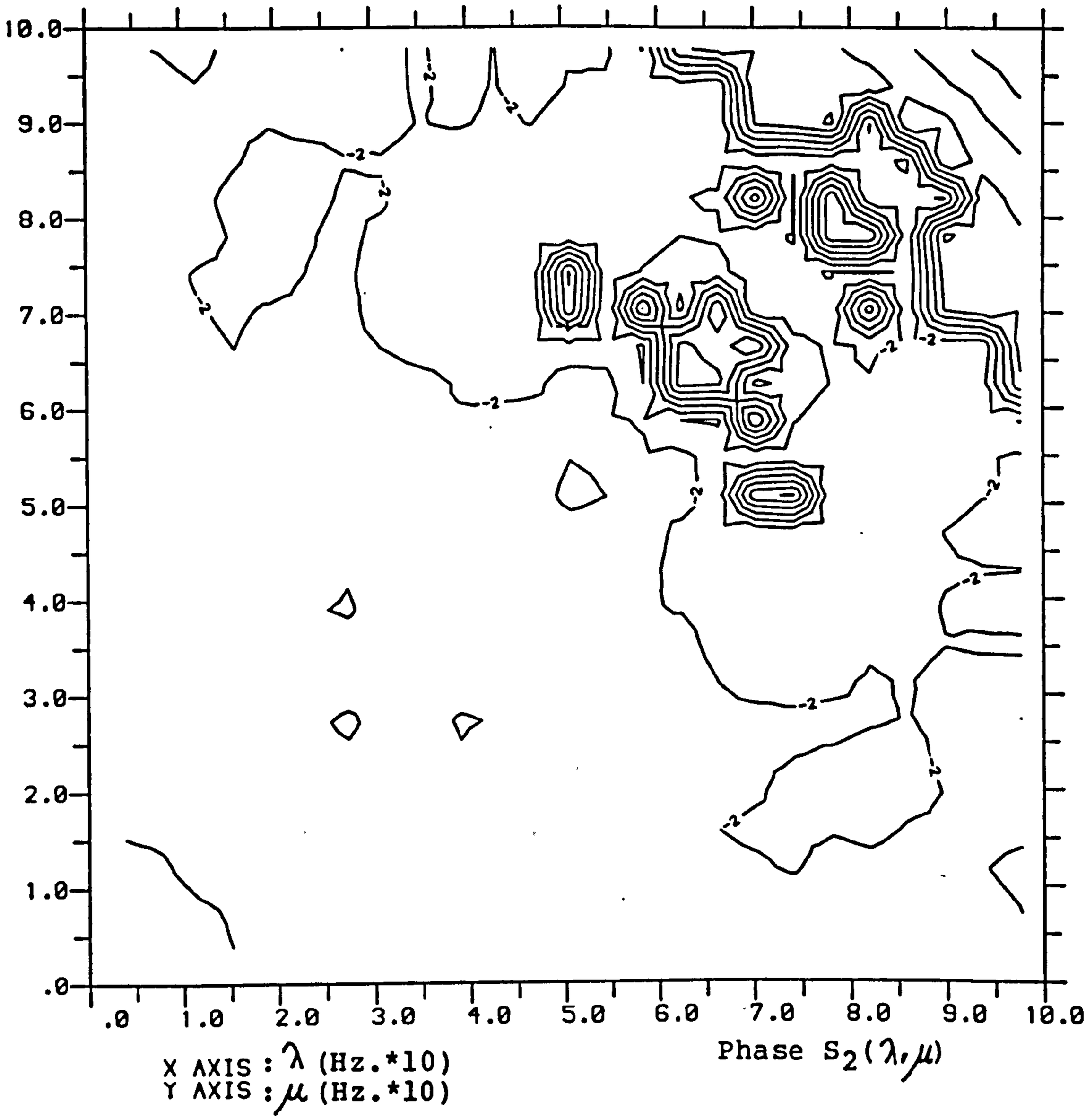

Fig. 5.8.14 Contour plot of restrained phase of smoothed estimate of $S_2(\lambda,\mu)$ for λ,μ=0 to 100Hz. and using simulated data with t_d=10msec. and G_m/t_m=14/15msec.. Estimated using (5.5.4), with T=256 in (2.3.29) and (5.3.13) and smoothed using 1 application of (5.7.2).

5.9 THE TWO INPUT QUADRATIC MODEL

The two input model introduced in section 5.6 can be extended to include non-linear interactive effects. This model is defined in (5.4.3) and estimates of the kernels $s_1(u)$ and $s_2(u)$ were considered in section 5.6. This section will consider the two second kernels $s_{11}(u,v)$ and $s_{22}(u,v)$, and the quadratic interaction between the two inputs will also be studied. The quadratic kernels are calculated exactly as the second kernel for the single input model, the other input spike-train is disregarded and the estimate (5.5.1) may be used if both inputs are Poisson. The results of section 5.6 have shown that the linear model is dominated by the $s_1(u)$ kernel, with the $s_2(u)$ kernel making an almost negligible contribution to the linear model, suggesting that the gammal input has a much stronger influence on the Ia discharge than the gamma2 input. This is also reflected in the estimates of the kernels $s_{11}(u,v)$ and $s_{22}(u,v)$.

In the time domain, the estimate of $s_{22}(u,v)$ has areas of facilitation and inhibition centred only about the main diagonal. At no other point does the magnitude of the estimate exceed the confidence band estimated using two Poisson spike-trains of the same mean rate. Figure 5.9.1 shows the surface plot of the estimate of $s_{11}(u,v)$, the contour plot is shown in figure 5.9.2. Processing two Poisson spike-trains of the same mean rate suggests that areas which exceed $\pm 100*10^{-4}$ indicate significant contributions from the kernel $s_{11}(u,v)$ to the two input model (5.4.3). These areas of significance are very similar in nature to the single input kernel discussed in section 5.7, with areas of facilitation and inhibition running parallel to the axes. Other areas of facilitation and inhibition are present, and are centred about the main diagonal. These are similar in nature to

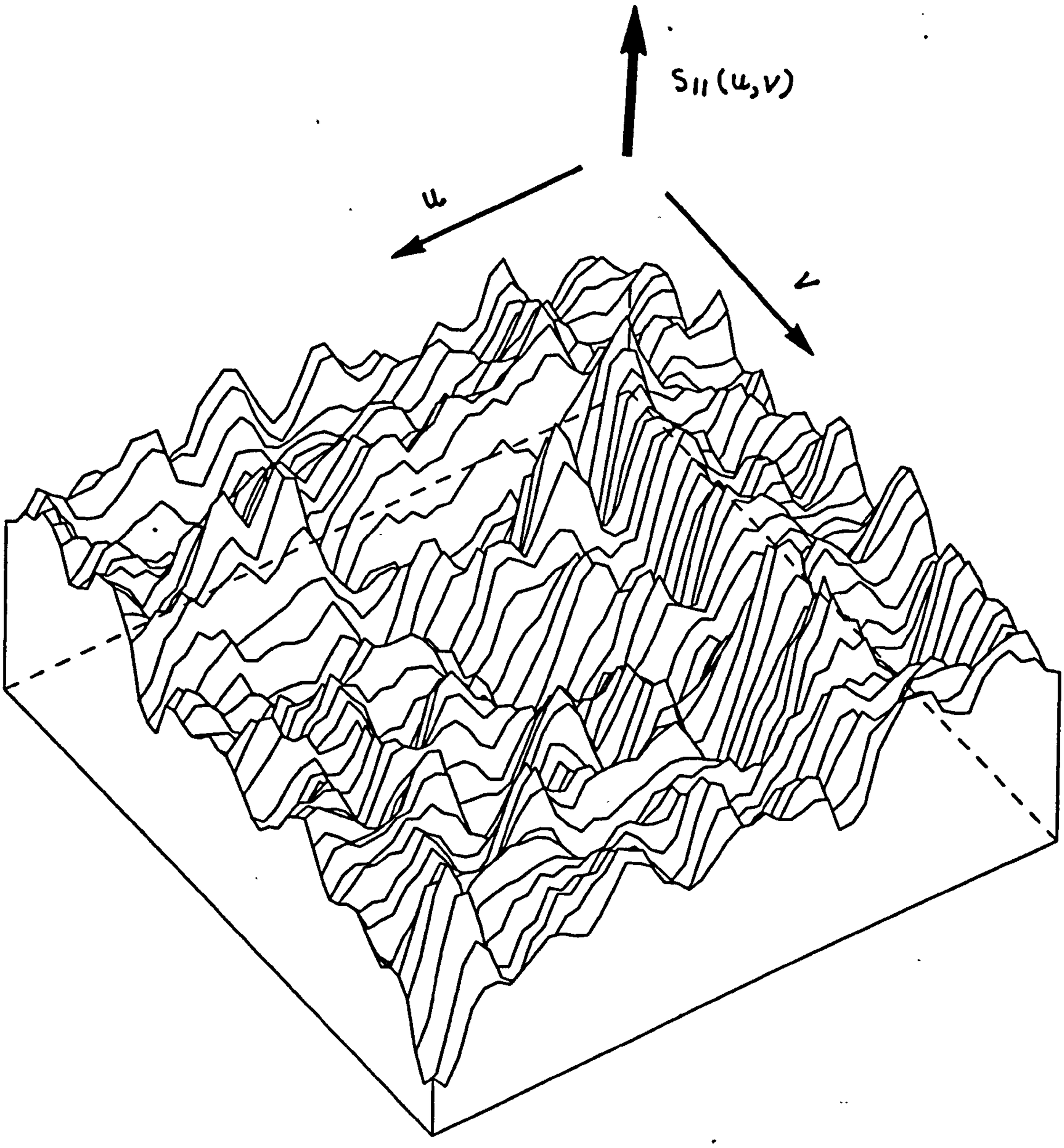

Fig. 5.9.1 Surface plot of smoothed estimate of second kernel $s_{11}(u,v)$ between gammal fusimotor input and Ia discharge in presence of gamma2 input. Estimated for u,v=0 to 50msec. using (5.5.1), with h=1.0 in (2.3.3), (2.3.8) and (5.3.1) and smoothed using 2 applications of (5.7.2).

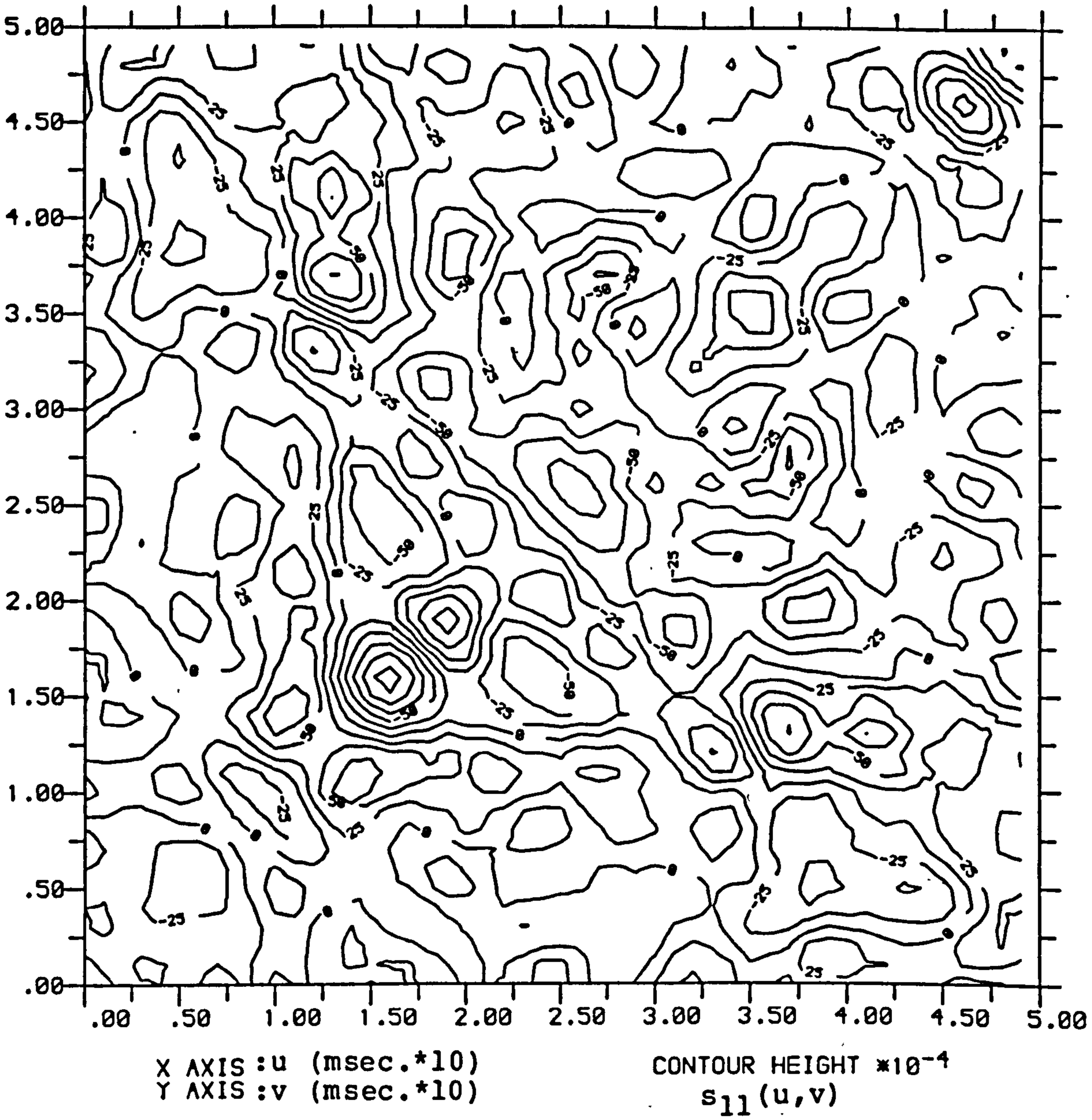

Fig. 5.9.2 Contour plot of smoothed estimate of second kernel $s_{11}(u,v)$ between gammal fusimotor input and Ia discharge in presence of gamma2 input. Estimated for u,v=0 to 50msec. using (5.5.1), with h=1.0 in (2.3.3), (2.3.8) and (5.3.1) and smoothed using 2 applications of (5.7.2). 95% confidence band estimated as $\pm 100*10^{-4}$ using (5.7.4).

the areas of facilitation and inhibition present in the estimate of $s_{22}(u,v)$, but are much larger in magnitude.

Thus with two inputs present, the interactive effect due to spike pairs from the dominant input is similar to that observed with a single input, with much weaker interactive effects from the second input only occurring due to short interspike intervals.

Figures 5.9.3 and 5.9.4 show the the magnitude of the frequency domain estimate of the kernel $S_{11}(\lambda,\mu)$, the phase estimate is shown in figures 5.9.5 and 5.9.6. These also resemble the single input kernel $S_2(\lambda,\mu)$ estimate discussed in section 5.7, with the magnitude being concentrated at lower frequencies, and the phase being consistent with that due to a delay in the system. The magnitude of the second kernel estimate of $S_{22}(\lambda,\mu)$ is 10 to 15 dB. less than the estimate in figure 5.9.4, suggesting a reduced dependence of the quadratic model (5.4.3) upon the kernel $s_{22}(u,v)$.

These results are consistent with the findings of section 5.6, in that for this particular muscle spindle either the gammal or gamma2 input separately will couple strongly with the Ia, as shown by the first and second kernel estimates for each input. If both inputs are applied simultaneously then the gammal input will dominate the primary discharge.

The final term in the model (5.4.3) is a cross quadratic kernel $s_{12}(u,v)$ whose arguments are the times to two distinct input spikes, one from each process. This gives a measure of the effect on the primary discharge of a gammal spike u time units previously interacting with a gamma2 spike v time units previously. The estimate (5.5.1) for the single input second

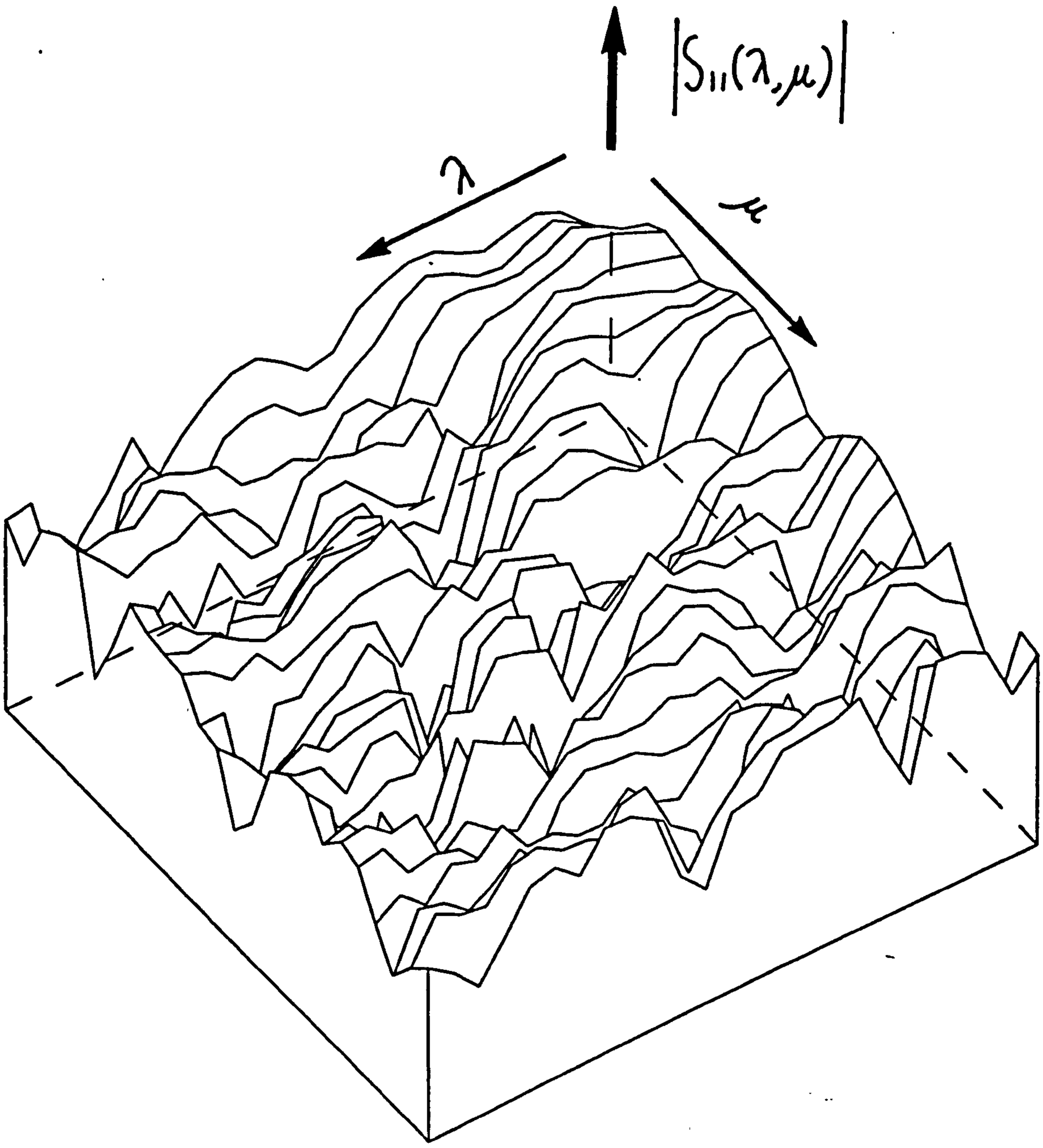

Fig. 5.9.3 Surface plot of magnitude of smoothed estimate of second kernel $S_{11}(\lambda,\mu)$ between gammal fusimotor input and Ia discharge in presence of gamma2 input and plotted as 20 Log_{10} $|S_{11}(\lambda,\mu)|$. Estimated for λ,μ=0 to 100Hz. using (5.5.4), with T=256 in (2.3.29) and (5.3.13) and smoothed using 1 application of (5.7.2).

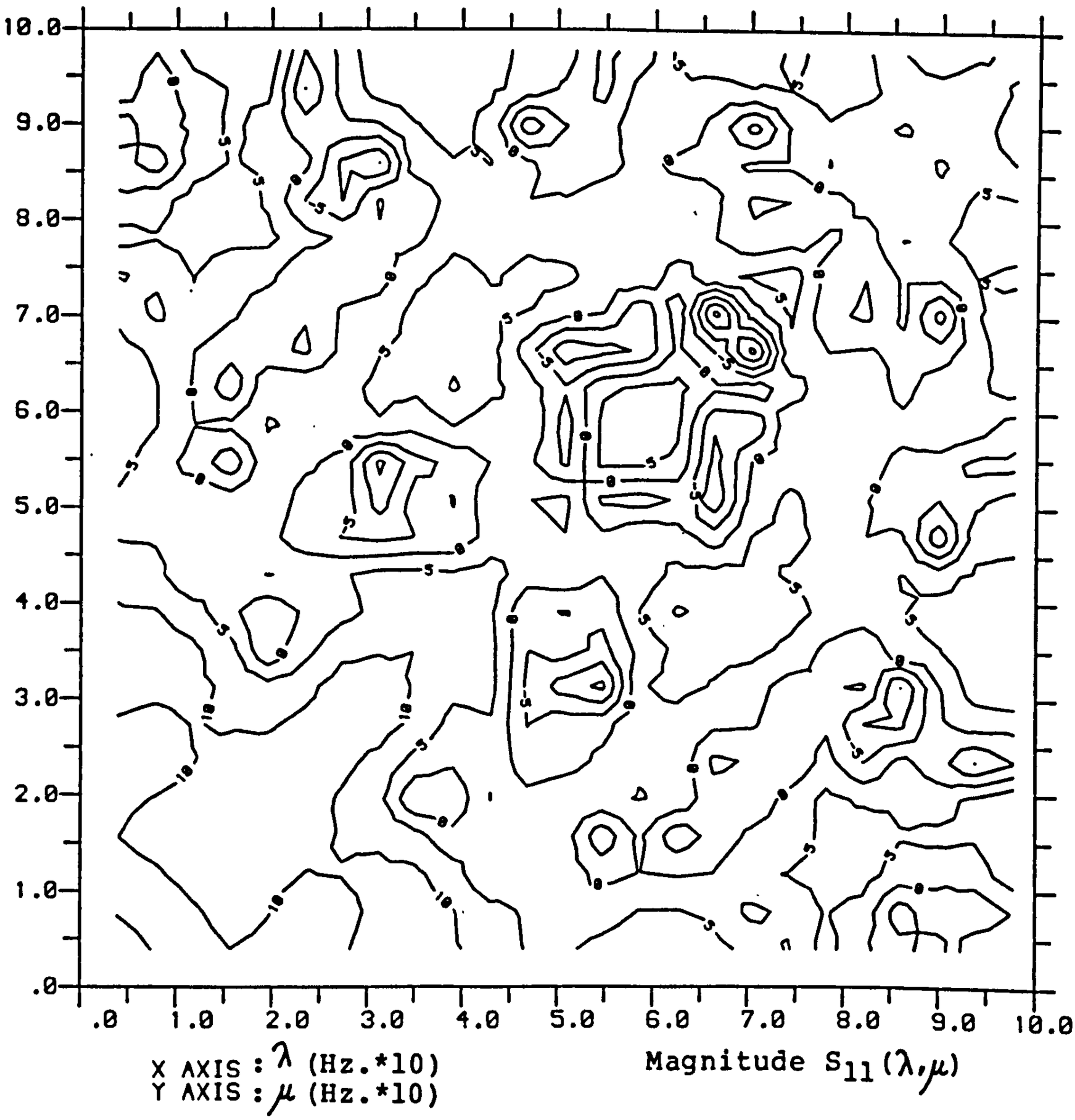

Fig. 5.9.4 Contour plot of magnitude of smoothed estimate of second kernel $S_{11}(\lambda,\mu)$ between gammal fusimotor input and Ia discharge in presence of gamma2 input and plotted as 20 Log_{10} $|S_{11}(\lambda,\mu)|$. Estimated for λ,μ=0 to 100Hz. using (5.5.4), with T=256 in (2.3.29) and (5.3.13) and smoothed using 1 application of (5.7.2).

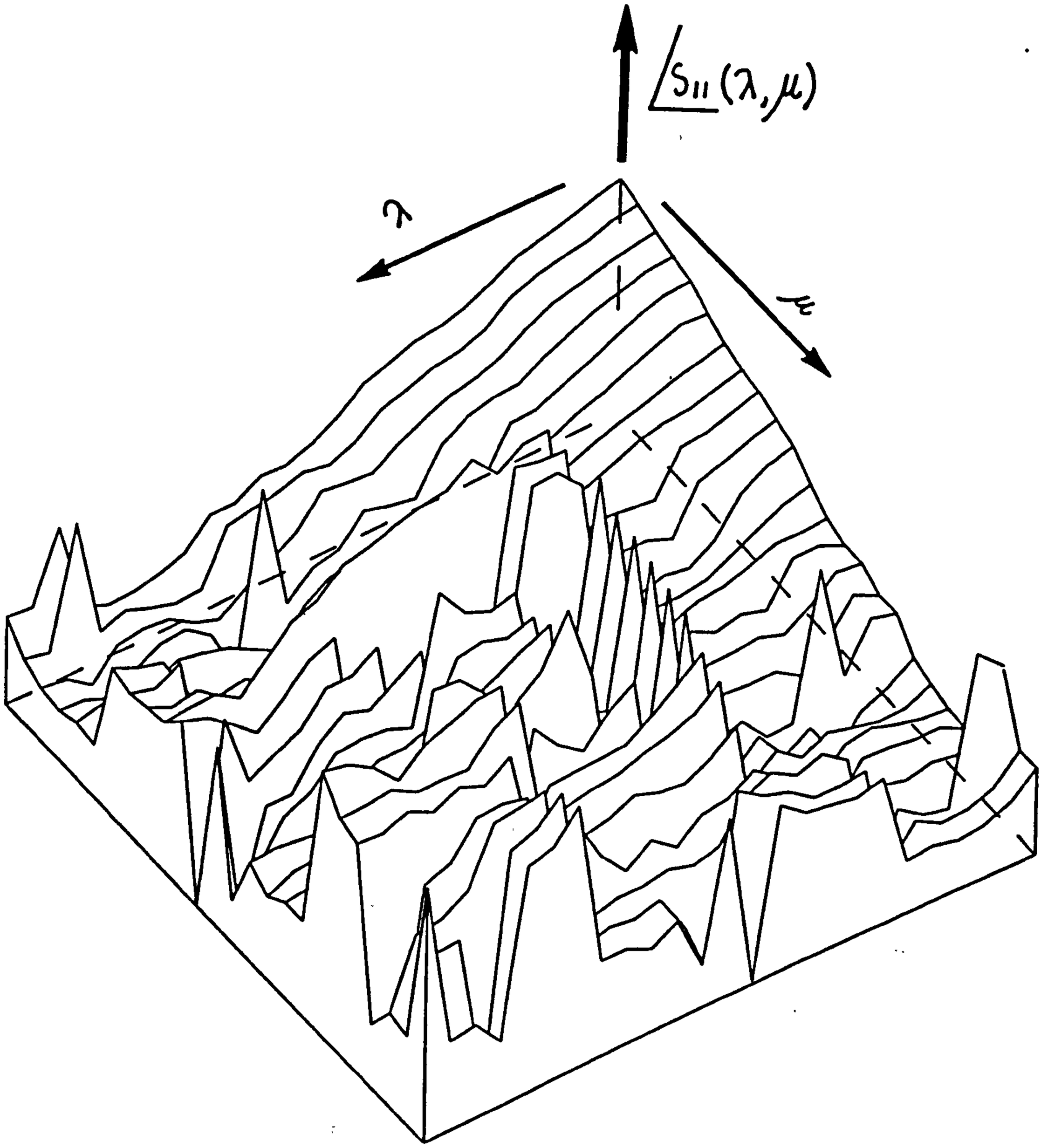

Fig. 5.9.5 Surface plot of unrestrained phase of smoothed estimate of second kernel $S_{11}(\lambda,\mu)$ between gammal fusimotor input and Ia discharge in presence of gamma2 input. Estimated for $\lambda,\mu=0$ to 100Hz. using (5.5.4), with T=256 in (2.3.29) and (5.3.13) and smoothed using 1 application of (5.7.2).

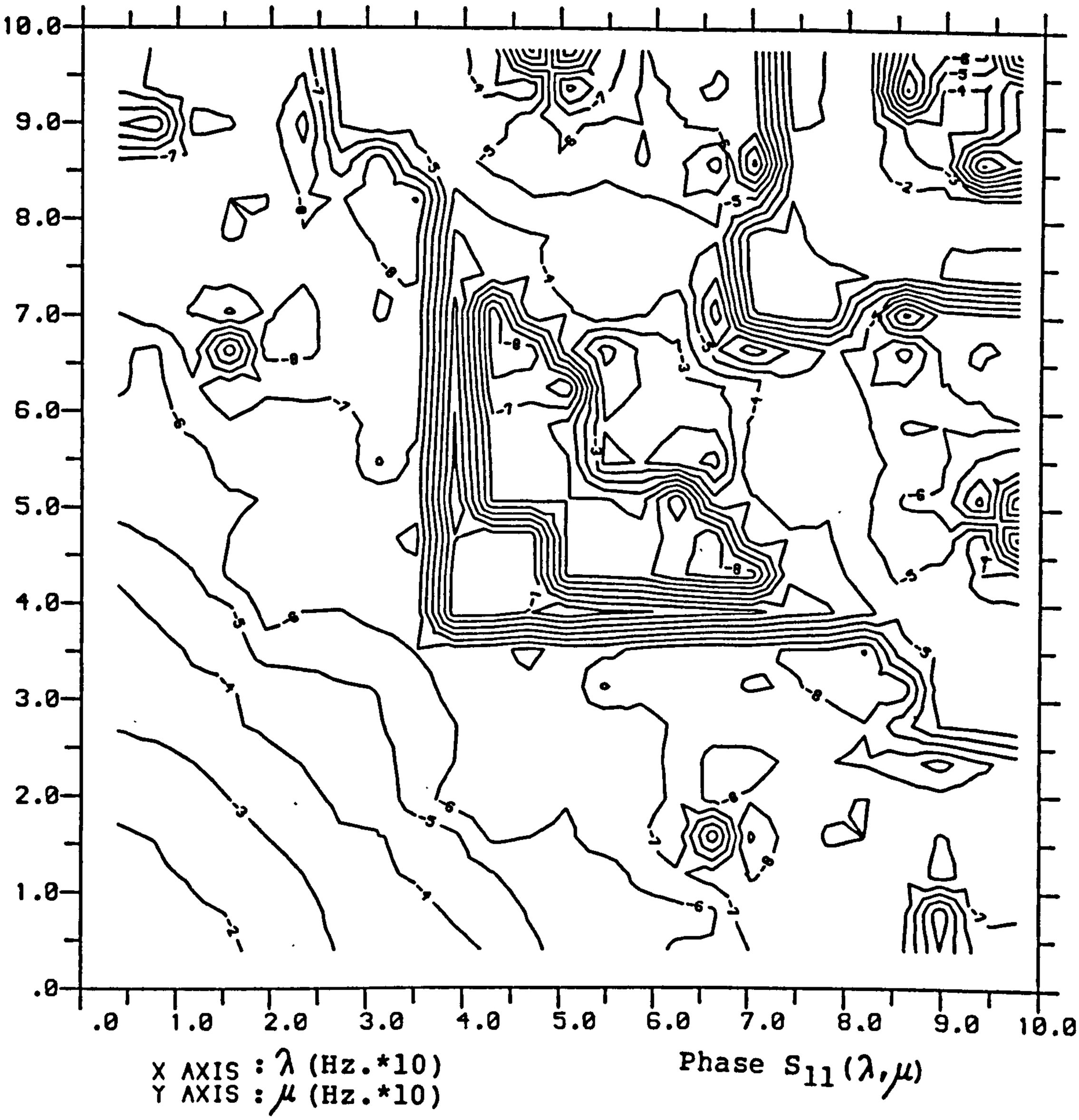

Fig. 5.9.6 Contour plot of unrestrained phase of smoothed estimate of second kernel $S_{11}(\lambda,\mu)$ between gammal fusimotor input and Ia discharge in presence of gamma2 input. Estimated for λ,μ=0 to 100Hz. using (5.5.4), with T=256 in (2.3.29) and (5.3.13) and smoothed using 1 application of (5.7.2).

kernel is based on the assumption that the kernel is symmetrical in the solution of the model (5.4.1). Since this assumption is not applicable to the two input case, this solution cannot be used. However the cumulant function $q_{nm2ml}(u,u-v)$ can be used. This will provide a measure of the statistical dependence of the output process N at time t+u upon the differential increments $dM_1(t)$ and $dM_2(t+v)$ as a function of u and u-v. See figure 5.3.1 for a timing diagram. The estimate for this cumulant function is based on (5.5.2), but is extended to deal with three spike-trains in a similar manner to (5.3.6). This is followed by two applications of the smoothing (5.7.2). Applying this estimate to the two input data set showed only a weak interactive effect, and this estimate was also applied to seven other two input data sets collected from the same muscle spindle. All of these data sets exhibited a weak interactive effect, but certain features were present in all the cumulant estimates.

Figures 5.9.7 and 5.9.8 show the result of averaging all eight of the smoothed estimates of the cumulant $q_{nm2ml}(u,u-v)$. This was done to provide a more consistent estimate of the interactive effect and to isolate the trends which are present in all the estimates from those which are particular to the individual data sets. Since all of the individual cumulant estimates had regions which exceeded the confidence band estimated from three Poisson spike-trains with the same mean rates as the data sets, then areas with the largest magnitudes in figure 5.9.8 can be considered as significant. From the definition of the cumulant function (5.2.13) the argument u in $q_{nm2ml}(u,u-v)$ represents the time to gammal spikes, and the argument u-v represents the time to gamma2 spikes. The main features in figures 5.9.7 and 5.9.8 are a region of facilitation

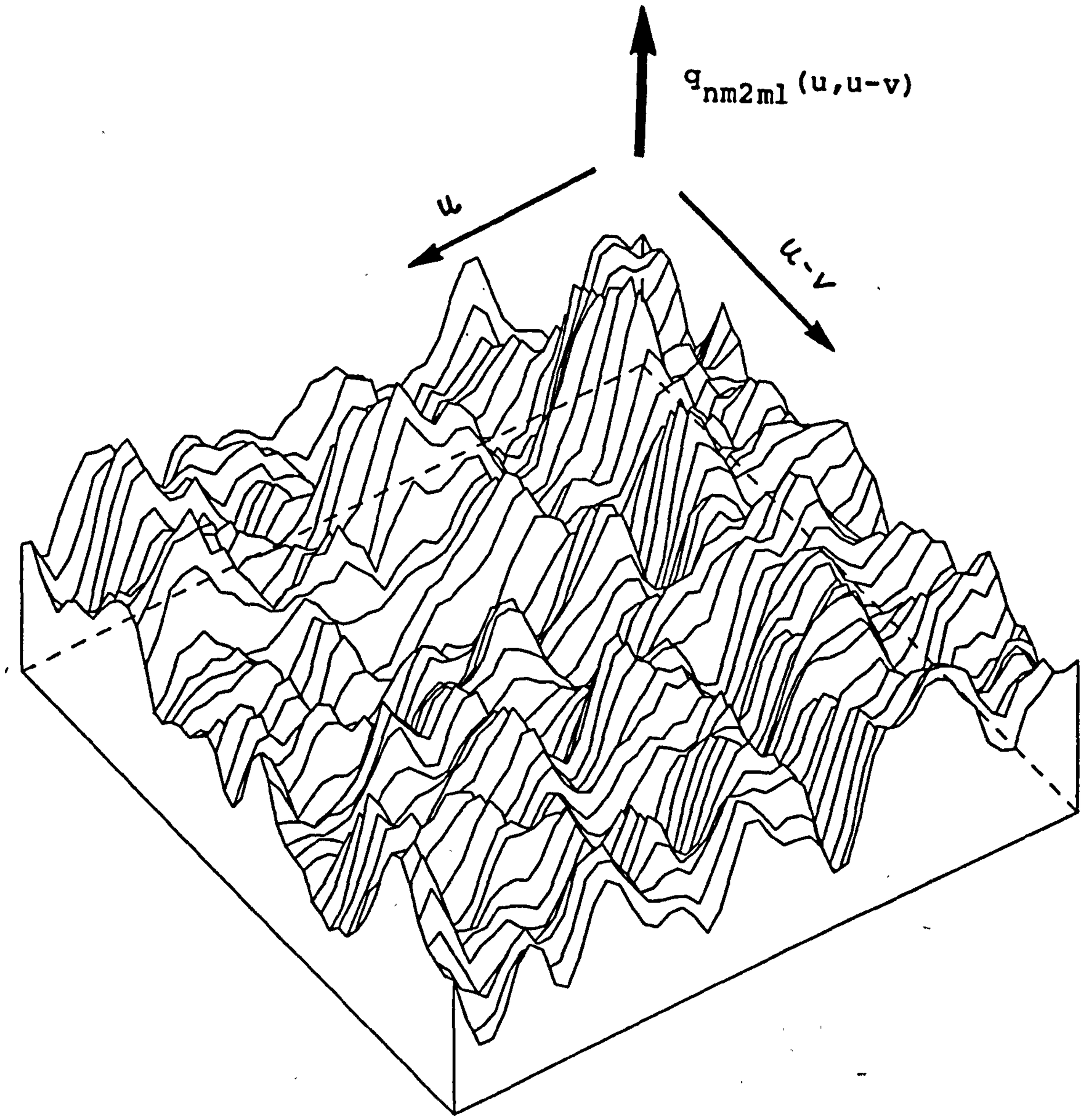

Fig. 5.9.7 Surface plot of smoothed estimate of $q_{nm2ml}(u,u-v)$ for u,v=0 to 50msec. and averaged over 8 files. Each estimate based on (5.5.2), with h=1.0, and smoothed using 2 applications of (5.7.2).

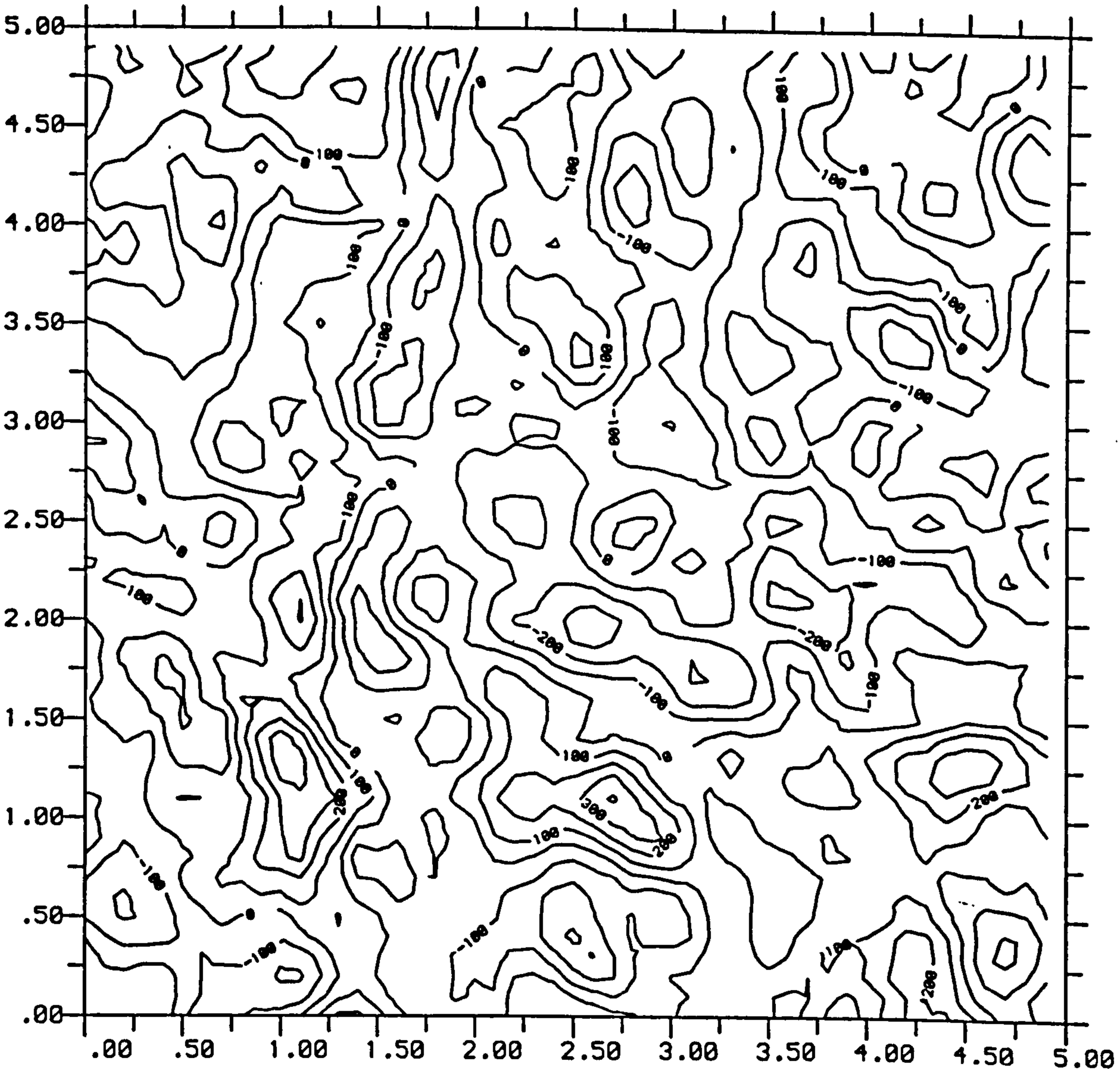

Fig. 5.9.8 Contour plot of smoothed estimate of $q_{nm2ml}(u,u-v)$ for u,v=0 to 50msec. and averaged over 8 files. Each estimate based on (5.5.2), with h=1.0, and smoothed using 2 applications of (5.7.2).

centred on u=11 msec. running parallel to the u-v axis, and a region of inhibition centred on u=14 msec. and also running parallel to the u-v axes. These regions of facilitation and inhibition occurring at fixed values of u suggest that any interactive effect is more dependent upon the time of occurrence of previous gammal spikes and therefore that cross-quadratic interactive effects have a stronger dependence on the gammal input. Other features of similar magnitude are present, including an area of facilitation centred on u=26 msec. v=11 msec., and an area of inhibition centred around u=26 msec. and v=20 msec.. These areas indicate the spike pair timings where a spike from process 1 can interact with a spike from process 2 and produce an interactive effect on the primary discharge.

5.10 SUMMARY

Extending to second order the point-process system identification model introduced in chapter two has allowed non-linear effects within the muscle spindle to be investigated. The development of a new algorithm has allowed higher order time domain parameters to be estimated very rapidly. Time and frequency domain representations of the second kernel have given different insights into how non-linear interactions between two spikes or two periodicities can affect the primary discharge. The effect of applying two simultaneous fusimotor inputs to the same muscle spindle has also been looked at. It was found that one input dominates the primary response, with first and second kernel estimates very similar to those obtained with this input separately. These findings indicate that as more fusimotor inputs to a muscle spindle become active, then the overall dependence of

the primary discharge upon each input may change.

CHAPTER SIX

6.1 SUMMARY AND CONCLUSIONS

In general terms, the work described in this thesis shows that stochastic point-process parameters can be used to characterize point-process representations of neuronal spike-train data, and can also form the basis for system identification techniques. Useful results can be obtained from estimates of the power spectrum in the analysis of single spike-trains, and a frequency domain approach provides more information about different discharge patterns than estimates in the time domain of the auto-intensity function reveal. Time and frequency domain parameters can relate changes in the activity of one spike-train which may be caused by activity in a second spike-train, the two approaches providing a different insight into the nature of any dependence of one process upon another.

The point-process identification procedure represents, in a series of kernels of increasing order, the relationship between the output and a Poisson input to a point-process system. The linear point-process model uses the kernel of order one to predict the average linear effect of the input process upon the output, and has time and frequency domain representations. In the frequency domain, a very useful measure of absolute dependence, the coherence, can be used to measure linear dependence on a scale from zero to one.

Based on the application to muscle spindle data of linear model estimates, a computer simulation of a spindle subsystem was constructed, and results from the simulation provided extra insight into the interpretation of experimental results. It was also found that varying gain and time-constants in the mathematical model of the simulation allowed different experimental conditions to be simulated. This fact, along with

the broad range of linear dependence of the primary discharge upon the fusimotor input, as shown by the coherence function, indicate that the linear point-process model is a powerful tool for investigating spindle response to a fusimotor input.

Comparison of the point-process approach with more conventional filtering and sampled data approach showed the point-process technique to be superior in terms of computational load and known statistical properties. Spectral estimates of filtered spike-trains containing a wide range of harmonic components showed up a problem in the choice of filter parameters which can lead to information loss in spectral estimates when compared with point-process spectral estimates.

The application of point-process parameter estimates to more general neurophysiological spike-train data showed that the frequency domain approach has increased sensitivity compared with the time domain approach, and can be used to provide a measure of dependence between two simultaneous spike-trains, including the ability to resolve coupling at individual harmonics. The extension of the coherence function to the analysis of multiple spike-trains which allows dependence on a common input to be distinguished from an actual connection was applied to different neuromuscular spike-train data, and was shown to provide valuable information about the formation of connections between active neurones.

Application of the point-process approach to analyse a particular phase-locking type response of the muscle spindle to a fusimotor input showed how similar information about this response can be obtained from two short experiments, as opposed to a repetitive trial and error approach required previously to

measure the range of frequencies affected by this phenomenon.

The extension of the definition of stochastic point-process parameters to higher order allows non-linear interactive effects to be studied and forms the basis for the solution of the quadratic point-process model. Time and frequency domain estimates for one and two input linear and quadratic model kernels were calculated and used to analyse the effect of applying two fusimotor inputs simultaneously to the same muscle spindle. It was shown that each fusimotor input on its own produces strong linear and non-linear dependence of the primary discharge upon this input. The application of both inputs together leads to one of the inputs dominating the primary discharge, with first and second kernel estimates very similar to the single input estimates, with the second input producing only a very weak dependence of the fusimotor input upon it. The time and frequency domain second kernel estimates, and higher order point-process parameters for two inputs, were used to determine the input spike-train patterns and input spike frequency range where higher order interactive effects are present. These may be linked to interactive effects in the muscle spindle such as after-firing refractory periods or fluctuations of electrochemical threshold levels. The study of higher order kernels and non-linear effects using the point-process model leads to suggestions for future work.

6.2 WHERE NOW?

The large sample properties for the time and frequency domain quadratic kernel estimates have still to be determined, along with the point-process equivalent of the quadratic coherence. This will allow a more precise dependence of the

spindle response to fusimotor stimulation upon non-linear interactions to be determined. Also the point-process model could be extended and estimates for kernels of order three derived to look at higher order interactive effects. This may allow more interesting features of the system to be investigated.

The simulation has provided a useful insight into the interpretation of experimental results, and the development of the simulation as more complex interactive experimental data sets are studied should prove a valuable aid in the interpretation of higher order interactions.

As higher order interactive effects within and between individual elements of the neuromuscular system are studied any results should be related, if possible, to the overall control function of the neuromuscular system. Only in this way can the understanding of the operation of higher levels within the central nervous system be extended.

Advances in the physiological field should make potentially more interesting neuronal spike-train data sets available, and application of the existing techniques outlined in this dissertation to a much wider range of neuronal data should help further the understanding of the operation of nervous and biological systems.

REFERENCES

ANDERSSON, B.F., LENNERSTRAND, G. and THODEN, U. (1968): Response characterisitics of muscle spindle endings at constant length to variation in fusimotor activity, Acta Physiol Scand, 74, 301-318.

ANGERS, D. and DELISLE, G.Y. (1971): Study of the action of static and dynamic fusimotor fibres with a mechanical model of the mammalian muscle spindle, IEEE Trans Bio-Med Engr, BME-18, 175-180.

BARTLETT, M.S. (1948): Smoothing periodograms from time series with continuous spectra, Nature, 161, 686-687.

BARTLETT, M.S. (1955): An introduction to stochastic processes, Cambridge univ press, Cambridge.

BARTLETT, M.S. (1963): The spectral analysis of point-processes, J R Statist Soc, B25, 264-280.

BESSOU, P. and PAGES, B. (1975): Cinematographic analysis of contractile events produced in intrafusal fibres by stimulation of static and dynamic fusimotor axons, J Physiol, 252, 397-427.

BHABHA, H.J. (1950): On the stochastic theory of continuous parametric systems and its application to electron cascades, Proc R Soc London, A202, 301-322.

BHABHA, H.J. and RAMAKRISHNAN, A. (1950): On the mean square deviation of the number of electrons and quanta in the cascade theory, Proc Indian Acad Sci, 32 , 141-157.

BLOOMFIELD, P. (1976): Fourier analysis of time series: An introduction, Wiley, New-York.

BOYD, I.A. (1980): The isolated mammalian muscle spindle, Trends in Neurosciences, 3, 258-265.

BOYD, I.A., GLADDEN, M.H., McWILLIAM, P.N. and WARD, J. (1977): Control of dynamic and static nuclear bag fibres and nuclear chain fibres by gamma and beta axons in isolated cat muscle

spindles, J Physiol, 265, 133-162.

BRILLINGER, D.R. (1970): The identification of polynomial systems by higher order spectra, J Sound and Vib, 12, 301-313.

BRILLINGER, D.R. (1972): The spectral analysis of stationary interval functions, Proc 6th Berkley Symposium, Vol 1, eds Le Cam, L. M., Neyman, J. and Scott, E.L., Univ of California Press, Berkely, 483-513.

BRILLINGER, D.R. (1974a): Cross spectral analysis of processes with stationary increments including the G/G/∞ queue, Ann Probab, 2, 815-827.

BRILLINGER, D.R. (1974b): Fourier analysis of stationary processes, Proc IEEE, 62, 1628-1643.

BRILLINGER, D.R. (1975a): Time series: data analysis and theory, 1st edn, Holt, Reinhart and Winston, Inc, London.

BRILLINGER, D.R. (1975b): Identification of point-process systems, Ann Probab, 3, 909-929.

BRILLINGER, D.R. (1975c): Statistical inference for stationary point-processes, in Stochastic processes and related topics, Vol 1, ed Puri, M.I., Academic Press, New-York, 55-79.

BRILLINGER, D.R. (1975d): Estimation of product densities, in Comp Sci Statist, 8th Ann Symp Interface, UCLA, Los Angeles, 431-438.

BRILLINGER, D.R. (1976a): Measuring the association of point-processes: a case history, Am Math Monthly, 83, 16-22.

BRILLINGER, D.R. (1976b): Estimation of the second order intensities of a bivariate stationary point-process, J R Statist Soc, B38, 60-66.

BRILLINGER, D.R. (1978): Comparative aspects of the study of ordinary time series and of point-processes, in Developments in

statistics, Vol 1, ed Krishnaiah, P.R., Academic Press, New-York, 33-134.

BRILLINGER, D.R., BRYANT, H.L.jr, and SEGUNDO, J.P. (1976): Identification of synaptic interactions, Biol Cybernetics, 22, 213-228.

BRILLINGER, D.R. and ROSENBLATT, M. (1967a): Asymptotic theory of estimates of k^{th} order spectra, in Spectral analysis of time series, ed Harris, B., Wiley, New-York, 153-188.

BRILLINGER, D.R. and ROSENBLATT, M. (1967b): Computation and interpretation of k^{th} order spectra, in Spectral analysis of time series, ed Harris, B., Wiley, New-York, 189-232.

BROWN, M.C., CROWE, A. and MATTHEWS, P.B.C. (1965): Observations on the fusimotor fibres of the tibialis posterior muscle of the cat, J Physiol, 177, 140-159.

BRYANT, H.L.jr, MARCOS A.R. and SEGUNDO, J.P. (1973): Correlation of neuronal spike discharges produced by monosynaptic connections and by common inputs, J Neurophysiology, 36, 205-255.

BURKE, R.M. and RUDOMIN, P. (1977): Spinal neurones and synapses, in Handbook of Physiology, Sect 1: The nervous system, Vol 1, Cellular biology of neurones, Part 2, eds Brookhart, J.M. and Mountcastle, V.B., American Physiological society, Bethesda, USA, 877-944.

CHATFIELD, C. (1980): The analysis of time series: An introduction, 2^{nd} edn, Chapman and Hall, London.

CHRISTAKOS, C.N., ROST, I. and WINDHORST, U. (1984): The use of frequency domain techniques in the study of signal transmission in skeletal muscle, Pflugers Archiv, 400, 100-105.

COX, D.R. (1955): Some statistical methods connected with series of events, J R Statist Soc, B17, 129-164.

COX, D.R. (1965): On the estimation of the intensity function of

a stationary point-process, J R Statist Soc, B27, 322-327.

COX, D.R. and LEWIS, P.A.W. (1966): The statistical analysis of series of events, Methuen, London.

COX, D.R. and LEWIS, P.A.W. (1972): Multivariate point-processes, Proc 6th Berkely Symp Math Statist Prob, 2, 401-448.

DALEY, D.J. (1971): Weakly stationary point-processes and random measures, J R Statist Soc, B33, 406-428.

DOOB, J.L. (1953): Stochastic processes, Wiley, New-York.

DOWNIE, I.C. and MURRAY-SMITH, D.J. (1981): Simulation of systems involving pulse frequency modulation with special reference to modelling of muscle spindles, Proc 1981 UKSC Conf on Comp Sim, Harrogate, Westbury House, Guilford, 143-152.

DUTIA, M.B., MURRAY-SMITH, D.J., ROSENBERG, J.R. and WILSON, R. (1977): The dependence of driving of Ia axons on muscle length and fusimotor stimulation frequency, J Physiol, 273, 30-31P.

ELLAWAY, P.H. (1977): An application of cumulative sum technique to neurophysiology, J Physiol, 265, 1-2P.

ELLAWAY, P.H., GARDNER-MEDWIN, A.R. and PASCOE, J.E. (1983): Decision limits for significance of changes in the cumulative sum (cusum) of the peristimulus time histogram, J Physiol, 341, 4-5P.

ELLAWAY, P.H., PASCOE, J.E. and TROTT, J.R. (1976): The effects upon fusimotor neurones of small, brief stretches of their muscles, J Physiol, 258, 48-49P.

EMONET-DENAND, F., LAPORTE, Y., MATTHEWS, P.B.C. and PETIT, J. (1977): On the subdivision of static and dynamic fusimotor axons on the primary ending of the cat muscle spindle, J Physiol, 268, 827-860.

FIENBERG, S.E. (1974): Stochastic models for single neuron firing trains: a survey, Biometrics, 30, 399-427.

FRENCH, A.S. and BUTZ, E.G. (1973): Measuring the kernels of a non-linear system using the fast Fourier transform, Int J Control, 17, 529-539.

FRENCH, A.S. and BUTZ, E.G. (1974): The use of Walsh functions in the Wiener analysis of non-linear systems, IEEE Trans Computers, 23, 225-232.

FRENCH, A.S. and HOLDEN, A.V. (1971): Alias free sampling of neuronal spike trains, Kybernetik, 8, 165-171.

GRIFFITH, J.S. and HORN, G. (1963): Functional coupling between cells in the visual cortex of the unrestrained cat, Nature, 199, 893-895.

HARRIS, F.J. (1978): On the use of windows for harmonic analysis with the discrete Fourier transform, Proc IEEE, 66, 51-83.

HARRIS, G.H. and LAPIDUS, L. (1967): The identification of non-linear systems, Industrial and Chemical Engr, 59, 66-81.

HASAN, Z. and HOUK, J.C. (1972): Non-linear behaviour of primary spindle receptors to small slow ramp stretches, Brain Res, 44, 680-683.

HOLDEN, A.V. (1976): Models of stochastic activity in neurones, in Lecture notes in biomathematics, Vol 12, ed Levin, S., Springer-Verlag, Berlin, 84-234.

HUNG, G., BRILLINGER, D.R. and STARK, L. (1977): Interpretation of kernels 2: Same signed 1^{st} and 2^{nd} degree kernels of the human pupillary system, Mathematical Biosciences, 46, 159-187.

HUNG, and STARK, L. (1977): The kernel identification method (1910-1977) - review of theory, calculation, application and interpretation, Mathematical Biosciences, 37, 135-190.

JENKINS, G.M. and WATTS, D.G. (1968): Spectrum analysis and its applications, Holden-Day, San Francisco.

KIRKWOOD, P.A. (1979): On the use and interpretation of cross-

correlation measurements in the mammalian central nervous system, J Neuroscience methods, 1, 107-132.

KROIN, J. (1974): Modeling of mammalian muscle receptors by means of spike-train correlation analysis, Ph.D. dissertation, University of Southern California.

KUZNETSOV, P.I. and STRATONOVICH, R.L. (1965): A note on the mathematical theory of correlated random points, in Non-linear transformations of stochastic processes, eds Kuznetsov, P.I., Stratonovich, R.L. and Tikhonov, V.I., Pergamon, Oxford, 101-115.

KUZNETSOV, P.I., STRATONOVICH, R.L. and TIKHNOV, V.I. (1965): The transmission of random functions through non-linear systems, in Non-linear transformations of stochastic processes, eds Kuznetsov, P.I., Stratonovich, R.L. and Tikhonov, V.I., Pergamon, Oxford, 29-58.

LEE, Y.W. and SCHETZEN, M. (1965): Measurement of the Wiener kernels of a non-linear system by cross-correlation, Int J Control, 2, 237-254.

LEWIS, P.A.W. (1970): Remarks on the theory, computation and application of the spectral analysis of series of events, J Sound and Vib, 12, 353-375.

LEWIS, P.A.W. (1972): Stochastic point-processes, Wiley, New-York.

MACLAINE, C.G., McWILLIAM, P.N., MURRAY-SMITH, D.J. and ROSENBERG, J.R. (1977): A possible mode of static fusimotor axons as revealed by system identification, Brain Res, 135, 351-357.

MARMARELIS, P.Z. and MARMARELIS, V.Z. (1978): Analysis of physiological systems, Plenum Press, New-York.

MATTHEWS, P.B.C. (1962): The differentiation of two types of fusimotor fibre by their effects on the dynamic response of

muscle spindle primary endings, Q J Exp Physiol, 47, 324-333.

MATTHEWS, P.B.C. (1981): Review lecture: evolving views on the internal operation and functional role of the muscle spindle, J Physiol, 320, 1-30.

MATTHEWS, P.B.C. and STEIN, R.B. (1969): The regularity of primary and secondary muscle spindle afferent discharges, J Physiol, 202, 59-82.

MEYER, A.U. (1961): Pulse frequency modulation and its effect in feedback systems, Ph.D. dissertation, Northwestern University, Evanston.

OLHSEN, R.A. (1967): Asymptotic properties of the periodogram of a discrete stationary process, J App Prob, 4, 508-528.

PAVLIDIS, T. and JURY, E.I. (1965): Analysis of a new class of pulse frequency modulated feedback systems, IEEE Trans Auto Control, 10, 35-43.

PETERKA, R.J., SANDERSON, A.C. and O'LEARY D.P. (1974): Practical considerations in the implementation of the French-Holden algorithm for sampling of neuronal spike-trains, IEEE Trans Bio-Med Engr, 25, 192-195.

PRIESTLY, M.B. (1963): Contribution to a discussion of paper by M.S. Bartlett, J R Statist Soc, B25, 288-290.

RAMAKRISHNAN, A. (1950): Stochastic processes relating to particles distributed in a continuous infinity of states, Proc Camb Phil Soc, 46, 595-602.

RAMAKRISHNAN, A. (1953): Stochastic processes associated with random divisions of a line, Proc Camb Phil Soc, 49, 473-485.

RIGAS, A.G. (1983): Point-process and time series analysis: theory and applications to complex physiological problems, Ph.D. dissertation, University of Glasgow, Glasgow.

ROSENBERG, J.R., MURRAY-SMITH, D.J. and RIGAS, A. (1982): An

introduction to the application of system identification techniques to elements of the neuromuscular system, Trans Inst Measurement and Control, 4, 187-201.

ROSENBLATT, M. (1956): A central limit theorem and a strong mixing condition, Proc Nat Acad Sci USA, 42, 43-47.

SAMPATH, G. and SRINIVASSAN, S.K. (1977): Stochastic spike-trains of single neurones, in Lecture notes in biomathematics, Vol 16, ed Levin, S., Springer-Verlag, Berlin, 1-188.

SCHETZEN, M. (1981): Non-linear system modeling based on the Wiener theory, Proc IEEE, 69, 1557-1573.

SHEPERD, G.M. (1974): The synaptic organisation of the brain, 1st edn, Oxford University Press, London, 79-110.

STEIN, R.B. (1970): The role of spike-trains in transmitting and distorting sensory signals, The Neurosciences second study program, ed Schmitt, F.O., Rockefeller Univ Press, New-York, 597-604.

TICK, L.J. (1961): The estimation of transfer functions of quadratic systems, Technometrics, 3, 563-567.

WIENER, N. (1958): Non-linear problems in random theory, MIT Press, Cambridge.